IMPACT OF UNDRAINED DEFORMATION ON THE HYDRAULIC CONDUCTIVITY OF CEMENT-BENTONITE BARRIER MATERIAL

By

NUHA JAMAL ALZAYANI

A thesis submitted to the University of Birmingham for the degree of

DOCTOR OF PHILOSOPHY

Department of Civil Engineering (Geotechnical)

School of Engineering

College of Engineering and Physical Sciences

University of Birmingham

May 2018

ABSTRACT

Cement-bentonite (CB) slurry is used to construct non-structural underground barriers of low hydraulic conductivity (i.e. 10^{-9} m/s or less) for retarding fluids migration in groundwater and waste containment systems. The hardened CB barrier material (after 7 days of curing) has brittle nature (similar to rocks and concrete) with strain-softening behaviour post-peak strength up on undrained loading that is akin to cemented clays or soils. Although, the strength and stiffness of the CB material increases with curing, the strain at which the undrained peak strength occurs was not found to significantly vary with curing as it typically ranged from 0.5% to 2.0%. Therefore, the problem of failure and cracking of the hardened CB material at small strains due to change in ground conditions (e.g. through seismic, vegetation or construction activities) might have a negative impact on the required low hydraulic conductivity to be achieved by the barrier as a performance criteria (i.e. 1 x 10^{-9} m/s after 90 days of curing).

This research aimed to investigate the unknown relationship between the deformation response under undrained loading and hydraulic conductivity of CB material in the triaxial cell. This was investigated using a CB mixture comprising of 80% GGBS as a cement-replacement material under triaxial unconsolidated-undrained (TXUU) loading expected to occur during short-term curing ages (i.e. for specimens cured up to 90 days). An extensive literature review was undertaken to gain the required knowledge to: understand the variation of CB deformation behaviour and hydraulic conductivity and develop a bespoke testing methodology that provides a combined approach to measure the hydraulic conductivity after TXUU shearing. Furthermore, laboratory investigation was carried out to examine different shearing methods (multiple-stage and single-stage) and hydraulic conductivity testing methods (constant head and constant flow) in the triaxial cell. This methodology was called 'single-stage' shearing with hydraulic conductivity measurement using constant flow technique.

The increase in CB hydraulic conductivity from the order of 10^{-9}m/s up to 10^{-6} m/s was confirmed to happen after exceeding the undrained peak strength (which occurred at axial strains ranging from 0.6% to 1.4%) through propagation of major failure planes that facilitated higher seepage. Therefore, deformation under undrained loading needs to be prevented throughout the whole service life of a CB barrier (regardless of the curing age and effective stress achieved) to avoid compromising its low hydraulic conductivity requirement. Hence, controlled drainage should be provided in order to prevent the build up of excess pore water pressures up on loading and maintain the hydraulic conductivity requirement.

Key Words: cement-bentonite, undrained deformation, undrained peak strength, hydraulic conductivity, triaxial cell

To

My Saver Allah,
My Believers Mother and Father,
and
My Hope Saud and Baby Aziz

ACKNOWLEDGMENTS

Special thanks are due to Dr Alexander Royal for his supervision and support throughout my PhD project, and his kind dedication to review this thesis. I am equally thankful to Prof. Ian Jefferson for his supervision and advice when I needed it the most. Heartfelt thanks to Dr Gurmel Ghataora for his supervision and advice during laboratory training and methodology development period.

I thank the technicians in the Civil Engineering laboratory for their help, especially Sebastian Ballard (former Geotechnics technician), and Luis Portela. I would also like to thank my colleague Christopher Shaw for his technical advice during the laboratory testing period.

A warm gratitude goes to Prof. John Burland, Senior Research Investigator at Imperial College London, for the inspirational discussions and comments on my final testing results.

I would like to express my sincere gratitude to the University of Bahrain for sponsoring my PhD study for four years. Special thanks to Dr. Hashim Almadani at the University of Bahrain for believing in my academic skills to become a Teaching and Research Assistant at the University of Bahrain. Also, I would like to thank Prof. Shamsul Haque Alvi at the University of Bahrain for motivating me to achieve a PhD degree in Civil Engineering.

I extend my gratitude to my Birmingham friends for their unlimited social and emotional support during my PhD research; special mention must go to Yasmeen and May. Also, special thanks to my brother Nasser Alzayani for his amity and unconditional support particularly during my stay in the UK.

Finally, I would like to thank my parents, Jamal Alzayani and Amal Hazeem for their financial support and endless motivation, and my husband, Saud Alzayani for his understanding and patience.

TABLE OF CONTENTS

ABSTRACT……..II

DEDICATION……III

ACKNOWLEDGEMENTS……IV

TABLE OF CONTENTS……..V

LIST OF FIGURES……...XII

LIST OF TABLES……..XX

LIST OF ABBREVIATIONS……XXIV

CHAPTER 1: INTRODUCTION

1.1 Background…….....1

1.2 Problem……3

1.3 Aim and Objectives of the Research……....6

1.4 Scope of the Research Work……....7

1.5 Thesis Layout..……9

CHAPTER 2: LITERATURE REVIEW

2.1 Introduction……11

2.2 Overview on Chemical Reactions and Microstructure of CB Slurries……..12

2.3 ICE Paper on Comparison of CB with Other Cemented Materials and Need for Improved Understanding of CB Deformation and Cracking Behaviour……..17

2.4 Undrained Triaxial Deformation Behaviour of CB Specimens Containing GGBS……...18

2.4.1 Joshi (2009) and Soga et al. (2013)…..……18

2.4.2 Manassero et al. (1995)……...23

2.4.3 Royal et al. (2017)……...28

2.4.4 Fratalocchi and Pasqualini (2007)……...30

2.4.5 Williams and Ghataora (2011)……31

2.4.6 Graham et al. (2012) and Xiao et al. (2015)……32

2.5 Hydraulic Conductivity of CB Measured in Oedometer and Falling Head Permeameter.....33

2.6 Hydraulic Conductivity of CB Measured in the Flexible-Wall Triaxial Cell….....35

2.6.1 Gill and Christopher (1985)……35

2.6.2 Khera and Tirumala (1992)…….37

2.6.3 Evans (1994)……...39

2.6.4 Deschênes et al. (1995)……...40

2.6.5 Manassero et al. (1995)……...41

2.6.6 Ted et al. (1997)……..42

2.6.7 philip (2001)……43

2.6.8 Joshi et al. (2010) and Soga et al. (2013)……44

2.6.9 Williams and Ghataora (2011)……45

2.6.10 Carreto (2014) and Carreto et al. (2015, 2016)…….47

2.7 Hydraulic conductivity Measurement in Laboratory…….49

2.7.1 Laboratory Measurement Methods Acknowledged in Literature……...49

2.7.2 Variation in Laboratory Measurements of Hydraulic Conductivity…...51

2.7.2.1 Effect of Hydraulic Gradient on Measurement of Hydraulic Conductivity…….53

2.7.2.2 Effect of Effective Confining Pressure on Measurement of Hydraulic Conductivity……56

2.7.3 Comparison between Triaxial Constant Flow and Conventional Constant Head Methods for Measuring Low Hydraulic Conductivities in the Laboratory ……..……58

2.7.4 Evaluation of Measurements Methods of Low Hydraulic Conductivities by Aiban and Znidarcic (1989)……60

2.8 Summary.....63

CHAPTER 3: METHODOLOGY

3.1 Introduction……65

3.2 Specimen Preparation……66

3.2.1 Mixture Composition…….....66

3.2.2 Specimen Size…….....68

3.2.3 Procedure of Specimen Preparation……68

3.2.4 Cutting Edges of Specimens prior Testing……..69

3.3 Basic Material Characteristics of Hardened CB Specimens……..70

3.4 Concept of the Laboratory Testing Methodology……..71

3.5 Measurement of Hydraulic Conductivity……...72

3.5.1 Constant Head Method in Triaxial Cell……..73

3.5.1.1 Apparatus……73

3.5.1.2 Procedure and Test conditions……75

3.5.1.3 Calculations of Coefficient of Hydraulic Conductivity……...77

3.5.1.4 Constant Flow Application with Constant Head method…….80

3.5.2 Constant Flow (Flow Pump) Method……..85

3.5.2.1 Apparatus……86

3.5.2.2 Procedure and Test Conditions……..……..87

3.5.2.3 Calculations of Coefficient of Hydraulic Conductivity……...92

3.6 Variation in the Performance of Pressure Regulators during Hydraulic Conductivity Testing. ……..95

3.7 Multi-Stage TXUU Shearing Method with Hydraulic Conductivity Testing……98

3.7.1 Introduction……98

3.7.2 Procedure……99

3.7.3 Summary of Outcomes……..101

3.7.4 Shortcomings……103

3.8 The Main testing Methodology: Single-Stage TXUU Shearing with Hydraulic Conductivity Measurement Using Constant Flow Method……104

3.8.1 Introduction……...104

3.8.2 Test Constraints and General Procedure……...107

3.8.3 Curing Ages to be Tested……..108

3.8.3.1 Testing Before 90 Days of Curing…….108

3.8.3.2 Main Testing after 90 Days of Curing……113

3.8.4 Displacement Rate and Stress Conditions…….114

3.8.5 TXUU Strain Limits for Assessment of Hydraulic Conductivity Change ……117

3.8.6 Procedure of Constant Flow Tests at Pre-Peak state and Just after $\bar{\varepsilon}_{peak}$ at 90 Days of Curing……..121

3.8.7 Procedure of constant flow tests at post-peak state……...124

3.8.8 Calculations of Hydraulic Conductivity at Pre-Peak and Post-Peak states ……127

3.8.9 Procedure and Calculations of TXUU Deformation…….128

3.8.10 Testing Procedure at Curing Ages Greater than 90 Days……...130

3.9 Summary.....131

CHAPTER 4: RESULTS (PART A)

4.1 Introduction……..133

4.2 TXUU Behaviour after 15 Days of Curing……..134

4.2.1 Behaviour under a CP of 50 kPa……...134

4.2.2 Behaviour under a CP of 150 kPa…….135

4.2.3 Behaviour under a CP of 300 kPa…….137

4.2.4 Variation at 15 Days of Curing…….138

4.2.5 Mean Behaviour and Variation at 15 Days of Curing Using the Filtered Data……139

4.2.6 Failure Modes at 15 Days of Curing…….142

4.3 TXUU Behaviour after 30 Days of Curing……..142

4.3.1 Behaviour under a CP of 50 kPa……...142

4.3.2 Behaviour under a CP of 150 kPa……143

4.3.3 Behaviour under CP of 300 kPa……145

4.3.4 Variation at 30 Days of Curing……146

4.3.5 Mean Behaviour and Variation at 30 Days of Curing Using the Filtered Data……147

4.3.6 Failure Modes at 30 Days of Curing……149

4.4 TXUU Behaviour after 60 Days of Curing……..150

4.4.1 Behaviour under a CP of 50 kPa……...150

4.4.2 Behaviour under a CP of 150 kPa……151

4.4.3 Behaviour under a CP of 300 kPa……153

4.4.4 Variation at 60 Days of Curing……155

4.4.5 Mean Behaviour and Variation at 60 Days of Curing Using Filtered Data ……155

4.4.6 Failure Modes at 60 Days……..157

4.5 TXUU Behaviour after 90 Days of Curing……..159

4.5.1 Behaviour under a CP of 50 kPa……...159

4.5.2 Behaviour under a CP of 150 kPa……160

4.5.3 Behaviour under a CP of 300 kPa……161

4.5.4 Variation at 90 Days of Curing……163

4.5.5 Mean Behaviour and Variation at 90 Days of Curing Using the Filtered Data……164

4.5.6 Failure Modes at 90 Days of Curing……166

4.6 Summary.....167

CHAPTER 5: RESULTS (PART B)

5.1 Introduction……..169

5.2 Hydraulic Conductivity at Intact State (No Deformation) after 90 Days of Curing..……..171

5.3 Hydraulic Conductivity at Pre-Peak State of Deformation after 90 Days of Curing…….172

5.4 Hydraulic Conductivity Just after the $\bar{\varepsilon}$peak at 90 Days of Curing……..173

5.5 Hydraulic Conductivity Just After the Post-Peak Deviator Stress State after 90 Days Curing……175

5.6 Hydraulic Conductivity at Post-Peak Deviator Stress State after 90 Days of Curing…….177

5.7 Summary.....180

CHAPTER 6: DISCUSSION OF RESULTS

6.1 Introduction……..183

6.2 Characteristics of the General TXUU Behaviour…….....184

6.3 Interpretation of Common MPWP and Deviator Stress Responses of CB Specimens at Post-Peak State in the TXUU test……188

6.4 Effect of Curing Age on the TXUU Behaviour……...192

6.5 Variation of TXUU Deformation Results……196

6.6 Cracking Phenomenon of CB Specimens under TXUU Deformation…….201

6.7 The Hydraulic Conductivity of Intact (Not Deformed) CB Specimens at 90 days of Curing and Comparison with Results Previously Published in Literature……204

6.8 Change of Hydraulic Conductivity with TXUU Deformation at 90 Days of Curing…….209

6.9 Variation of Hydraulic Conductivity Results……...212

6.10 Implications for CB Performance When Exposed to Undrained Deformation ……216

6.11 Summary.....221

CHAPTER 7: CONCLUSIONS

7.1 Introduction……..223

7.2 Conclusions……..224

7.3 Recommendations for Further Work……227

7.3.1 Study of Microcracking Process Using Advanced Laboratory Testing Equipments…….228

7.3.2 Study of Effect of Consolidation (Drained Loading) on the Performance of Juvenile Fissured CB Specimens in the Triaxial Cell……229

7.3.3 Study of Drainage Implications on Performance of Small Scale CB Slurry Wall in the Laboratory……229

REFERENCES…..……...……231

APPENDIX A
Published Literature Review Paper

APPENDIX B
Data Sheets of CB Materials Used

APPENDIX C
Properties and Digital Keypad Operation Guide of Standard GDS Controller Model

LIST OF FIGURES

CHAPTER 1: INTRODUCTION

Figure 1.1 Generalised stress-strain behaviour of CB specimens (for the same mixture and duration of curing) in the laboratory under varying triaxial test conditions: TXUU or UCS (brittle response, tensile failure with strain-softening post peak), TXCU (brittle response, tensile or shear failure with strain-softening post peak depending on the effective confining pressure) and TXCD (strain-hardening)……4

Figure 1.2 Application of slurry cutoff wall under embankment, after Millet et al. (1992).....5

CHAPTER 2: LITERATURE REVIEW

Figure 2.1 SEM images of CB slurry at different curing times (t_a) measured in hours (h) (Plee et al., 1990)……13

Figure 2.2 'Foil' like formation of CSH in blended paste of Ordinary Portland Cement and GGBS (after Taylor et al. 2007)……...14

Figure 2.3 Common structure properties between (a) dried CB material, and (b) metallic foam (Joshi, 2009; Soga et al., 2013)……16

Figure 2.4 Stress-strain relationships at 35 days of curing in TXCU tests, after Joshi (2009)……...19

Figure 2.5 Excess pore water pressure versus axial strain at 35 days of curing in TXCU tests, after Joshi (2009)……19

Figure 2.6 Effective stress paths at 35 days of curing in TXCU tests, after Joshi (2009)…….....……..20

Figure 2.7 Failure modes in CUTX tests (Soga et al., 2013). (a) Shear failure (b) Tension failure……..22

Figure 2.8 Tentative elasto-plastic-work hardening model based on laboratory tests on a CB mixture containing GGBS, after Manassero et al. (1995)……..25

Figure 2.9: Stress-Strain relationships and modes of failure in TXCU tests (after Manassero et al., 1995). (a) brittle-softening, tension failure (Zone A in Figure 2.8) (b) brittle-softening, shear failure (Zone B in Figure 2.8).....……..26

Figure 2.10 Typical normalised stress paths from TXCU tests, after Manassero et al. (1995)……...27

Figure 2.11 Failure modes in TXCU tests at different initial isotropic consolidation stresses referred to unconfined compression strength, after Manassero et al. (1995)..28

Figure 2.12 Failure mechanisms of CB specimens: (a) and (b) tested in UCS at 7 days; (c) and (d) tested in UCS at 14 days; (e) tested in TXUU at 28 days under 200 kPa confinement; (f) tested in UCS at 60 days; (g) tested in UCS at 90 days; (h) tested in TXUU at 90 days under 50 kPa confinement (Royal et al., 2017)……..30

Figure 2.13 Effect of curing age and effective confining pressure on the undrained shear strength of CB specimens, after Fratalocchi and Pasqualini (2007)……...31

Figure 2.14 Stress-strain behaviour of CB specimens in TXCU tests at σ'_3 = 60 kPa and different curing ages, after Williams and Ghataora (2011)……...32

Figure 2.15 Effect of effective confining stress on hydraulic conductivity (k) of CB specimens from borehole BH2 at 3.5 m depth (Philip, 2001)……..34

Figure 2.16 A typical cumulative time versus cumulative flow curve (Khera and Tirumala, 1992)……38

Figure 2.17 Effect of Bentonite content on SB hydraulic conductivity (Evans 1994 after Barvenik 1992)……40

Figure 2.18 Effect of curing age on laboratory CB hydraulic conductivity, after Joshi (2009)……...44

Figure 2.19 Variation of hydraulic conductivity during permeation up to 9 days; (a) at 28 days of curing, and (b) at 60 and 90 days of curing, after Williams and Ghataora (2012)……...46

Figure 2.20 Hydraulic conductivity results of CB specimens with different mixture proportions at 2 months of curing (Carreto et al., 2015)……..48

Figure 2.21 Hydraulic conductivity of CB specimens of mixture composition A at varying curing periods (Carreto et al., 2015)……...48

Figure 2.22 Effect of hydraulic gradient on the hydraulic conductivity of SB specimens and the testing duration, after Evans and Fang (1988). The SB specimens comprised of; 7% bentonite, and medium to fine sand (5% medium sand, 93% fine sand, and less than 2% silt)…….....53

Figure 2.23 Effect of hydraulic gradient and specimen size on the hydraulic conductivity of reconstituted clayey material comprised of; 55 to 65% smectite, 10 to 20% illite, 10 to 20% kaolinite, 5 to 15% quartz, and less than 0.001% heavy minerals (after Carpenter and Stephenson, 1986)……...54

Figure 2.24 Effect of consolidation effective stress on the hydraulic conductivity of reconstituted clayey specimens, after Carpenter and Stephenson (1986)……57

Figure 2.25 Hydraulic conductivity measurements at varying effective stresses (a) Sandstone specimens, (b) Shale specimens (after Olsen et al., 1991)……..57

Figure 2.26 Hydraulic conductivity results on kaolinite in triaxial cell using: (a) flow pump method, (b) constant head method (after Aiban and Znidarcic, 1989)……..61

CHAPTER 3: METHODOLOGY

Figure 3.1 Triaxial cell configuration for hydraulic conductivity tests using constant head method with two back pressure systems in this study…….74

Figure 3.2 Triaxial apparatus for hydraulic conductivity tests using constant head method with two back pressure systems in this study……..75

Figure 3.3 (a) Example of calculations of flow rate, hydraulic gradient and hydraulic conductivity for triaxial hydraulic conductivity test as graphically described by Head and Epps (2014), (b) Example of top and bottom volume change data of a constant head test trial in this study……80

Figure 3.4 The standard hydraulic pressure or volume controller by GDS Instruments (GDS Instruments, 2009)……83

Figure 3.5 Apparatus configuration for hydraulic conductivity measurements with addition of the GDS hydraulic controller…….83

Figure 3.6 Apparatus configuration for hydraulic conductivity measurements with addition of the GDS hydraulic controller in this study……84

Figure 3.7 Effect of high pumping inflow rate on volume change readings……...84

Figure 3.8 Example of flow measurement data and calculations for the second method of triaxial hydraulic conductivity testing…….85

Figure 3.9 Triaxial cell configuration for hydraulic conductivity measurement through the constant flow (flow pump) method……...86

Figure 3.10 Example of the calculations and analysis of the constant flow test in this study…….95

Figure 3.11 Variation of hydraulic pressure difference with time in triaxial constant flow test under Q_{In} of 0.001 ml/min…….97

Figure 3.12 Variation of hydraulic pressure difference with time in triaxial constant flow test under Q_{In} of 0.01 ml/min……...97

Figure 3.13 Variation of hydraulic pressure difference between with time in triaxial constant flow test under Q_{In} of 0.1 ml/min……...98

Figure 3.14 Example of variation of the cell pressure with time in triaxial tests……98

Figure 3.15 Stress-strain behaviour in a multi-stage test (consisted of 10 shearing stages) on a CB specimen at 19 months curing age……...103

Figure 3.16 Example of cumulative volume change measurements in a constant flow test on a CB specimen at 14 days of curing. The constant inflow rate by GDS pump was 0.001 ml/min. (a) Cumulative outflow volume through the TBP system until 2 days of permeation. (b) Cumulative outflow volume through the TBP system until 7 days of permeation. (c) Pressure difference variation across the test specimen……109

Figure 3.17 Example of cumulative volume change measurements in a constant flow test on a CB specimen at 28 days of curing. The constant inflow rate by GDS pump was 0.001 ml/min. (a) Cumulative outflow volume through the TBP system (b) Pressure difference variation across the test specimen……..110

Figure 3.18 Cumulative volume change measurements in a constant flow test on CB specimen at 60 days of curing under varying confining pressures. The constant inflow rate by GDS pump was 0.001 ml/min……111

Figure 3.19 Pressure difference and outflow from the specimen at 14 days. The inflow rate by the GDS pump was 0.001 ml/min……...112

Figure 3.20 Pressure difference and outflow from the specimen at 28 days of curing. The inflow rate by the GDS pump was 0.001 ml/min……...113

Figure 3.21 Pressure difference and outflow from the specimen at 90 days of curing. The inflow rate by the GDS pump was 0.001 ml/min……...114

Figure 3.22 TXUU stress-strain relationships for three CB specimens at 91 days of curing tested under different CPs at 1 mm/min……..116

Figure 3.23 TXUU stress-strain relationships for three CB specimens 96 days of curing tested under different CPs at 0.02 mm/min……...……..117

Figure 3.24 Two CB specimens showing visible crack developed at the top and bottom ends through TXUU shearing up to 2% strain at CP of 300 kPa. (a) CB specimen at 58 days of curing tested under 0.02mm/min strain rate, with ε_{peak} of 0.8%. (b) CB Specimen at 94 days of curing tested under 1 mm/min strain rate, with $\boldsymbol{\varepsilon_{peak}}$ of 1.5%). Note that the middle sections of the specimens were smeared with silicone gel, and the colours were adjusted for better visibility...……..119

Figure 3.25 Two CB specimens showing no visible crack when sheared up to a strain not exceeding their ε_{peak}, under TXUU at 1 mm/min strain rate and CP of 300 kPa. (a) CB specimen at 91 days of curing sheared up to 0.6% strain. (b) CB specimen at 93 days of curing sheared up to 1.1% strain. Note that the middle sections of the specimens were smeared with silicone gel, and the colours were adjusted for better visibility.....……119

CHAPTER 4: RESULTS (PART A)

Figure 4.1 Stress-strain behaviour at 15 days of curing under a CP of 50 kPa…….134

Figure 4.2 MPWP and axial strain relationships at 15 days of curing under a CP of 50 kPa……..135

Figure 4.3 Effective stress paths at 15 days of curing under a CP of 50 kPa……135

Figure 4.4 Stress-strain behaviour at 15 days of curing under a CP of 150 kPa…...136

Figure 4.5 MPWP and axial strain relationships at 15 days of curing under a CP of 150 kPa……...136

Figure 4.6 Effective stress paths at 15 days of curing under a CP of 150 kPa……..137

Figure 4.7 Stress-strain behaviour at 15 days of curing under a CP of 300 kPa…...137

Figure 4.8 MPWP and axial strain relationships at 15 days of curing under a CP of 300 kPa……...138

Figure 4.9 Effective stress paths at 15 days of curing under a CP of 300 kPa……..138

Figure 4.10 Mean stress-strain curves at 15 days of curing under different CPs, using filtered data…….140

Figure 4.11 Mean Change of MPWP with axial strain at 15 days of curing under different CPs, using filtered data……141

Figure 4.12 Failure modes at 15 days of curing in TXUU tests. Note that the colours were adjusted for better visibility.....……142

Figure 4.13 Stress-strain behaviour at 30 days of curing under a CP of 50 kPa…...142

Figure 4.14 MPWP and axial strain relationships at 30 days of curing under a CP of 50 kPa…….143

Figure 4.15 Effective stress paths at 30 days of curing under a CP of 50 kPa……..143

Figure 4.16 Stress-strain behaviour at 30 days of curing under a CP of 150 kPa….144

Figure 4.17 MPWP and axial strain relationships at 30 days of curing under a CP of 150 kPa……...144

Figure 4.18 Effective stress paths at 30 days of curing under a CP of 150 kPa……145

Figure 4.19 Stress-strain behaviour at 30 days of curing under a CP of 300 kPa….145

Figure 4.20 MPWP and axial strain relationships at 30 days of curing under a CP of 300 kPa……...146

Figure 4.21 Effective stress paths at 30 days of curing under a CP of 300 kPa……146

Figure 4.22 Mean stress-strain curves at 30 days of curing under different CPs, using the filtered data……...148

Figure 4.23 Mean Change of MPWP with axial strain at 30 days of curing under different CPs, using filtered data……149

Figure 4.24 Failure modes at 30 days of curing in TXUU tests. Note that the colours were adjusted for better visibility.....……150

Figure 4.25 Stress-strain behaviour at 60 days of curing under a CP of 50 kPa…...150

Figure 4.26 MPWP and axial strain relationships at 60 days of curing under a CP of 50 kPa…….151

Figure 4.27 Effective stress paths at 60 days of curing under a CP of 50 kPa……..151

Figure 4.28 Stress-strain behaviour at 60 days of curing under a CP of 150 kPa….152

Figure 4.29 MPWP and axial strain relationships at 60 days of curing under a CP of 150 kPa……...152

Figure 4.30 Effective stress paths at 60 days of curing under a CP of 150 kPa……153

Figure 4.31 Stress-strain behaviour at 60 days of curing under a CP of 300 kPa….153

Figure 4.32 MPWP and axial strain relationships at 60 days of curing under a CP of 300 kPa……...154

Figure 4.33 Effective stress paths at 60 days of curing under a CP of 300 kPa……154

Figure 4.34 Mean stress-strain curves at 60 days of curing under different CPs, using filtered data…….156

Figure 4.35 Mean Change of MPWP with axial strain at 60 days of curing under different CPs, using filtered data……157

Figure 4.36 Failure modes at 60 days of curing in TXUU tests. Note that the colours were adjusted for better visibility.....……158

Figure 4.37 Stress-strain behaviour at 90 days of curing under a CP of 50 kPa…...159

Figure 4.38 MPWP and axial strain relationships at 90 days of curing under a CP of 50 kPa…….159

Figure 4.39 Effective stress paths at 90 days of curing under a CP of 50 kPa……..160

Figure 4.40 Stress-strain behaviour at 90 days of curing under a CP of 150 kPa….160

Figure 4.41 MPWP and axial strain relationships at 90 days of curing under a CP of 150 kPa……...161

Figure 4.42 Effective stress paths at 90 days of curing under a CP of 150 kPa……161

Figure 4.43 Stress-strain behaviour at 90 days of curing under a CP of 300 kPa….162

Figure 4.44 MPWP and axial strain relationships at 90 days of curing under a CP of 300 kPa……...162

Figure 4.45 Effective stress paths at 90 days of curing under a CP of 300 kPa……163

Figure 4.46 Average stress-strain curves at 90 days of curing under different CPs, using filtered data……...165

Figure 4.47 Mean Change of MPWP with axial strain at 90 days of curing under different CPs, using filtered data……165

Figure 4.48 Failure modes at 90 days of curing in TXUU tests. Note that the colours were adjusted for better visibility**.....**……166

CHAPTER 6: DISCUSSION OF RESULTS

Figure 6.1 Idealised model of stress-strain relationship, modelled on behaviour exhibited by CB specimens in TXUU tests……185

Figure 6.2 The idealised MPWP-strain response, modelled on behaviour exhibited by CB specimens in TXUU tests…….186

Figure 6.3 Proposed model of typical effective stress path of CB specimens in TXUU tests……187

Figure 6.4 Stretching of rubber membrane due to single plane slip (Head and Epps, 2014)……...189

Figure 6.5 Examples of failed CB specimens showing the uneven stretching of the rubber membranes in TXUU tests……..189

Figure 6.6 Refined idealised modelled stress-strain behaviour that redefines (dotted line) the stress-strain behaviour post-peak strength under TXUU loading……190

Figure 6.7 Refined idealised MPWP response (dotted line) expected to be exhibited under TXUU loading……191

Figure 6.8 Proposed model of relative displacements within the fragmented CB specimen in TXUU tests with increasing axial compressive strain post undrained peak strength……...192

Figure 6.9 Mean stress-strain relationships in TXUU tests for CB specimens at varying curing ages…….....193

Figure 6.10 Variation of strength parameters (q_{peck} and q_{end}) showing their independence of variation of CP in TXUU tests at the different curing ages……197

Figure 6.11 Variation of $\boldsymbol{q_{peak}}$ with curing age in TXUU tests, where total count of tests per curing age is presented in Table 6.2…….199

Figure 6.12 Variation of $\boldsymbol{q_{min}}$ with curing age in TXUU tests, where total count of tests per curing age is presented in Table 6.2……199

Figure 6.13 Variation of $\boldsymbol{q_{end}}$ with curing age in TXUU tests, where total count of tests per curing age is presented in Table 6.2…….200

Figure 6.14: Variation of $\boldsymbol{\varepsilon_{peak}}$ with curing age in TXUU tests, where total count of tests per curing age is presented in Table 6.2…….200

Figure 6.15 Variation of $\boldsymbol{\varepsilon_{min}}$ with curing age in TXUU tests, where total count of tests per curing age is presented in Table 6.2…….201

Figure 6.16 Variation of $\boldsymbol{\varepsilon_{\Delta MPWP}}$ with curing age in TXUU tests, where total count of tests per curing age is presented in Table 6.2…….201

Figure 6.17 Idealised stress-strain relationship of CB specimens in TXUU tests with mapping of cracking visualisation points ($A - E$)…….....202

Figure 6.18 Growth of visible cracks of some CB specimens in TXUU tests with respect to the cracking visualisation points described in Table 6.3. Note that the colour of images was adjusted to capture the cracks in a clearer vision, and the middle section of some of the specimens was coated with silicone gel. Cracks at points A and B are annotated with white circles and arrows.....……203

Figure 6.19 Idealised model of the impact of TXUU loading on the CB hydraulic conductivity at 90 days of curing……...211

Figure 6.20 Variation of $\boldsymbol{k_{Outflow}}$ and $\boldsymbol{\bar{k}_{Outflow}}$ of CB specimens at 90 days with increasing axial strain in repeated single-stage TXUU and constant flow tests……216

LIST OF TABLES

CHAPTER 2: LITERATURE REVIEW

Table 2.1 Summary of CB hydraulic conductivity results for selected CB mixtures (after Gill and Christopher, 1985)……36

Table 2.2 CB mixtures compositions and coefficients of hydraulic conductivity for permeation duration from 4 days to 38 days (after Khera and Tirumala, 1992)……..38

Table 2.3 CB mixture compositions by considered in this review (after Deschênes et al., 1995). Where: B = bentonite, C = cement, W = water, R = retarding agent, and all percentages by total weight……..40

Table 2.4: Laboratory triaxial hydraulic conductivity results (after Deschênes et al., 1995) **.....**……...40

Table 2.5: Laboratory hydraulic conductivity test results of the accepted field CB specimens (after Philip, 2001)**.....**……...43

Table 2.6 Hydraulic conductivity results (after Williams and Ghataora, 2012)….....45

Table 2.7 CB slurry compositions used in the laboratory study of Carreto (2014) and Carreto et al. (2015, 2016)……46

Table 2.8 Long-term triaxial permeability testing variables, after Evans and Fang (1988)……...52

Table 2.9 Comparison of constant flow method with conventional constant head method……..59

Table 2.10 Hydraulic conductivity results on kaolinite, after Aiban and Znidarcic (1989)……...60

CHAPTER 3: METHODOLOGY

Table 3.1 Mixture composition in previous studies on CB material……...66

Table 3.2 CB mixture composition used in this study…….....67

Table 3.3 Basic material characteristics of hardened CB specimens in this study…..70

Table 3.4 Flow rates measured in triaxial constant flow tests using porous stones only……...97

Table 3.5 Triaxial multi-stage test conditions and results of hydraulic conductivity measurements on a CB specimen at 19 months curing age……...102

Table 3.6 The main testing constrains and the corresponding procedures……107

Table 3.7 Peak deviator stresses and corresponding strains at different CPs and displacement rates in TXUU tests after 90 days of curing .....……..115

Table 3.8 Axial strain limits and their corresponding testing states used in the single-stage method……...120

CHAPTER 4: RESULTS (PART A)

Table 4.1 The count of TXUU tests conducted in the main testing period at different curing ages…….....……134

Table 4.2 Variation of q_{peak} and ε_{peak} at 15 days of curing in TXUU tests……...139

Table 4.3 Variation of q_{peak} and ε_{peak} of filtered data (i.e. mean trends) at 15 days of curing in TXUU tests under different CPs…….141

Table 4.4 Variation of q_{peak} and ε_{peak} at 30 days of curing in TXUU tests……...147

Table 4.5 Variation of q_{peak} and ε_{peak} of filtered data (i.e. mean trends) at 30 days of curing in TXUU tests under different CPs…….149

Table 4.6 Variation of q_{peak} and ε_{peak} at 60 days of curing in TXUU tests……..155

Table 4.7 Variation of q_{peak} and ε_{peak} of filtered data (i.e. mean trends) at 60 days of curing in TXUU tests under different CPs…….157

Table 4.8 Variation of q_{peak} and ε_{peak} at 90 days of curing in TXUU tests……...163

Table 4.9 Variation of q_{peak} and ε_{peak} of filtered data (i.e. mean trends) at 90 days of curing in TXUU tests…….166

CHAPTER 5: RESULTS (PART B)

Table 5.1 The count of hydraulic conductivity tests undertaken at 90 days of curing and different states of deformation…….171

Table 5.2 Flow rates and mean hydraulic gradient at steady state of intact CB specimens ……..172

Table 5.3 Hydraulic conductivity results at steady state of intact CB specimens….172

Table 5.4 Flow rates and mean hydraulic gradient at steady state of deformed CB specimens up to 0.6% axial strain……..173

Table 5.5 Hydraulic conductivity results at steady state of deformed CB specimens up to 0.6% axial strain…….173

Table 5.6 Flow rates and mean hydraulic gradient at steady state of deformed CB specimens up to 1.1% axial strain……..175

Table 5.7 Hydraulic conductivity results at steady state of deformed CB specimens up to 1.1% axial strain…….175

Table 5.8 Flow rates and mean hydraulic gradient at steady state of deformed CB specimens up to just post-peak deviator stress……...177

Table 5.9 Hydraulic conductivity results at steady state of deformed CB specimens up to just post-peak deviator stress…….177

Table 5.10 Flow rates and mean hydraulic gradient at steady state of deformed CB specimens up to 2.2% axial strain……..178

Table 5.11: Hydraulic conductivity results at steady state of deformed CB specimens up to 2.2% axial strain……179

Table 5.12 Flow rates and mean hydraulic gradient at steady state of deformed CB specimens up to 3.3% axial strain……..179

Table 5.13 Hydraulic conductivity results at steady state of deformed CB specimens up to 3.3% axial strain……179

Table 5.14 Flow rates and mean hydraulic gradient at steady state of deformed CB specimens up to 4.4% axial strain……..179

Table 5.15 Hydraulic conductivity results at steady state of deformed CB specimens up to 4.4% axial strain……180

Table 5.16 Flow rates and mean hydraulic gradient at steady state of deformed CB specimens up to 5.5% axial strain……..180

Table 5.17 Hydraulic conductivity results at steady state of deformed CB specimens up to 5.5% axial strain……180

CHAPTER 6: DISCUSSION OF RESULTS

Table 6.1 Comparison of TXUU results of CB specimens at different curing ages…….194

Table 6.2 Variation of TXUU results of CB specimens at different curing ages…..198

Table 6.3 Description of the cracking visualisation points with respect to axial strain……...203

Table 6.4 Comparison of $\bar{k}_{Outflow}$ at the intact state of this study with other studies with respect to their; mixture composition, triaxial testing conditions, and specimen size……..207

Table 6.5 The change of $\bar{k}_{Outflow}$ at 90 days with increasing axial strain……...210

Table 6.6 Variation of mean hydraulic conductivity results at 90 days with increasing axial strain……..213

Table 6.7 Variation of hydraulic conductivity of CB specimens at 90 days with increasing axial strain in repeated single-stage TXUU and constant flow tests……216

LIST OF ABBREVIATIONS

CB	Cement-bentonite
UCS or q_u	Unconfined compression strength
GGBS	Ground granulated blastfurnace slag
PFA	Pulverised fuel ash
CSH	Calcium-Silicate-Hydrate
CAH	Calcium-Aluminate-Hydrates
TXUU	Triaxial unconsolidated-undrained
TXCU	Triaxial consolidated-undrained
TXCD	Triaxial consolidated-drained
kPa	Kilo Pascal(s)
MPa	Mega Pascal(s)
m	Metre(s)
cm	Centimetre(s)
mm	Millimetre(s)
s	Second(s)
msec	Millisecond(s)
min	Minute(s)
ml	Millilitre(s)
cc	cubic-centimetre
g	Gram(s)
p'_o	Initial mean effective principal stress
p'	Mean effective principal stress
q	Principal stress difference or deviator stress
ε	Axial strain

σ_3	Minor total principal (confining) pressure or cell pressure
σ'_3	Minor effective principal (confining) pressure
σ_1	Major total principal pressure or cell pressure
σ'_1	Major effective principal pressure
A	Skempton parameter or cross-sectional area of the specimen
A'	Corrected cross-sectional area of the specimen
σ'_{3c}	Isotropic effective consolidation pressure
e_o	Initial void ratio
e	Void ratio
t	Mean principal stress difference in plane-strain
s'	Mean effective principal stress in plane-strain
Hz	Hertz
v	Specific volume
SB	Soil-bentonite
CP	Cell pressure or minor effective principal (confining) pressure
TBP	Top back pressure
BBP	Bottom back pressure
k	Coefficient of hydraulic conductivity
BPWP	Bottom pore water pressure
Q_{In}	Inflow rate or pumping flow rate
Q_{Out}	Outflow rate
i	Hydraulic gradient
g	Gravity
L	Length of specimen
D	Diameter of specimen
k_{Inflow}	Inflow coefficient of hydraulic conductivity

$k_{Outflow}$	Outflow coefficient of hydraulic conductivity
$\bar{k}_{Inflow}$	Mean inflow coefficient of hydraulic conductivity
$\bar{k}_{Outflow}$	Mean outflow coefficient of hydraulic conductivity
GDS	Global Digital Systems Ltd
Δ	Mathematical difference or change
PWP	Pore water pressure
MPWP	Mean pore water pressure across the specimen
$\bar{\Delta}$MPWP	Mean change of mean pore water pressure
q_{peak}	Peak deviator stress or undrained peak strength
ε_{peak}	Axial strain corresponding to peak deviator stress
$\bar{q}_{peak}$	Mean peak deviator stress or mean undrained peak strength
$\bar{\varepsilon}_{peak}$	Mean axial strain corresponding to the mean peak deviator stress
q_{min}	Minimum deviator stress
$\bar{q}_{min}$	Mean minimum deviator stress
ε_{min}	Axial strain corresponding to the minimum deviator stress
$\bar{\varepsilon}_{min}$	Mean axial strain corresponding to the minimum deviator stress
q_{end}	Final deviator stress or apparent constant strength
$\bar{q}_{end}$	Mean final deviator stress or apparent constant strength
$\varepsilon_{\Delta MPWP}$	Axial strain at which mean pore water pressure changes
$\bar{\varepsilon}_{\Delta MPWP}$	Mean axial strain at which mean pore water pressure changes
E_u	Undrained Young's Modulus
$\bar{E}_u$	Mean undrained Young's Modulus
G_u	Undrained Shear Modulus
$\bar{G}_u$	Mean undrained Shear Modulus

CHAPTER 1
INTRODUCTION

1.1 BACKGROUND

There are two broad types of slurry cut-off wall: those that are involved in the construction of structural members (such as panel walls, diaphragm walls, etc.) and those that create 'non-structural' members (such as barriers for groundwater or contaminated waste control), i.e. not expected to transmit significant loads (Millet et al., 1992). This thesis is concerned with cement-bentonite (CB) slurry cut-off walls. These are non-structural barriers that cure to form low hydraulic conductivity structures that significantly reduce the movement of groundwater or other fluids; such as those encountered in contaminated plumes.

As explained by Jefferis (1997), CB barriers (typically 0.6 m wide and up to 12 m deep) are constructed through a single phase construction technique that begins with excavating a trench then backfilling it with CB slurry (although in deeper excavations, bentonite slurry can be used to maintain excavation stability until the desired depth is reached at this point the bentonite slurry is displaced by the CB, in a double phase construction technique). Geomembranes have also been installed that run along the centre line of the CB barrier in an effort to reduce the low hydraulic conductivity still further (Jefferis, 1997; and Daniel and Koerner, 2007).

The ICE (1999) recommend that the CB barriers have a hydraulic conductivity of 1×10^{-9} m/s or lower after 90 days of curing as a performance criteria to be satisfied for effective containment of fluids. CB barriers are not capable of supporting bending moments or significant shear stress higher than those which exists in situ (Ryan, 1985; Jefferis, 1997; and Gravin and Hayles, 1999). Although, the ICE (1999) recommend a minimum value of unconfined compressive strength (UCS) of 100 kPa after 28 days of curing.

In the CB barrier construction process, particularly practiced in Europe, cementitious materials (cement and cement replacement materials such as ground granulated blastfurnace slag, GGBS, or pulverised fuel ash, PFA) are added to fully hydrated (sodium activated) bentonite-water suspension; then this slurry mixture is used to both stabilise the trench wall during excavation, and form the permanent cut-off wall itself upon setting and hardening (Millet et al., 1992; Daniel and Koerner, 2007).

Cement replacement with GGBS (from 65% to 80% of the total cementitious content) was justified to lower the hydraulic conductivity of CB significantly (Jefferis, 1997; Evans and Dawson, 1999; and Opdyke and Evans, 2005). In addition, significant increase in shear strength was achieved with increasing percentage of GGBS as studied by Guner (1978) and Jefferis (1981, and 1997). The beneficial decrease of hydraulic conductivity and increase of strength was more rapid at mixtures containing 20% cement (by total weight) with 80% GGBS cement replacement (Jefferis, 1997; and Opdyke and Evans, 2005). Furthermore, Evans (1994) found that lower hydraulic conductivity was obtained with increasing bentonite content, with 3% to 4% (by total weight) being the optimum content giving the lowest hydraulic conductivity.

CB material varies; chemically, physically and mechanically with time upon curing. Initially it is governed by colloidal bentonite slurry fabric (before hardening), then as the Calcium-Silicate-Hydrate (CSH) and Calcium-Aluminate-Hydrates (CAH) gels form from hydration reactions of cementitious materials, these dominate the behaviour in the intermediate and long terms (i.e. initially after hardening and then with completion of cement hydration processes and dissolution of the bentonite particles; Royal et al., 2017). These cementitious products are sensitive to the physico-chemcial conditions of the surrounding environment (Taylor, 1997) and as such may weather, or be chemically altered, over time in active environments. However, this thesis considers an aspect of CB behaviour (for groundwater control applications) and thus the effect of other fluids on CB properties and chemical compatibility is not considered herein.

1.2 PROBLEM

Several laboratory investigations on the CB material in the triaxial cell revealed that it undergoes different deformation responses depending on the drainage conditions during loading post hardening (Alzayani et al., 2016). Under undrained loading (i.e. UCS, triaxial unconsolidated-undrained, TXUU, and triaxial consolidated-undrained, TXCU), CB exhibits brittle behaviour with strain-softening post peak strength. In addition, it undergoes tensile failure at effective confining stresses less than or equal to 200 kPa, and shear failure at higher effective confining stresses (Joshi, 2009; and Soga et al., 2013). Whereas under drained loading (i.e. triaxial consolidated-drained, TXCD), CB shows significantly higher strength as it undergoes ductile strain-hardening behaviour when the effective confining pressure exceeds its compressive yield stress (or pre-consolidation pressure). This unusual variation of deformation

behaviour is generalised in **Figure 1.1**, this figure is based on previous findings published in the literature (as reviewed in Alzayani et al.,2016).

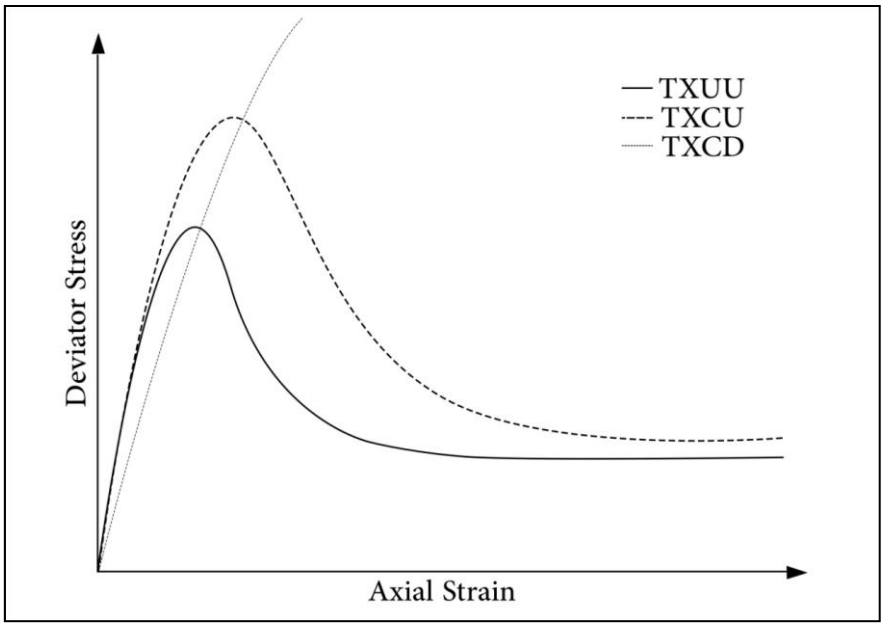

Figure 1.1: Generalised stress-strain behaviour of CB specimens (for the same mixture and duration of curing) in the laboratory under varying triaxial test conditions: TXUU or UCS (brittle response, tensile failure with strain-softening post peak), TXCU (brittle response, tensile or shear failure with strain-softening post peak depending on the effective confining pressure) and TXCD (strain-hardening).

CB develops a structure of low hydraulic conductivity (i.e. 10^{-9} m/s or less) up on curing, therefore the undrained condition is expected to govern for a considerable time whenever loading is applied post hardening as the consolidation process might require years to complete. For instance, such undrained loading conditions can be induced shortly after constructing a CB barrier (as being a part of a groundwater control system) as shown in **Figure 1.2**. This illustrates an example of a CB barrier that is constructed under a proposed earth dam to control groundwater seepage. Construction traffic, creation of the embankment and filling of the reservoir will all apply loads onto the barrier.

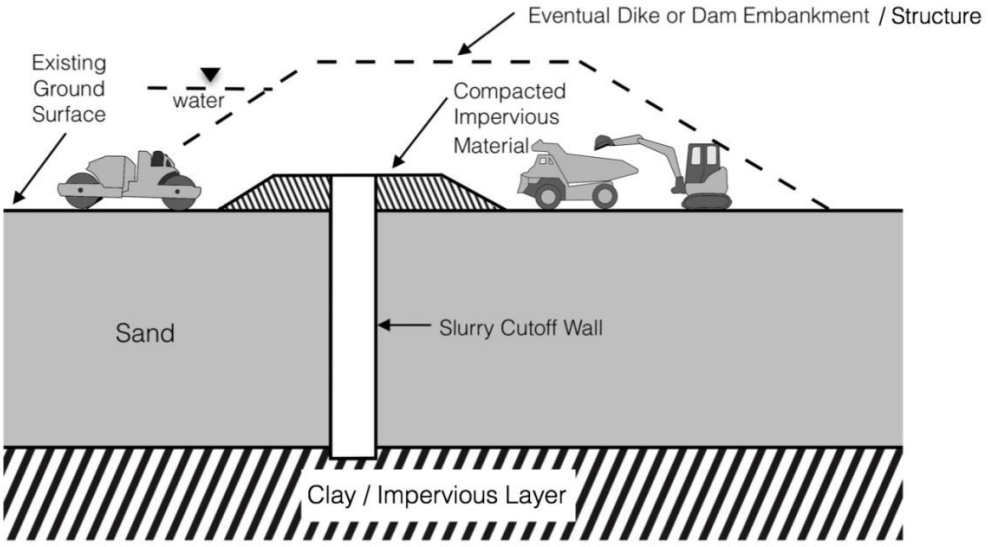

Figure 1.2: Application of slurry cutoff wall under embankment, after Millet et al. (1992)

The process of earth dam construction will impose an increase in the total stresses acting on the CB barrier; initially through traffic loads and increasing mass of the earth dam, and at later stage through increasing water level of the retained reservoir and establishment of seepage forces. Thus, if the brittle deformation response of CB is mobilised and the strength of the barrier (so far achieved through curing) is exceeded under such circumstances (**Figure 1.2**), what implications does this have for the hydraulic conductivity (i.e. performance) of the CB barrier in the short and long terms? In addition, at what point of stress and strain relative to the peak strength achieved by curing, the CB material will start to crack under undrained deformation and how this changes the hydraulic conductivity? Furthermore, in case the hydraulic conductivity has increased during the short-term due to cracking, does the CB material has the ability to recover through curing and/or consolidation? Or under what conditions it could recover and fulfil the desired performance criteria in the long-term?

1.3 AIM AND OBJECTIVES OF THE RESEARCH

As stated previously, the CB material is mostly expected to exhibit undrained deformation upon loading, as the consolidation might still not here commenced/progressed. In undrained conditions, the material is brittle (hence is likely to crack), yet the relationship between deformation response (in undrained conditions) and the hydraulic conductivity of CB does not appear to have been considered previously. Therefore the aim of this study is:

To investigate the relationship between hydraulic conductivity and deformation response of cement-bentonite barrier material in undrained conditions.

To achieve this aim, the following objectives were developed:

1. Develop a CB mixture that meets the material requirements reported in the literature, or been used previously.
2. Characterise the deformation behaviour of CB specimens in undrained conditions.
3. Develop an understanding of how cracks form within the specimens during undrained deformation.
4. Develop a laboratory testing methodology for measuring the (low) hydraulic conductivity of the specimens in conjunction with undrained deformation.
5. Evaluate the change in hydraulic conductivity of CB with increasing undrained deformation.
6. Consider the implications, and potential negative impact, of undrained deformation on the CB performance in the short and long term of curing.

In an attempt to meet the aim and objectives, an experimental study was undertaken to determine the relationship between undrained deformation behaviour under zero effective stress (i.e. TXUU loading- worst case conditions) and hydraulic conductivity, for a CB mixture containing GGBS as a cement replacement material in the triaxial cell. This aims to assess the impact of undrained deformation on the hydraulic conductivity of CB specimens in the short-term (i.e. up to 90 days of curing), during which consolidation might not yet progressed.

1.4 SCOPE OF THE RESEARCH WORK

The aim and objectives of this research have been addressed through accomplishing the following work packages:

- A literature review was undertaken that considered: undrained and drained deformation behaviour of CB material; the deformation behaviour of CB when compared to other cemented materials, in an attempt to understand the CB behaviour (as published in collaboration with this thesis in Alzayani et al., 2016) in a wider material context; the types of approaches used to measure low hydraulic conductivities within the laboratory; the results of CB hydraulic conductivity previously reported.
- A bespoke testing methodology was developed for the project. Two different hydraulic conductivity methods were evaluated (constant head and constant flow) along with two shearing procedures to develop a combined approach of shearing and hydraulic conductivity testing. This initially resulted in the development of the 'multi-stage undrained shearing' method, which was eventually abandoned in favour of the 'single-stage undrained shearing' method.

- The TXUU deformation behaviour and cracking response of CB specimens, at varying short-term curing ages from 15 days to 90 days, was investigated in the laboratory. In addition, the effect of curing on the variation of TXUU behaviour encountered was evaluated.
- The hydraulic conductivity of intact CB specimens (i.e. not deformed) was measured using constant flow method in the flexible-wall triaxial cell to establish the minimum threshold of CB hydraulic conductivity achieved after 90 days of curing.
- The hydraulic conductivity of CB specimens, cured for at least 90 days, was measured after the specimens were exposed to various amounts of axial strain using the single-stage TXUU shearing procedure (developed specially for this research).

In order to produce a robust investigation into the relationship between deformation response in undrained loading conditions and hydraulic conductivity, the scope of study has been limited to a relatively small number of parameters. This is a function of the time required to develop the bespoke method (which required significant research effort, as illustrated in Chapter 3) and the duration of the tests to assess the hydraulic conductivity of specimens in the 'intact state' (i.e. not deformed). Therefore, only one CB mixture was considered. The mixture comprised: 76% water (by total weight), 4% bentonite (by total weight), and 20% cement (by total weight with 80% replacement by GGBS). In addition, the research was limited to investigating CB specimens of short-term curing ages (i.e. up to approximately 90 days), using the flexible-wall triaxial cell for the hydraulic conductivity testing, as this was believed to consider the short and longer term strengths (the strength of this

material is not expected to increase significantly after 90 days curing; Alzayani et al., 2016). Finally, the hydraulic conductivity testing has been conducted using tap water, thus the impact of other fluids on the CB performance is not included in the scope of this research work. It is suggested that the successful development of the methodology herein permits the study of these important factors in subsequent investigations.

1.5 THESIS LAYOUT

This thesis is divided into seven chapters that are briefly described as follows:

Chapter 2: Literature Review. This chapter gives a brief review of the chemical reactions and microstructure of CB and the physical properties of the cured material. It also summarises the knowledge gained from literature reviewed and published in Alzayani et al. (2016), which includes: CB deformation behaviour (under varying effective confining stresses and drainage conditions in the laboratory), the need for improved understanding of this behaviour and the CB cracking process, and comparison with other cemented materials. Furthermore, this chapter reviews literature that covers the CB hydraulic conductivity results obtained in the laboratory and hydraulic conductivity testing methods in the flexible-wall triaxial cell.

Chapter 3: Methodology. This chapter describes the procedure of CB specimen preparation adopted in this study, and explains the constant head and constant flow methods for hydraulic conductivity measurements in the flexible-wall triaxial cell. In addition, it explains the development and testing of the combined testing approaches (multi-stage and single-stage methods), comments on the relative merits and

shortcomings of each. The single-stage method was finally selected and the chapter details validation testing undertaken to ensure the method was robust.

Chapters 4 and **5: Results.** These chapters presents the TXUU deformation tests results at varying curing ages from 15 days to 90 days (Chapter 4), and the hydraulic conductivity tests results after 90 days of curing using constant flow and single-stage testing methods (Chapter 5).

Chapter 6: Discussion. This chapter discusses the results presented in Chapters 4 and 5. It also describes the findings of the visible cracking investigation in the UCS and TXUU tests. In addition, it discusses the determined relationship between the TXUU deformation and CB hydraulic conductivity and its implications on CB performance during the short and long terms of curing.

Chapter 7: Conclusions and Recommended Further Work: This chapter summarises the findings and concludes the thesis, and suggests further work.

Appendices A, B, and C: **Published Literature Review Paper, and Data Sheets**. Appendix A comprises the ICE journal paper published in 2016 as part of the extensive literature review undertaken in this study. Appendix B presents the data sheets of materials (i.e. bentonite, cement, and GGBS) used in creating the CB slurry tested in this study. Appendix C presents properties and digital keypad operation guide of the standard GDS controller model used in this study.

CHAPTER 2
LITERATURE REVIEW

2.1INRODUCTION

In this chapter, the chemical reactions happening in the CB slurry upon curing and development of the structure that affects the variability of the CB physical and mechanical properties, is briefly reviewed. In addition, the literature concerned about the CB deformation behaviour is reviewed with a focus on the behaviour under undrained loading conditions. The previous CB deformation behaviour results are contrasted in a published review paper as a part of this thesis (See **Appendix A**). This paper also compares the CB deformation behaviour with the deformation behaviour of other cemented materials as an attempt for further understanding.

In addition, the previous CB hydraulic conductivity results are reviewed in this chapter. These results were determined using different methodologies (i.e. conventional and advanced) and specimen types (i.e. casted in the laboratory or the field). Therefore, the previous research is reviewed on an individual paper basis as it could not be properly compared. However, the CB hydraulic conductivity results obtained using the flexible-wall triaxial cell (including the results determined in this thesis) are compared in **Chapter 6**.

Furthermore, the low hydraulic conductivity testing methodologies using the flexible-wall triaxial cell are reviewed and compared in this chapter. Also, the effects of variation in the hydraulic gradient and effective confining pressure on the results of

the low hydraulic conductivity testing are reviewed. This provides the fundamental knowledge required to develop the laboratory testing methodology of this study.

2.2 OVERVIEW ON CHEMICAL REACTIONS AND MICROSTRUCTURE OF CB SLURRIES

Both the bentonite and the cementitious materials within the CB mixture have important roles in the formation and chemical response of the barrier. The hydrated bentonite supports both the excavation and the cementitious materials until the cement cure (Soga et al., 2013). The cementation process starts as soon as the Portland cement constituents react with water of bentonite slurry and GGBS to produce a range of hydration products (Joshi, 2009). The primary cementitious products are Calcium-Silicate-Hydrate (CSH), Calcium-Aluminate-Hydrates (CAH), and calcium hydroxide or hydrated lime (CH), or portlandite (Hewlett, 1998), are formed (Carreto et al., 2016). These cementitious materials cure to form a hardened structure that results in shear strength and low hydraulic conductivity.

The proportion of each cementitious product is dependent upon the nature of the constituent cementitious materials included within the mixture. Scanning electron microscopy (SEM) images were taken by Plee et al. (1990) for a CB slurry mixture up to 24 hours of curing as shown in **Figure 2.1**.

The cementitious products (CSH and CAH) forms an amorphous and colloidal gel structure (Taylor, 1997) that solidifies with curing time (Zhao et al., 2016). After 7 days of curing, the structure shows a folded pattern of the surface that is most probably developed due to the shrink of the gel during solidification (Zhao et al., 2016) as shown in **Figures 2.1**. Also, solidification results in a needle-shaped pattern of CSH within the structure (Zhao et al., 2016) as shown in **Figure 2.1** (after 24 hours

curing). Note that CB containing significant proportions of GGBS form very different structures; described as 'foil' like (**Figure 2.2**), and it is argued that this difference in CSH/CAH structure results in the significantly greater strength associated with those containing GGBS as a cement replacement (greater than 80% replacement level) (Royal et al., 2017).

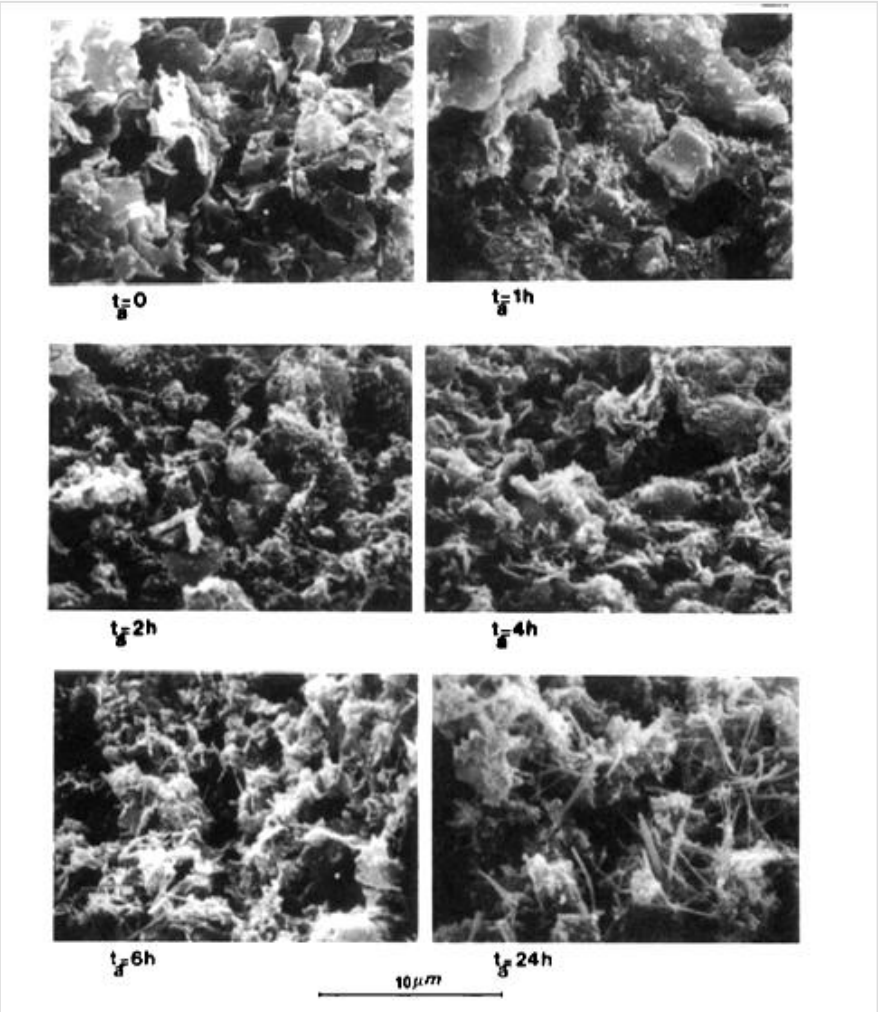

Figure 2.1: SEM images of CB slurry at different curing times (t_a) measured in hours (h) (Plee et al., 1990)

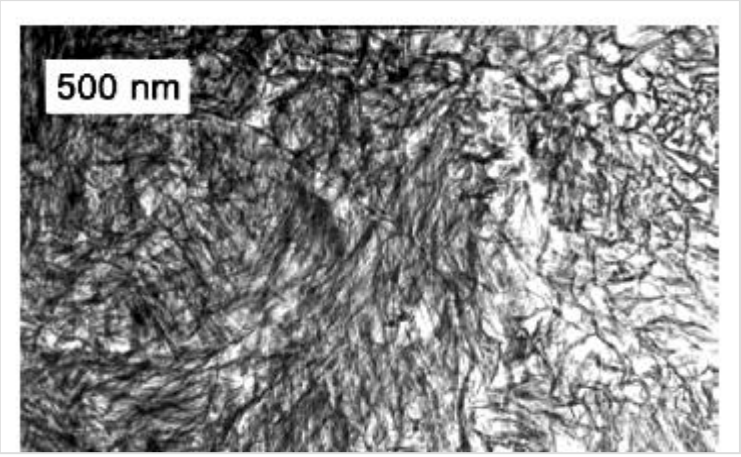

Figure 2.2: 'Foil' like formation of CSH in blended paste of Ordinary Portland Cement and GGBS (after Taylor et al. 2007)

The pH rises due to cement hydration and leads to the solubility of the inherently acidic or hydrous silica (SiO_2) and alumina (Al_2O_3) of bentonite (Plee et al, 1990). In high pH environments (approximately 12.6; Pusch et al., 2003; Jefferis, 1996 and 2008), the bentonite structure can be expected to deteriorate over time, forming additional CSH structures (Royal et al., 2017). The hydrous silica and alumina will then gradually react with the calcium and hydroxyl ions released by cement hydration to form secondary (additional) cementitious materials (i.e. CSH and CAH) on the surface of the bentonite particles; thus enhancing the bond between particles (Chew et al., 2004). These secondary (pozzolanic) reactions are likely to add to the strength of the material (Chew et al., 2004; Carreto et al., 2016), although is still secondary to the contribution from the cementitious materials added from the outset.

GGBS primarily consists of silicates, alumina-silicates, and calcium- alumina-silicates; therefore it is an intermediate chemical composition between pozzolanic material and cement (Hill and Sharp, 2002). When GGBS is used as a cement replacement material; it participates in the hydraulic/pozzolanic reactions (depending upon the temperature of the system, Hill and Sharpe, 2002) similar to cement,

contributing significantly to the composition and microstructure of the hydrated product (Hill and Sharp, 2002). GGBS reacts with hydrated lime (portlandate) produced during the early hydration of Portland cement (or naturally occurring in the GGBS) and water to form CSH gel as a principal hydration product which contributes to the strength of the cement paste (Hill and Sharp, 2002). It was observed that at high cement-replacement levels (70% or greater) the gel structure varies significantly from cement derived CSH; instead of forming 'fiberillar' structure, a far finer and more distributed 'foil' like structure is formed (Taylor et al., 2007; Richardson and Groves, 1997). This difference is attributed to CB specimens containing GGBS (70% replacement levels or greater) forming stronger materials, and improved early curing strength, than those CB containing Ordinary Portland cement (with or without PFA) and CB containing PFA as the cementitious materials (Royal et al., 2017).

The temperature is an important driver in these reactions, and in low temperature environments (10° C; that is like the shallow ground temperature expected in the UK up to 15 m that ranges from 8° C to 12° C, Busby, 2016), these reactions may take a considerable period of time (Taylor, 1997). In addition, the presence of clay becomes less and less visible as the CSH and CAH phases expand, as confirmed by an X-ray diffraction (XRD) analysis of old CB slurries (Evans, 1996; Jefferis, 1997, 2012 as cited by Carreto et al., 2016). This is also confirmed through XRD analysis by Zhao et al. (2016), as they stated that there were no clear observable peaks for clay minerals after a curing age of 1.5 years.

Finally, in an attempt to idealise the CB structure, Joshi (2009) and Soga et al. (2013) suggested that the structure of dried CB wall material could be compared to the structure of a metallic foam as shown in **Figure 2.3** (although this is not a perfect

analogue for CB structure). Soga et al. (2013) stated that the dried CB material has a porous and rigid structure that contributes; high void ratio, high strength and low hydraulic conductivity as shown in **Figure 2.3 (a)**. Similarly, metallic foam has network of alloy forming closed pores; thus it has low density, high porosity but very low hydraulic conductivity (Soga et al., 2013; **Figure 2.3b**). However, the rigidity of CB structure is limited by its yield stress; meaning once the applied load exceeds its yield stress, the porous network rapidly collapses generating large volumetric compression (Soga et al., 2013).

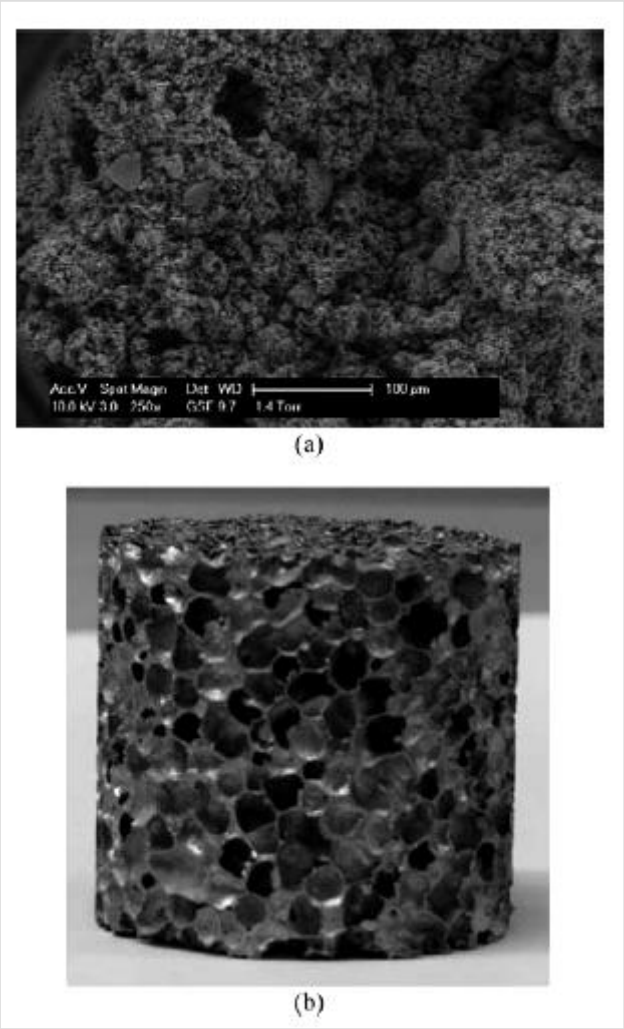

Figure 2.3: Common structure properties between (a) dried CB material, and (b) metallic foam (Joshi, 2009; Soga et al., 2013)

2.3 ICE PAPER ON COMPARISON OF CB WITH OTHER CEMENTED MATERIALS AND NEED FOR IMPROVED UNDERSTANDING OF CB DEFORMATION AND CRACKING BEHAVIOUR

Undertaking the review of CB barriers it became clear that the deformation response of CB was relatively poorly understood yet potentially critical to the long term integrity of the barrier (especially as strength and hydraulic conductivity would appear to be linked). Therefore, a review of CB deformation response compared to the more commonly reported deformation responses of other, potentially comparable, materials (cemented clays and soils, concretes, plastic concretes, 'soft' sedimentary rocks, such as mudstones and chalks) was undertaken to determine if understanding developed in other research areas could be applied to CB. In addition, whilst strength and hydraulic conductivity criteria may be specified for CB it is not clear how these parameters are interlinked, nor how change in one (i.e. deformation) impacts upon the other. This review was published in the Journal of Environmental Geotechnics, ICE (reference details below, paper located in **Appendix A**):

Alzayani NJ, Royal ACD, Ghataora GS and Jefferson IN (2016) A Review of Cement-Bentonite in Comparison with Concrete, Rocks and Cemented Soils. Journal of Environmental Geotechnics, Institution of Civil Engineers: Online publication from April 2016, http://dx.doi.org/10.1680/jenge.14.00050.

The outcome of this review suggests that a direct comparison of physical behaviour between CB and other cemented materials is problematic due to the differences observed. Furthermore, the formation of mircocracks prior to reaching the peak strength in brittle cemented materials (e.g. rocks) is an area that does not appear to

have been studied previously with CB materials; yet microcrack formation could have a significant impact on the CB ability to retard groundwater migration. Backfills enriched with Portland cement that hardens (like CB) are susceptible to cracking, leaving unknown and almost undocumentable preferential pathways for retarded water flow (Grube, 1992). Therefore, additional research is required into CB behaviour, prior to achievement of the peak strength, to determine if cracking in CB is a significant hazard as aimed in this study.

2.4 UNDRAINED TRIAXIAL DEFORMATION BEHAVIOUR OF CB SPECIMENS CONTAINING GGBS

Research on deformation behaviour of CB (containing GGBS as a cement replacement material) under undrained triaxial compression is reviewed without considering their chronological order; instead they are presented based on their findings of interest to the study herein.

2.4.1 JOSHI (2009) AND SOGA ET AL. (2013)

The undrained compression behaviour of CB was studied by Soga et al. (2013) based on Joshi (2009). TXCU tests were conducted under different confining pressures; i.e. undrained deformation is investigated after a change in the CB material structure (due to consolidation). The laboratory specimens (termed 'mixer') were tested at 35 days, 90 days, and 3.25 years of curing. The field specimens (termed 'block') were tested at 11.5 years after casting in situ. The mixture design by weight was: 3.4% bentonite, 2.5% ordinary Portland cement, 10.1% GGBS (i.e. 80.1% cement replacement), and 84% water.

It was observed that the undrained strength was generally constant and independent on the change of effective confining pressure particularly at 90 days (curing) and older, which was expected due to the very high pore water pressures building up during undrained shearing. The stress-strain relationships at different confining pressures (or initial minor effective principal stresses) for 'mixer' specimens at 35 days is shown in **Figure 2.4**, and the corresponding increase in excess pore water pressure during undrained shearing is shown in **Figure 2.5**.

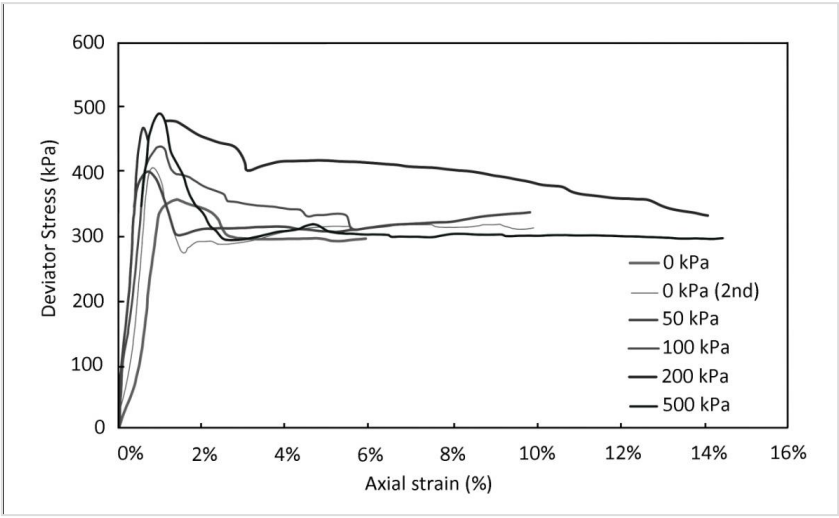

Figure 2.4: Stress-strain relationships at 35 days of curing in TXCU tests, after Joshi (2009)

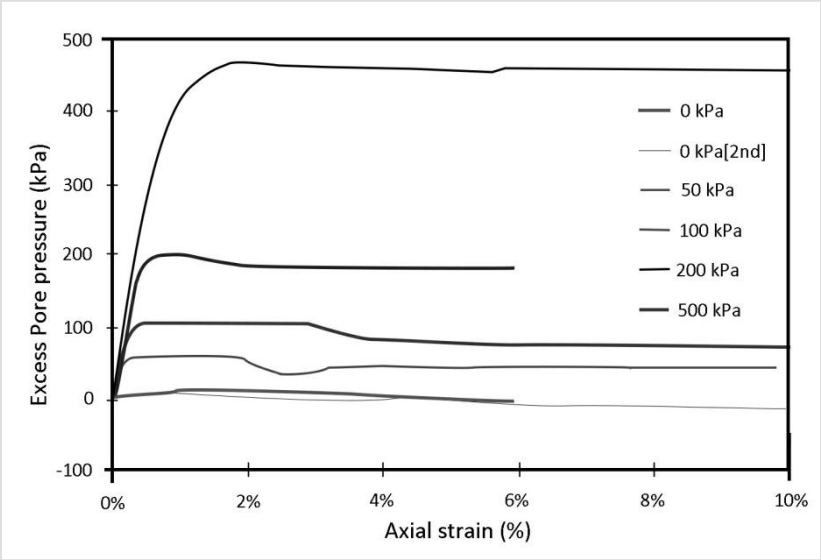

Figure 2.5: Excess pore water pressure versus axial strain at 35 days of curing in TXCU tests, after Joshi (2009)

Figure 2.4 shows consistent pattern of undrained deformation behaviour at the varying confining pressures, i.e. brittle pre-peak behaviour, well defined peak, followed by post-peak strain softening. The post-peak behaviour initiates as structure collapse and the deviator stress drops, then the stress-strain curve appears to approach an asymptote as the deviator stress becomes constant with the increasing strain. **Figure 2.5** shows that the excess pore water pressures increase under undrained shearing following the same pattern of increasing deviator stresses pre-peak, then reach a steady value at and during the post-peak states. This implies that the undrained deformation behaviour is significantly influenced by pore water pressure condition regardless of the age.

Through observing the effective stress paths shown in **Figure 2.6**, more details of deformation behaviour could be indicated. The CB 'mixer' specimens at 35 days, exhibited two different patterns of undrained behaviour, with the initial mean effective principal stress (**p'$_o$**) being the reference variable, whether it was below or above 200 kPa.

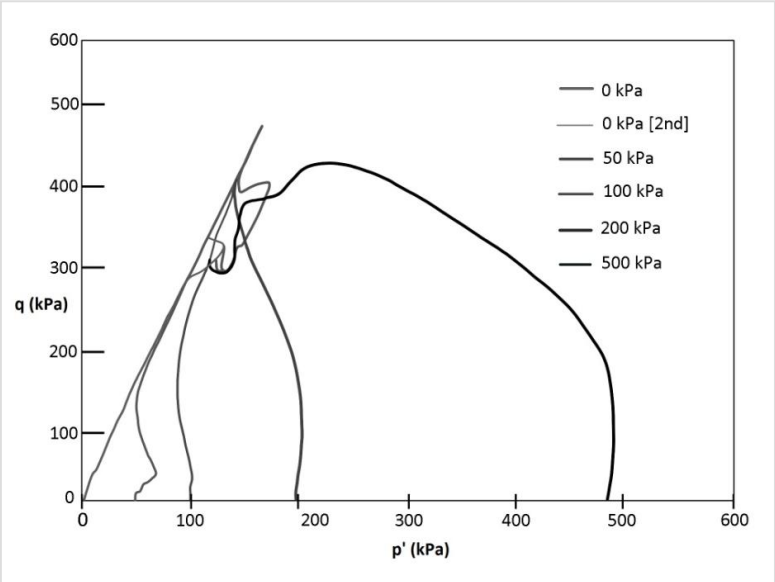

Figure 2.6: Effective stress paths at 35 days of curing in TXCU tests, after Joshi (2009)

Figure 2.6 shows the stress paths occurred under TXCU tests. At $\mathbf{p'_o} \leq$ 200 kPa (**Figure 2.6**), the path started by moving up vertically as the specimens behaved elastically until reaching the minor effective principal stress (σ'_3)=0 line (or tension cut-off line, q=3p'). Soga et al. (2013) stated that even if the specimen failed in tension, the point at which the stress state reach the σ'_3=0 line, is not necessarily the point at which the first tensile crack occur. This was interpreted due to limited pore water pressure measurement within the specimen that was possible at the bottom end only; therefore the pore pressure change at the formation of first crack might be missed. After reaching the σ'_3=0 line, the stress state travelled along this line through mobilising the remaining strength. Eventually, after reaching the maximum deviator stresses, large strains was induced due to development of tensile cracks.

In contrast, the effective stress paths of specimens at $\mathbf{p'_o} \geq$500 kPa (**Figure 2.6**), began by moving upwards, then tilting to the left towards the σ'_3=0 line and the Hvorslev line (shear failure envelope), indicating a decrease in the mean effective principal stress (**p'**) that is controlled by the increasing excess pore water pressure (**Figure 2.5**). The specimens failed before touching the σ'_3=0 line as per the declining deviator stress (**q**). Eventually, the stress state generally moves towards the σ'_3=0 line, with continuing post peak- strain softening similar to $\mathbf{p'_o} \leq$ 200 kPa stress paths. Soga et al. (2013) noted that the specimens following that pattern (at $\mathbf{p'_o} \geq$500 kPa), have failed in shear not tension; because at both the peak and post-peak strengths, the pore water pressures was not high enough to cancel out the effective confining pressure (i.e. $\boldsymbol{\sigma'_3} > 0$).

The shear strength and its corresponding axial strain at 90 days were found to be of similar ranges to that for the 3.25 years specimens that were between 535 kPa and 745

kPa and between 0.5% and 2%, respectively, indicating that the CB mix gains stable mechanical properties by reaching this age and further.

Two failure modes were observed: shear and tension failures (**Figure 2.7**). Those failure modes are dependent on the effective confining pressure. The undrained strength is highly characterised by the ability of the structure to withstand the tensile stress and resist fragmentation. Joshi (2009) observed that tension failure happened in the majority of specimens which were consolidated below 200 kPa (i.e. $\mathbf{p'_o} \leq 200$ kPa).

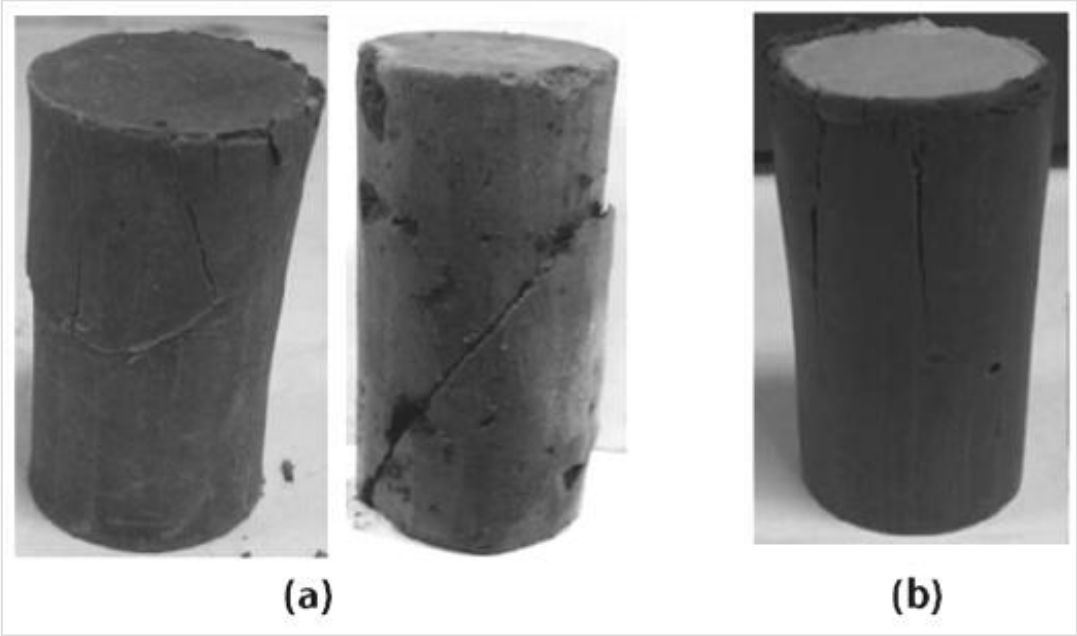

Figure 2.7: Failure modes in CUTX tests (Soga et al., 2013). **(a)** Shear failure **(b)** Tension failure

Soga et al. (2013) stated that all the stress paths encountered, didn't exceed the slope of 3 to 1 as tending to the $\sigma'_3=0$ line, and this was expected as the CB specimens do not have the required tensile resistance to cross the $\sigma'_3=0$ line.

In addition, the maximum pore water pressures above the cell pressures applied could not be recorded due to a limitation in the triaxial apparatus used. In reality, the pore pressure might have exceeded the cell pressure in the interior of the specimen, while

experiencing tensile stresses; therefore, the real stress path in the field could be on the left of the σ'_3=0 line (Soga. et al., 2013). In contrast, during TXCU tests at effective confining pressures of 500 kPa and 900 kPa (i.e. $\mathbf{p'_o}$≥200 kPa); the excess pore water pressures did not increase over the initial effective confining pressure. Skempton parameter (**A**) at failure in shear was higher than one, and collapse of structure was due to the high water content, this propagated the creation of inclined cracks. In addition, Soga et al. (2013) expect that shear failure could happen before reaching the σ'_3=0 line in tests at $\mathbf{p'_o}$≤200 kPa at young specimens (e.g. 7 days old); due to insufficient cement hydration (strength development).

2.4.2 MANASSERO ET AL. (1995)

Manassero et al. (1995) conducted various triaxial tests on CB specimens containing GGBS to propose a conceptual elasto-plastic-work hardening model (**Figure 2.8**). The tests were conducted on a CB mixture containing (by total weight): 76.8% water, 4% bentonite, and 19.2% blast furnace cement (containing 60% GGBS). The curing ages was from 5 to 7 months. The undrained triaxial behaviour was studied through TXCU tests.

The specimens were consolidated at different initial isotropic consolidation pressures ($\mathbf{\sigma'_{3c}}$ or $\mathbf{p'_o}$ as noted in the previous **Section 2.4.1**). When the $\mathbf{p'_o}$ were below 100 kPa, the excess pore water pressures were very low or negative, resulting in failure in tension (Zone A in **Figures 2.8 and 2.9**). However, when the $\mathbf{p'_o}$ were higher than 400 kPa, high positive pore pressures developed (Skempton parameter (A) at failure was greater than unity) due to the collapse of the CB structure, leading to failure in shear (Zone B in **Figures 2.8 and 2.9**). In **Figure 2.8**, the effective stress paths of specimens consolidated at $\mathbf{p'_o}$≤100 kPa (Zone A), started with vertical climb up until

reaching the tension cutoff surface (σ'_3=0 line), mobilising the remaining strength and travelled on this surface until failure in tension and decay of the maximum deviator stress. On the other hand, the effective stress paths of specimens consolidated at $\mathbf{p'_o}$≥500 kPa (Zone B), had not all succeeded to reach the tension cutoff surface, as they got more distance to travel to it, thus failure happened in shear. **Figure 2.9** shows that the stress-strain behaviour in undrained loading is brittle; peak strength was reached at very small strains, post peak -strain softening was more dramatic when the $\mathbf{p'_o}$>400 kPa.

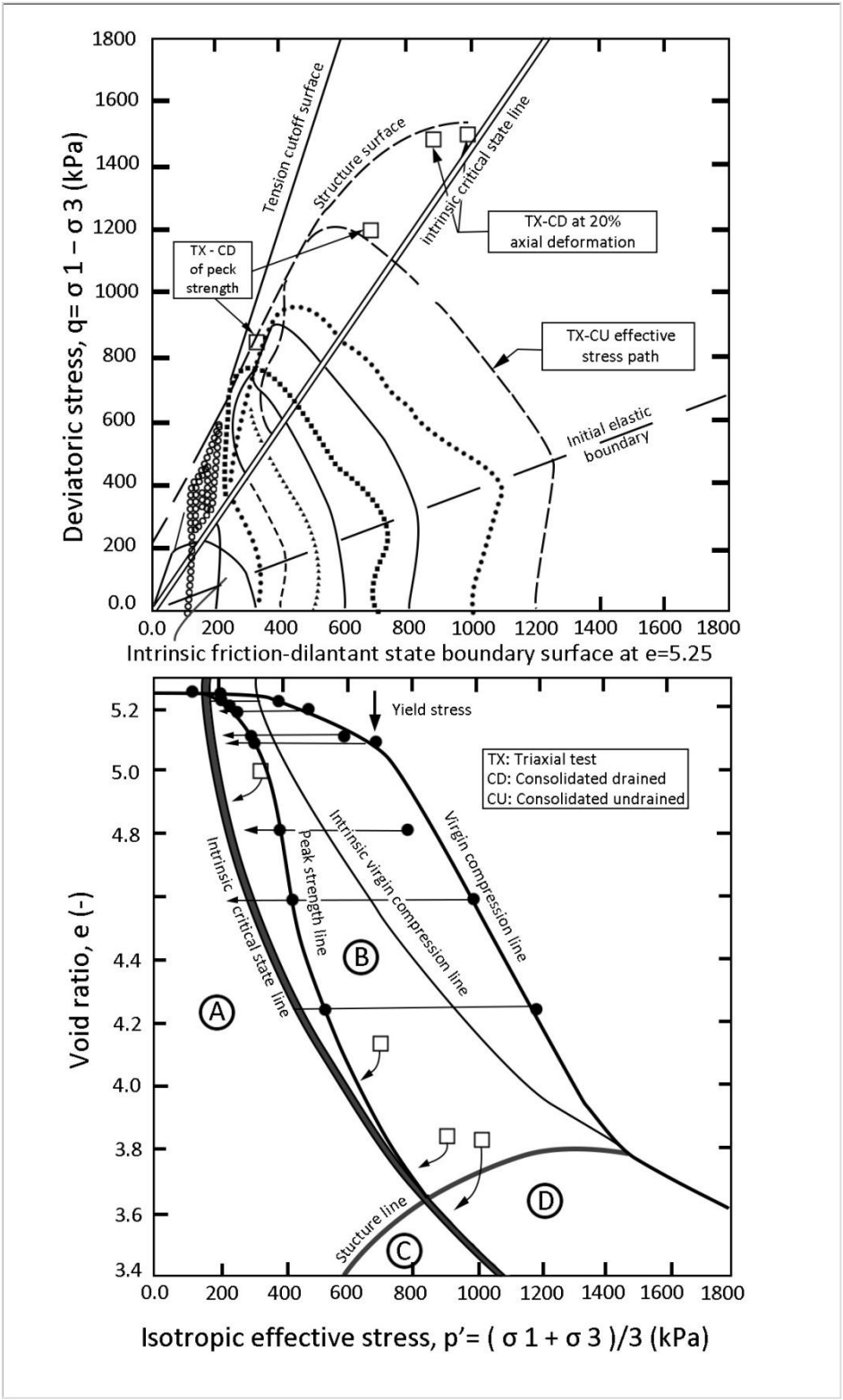

Figure 2.8: Tentative elasto-plastic-work hardening model based on laboratory tests on a CB mixture containing GGBS, after Manassero et al. (1995)

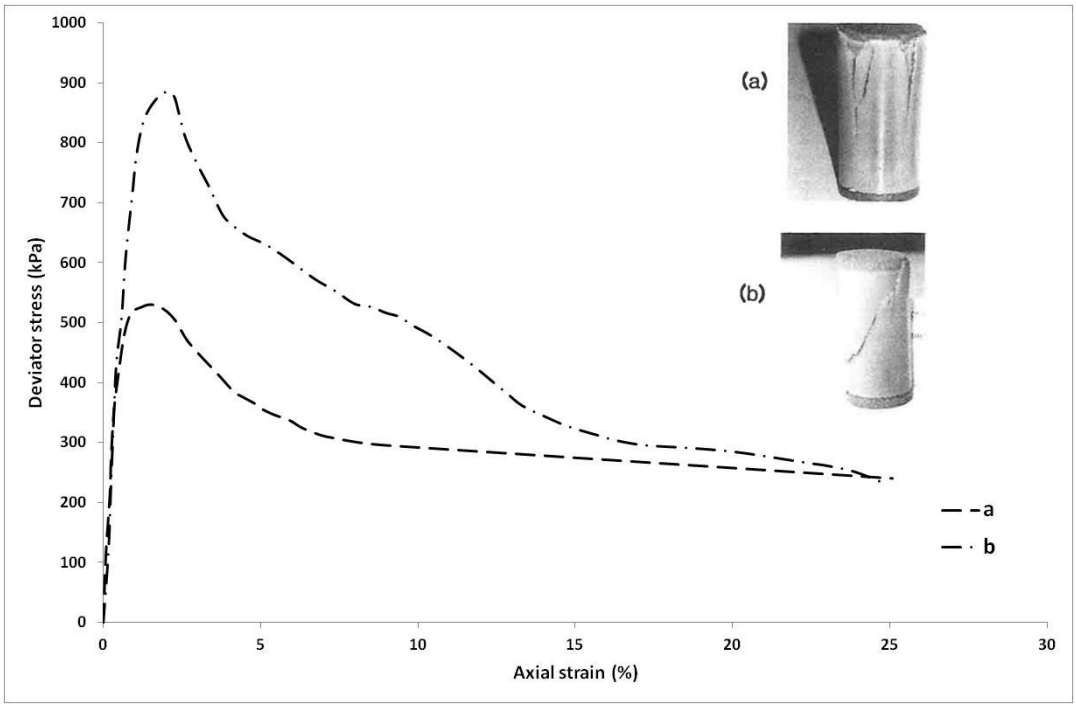

Figure 2.9: Stress-Strain relationships and modes of failure in TXCU tests (after Manassero et al., 1995). (a) brittle-softening, tension failure (Zone A in Figure 2.8) (b) brittle-softening, shear failure (Zone B in Figure 2.8).

Furthermore, Manassero et al. (1995) normalised the effective stress paths by taking out the effect of variable initial consolidation pressures, and by this they all started at unity (**Figure 2.10)**. Through these dimensionless stress paths, there are two apparent behaviours: the first showing post-peak dilatant tendency at low effective confining pressures (less than 100 kPa – Zone A), and the second showing contractive behaviour at higher effective confining pressures (higher than 100 kPa – Zone B). The normalised stress paths ended all at the critical state line (i.e. at a constant volume friction angle of 35.5° obtained in Ring Shear laboratory tests). Manassero et al. (1995) separated these two behaviours (dilatant-tension failure, and contractive-shear failure) by a frictional dilatant intrinsic state boundary surface (at e_o=5.25) that is controlled by the current effective confining pressures as shown in **Figure 2.8**.

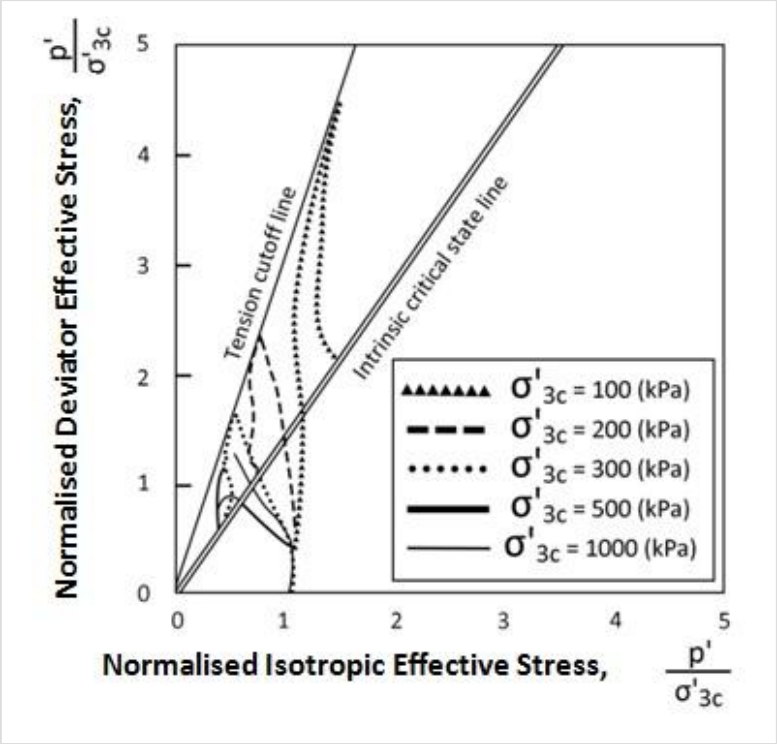

Figure 2.10: Typical normalised stress paths from TXCU tests, after Manassero et al. (1995)

Manassero et al. (1995) work suffered from the limitation of the triaxial equipment used; the inability to measure the actual pore water pressure that developed when the tensile strength is mobilised. They suggested that this might be overcome by insertion of pore water pressure gauge at the middle of the specimen. That limitation of equipment, did not justify the location of the actual failure envelope; they expect it to be on the left of the $\sigma'_3=0$ line. Thus, this verifies the occurrence of shear failures even at low effective confining pressures, as the actual pore water pressures leading to failure (expected to be in the middle of the specimens) were not known.

Manassero et al. (1995) modelled the failure modes observed in undrained triaxial loading as shown in **Figure 2.11**. In this model, the mean principal stress difference in plane-strain ($t = 0.5\ (\sigma_1 - \sigma_3)$) was normalised with respect to the mean effective principal stress in plane-strain ($s' = 0.5\ (\sigma'_1 + \sigma'_3)$), and plotted against $\boldsymbol{\sigma'_{3c}}$ or $\mathbf{p'_o}$ that

is normalised with respect to the UCS or q_u determined in UCS tests to eliminate the effect of the ultimate strength of CB structure in unconfined undrained compression conditions. Through this model (**Figure 2.11**), the two failure modes under undrained loading are separated by the ratio σ'_{3c}/ q_u of 0.7. Manassero et al. (1995) suggested that below this particular ratio ($\sigma'_{3c}/ q_u = 0.7$), the failure modes were tension failures, as the deviator stress to total effective principal stress ratio is equal to unity (meaning the change in deviator stress equal the increment in effective principal stresses), whereas above that shear failures occurred with descending deviator stress to total effective principal stress ratio and increasing σ'_{3c}/ q_u ratio.

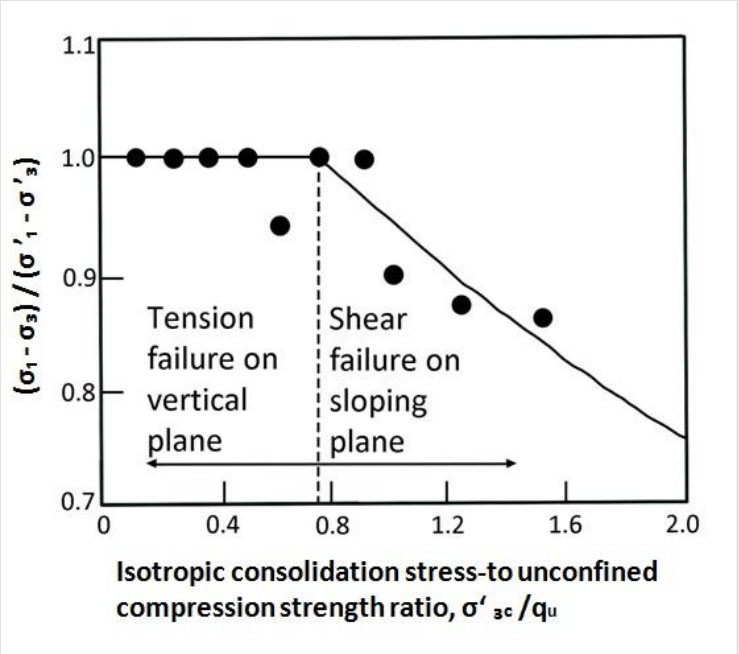

Figure 2.11: Failure modes in TXCU tests at different initial isotropic consolidation stresses referred to unconfined compression strength, after Manassero et al. (1995)

2.4.3 ROYAL ET AL. (2017)

Royal et al. (2017) investigated a CB mixture that contained the following proportions (by total weight): 76% water, 4% bentonite, and 20% cementitious materials consisting of 4% Portland cement, and 16% GGBS (i.e. 80% cement replacement).

Specimens were tested under TXUU at 1 mm/min strain rate, at various curing ages from 7 days to 90 days, and cell pressures or total minor confining pressures (σ_3) from 50 kPa to 200 kPa.

Considerable variation in deformation characteristics were found in the TXUU behaviour with respect to the variable curing age, whereas the variation was very minor with respect to increasing σ_3. The peak deviator stress was the highest at 90 days varying from around 700 kPa to 1000 kPa (in 3 to 4 repeated tests per confining pressure), and the lowest at 7 days being as low as average 300 kPa (in 5 to 6 repeated tests per confining pressure). Those peak deviator stress values were reached at small strains; that were the highest at 7 days (range from 1.2% to 1.8% (mean values)) and slightly decreased with increasing curing age (0.8% to 1.2% (mean values) at 90 days). This indicates the increasing brittleness and stiffness of CB with development of structure under increasing curing age due to processes of cement hydration. This observed an increase in brittleness and stiffness with increasing age of curing, was not linear and showed increased non-linearity at higher curing ages.

Royal et al. (2017) observed that failure modes in TXUU and UCS tests are similar. Most of the specimens failed through development of combination of inclined and vertical cracks forming a cone (or wedge) at the base that connect to longer vertical tension cracks as shown in **Figure 2.12**. Furthermore, failure through development of inclined shear plane happened mainly at young curing ages that were 7 and 14 days (**Figure 2.12**). Royal et al. (2017) did not measure the change of pore water pressures during shearing; so further beneficial interpretation on the undrained deformation behaviour cannot be made.

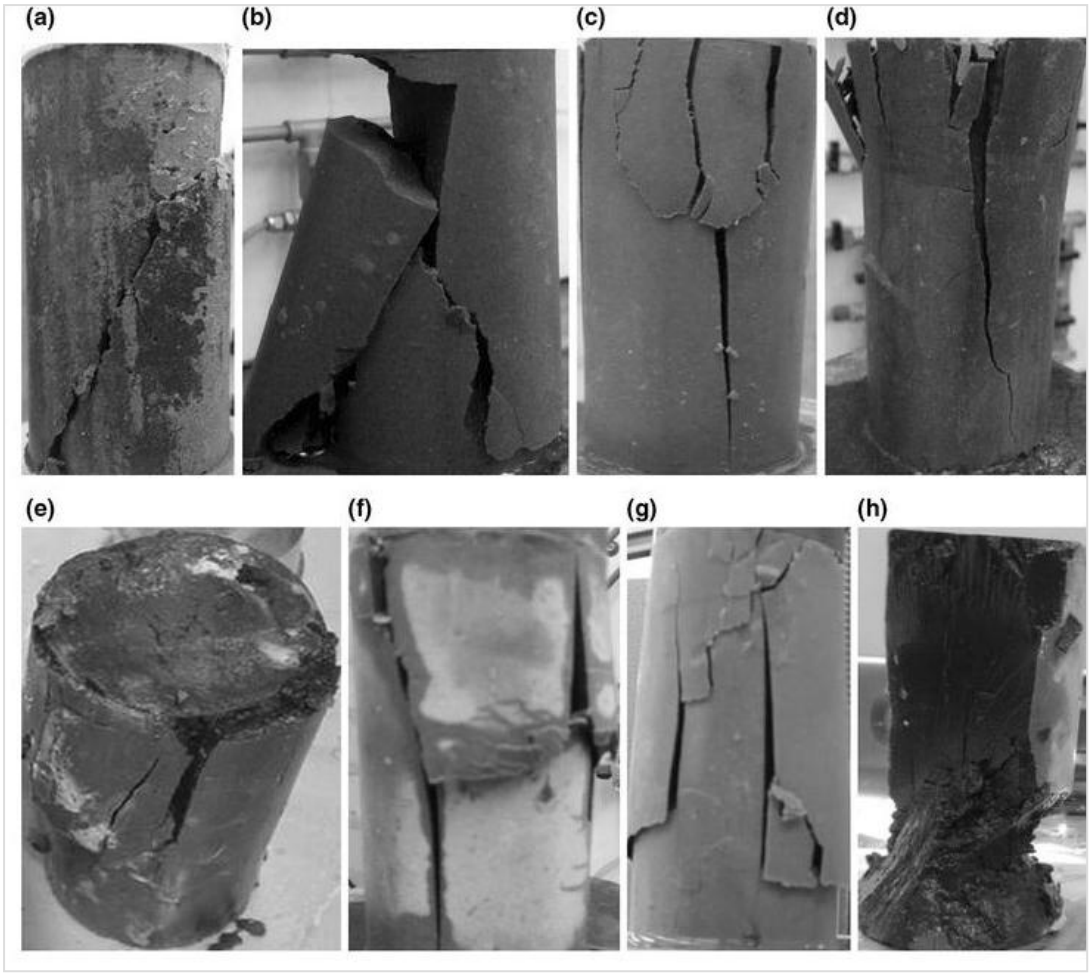

Figure 2.12: Failure mechanisms of CB specimens: (a) and (b) tested in UCS at 7 days; (c) and (d) tested in UCS at 14 days; (e) tested in TXUU at 28 days under 200 kPa confinement; (f) tested in UCS at 60 days; (g) tested in UCS at 90 days; (h) tested in TXUU at 90 days under 50 kPa confinement (Royal et al., 2017).

2.4.4 FRATALOCCHI AND PASQUALINI (2007)

Fratalocchi and Pasqualini (2007) investigated the undrained deformation behaviour of a CB mixture having a cement to water ratio between 0.2-0.3, bentonite to water ratio between 0.04-0.07, and cement with GGBS content between 66 %-80%. **Figure 2.13** shows the influence of increasing curing age and σ'_3 on the undrained shear strength of the tested CB specimens. There was a considerable increase in the undrained shear strength with increasing age of curing and increasing effective confining pressure. In addition, the variation of undrained shear strength with σ'_3

decayed at age of 300 days as the CB structure become more stable (**Figure 2.13**). Therefore, the effect of confining pressure will be negligible in the long-term in contrast to the short-term. The undrained shear strengths were achieved at axial strains of 0.5% to 2%. However, the repeatability of the results was not mentioned.

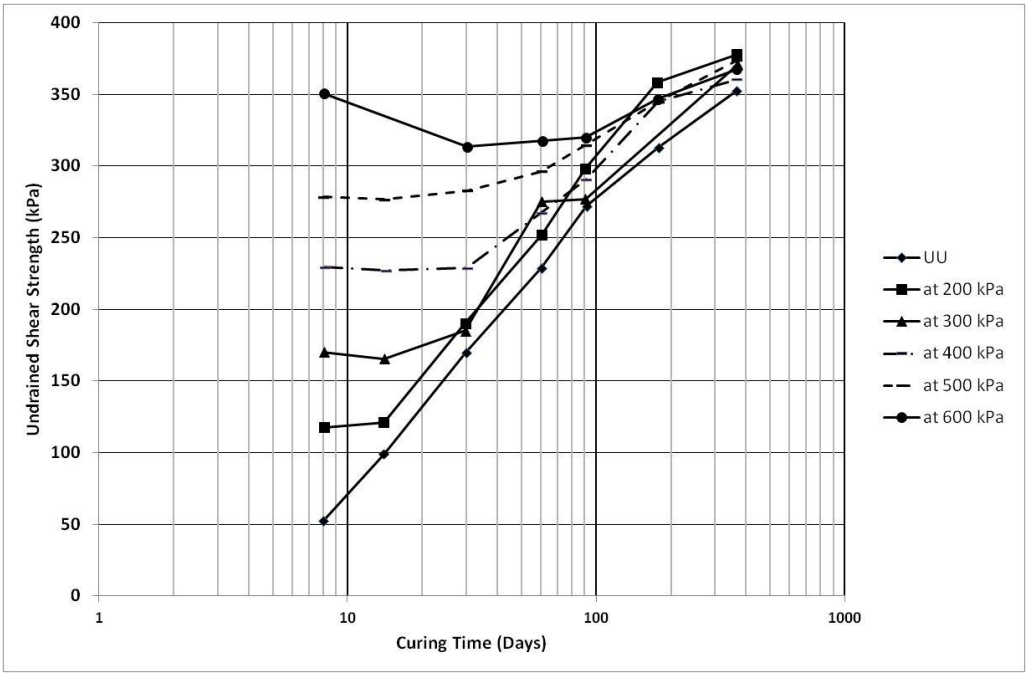

Figure 2.13: Effect of curing age and effective confining pressure on the undrained shear strength of CB specimens, after Fratalocchi and Pasqualini (2007)

2.4.5 WILLIAMS AND GHATAORA (2011)

Williams and Ghataora (2011) investigated a CB mixture containing 80% GGBS (as cement-replacement) that was similar to that used by Royal et al. (2017). TXUU tests were conducted at σ'_3 of 60 kPa and 120 kPa, and strain rate of 0.4 mm/min. **Figure 2.14** shows that stress-strain behaviour exhibited increasing brittleness and stiffness with increasing age of curing from 28 days to 90 days. The peak undrained deviator stress increased from around 400 kPa at 28 days to around 630 kPa at 90 days. The post peak-strain softening at 90 days was more dramatic. The strain corresponding to peak deviator stress ranged from 0.9 (at 28 days) to 0.6 (at 90 days); when σ'_3 was 60

kPa, and ranged from 0.8 (at 28 days) to 0.95 (at 90 days); when σ'_3 was 120 kPa. Thus, this shows insignificant variation in values of strain at peak strength with increasing effective confining pressure and curing age.

The confining pressures used by Williams and Ghataora (2011) are quite low; thus it would be so beneficial to review the pore water pressure change during shearing and failure modes happen under this low confinement. However, these findings were not reported in their publication.

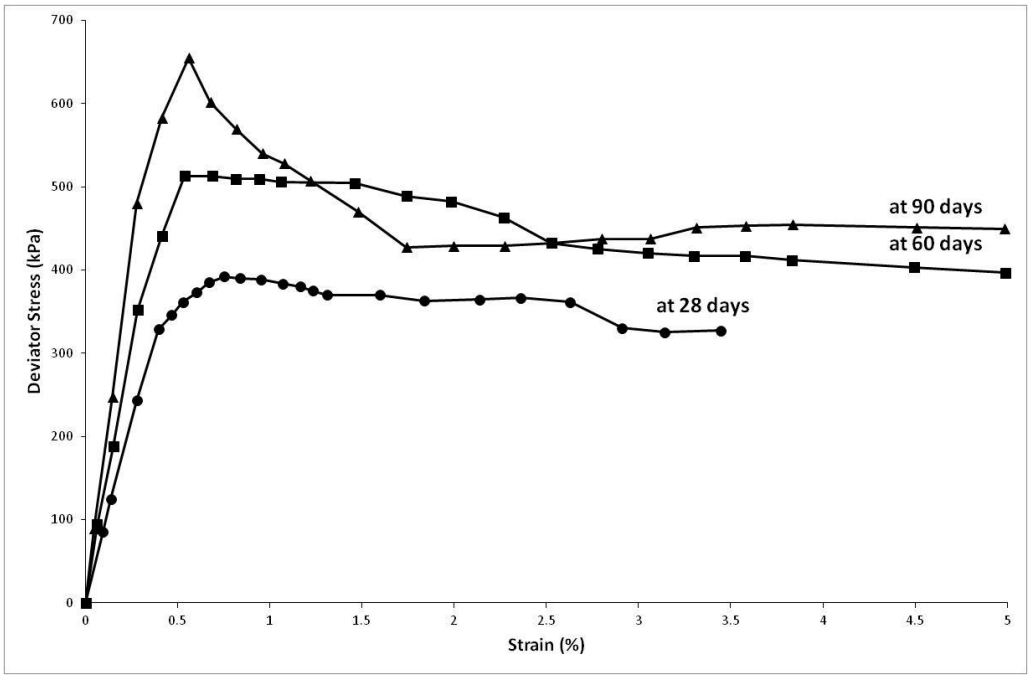

Figure 2.14: Stress-strain behaviour of CB specimens in TXCU tests at σ'_3 = 60 kPa and different curing ages, after Williams and Ghataora (2011)

2.4.6 GRAHAM ET AL. (2012) AND XIAO ET AL. (2015)

In areas that are susceptible to seismic activity, the slurry wall inside a levee could clearly be damaged under seismic load: micro and macro cracks can develop, large lateral deformations can occur, and hydraulic conductivity may significantly increase (Graham et al., 2012). Thus, Graham et al. (2012) investigated the CB response to seismic loading conditions (as did Xiao et al., 2015). Both studies used a shaking

table test on a small scale CB slurry wall using the 1997 Loma Prieta earthquake motions and sinusoidal sweep-frequency motions (from 0.2 to 6.0 Hz). The dimensions of the tested slurry wall section were 150 cm long, 160 cm tall, and 20 cm wide. The CB mixture comprised of (by weight): 4.2% bentonite, 0.8% Portland cement, 10.5% GGBS and 0.3% defloc agent (a detailed testing methodology is given in Graham et al.,2012, and Xiao et al.,2015). The results suggested that the shaking at least did not weaken the CB slurry wall (Xia et al., 2015). The CB wall performed well without any visible cracks under shaking (Graham et al., 2012).

The authors stated that they aim to conduct triaxial compression tests and flexible wall hydraulic conductivity tests on CB specimens before and after shaking to justify if any microcracks and inner structural damages may be caused by the shaking. However, no work appears to have been published on this subject at the time of writing the thesis. Hence, the outcomes of this thesis would be very helpful in evaluating the effect of undrained deformation due to seismic activity on CB hydraulic conductivity; as it provides a convenient methodology to measure the hydraulic conductivity through flexible-wall triaxial hydraulic conductivity tests after triaxial shearing.

2.5 HYDRAULIC CONDUCTIVITY OF CB MEASURED IN OEDOMETER AND FALLING HEAD PERMEAMETER

Conventional methods of measuring low hydraulic conductivities in the oedometer and falling head permeameter might produce questionable results and apply unknown and unrealistic boundary conditions (i.e. effective stresses and hydraulic gradients). Therefore, in this study the measurement, in flexible wall triaxial cell was selected to evaluate the CB hydraulic conductivity with maximum confidence.

Royal (2006) and Royal et al. (2017) investigated the same CB mixture as herein using the falling head permeameter and oedometer. The results encountered hydraulic conductivities in the order of 10^{-10} m/s and occasionally 10^{-11} m/s in the falling head permeameter, and 10^{-9} m/s (for juvenile specimens) and 10^{-10} m/s in the oedometer under effective stress of 1000 kPa.

Furthermore, the effect of increasing the consolidation pressure in oedometer tests on the hydraulic conductivity on the CB specimens is shown in **Figure 2.15**. At high effective stresses inelastic deformation took place and the specimen was quite sensitive to changes in effective stress; however, at lower values of effective stress, elastic deformation takes place and changes in hydraulic conductivity were insignificant (Philip, 2001). The highest hydraulic conductivity was in the order of 10^{-7} m/s at the lowest effective stress of 100 kPa; whereas the lowest hydraulic conductivity was in the order of 10^{-11} m/s at the highest effective stress of 2500 kPa. However, Philip (2001) suggested the maximum effective confining pressure that a CB cut-off wall will be under in the field is expected to be about 200 kPa.

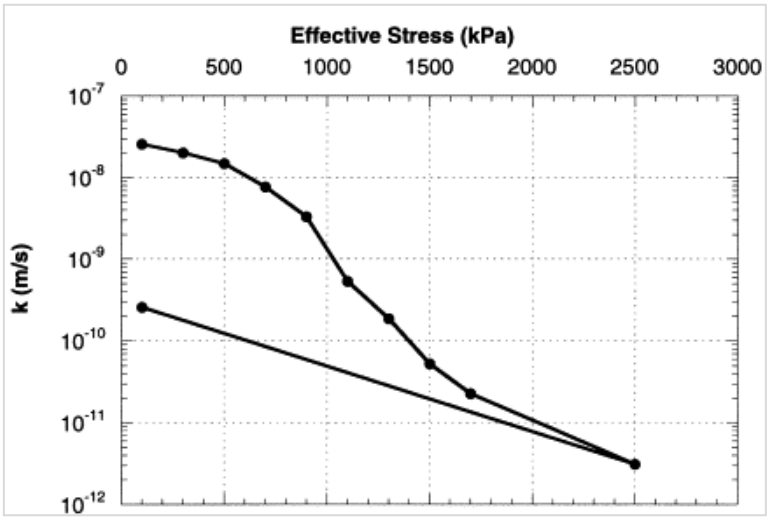

Figure 2.15: Effect of effective confining stress on hydraulic conductivity (k) of CB specimens from borehole BH2 at 3.5 m depth (Philip, 2001)

2.6 HYDRAULIC CONDUCTIVITY OF CB MEASURED IN THE FLEXIBLE-WALL TRIAXIAL CELL

In this section the previous laboratory studies on the hydraulic conductivity of CB material measured in the flexible-wall triaxial cell using different testing methods is reviewed. The triaxial testing methods of low hydraulic conductivities include the conventional constant and falling head methods to more advanced measurements through the constant flow method.

2.6.1 GILL AND CHRISTOPHER (1985)

Gill and Christopher (1985) measured the hydraulic conductivity of different CB slurry mixtures that did not contain GGBS using the falling head method in the flexible-wall triaxial cell. They also measured the hydraulic conductivity change before and after TXCD tests. The results of the CB mixtures considered in this review are shown in **Table 2.1**. The CB specimens tested had diameter of 51 mm and length of 102 mm (i.e. specimen length to diameter ratio was 2:1).

Gill and Christopher (1985) first measured the initial hydraulic conductivity (i.e. before consolidation) under; cell pressure of 405 kPa, back pressure of 392 kPa, and hydraulic gradient of 8 to 10 across the specimen to establish an upwards direction flow. After that, these test conditions were changed to measure the hydraulic conductivity TXCD deformation. Gill and Christopher (1985) stated that the hydraulic conductivity was measured after 10% strain drained deformation to simulate the condition during the initial construction of the slurry trench and embankment. They also stated that the testing encountered problems that required further modifications. However, the final modifications made to the testing procedure after consolidation and/or drained deformation were not detailed. The results in **Table 2.1** show that it

was not possible to obtain hydraulic conductivity less than 1 $x10^{-8}$ m/s for the CB mixtures tested up to 90 days of curing.

Gill and Christopher (1985) stated that the increase of bentonite content from 4% to 6% yielded to a decrease in the hydraulic conductivity by one order of magnitude. In addition, an increase in the cement content tended to increase the hydraulic conductivity (Gill and Christopher, 1985). There were two types of water used as the permeant; site water and distilled water. These kinds of water did not make considerable difference in the hydraulic conductivity of CB specimens. Furthermore, the influence of curing age found to be more significant in decreasing the hydraulic conductivity before 60 days of curing that was a decrease of one order of magnitude. Similar magnitude of reduction of the hydraulic conductivity occurred after consolidation and/or drained deformation. This confirms the findings by Jefferis (1981) that the increase of effective confining pressure reduces the hydraulic conductivity (Gill and Christopher, 1985). However, no graphical representation for the tests results is provided in their publication.

Table 2.1: Summary of CB hydraulic conductivity results for selected CB mixtures (after Gill and Christopher, 1985)

Mix No.	Cement	Bentonite	Water	Hydraulic Conductivity (m/s)		
				Curing Age		
	(% by total weight)			60 Days*		90 Days
2	14	5	81	$1*10^{-7}$	($3*10^{-8}$)	$6*10^{-8}$
4	15.4	5	79.6	$6*10^{-8}$	($2*10^{-8}$)	$6*10^{-9}$
6	16.5	5	78.5	$9*10^{-8}$	($2*10^{-8}$)	$9*10^{-8}$
9	12.97	5	82.03	$4*10^{-8}$	($2*10^{-8}$)	$2*10^{-8}$
11	14.15	5	80.85	$3*10^{-8}$		$9*10^{-8}$
* Values in parentheses indicate hydraulic conductivity after triaxial consolidation						

2.6.2 KHERA AND TIRUMALA (1992)

Khera and Tirumala (1992) stated that the CB mixtures yield a hydraulic conductivity of about 10^{-8} m/s which is an order of magnitude higher than that specified for slurry trench cutoff walls by; BRE (1994), ICE (1999), and Gravin and Hayles (1999). The authors expect that the higher hydraulic conductivity is due to calcium in cement replacing some of sodium in bentonite (as reviewed in **Section 2.2**). Therefore, Khera and Tirumala (1992) stated that the properties of a clay which undergone an ionic exchange (i.e. sodium bentonite) can differ considerably from the original clay (i.e. calcium bentonite).

Khera and Triumala (1992) conducted hydraulic conductivity measurements of CB specimens using constant head method in the triaxial cell. The cell pressure applied was 345 kPa, and the back pressure was 290 kPa. The hydraulic gradients applied were ranging from 20 to 60. CB mixtures were made using different calcium bentonite types and variable cement and slag cement replacement contents. The coefficient of hydraulic conductivity was obtained through the cumulative flow curve with cumulative time. A typical cumulative time versus cumulative flow curve is shown in **Figure 2.16**. Whenever the slope of this curve reached a constant value, the hydraulic conductivity was considered to be steady value (i.e. steady state flow condition). The measured coefficients of hydraulic conductivity at steady state of the different CB mixtures is summarised in **Table 2.1**.

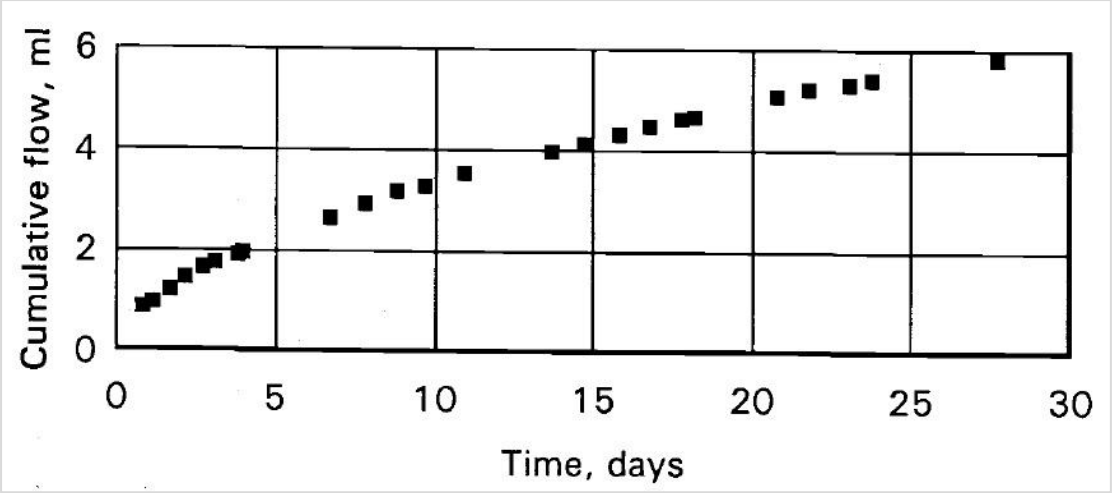

Figure 2.16: A typical cumulative time versus cumulative flow curve (Khera and Tirumala, 1992)

Table 2.2: CB mixtures compositions and coefficients of hydraulic conductivity for permeation duration from 4 days to 38 days (after Khera and Tirumala, 1992)

Specimen No.	Bentonite Type	Mixture content	Hydraulic conductivity (m/s)
AC-8W	Calcium bentonite from American Colloid	12% bentonite + 15% Cement	$1.8 * 10^{-8}$
ACL-1W		12% bentonite + 15% Cement:slag (1:1)	$1.5 * 10^{-8}$
ACL3-W		12% bentonite + 15% Cement:slag (1:3)	$3.8 * 10^{-9}$
IC-1W	Calcium bentonite from AIMCOR	12% bentonite + 15% Cement	$6.5 * 10^{-8}$
ICL-W		12% bentonite + 15% Cement:slag (1:1)	$1.9 * 10^{-7}$
GC-2W	Calcium bentonite from Greece	12% bentonite + 15% Cement	$2.3 * 10^{-8}$
GCL-1W		12% bentonite + 15% Cement:slag (1:1)	$5.0 * 10^{-11}$
TC-1W	Tixoton CV 15 [1]	12% bentonite + 15% Cement	$4.0 * 10^{-9}$
TCL-1W		12% bentonite + 15% Cement:slag (1:1)	$7.0 * 10^{-9}$

[1] is calcium bentonite treated with Na_2Co_3 from Germany

The hydraulic conductivity of the mixtures with slag cement-replacement was found to be generally lower than the mixtures without slag (**Table 2.2**). In addition, the specimens with Tioxton bentonite showed lower hydraulic conductivity values than the other types of bentonite (**Table 2.2**). This might be attributed to the abundance of sodium ions due to the treatment with sodium carbonate resulting in a very high water absorption capacity (Tirumala, 1989). Khera and Tirumala (1992) stated that none of these hydraulic conductivity values are suitable for waste containment structures. However, the test GCL-IW which contained calcium bentonite from Greece indicated an acceptable value of hydraulic conductivity for containment purposes (5×10^{-11}

m/s), and showed the most dramatic decrease in hydraulic conductivity with the addition of slag.

2.6.3 EVANS (1994)

Evans (1994) reviewed different types of vertical cutoff walls including the one comprising of CB. He found that bentonite had the same effect on the hydraulic conductivity of SB and CB compositions. This effect is illustrated in **Figure 2.17**. Lower hydraulic conductivity was obtained with increasing bentonite content, with 3% to 4% (by total weight) being the optimum content giving the lowest hydraulic conductivity. Therefore, the bentonite content of 4% is used in this thesis, same as Soga et al. (2013) and Royal et al. (2017).

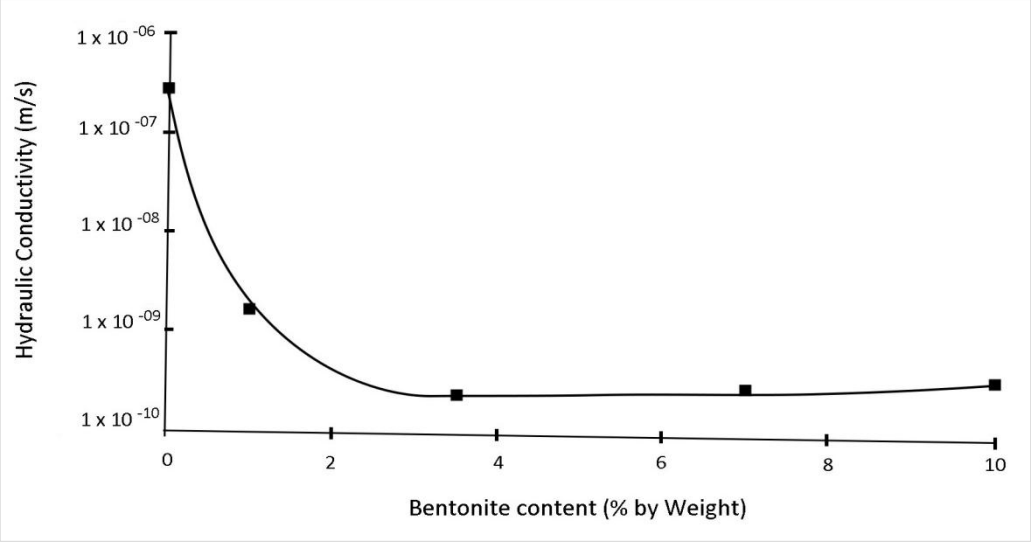

Figure 2.17: Effect of Bentonite content on SB hydraulic conductivity (Evans 1994 after Barvenik 1992)

2.6.4 DESCHÊNES ET AL. (1995)

Deschênes et al. (1995) measured the hydraulic conductivity of CB laboratory specimens at different mixture compositions (that did not contained GGBS) and curing ages from 7 days to 98 days. The two CB mixtures considered in this review is

described in **Table 2.3**. The hydraulic conductivity of CB specimens was measured through constant head method in flexible-wall triaxial cell under effective confining pressure of 100 kPa and back pressure of 690 kPa. The hydraulic gradient varied through tests from 12 to 24.

Deschênes et al. (1995) observed that hydraulic conductivity of mixes BJ-1 and BJ-4 slightly decreased with time during measurement, whereas the one of mix BJ-2 stayed almost constant. From results summarised in **Table 2.4**; the measured hydraulic conductivity of all mixes after 90 days of curing generally fall within the same order of magnitude that was approximately 1 x 10^{-8}m/s. The lowest hydraulic conductivity was achieved for mix BJ-1 which contained the highest cement content. Deschênes et al. (1995) suggested that to decrease the hydraulic conductivity to be 1 x 10^{-9} m/s, the bentonite content should be increased to be 5% to 6% as advised by Gill and Christopher (1985).

Table 2.3: CB mixture compositions by considered in this review (after Deschênes et al., 1995). Where: B = bentonite, C = cement, W = water, R = retarding agent, and all percentages by total weight.

Mix No.	BJ-1	BJ-2	BJ-4
B/W (%)	3.72	3.68	3.68
C/W (%)	35	30	30
R/W (%)	0.17	0.11	0.11

Table 2.4: Laboratory triaxial hydraulic conductivity results (after Deschênes et al., 1995)

Mix No.	Curing age (days)	k (m/s)
BJ-1	8	1.9×10^{-8}
	18	8.1×10^{-9}
	28	6.5×10^{-9}
	98	4.4×10^{-9}
BJ-2	21	1.5×10^{-8}
	28	1.2×10^{-8}
	90	1.9×10^{-8}
BJ-4	20	1.2×10^{-8}
	28	9.1×10^{-9}
	98	6.2×10^{-9}

2.6.5 MANASSERO ET AL. (1995)

Manassero et al. (1995) measured the hydraulic conductivity of a CB mixture (containing 60% GGBS cement-replacement) at curing ages from 5 to 7 months in the triaxial cell using constant head method at constant hydraulic gradient of 12. The major decrease in the hydraulic conductivity occurred in the first two months of aging (Manassero et al., 1995), and tended to stabilise to an upper boundary of about 1×10^{-9} m/s after 4 months of curing (Schweitzer, 1989; Manassero and Viola, 1992). The hydraulic conductivity of the considered CB mixture stabilised at 1×10^{-8} m/s at 60 days.

The hydraulic conductivity of CB mixtures is typically insensitive to variation in the effective confining pressures below the isotropic effective threshold stress in compression, which causes the failure of cementation bonds and the consequent significant volumetric strain due to the collapse of the solid skeleton (Manassero 1994). However, an appreciable hydraulic conductivity decrease can be observed when effective confining pressures during the setting time of the specimens are greater than the current threshold stress of the mixture (Jefferis, 1981).

The results of hydraulic conductivity justified that the hydraulic conductivity decreased by one order of magnitude from 10^{-7} m/s to 10^{-8} m/s , when the effective confining pressure increased from 20 kPa to 200 kPa after 90 days of curing.

2.6.6 TED ET AL. (1997)

Ted at al. (1997) measured the CB hydraulic conductivity through flexible-wall triaxial cell using the constant head method. The specimens tested were laboratory mixer casted, and field (trench) specimens. Unfortunately, the CB mixture proportions

used in this study is not mentioned, however it is stated that it was in accordance to specifications used in the UK.

The hydraulic conductivity for the CB laboratory mixed specimens achieved the value of 1 x 10^{-10} m/s after 90 days of curing. However, the trench specimens indicated significant contamination of CB slurry; hydraulic conductivity values varied with curing age and were higher than mixer specimens by at least one order of magnitude.

Ted et al. (1997) mentioned that a decrease in specimen volume was noticed after test completion to be around 0.35 ml/day (i.e. 2.2% of permeated volume), and it was unknown if it contributed to the observed decrease in the measured hydraulic conductivity. This loss of specimen volume might be due to the limitations of the constant head method used. Volume loss due to seepage induced consolidation could take place under such prolong measurements **(Section 2.7)**.

2.6.7 PHILIP (2001)

Philip (2001) carried out a laboratory study on CB field specimens containing GGBS that were sampled at age of three years from three boreholes drilled in an existing CB slurry wall located in Yorkshire, UK. This CB slurry wall was installed in 1995 to contain leachates from a landfill site. The tested CB specimens contained (by weight); 3.5% bentonite, and 16.5% ordinary Portland cement with 79% GGBS cement replacement.

Philip (2001) used the method of constant flow for measurement of the laboratory hydraulic conductivity in the triaxial cell. This method is more advanced than the conventional constant and falling head methods, and provides much quicker results in case low hydraulic conductivities need to be measured. This method is reviewed in

detail in **Section 2.7**. Philip (2001) used cell pressure of 600 kPa and back pressures of 500 kPa (i.e. σ'_3 of 100 kPa). The applied inflow rates varied from 0.001 ml/min to 0.01 ml/min, and the constant hydraulic gradients ranged from 3 to 70. The measurements (permeation times) under that method took from 20 minutes to 2 days.

The results summary is shown in **Table 2.5**. These values varied from the order of 10^{-8} m/s to 10^{-10} m/s measured after three years of curing.

Philip (2001) suggested that this variation of the hydraulic conductivity was neither dependent on the depth that was from 1 to 5 metres below ground level nor the hydraulic gradient up to 140; although it might be due to the variation of CB slurry material.

Table 2.5: Laboratory hydraulic conductivity test results of the accepted field CB specimens (after Philip, 2001)

Values for all tests	Coefficient of hydraulic conductivity (m/s)
Maximum	2.6×10^{-8}
Mean	5.9×10^{-9}
Median	3.1×10^{-9}
Minimum	1.3×10^{-10}

2.6.8 JOSHI ET AL. (2010) AND SOGA ET AL. (2013)

Joshi et al. (2010) and Soga et al. (2013) has discussed the behaviour of CB material (that contains GGBS) based on the findings from Joshi (2009). The CB specimens prepared in laboratory was termed 'mixer' specimens and were uncontaminated and homogeneous unlike the other types of specimens that are not covered in this review. Joshi et al. (2010) investigated the evolution of the hydraulic conductivity over curing time from 4 weeks to 10.7 years. The hydraulic conductivity was measured through a triaxial cell using the constant flow method. The applied back pressure was 100 kPa, and the initial effective confining pressure was 100 kPa. The injection flow rates was

applied through a syringe infusion pump and varied to produce hydraulic gradients from 5 to 30.

The results of laboratory hydraulic conductivity of the 'mixer' specimens at different curing ages are shown in **Figure 2.18**. Joshi et al. (2010) stated that the reduction of the CB hydraulic conductivity was most rapid at the first 90 days of curing. The general hydraulic conductivity of the 'mixer' specimens was lower than the value specified by ICE (1999) that is 10^{-9} m/s at 90 days (**Figure 2.18**). The lowest hydraulic conductivity of the 'mixer' specimens was achieved at the age of 10.7 years (around 4000 days), that ranged from 1.1 x 10^{-11} to 8 x 10^{-11} m/s (**Figure 2.18**). The variation in the hydraulic conductivity of the 'mixer' specimens was found to be lower at curing ages less than 100 days than older curing ages (**Figure 2.18**) as it became of one order of magnitude; however, the authors did not interpreted the reason of that. Soga et al. (2013) stated that more test repeats should be conducted to be able to justify the variability in results.

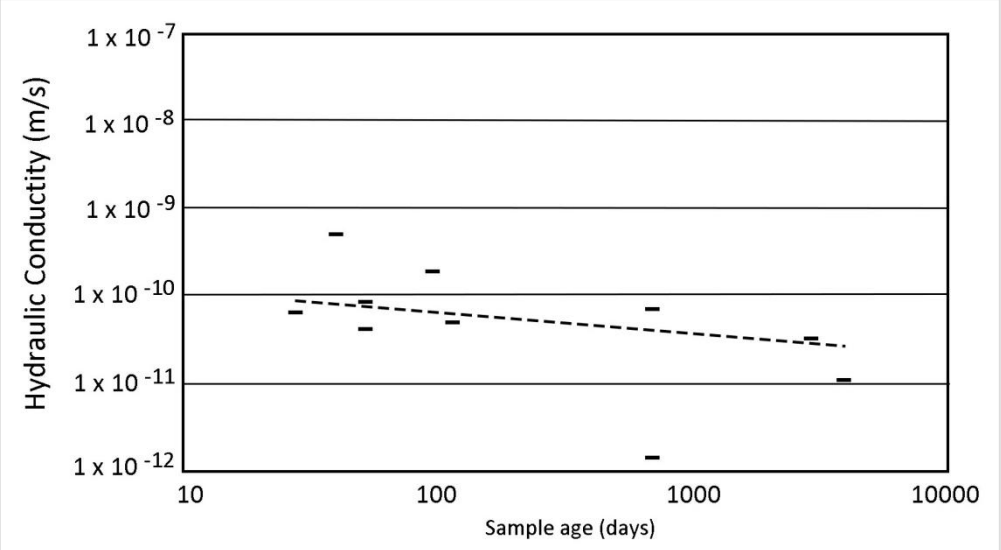

Figure 2.18: Effect of curing age on laboratory CB hydraulic conductivity, after Joshi (2009)

2.6.9 WILLIAMS AND GHATAORA (2011)

Williams and Ghataora (2011) conducted constant head tests using flexible-wall triaxial cell to measure the hydraulic conductivity of CB slurry specimens containing GGBS. The CB mix design was similar to the one used by Royal et al. (2017); that is containing 80% GGBS as cement-replacement. The tests were carried out at effective confining pressure of 60 kPa, and hydraulic gradient 27. Permeation under constant hydraulic gradient continued until steady state flow condition was achieved after at least 9 days. The results after 9 days of permeation at varying curing ages are shown in **Table 2.6**. The hydraulic conductivity values up to 90 days of curing fall within the same order of magnitude that was 10^{-9} m/s. However, they varied during the permeation period mostly at young curing ages (i.e. 28 days) as shown in **Figure 2.19**. Williams and Ghataora (2011) could not interpret the reason of this change. However, this can be due to the rapid cement hydration processes exhibited at curing ages less than 90 days, thus hydration continues through permeation and this is observed through comparing the change rate from 28 days (**Figure 2.19a**) and higher ages (**Figure 2.19b**).

Table 2.6: Hydraulic conductivity results (after Williams and Ghataora, 2012)

Curing age (Days)	k (m/s)
28	2.75×10^{-9}
60	0.35×10^{-9}
90	0.2×10^{-9}

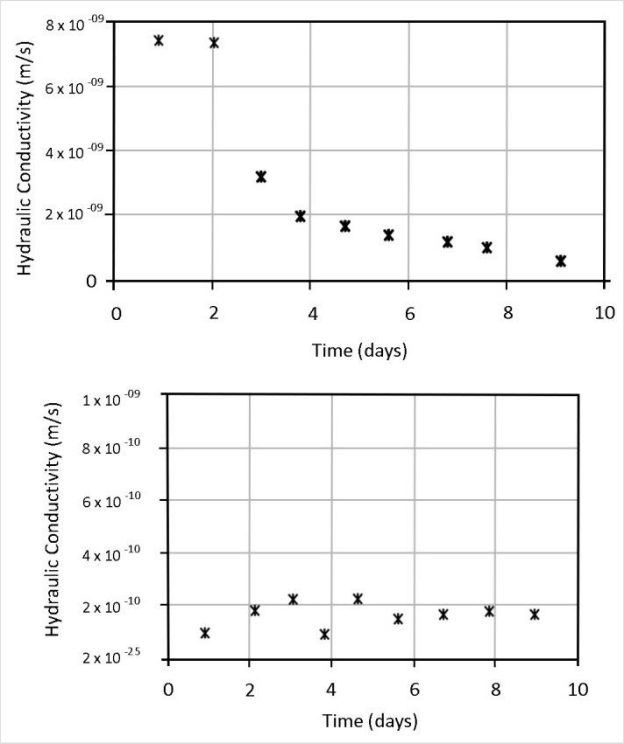

Figure 2.19: Variation of hydraulic conductivity during permeation up to 9 days; (a) at 28 days of curing, and (b) at 60 and 90 days of curing, after Williams and Ghataora (2012)

2.6.10 CARRETO (2014) AND CARRETO ET AL. (2015, 2016)

Carreto (2014) studied CB mixtures without cement replacement by slag. **Table 2.7** shows the three different CB mixtures; that were made using CLARSOL FTP 2S sodium activated bentonite from CECA (Paris, France), CEM II-32.5N Portland cement, and tap water. One of the CB mixtures (called A) was based on the Santa Clara-a-Velha Monastery cut-off slurry wall in Portugal that was built in 2001-2002. The hydraulic conductivities of those mixtures were measured through the conventional constant head method in a triaxial cell.

Table 2.7: CB slurry compositions used in the laboratory study of Carreto (2014) and Carreto et al. (2015, 2016)

CB Composition	Bentoite	Cement
	(% by weight per 1 cubic meter of water)	
A	2.83	16.19
B	4	16.2
C	2.95	12.658

Carreto et al. (2015) also measured the hydraulic conductivity after triaxial consolidation same as Gill and Christopher (1985). The results at 2 months of curing at varying specific volume (**v** = 1 + void ratio (**e**)) corresponding to different **p'** values is shown in **Figure 2.20**. The used range of p' were almost equivalent to the range of primary yield stresses (maximum deviator stress in TXCU tests) of the different tested CB mixtures. These stresses were ranging from 50 kPa to 400 kPa. Carreto et al. (2015) stated that measurement of the hydraulic conductivity at stresses lower than the primary yield stress was not successful due to difficulty in maintaining constant pressures. However, the coefficient of hydraulic conductivity of lab-made CB mixtures, consolidated under their self-weight, is considered to be typically insensitive to variations in the effective confining pressures lower than the primary yield stress (Carreto et al., 2015). In contrast, the hydraulic conductivity decreases with increasing effective confining stresses due to a significant decrease in the number and size of voids (Carreto et al., 2015); this can be clearly seen in **Figure 2.20**. At the lowest effective consolidation stress (i.e. 50 kPa) the coefficient of hydraulic conductivity is in the order of 10^{-6} m/s, whereas at the highest effective consolidation stress (i.e. 400 kPa) the coefficient of hydraulic conductivity was in the order of 10^{-8} m/s. Furthermore, the coefficients of hydraulic conductivity (k) of mixtures C and B were lower than mixture A by one order of magnitude (at the same effective consolidation stresses). This is because whenever the ratio between bentonite and cement increases, the ratio between the pozzolanic CSH gel and the primary CSH gel increases and hydraulic conductivity decreases (Carreto et al., 2015). The bentonite/cement ratio in mixtures B and C were 0.25 and 0.23 respectively, whereas the one in mixture A was 0.18.

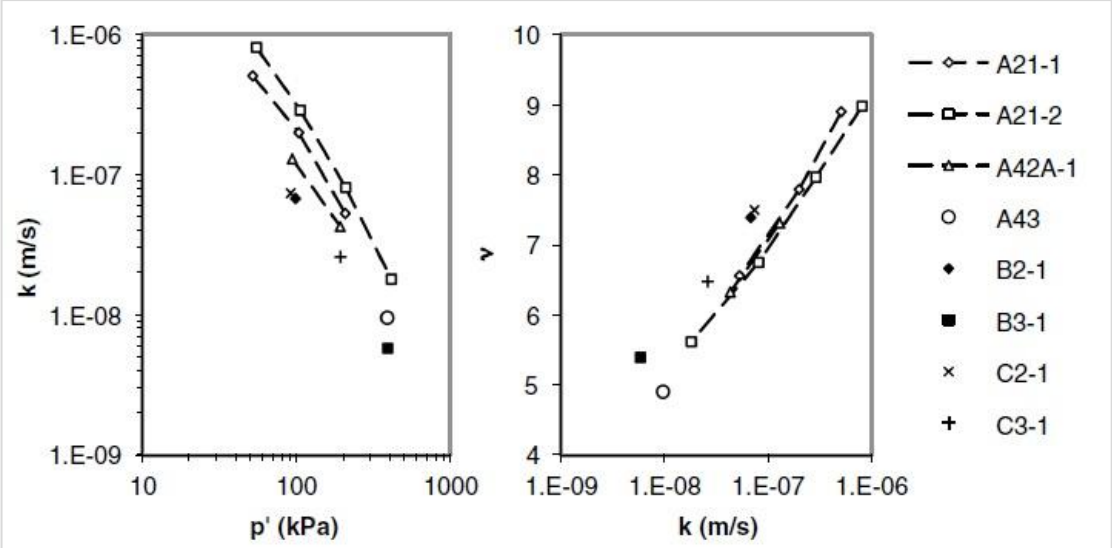

Figure 2.20: Hydraulic conductivity results of CB specimens with different mixture proportions at 2 months of curing (Carreto et al., 2015)

Carreto et al. (2015) expected to find a decrease in the hydraulic conductivity with increasing curing age; however this was not justified in their results as shown in **Figure 2.21**. The authors suggested that this might be because the major chemical reactions of tested CB mixtures had happened by the curing age of 30 days; hence the remaining further chemical reactions and development of CB structure might not be significant between 30 days to 90 days of curing.

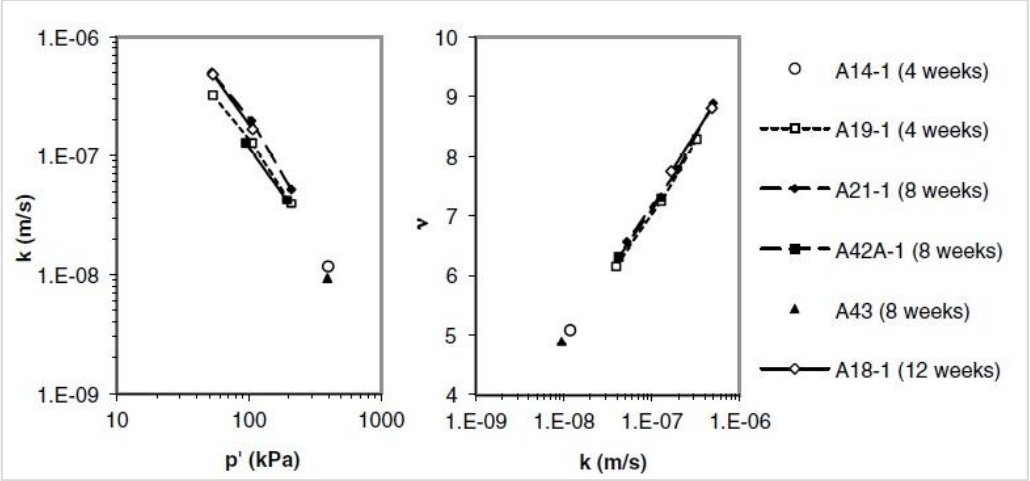

Figure 2.21: Hydraulic conductivity of CB specimens of mixture composition A at varying curing periods (Carreto et al., 2015)

2.7 HYDRAULIC CONDUCTIVITY MEASUREMENT IN LABORATORY

2.7.1 LABORATORY MEASUREMENT METHODS ACKNOWLEDGED IN LITERATURE

There are several methods to measure the hydraulic conductivity of saturated materials in laboratory; these range from conventional (i.e. falling and constant head methods or derived from 1D consolidation testing in the oedometer; BS 1377-6: 1990) to more advanced methods that facilities more control of flow (i.e. constant flow or flow pump method, Aiban and Znidarcic, 1989). Methods can result in direct measurement (through the triaxial cells or other permeameter cells), or indirect measurement (as noted above, through the oedometer or consolidation tests), and each method has its own advantages and disadvantages.

In the constant head method, water flows through a specimen under constant head or pressure difference indicating a constant hydraulic gradient that should produce a laminar flow across the test specimen. Therefore, the coefficient of hydraulic conductivity is calculated after a certain volume of water has passed through the specimen during a known time indicating constant (steady state) flow using Darcy' s law as in **Equation 2.1** (Das, 2010; Heads and Epps, 2011).

$$\mathbf{k} = \frac{\boldsymbol{Q}}{\boldsymbol{Ait}} \qquad \textbf{(2.1)}$$

Where; A is the area of cross-section of specimen, k is the coefficient of hydraulic conductivity of the soil and has the dimensions of velocity (that is usually expressed in metres per second – m/s), i is the hydraulic gradient (dimensionless), Q is the discharge and t is the time.

The steady state flow condition is achieved whenever the inflow rate equals outflow rate. If used without forced flow (i.e. without pumping) this method is recommended for coarse soils.

In the falling head method, the lower head is maintained whilst the upper head is allowed to decrease with the flow of fluid through the soil. The hydraulic conductivity of fine grained soils at any time under any head difference under laminar flow condition is obtained using Darcy's law as in **Equation 2.2**.

$$\boldsymbol{k = \frac{aL}{A(t_2 - t_1)}\, ln\, \frac{h_1}{h_2}} \qquad \textbf{(2.2)}$$

Where; h_1 and h_2 are the head differences at time t_1 and t_2, respectively, L is the length of the specimen, and a is the area of cross-section of measurement standpipe tube.

In the constant flow (flow pump) method, a certain constant and slow infiltration rate (based on the type of soil tested) is applied until a constant hydraulic gradient and equivalent outflow rate are achieved (i.e. steady state flow condition is achieved). The hydraulic conductivity is obtained using **Equation 2.1** similar to the constant head method. The constant inflow rate is provided by an automated syringe pump and the direction of the generated flow across the test specimen can be controlled same as the constant head method. This method is beneficial for measuring low hydraulic conductivities in relatively short periods using low hydraulic gradients (Aiban and Znidarcic, 1989).

2.7.2 VARIATION IN LABORATORY MEASUREMENTS OF HYDRAULIC CONDUCTIVITY

The hydraulic conductivity is an extremely variable parameter, possibly the most variable in geotechnical engineering (Dunn and Mitchell, 1984) and this is reflected in values measured in situ or in the laboratory (as illustrated in **Section 2.6**).

In addition, there are limitations with the testing, for example Aiban and Znidarcic (1989) stated that the falling head test suffers from continuous variation of gradient that result in variation of effective stress within the test specimen; hence variation of volume and hydraulic conductivity. In order to avoid, or minimise, the problem of varying gradient, the constant head method (for measuring hydraulic conductivities of coarse grained soils) was used to measure low hydraulic conductivities (Tavenas et al., 1983; Dunn and Mitchell, 1984; Aiban and Znidarcic, 1989). Carpenter and Stephenson (1986) stated that the short-term testing (through falling head method) varies with respect to boundary influences (either fixed or flexible membrane), smear zones on specimens ends, gradient, length-to-diameter ratio, duration of testing, high effective stresses at outflow end, and degree of saturation. In addition, if used over long durations the constant head method experiences variations in measurement due to variations in hydraulic gradient, effective stress, particle migration, differential consolidation, diffusion through the membrane, and changes in water chemistry (Evans and Fang, 1988). These variables were described thoroughly by Evans and Fang (1988) and summarised in **Table 2.8**.

Table 2.8: Long-term triaxial permeability testing variables, after Evans and Fang (1988)

Variable	Typical Cause	Potential Errors	Potential Solutions
Gradient	Typically high (100 +) to achieve adequate pore volume displacement in a reasonable testing period	•Does not represent field conditions •May cause migration of fines	Conduct replicate tests at "low" gradients to determine hydraulic conductivity and "high" gradients to determine compatibility
Effective stress	High enough to maintain positive effective stress at influent end of the sample	•May cause differential consolidation •May not represent field stress conditions •May result in hydraulic conductivity measurments lower than actual	•See above
Particle migration/reorientation	Induced by high gradients	•May result in hydraulic conductivity measurments lower than actual	•See above •Perform grain size distribution analysis after testing to check for migration
Differential consolidation	See above	•Reduced cross-sectional flow area; impeding flow	•See above •Use shorter samples
Maintaining saturation	Consolidation and back pressure typically applied using compressed air; tests may run for weeks causing air in solusion	•Steady decrease in hydraulic conductivity observed due to entrappted air	•Refresh permeant frequently •Eliminate air-permeant interface •Other equipment moifications
Influent/equilibrium	Volatilisation of organics from influent	•Permeant chemstry may not represent field conditions	•Refresh permeant frequently •Eliminate air-permeant interface •Other equipment moifications
Diffusion through membrane	Molecular diffusion of under containments through membrane chemical diffusion gradient	•See above	•Eliminate diffusion gradient by using contaminated cell water •Use alternative membrane systems •Use silicone oil as cell fluid
Biologic activity	Biologic growth due to long-term nature of tests	•May cause decrease in flow rate due to biologic plugging	•Use biocides
Type of "water"	Distilled water, tap water, 0.01N $CaSO_4$, 0.005N $CaSO_4$, 1.0 g/L $MgSO_4$ are all 'standard" water	•Water may alter hydraulic conductivity due to pore fluid-soil interactions	•Avoid distilled water •Use original pore fluid where possible •0.01N $CaSO_4$ or 0.005N $CaSO_4$ impact
Low gradients	Used to simulate field conditions	•Not practical for compatibility testing •Equipment precision may be inadequate	•Procedures and equipment needs are different for short-term, low-gradient testing than for long-term, high-gradient compatibility testing

2.7.2.1 EFFECT OF HYDRAULIC GRADIENT ON MEASUREMENT OF HYDRAULIC CONDUCTIVITY

The effect of hydraulic gradient in the long-term testing on a soil bentonite (SB) material is shown in **Figure 2.22**, and short-term testing on clayey material is shown in **Figure 2.23**. Establishment of a hydraulic gradient (in hydraulic conductivity measurements) results in an effective stress gradient across the specimen, causing it to undergo consolidation (Lentz et al., 1985), hence having an influence on the derived value for the hydraulic conductivity.

Figure 2.22 illustrates that as the hydraulic gradient increased (from 75 to 750), the hydraulic conductivity of SB specimens decreased (up to one order of magnitude) due to increase in effective stress and the resulting specimen consolidation (Evans and Fang, 1988). **Figure 2.23** shows that the hydraulic conductivity of clay specimens was less sensitive to the increase of hydraulic gradient under short-term testing whenever the specimen size was larger than 73 mm diameter and 53.3 mm length; whereas for smaller sizes, it decreased by around 30% as the gradient increased from 50 to 300.

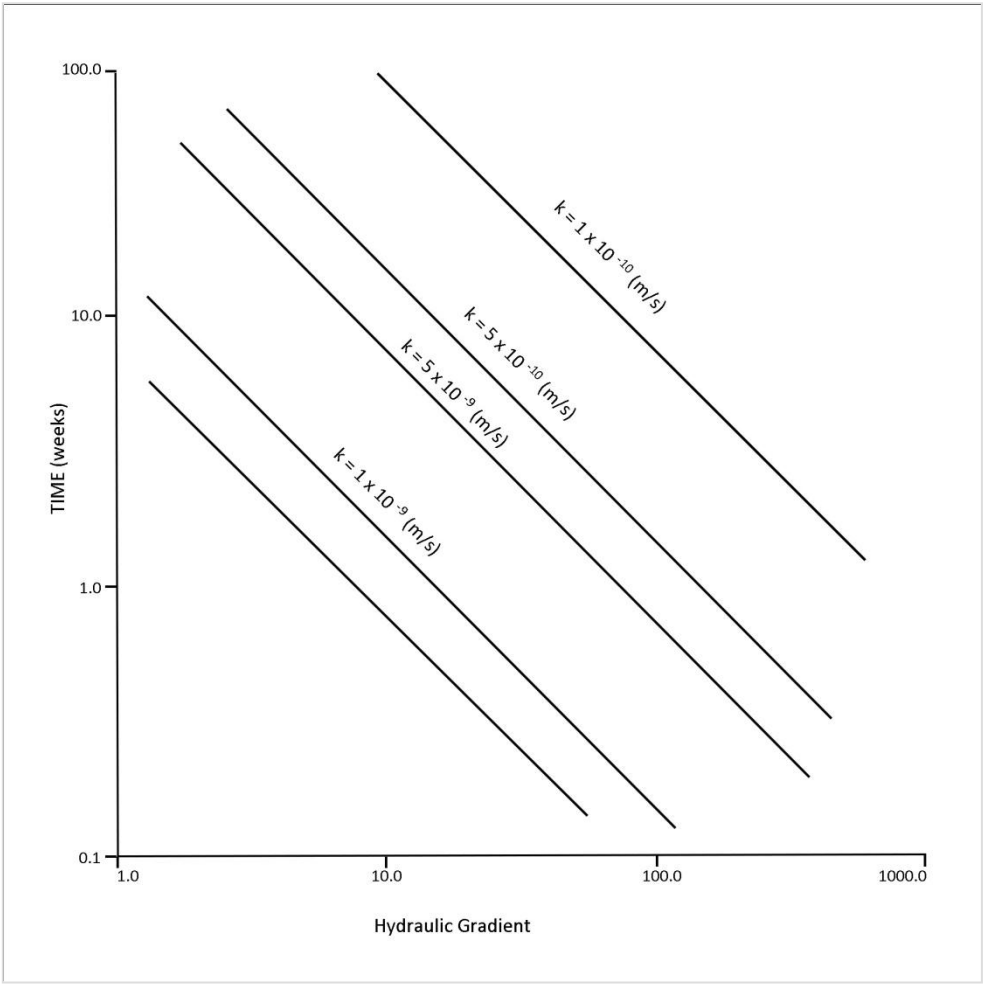

Figure 2.22: Effect of hydraulic gradient on the hydraulic conductivity of SB specimens and the testing duration, after Evans and Fang (1988). The SB specimens comprised of; 7% bentonite, and medium to fine sand (5% medium sand, 93% fine sand, and less than 2% silt).

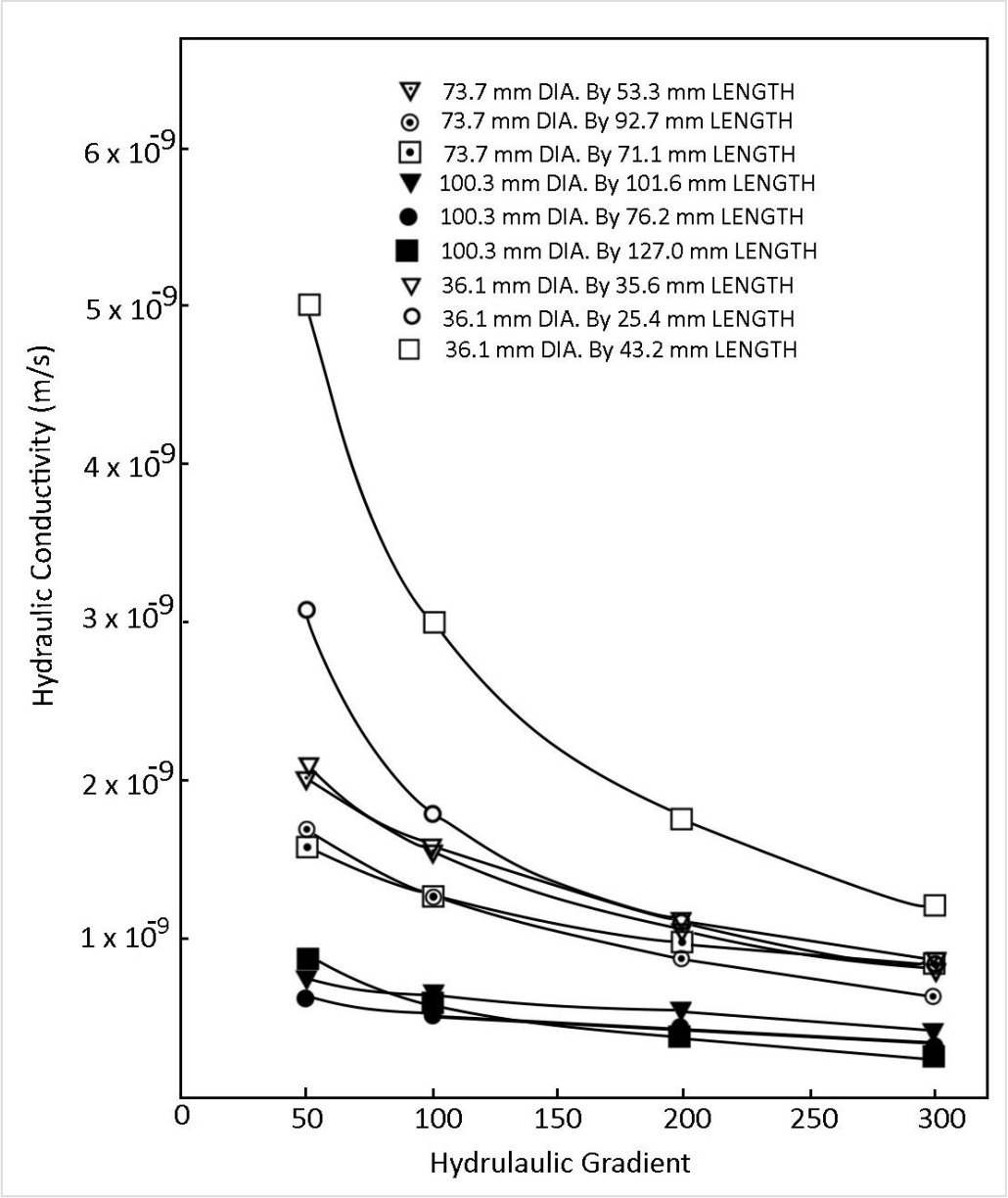

Figure 2.23: Effect of hydraulic gradient and specimen size on the hydraulic conductivity of reconstituted clayey material comprised of; 55 to 65% smectite, 10 to 20% illite, 10 to 20% kaolinite, 5 to 15% quartz, and less than 0.001% heavy minerals (after Carpenter and Stephenson, 1986).

Evans and Fang (1988) agreed with Olsen et al. (1985) that low hydraulic gradients are impractical and unreliable for long-term testing (i.e. through constant head method). Evans and Fang (1988) stated that, although high gradients are not representative of those encountered in the field; a minimum gradient of 200 is required to measure a hydraulic conductivity of 1 x 10^{-10} m/s in one month through

long-term testing. In naturally occurring groundwater systems hydraulic gradients are generally one or less (Dunn and Mitchell, 1984). Higher gradients often exist across seepage blankets or compacted soil liners, but they are unlikely to exceed 10 or 20 in most cases (Dunn and Mitchell, 1984). However, in the laboratory conventional hydraulic conductivity testing methods gradients of 150 to 200 or more are not at all unusual for reasons of speed and economy (Dunn and Mitchell, 1984). High hydraulic gradients have been reported to increase hydraulic conductivity in some cases and to decrease it in others (Olson and Daniel, 1981). Particle migration or erosion of specimen material particularly of low density might be experienced under high gradients producing hydraulic conductivity values lower than expected (Dunn and Mitchell, 1984; Lentz et al., 1985; Evans and Fang, 1988). Dunn and Mitchell (1984) suggested that gradient values as close as to those expected to occur in the field should be used, and in the same time should allow the completion of measurement with in a tolerable time. Furthermore, Tavenas et al. (1983) confirmed that Darcy's law in natural clays is valid when subjected to hydraulic gradients of 0.1 to 50.

2.7.2.2 EFFECT OF EFFECTIVE CONFINING PRESSURE ON MEASUREMENT OF HYDRAULIC CONDUCTIVITY

The hydraulic conductivity of soils also depends significantly on the void ratio of the soil and the effective stress experienced by the soil. A decrease in the void ratio results in an increase in the effective stress and hence a decrease in the hydraulic conductivity. The effect of consolidation effective stress applied in the oedometer or consolidation cells on the hydraulic conductivity (i.e. indirect measurement) is well presented in literature.

Anderson et al. (1985) stated that testing in in flexible-wall cells under high effective confining pressure may reduce the hydraulic conductivity of soft slurry wall backfills. The effect of effective confining pressure on triaxial hydraulic conductivity testing was studied by Carpenter and Stephenson (1986) as illustrated in **Figure 2.24**. The hydraulic conductivity was found to be sensitive to the consolidation effective stress particularly for smaller specimens (71.1 mm diameter or less); as it decreased from 2 x 10^{-9} m/s at effective stress of around 15 kPa to 7.5 x 10^{-10} m/s at an effective stress of around 130 kPa (**Figure 2.25**). Similar findings were presented by Olsen et al. (1991) as shown in **Figure 2.25**. Olsen et al. (1991) evaluated the hydraulic conductivity of sandstone (**Figure 2.25a**) and shale (**Figure 2.25b**) at different effective stress representing their stress history using triaxial constant flow method. The sandstone specimens had a diameter of 50.08 mm and thickness of 25.5, and the shale specimens had a diameter of 100.16 mm and thickness of 25.4 mm. **Figure 2.25a** indicates that the highest hydraulic conductivity for the sandstone specimen which was in the order of 10^{-7} m/s was achieved at the lowest effective stress of 70 kPa. Olsen et al. (1991) stated that this value was relatively higher than expected for sandstone, and might be due to sampling disturbance or undetected fissures. Furthermore, the shale specimens showed similar pattern of decreasing hydraulic conductivity with increasing effective stress; however, the values of hydraulic conductivity were generally lower that the values for sandstone specimens by three to four orders of magnitude (**Figure 2.25b**).

Grube (1992) advised that stress applied during hydraulic conductivity testing should not exceed the overburden stress expected near the top of the barrier wall.

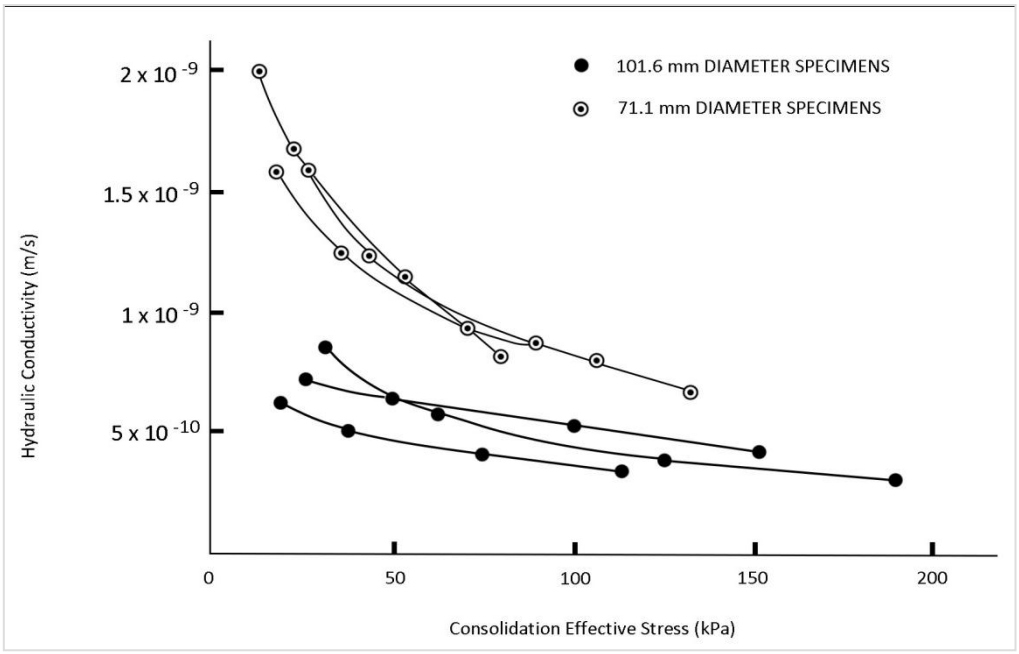

Figure 2.24: Effect of consolidation effective stress on the hydraulic conductivity of reconstituted clayey specimens, after Carpenter and Stephenson (1986)

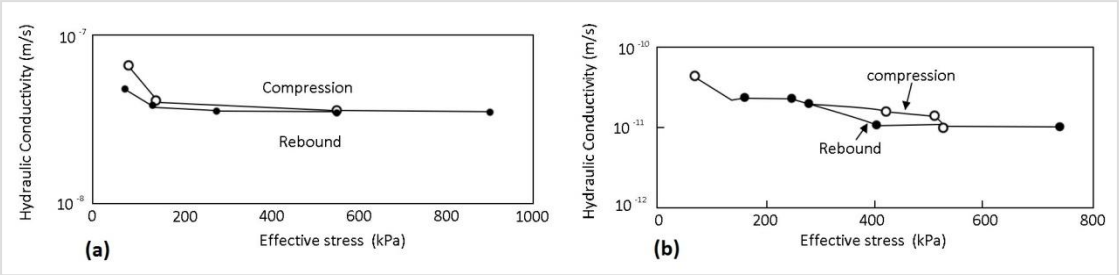

Figure 2.25: Hydraulic conductivity measurements at varying effective stresses (a) Sandstone specimens, (b) Shale specimens (after Olsen et al., 1991)

2.7.3 COMPARISON BETWEEN TRIAXIAL CONSTANT FLOW AND CONVENTIONAL CONSTANT HEAD METHODS FOR MEASURING LOW HYDRAULIC CONDUCTIVITIES IN THE LABORATORY

The constant flow method has several advantages that make it more preferable than the conventional constant head method particularly for testing materials of low hydraulic conductivities. One of the major advantages is that small flow rates can be generated at substantially smaller hydraulic gradients to be more suitable for fine grained materials of very low hydraulic conductivities (Olsen et al., 1985; Olsen et al., 1988; Aiban and Znidarcic, 1989; Olsen et al., 1991). The time required to carry out a

hydraulic conductivity test is controlled by the response time to achieve the steady state flow condition. This time is much shorter for a flow pump test than that required for conventional constant head and falling head tests (Olsen et al., 1991). In addition, because the response time is governed by the consolidation process, it varies with the square of the drainage path and therefore can be shortened substantially by reducing the height of a specimen (Olsen et al., 1991). When large hydraulic gradients are externally imposed or induced across compressible specimens in stress controlled triaxial cells, seepage induced volume changes can be of sufficient magnitude to cause substantial errors in hydraulic conductivity measurements (Olsen et al., 1991). Pane et al. (1983) summarised the advantage of the constant flow method for minimising this error as follows: "In using conventional tests one is faced with a paradox. The use of high gradients reduces the time of testing but introduces substantial errors in the test results. However, the use of low gradients extends the testing time to unacceptable limits. The flow pump test (constant flow method) solves both these problems".

Opdyke and Evans (2005) measured the UCS of CB specimens using falling head triaxial hydraulic conductivity tests and compared it to the UCS of fresh specimens (i.e. not subjected to permeation) at 28 days. The results showed higher UCS values for permeated specimens than fresh specimens; indicating the considerable effect of consolidation observed in the permeated specimens (permeated for quite long time that was 4 days to 7 days). This agrees with the conclusions of Pane et al. (1983) and Olsen et al. (1991). This indicates that any test used to measure the hydraulic conductivity of CB must be sufficiently rapid to minimise the consolidating processes (and hence underestimate the hydraulic conductivity of the material). The flow pump technique has recently been successfully used in laboratory measurements of CB

hydraulic conductivity; this is seen in recent laboratory studies of Philip (2001) and Joshi et al. (2010) as reviewed in more detail **Section 2.6** and is far quicker than a falling head test. A brief comparison between the constant flow (flow pump) method and the conventional constant head method is carried out in **Table 2.9.**

Table 2.9: Comparison of constant flow method with conventional constant head method

Property	Constant Head Method	Influence (shortage)	Constant flow Method (flow-pump test)	Influence(advantage)
Applicable Materials to be tested	Fine and coarse grained materials, but mostly suitable for coarse grain materials (Aiban and Znidarcic ,1989)	-	Fine and coarse grained materials, but mostly effective for fine grain materials (Aiban and Znidarcic ,1989)	-
Applicable Flow rates	To be known at the end of measurement; when steady state (SS) condition arrives	Prolong permeation time required to achieve the flow rate at SS especially for fine grained materials	Very low flow rates as low as 0.001 ml/min and higher could be applied by precise electronic pumps	Measures the permeability of fine grained materials in relatively short period
Hydraulic gradient	Constant throughout the test, but start to decay after prolong application of hydraulic difference across the specimen (Aiban and Znidarcic ,1989)	Drainage into the back pressure system as response time to SS increases particularly in case of testing low permeability materials. Hence, resulting in seepage induced consolidation; outflow is higher than inflow, and SS condition is not clearly confirmed (Aiban and Znidarcic ,1989)	Gradually increases across the specimen until SS condition arrives, and it become constant at SS condition	Arrival of SS condition is confidently confirmed; the permeability can be estimated during the beginning of the test as the outflow would nearly equal the inflow (from the pump), and the hydraulic gradient becomes constant as soon as SS condition is achieved
Measurement time	Long particularly in case of fine grained materials (in order of weeks to months (Evans and Fang, 1988), if low hydraulic gradients are applied	Risk of algae and bacterial growth within the membrane and triaxial system pipelines. Potential fabric change and fine particles migration in case high hydraulic gradients are applied to speed up the testing period	Relatively short (in order of minutes to few days)	Avoidance of fabric change and bacteria growth risks

2.7.4 EVALUATION OF MEASUREMENTS METHODS OF LOW HYDRAULIC CONDUCTIVITIES BY AIBAN AND ZNIDARCIC (1989)

Both constant head and flow pump tests are expected to give similar results; because they impose near identical conditions on the specimen (Aiban and Znidarcic, 1989). Therefore, those methods were compared experimentally to justify their impact on hydraulic conductivity results.

Table 2.10 compares hydraulic conductivity results from flow pump tests with constant head tests using Specwhite clay (kaolinite) specimens. The kaolinite specimens were prepared at a moisture content of 133%, and consolidated one-

dimensionally under an axial stress of about 100 kPa. Hydraulic conductivity tests were then conducted in the triaxial cell after achieving an initial isotopic effective pressure of 30 kPa. The coefficient of hydraulic conductivity (k) was obtained at; varying effective confining pressures (higher than 30 kPa) corresponding to varying void ratios, and different pressure difference (p) across the test specimens corresponding to variable hydraulic gradients (i) as shown in **Table 2.10**.

Table 2.10: Hydraulic conductivity results on kaolinite, after Aiban and Znidarcic (1989).
* All values corresponded to steady state flow condition

Void Ratio (e)	Flow pump test *					Constant head test *				
	k (m/s)		*Δk from average (%)*	i	p (kPa)	*k* (m/s)		*Δk from average (%)*	i	p (kPa)
	Inflow x 10^{-9}	Outflow x 10^{-9}				Inflow x 10^{-9}	Outflow x 10^{-9}			
1.63	2.3	2.9	23.08	11.5	8.8	2.8	2.8	0	8.4	6.4
1.63	2.4	2.8	15.38	12	9.2	2.8	2.8	0	10.4	7.9
1.52	1.7	2.5	38.10	14.1	10.6	2	2	0	10	7.5
1.52	1.7	2.3	30.00	7.1	5.8	-	-	-	-	-
1.39	1.5	1.6	6.45	11	8.2	1.6	1.6	0	10.9	8.1
1.32	1	1.6	46.15	11.6	8.5	1.2	1.4	15.38	11.8	8.7
1.27	0.93	1.3	33.18	14.3	10.4	1	1	0	12.6	9.2
1.22	0.83	1.2	36.45	6.4	4.6	-	-	-	-	-
1.22	0.93	1	7.25	17.9	13	-	-	-	-	-
1.19	0.73	1	31.21	6.9	5	0.87	0.87	0	13.1	9.4
1.19	0.85	0.96	12.15	19.9	14.3	-	-	-	-	-

The gradients were varied in flow pump tests through applying different outflow rates as the pump was set in withdraw mode to produce downwards flow direction from top to bottom of the test specimen. Whereas, the variable pressure difference were directly applied to the specimen to impose a constant gradient during each constant head test.

In the flow pump tests, Aiban and Znidarcic (1989) advised that the first flow rate to be applied by the pump should the smallest possible, and then gradually increased until achieving a measurable (or required) pressure difference. In addition, the steady state flow condition is confirmed when the inflow rate is approximately equal to the

applied outflow rate and both rates are nearly constant Aiban and Znidarcic (1989) as illustrated in **Figure 2.26**.

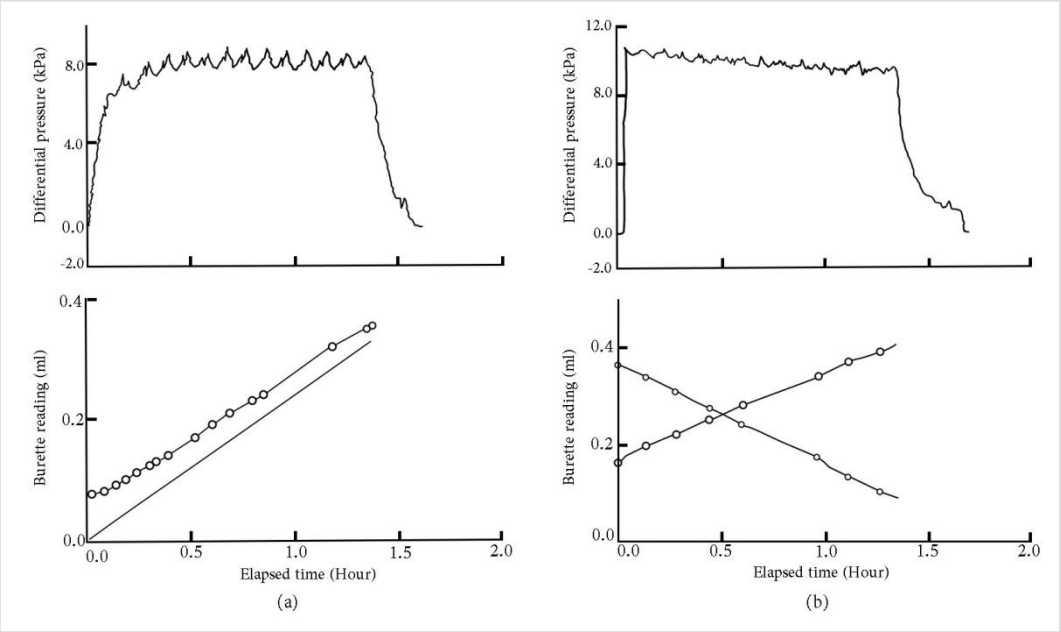

Figure 2.26: Hydraulic conductivity results on kaolinite in triaxial cell using: (a) flow pump method, (b) constant head method (after Aiban and Znidarcic, 1989)

Figure 2.26 shows an example of results using a hydraulic gradient of 11 in the flow pump test and a hydraulic gradient of 12.6 in the constant head test, where specimen thickness was 76 mm. In case of flow pump method, as soon as pumping with selected outflow rate was initiated, the pressure difference across the specimen increased gradually across the specimen and apparently stabilised after around 0.7 hours. This difference then dropped instantly once the pumping was stopped at the end of the measurement after confirmation of the steady state condition (**Figure 2.26a**). Similar observations were seen in the case of constant head method as soon as the desired pressure difference was applied (**Figure 2.26b**).

Small cyclic pressure variations were seen in the differential pressure readings (**Figure 2.26**) using both methods; this was caused by the operation of the air pressure regulator that controlled the back pressure (Aiban and Znidarcic, 1989). Aiban and Znidarcic (1989) stated that for the flow pump results, ideally the inflow and outflow (pump) rates should be identical at steady state condition; however a noticeable difference between them existed, and resulted in a difference between the inflow and outflow k values (**Table 2.10** and **Figure 2.26a**). This difference should be considered insignificant as long as it is within the same order of magnitude of the hydraulic conductivity accuracy (i.e. the pumping flow rate). Aiban and Znidarcic (1989) advised that this accuracy is evaluated through the applied outflow (pump) rate (considered in further detail in the Methodology Chapter: **Section 3.5.2.3)**.

Such difference between the inflow and outflow hydraulic conductivity values did not occur using the constant head method (**Table 2.10** and **Figure 2.26b**). However, the outflow rates were consistently higher than the inflow rates, indicating that the volume of the specimen decreased during the flow pump test (Aiban and Znidarcic, 1989). This justified the findings and conclusions of: Pane et al. (1983), Olsen et al. (1991), and Opdyke and Evans (2005). It was concluded that seepage induced consolidation was taking place (Aiban and Znidarcic, 1989). Differences between the inflow and outflow (pump) rates and seepage induced consolidation were not seen in the results when high gradients were applied (100 or more) or less compressible materials such as silt was tested as presented by Aiban and Znidarcic (1989) (not presented herein). Aiban and Znidarcic (1989) suggested that the seepage induced consolidation might be reduced if shorter specimens with smaller gradients are to be tested.

Through the constant head method, the inflow and outflow rates had similar slopes towards the end of the constant head test, although the differential pressure across the specimen continuously reduced during the test as shown in **Figure 2.26b**. This was due to the reducing water level in the inflow burette and corresponding increase of water level in the outflow burette; thus this head variation caused the flow rates to change continuously throughout the test and steady state flow could not be confirmed (Aiban and Znidarcic, 1989).

2.8 SUMMARY

This chapter summarises the chemical reactions happening in the CB material upon curing and the structure forming upon hardening. Furthermore, this chapter refers to a published review paper (**Appendix A**), which summarises the variable CB deformation behaviour and compares it with the behaviour of other cemented materials as a part of this research. This paper emphases the need of understanding the CB deformation and cracking behaviour, which plays great role in achieving the required performance criteria.

In addition, this chapter summarises the key findings of the previous published research on the CB specimens containing GGBS under undrained triaxial deformation. The undrained peak strength at curing ages less than 90 days was found to increase with increasing age of curing and increasing effective confining pressure. However, this strength was generally constant and independent of the change of effective confining pressure after 90 days of curing. The CB specimens exhibited brittle strain-softening behaviour under undrained deformation regardless of the curing age and effective stress achieved. This behaviour seemed to be controlled by the pore water pressure. However, the published literature did not provide any data on

the pore water pressure changes yielding failure in the middle of the CB specimens or at the initial cracking points. The failure modes under undrained deformation varied from tensile failure (when the effective stresses were less than 200 kPa) and shear failure (when the effective stresses exceeded 400 kPa). The literature reviewed in this chapter has justified that the undrained deformation behaviour is critical throughout the whole service life of the CBB regardless of the effective stress achieved. Furthermore, this literature review has justified that the application of effective confining pressure before undrained shearing is unnecessary for achieving the aim of this thesis (as followed in the developed testing methodology that is explained in **Chapter 3**).

The results of testing the hydraulic conductivity of the CB specimens using different methods and their variation have been reviewed. The previous results that were determined using the flexible-wall triaxial cell have been compared with the results determined in this thesis in **Chapter 6**. The need of investigating the impact of the undrained shearing on the CB hydraulic conductivity in the triaxial cell was suggested by; Gill and Christopher (1985), Graham et al. (2012) and Xiao et al. (2015). This suggestion is ideally the aim of this PhD thesis, as no work appears to have been published on this subject at the time of writing the thesis. Hence, the outcomes of this thesis will contribute to knowledge through identifying the unknown relationship between the undrained deformation and the CB hydraulic conductivity.

Two hydraulic conductivity testing methods using the flexible-wall triaxial cell are reviewed and compared, which are the constant head and the constant flow. The effects of the hydraulic gradient and effective confining pressure on the measurement

of low hydraulic conductivities are reviewed. This aided in designing the testing methodology for this thesis as explained in **Chapter 3**.

CHAPTER 3
METHODOLOGY

LABORATORY INVESTIGATION OF HYDRAULIC CONDUCTIVITY AND DEFORMATION OF CEMENT-BENTONITE (CB) SPECIMENS

3.1 INTRODUCTION

This chapter details the development of the methodology required to investigate the changing hydraulic conductivity of the Cement-Bentonite (CB) under undrained strain. The methodology was developed to: (1) determine the undrained stress-strain behaviour of CB specimens containing GGBS at varying curing ages, and (2) measure the hydraulic conductivity of CB and assess its variation after TXUU shearing (i.e. the worst case scenario of loading as CB is likely to be weakest during this kind of deformation as reviewed in **Chapter 2**.

Trial tests have been used to investigate and establish procedures of hydraulic conductivity measurement using the flexible-wall triaxial cell. From this the bespoke testing method was established and is detailed in this Chapter. Once a suitable methodology was developed the main programme of work was undertaken (see Chapter 4, 5 and 6).

3.2 SPECIMEN PREPARATION

As part of the research presented in this thesis, test specimens were cured for up to 90 days. Unfortunately, specimens casted in 2014 up to 2015 were found to be contaminated with biological film on their surface. The source of contamination was found to be the purified water that was used for preparing and curing the specimens. Therefore, another water source was subsequently used to cast specimens. The affected specimens were disposed of, as they were considered inappropriate to be used for the main testing.

3.2.1 MIXTURE COMPOSITION

As discussed in Chapter 2 increasingly cement replacements, such as GGBS, have been used in CB slurries (see **Table 3.1**). This was seen in much of the previous work of CB testing as reviewed in **Chapter 2**. For this reason and in conjunction with the performance criteria set out in the ICE specification (see ICE 1999), the final mix design shown in **Table 3.2** was selected. Data sheets of the bentonite, cement and GGBS used in this study are shown in **Appendix B**.

Table 3.1: Mixture composition in previous studies on CB material

Previous Study	Bentonite- Water Slurry Content	Cementatious Material Content
Barker et al. (1997)	3% bentonite and 83% water	3% Ordinary Portland cement and 11% GGBS (80% cement-replacement)
Manassero et al. (1995)	4% bentonite and 76.8% water	19.2% blast furnace cement containing 60% GGBS
Philip (2001)	3.5% bentonite and 80% water	13% Ordinary Portland cement with 79% GGBS cement-replacement
Opdyke & Evans (2005)	5% bentonite and 95% water	15% cement with 75% GGBS replacement
Williams & Ghatoara (2011)	3% bentonite and 83.5% water	13.5% cement with 80% GGBS cement-replacement
Joshi (2009) and Soga et al. (2013)	3.4% bentonite and 84% water	2.5% Ordinary Portland cement and 10.1% GGBS (80.1% cement-replacement)
Royal et al. (2017) and the Current Study	4% bentonite and 76% water	4% cement containing Fly Ash and 16% GGBS (80% cement-replacement)

Table 3.2: CB mixture composition used in this study

Ingredient	Mass (g)	Percentage by total mass (%)
Water	2000	76
Bentonite	80	4
Cement (CEM II / B-V 32,5 N)	80	4 (20% by mass of cementitious material)
GGBS	320	16 (80% by mass of cementitious material)

It should be noted that as part of the selection of the mix design shown in **Table 3.2**, the achievement of higher strength and corresponding strain at failure due to cement-replacement with GGBS that coincides with the achievement of the lower hydraulic conductivities was taken account of. This is seen at around 70% to 90% replacement percentages, with the 80% replacement being the optimum content.

However, the variation in GGBS percentage by weight of cementitious material from 70% to 90% results in variation of texture of the CB material noticed during preparation of the specimens. At 90% GGBS cement replacement specimens are noticed to be much softer than at 80% even after 7 days of curing in the moulds, and no colour changes are detected since casting (i.e. grey did not turned to dark green). A similar observation is noticed at 70% GGBS cement replacement. Hence, the overall assessment of selecting 80% GGBS cement replacement for testing in this research is justified as it falls in range of lowest and constant hydraulic conductivity achieved, whilst producing specimens sufficiently robust to be taken out of the moulds to cure after 7 days of hardening.

Thus, the ideal cementitious material content was considered to be 20% (by weight) with GGBS cement-replacement of 80%. It should be noted that whilst PFA has been used as an alternative cement replacement material, it does not provide the marked hydraulic conductivity reduction and strength enhancement of high slag replacement

levels (Jefferis, 2012) – see Royal et al. (2013) and Alzayani et al. (2016) for further details.

Curing ages were selected to be as follows: 7 days, 14 days, 28 days, and 90 days. These ages were chosen as they describe the early changes in CB physical properties with curing and they are commonly used in recent research on CB material (Williams and Ghataora, 2011; Joshi et al., 2010; and Soga et al., 2013); hence providing a means to compare findings from this study with the outcomes of others.

3.2.2 SPECIMEN SIZE

The size of specimen was 50 mm in diameter as this was the minimum diameter available for pipes used for casting. The length of the specimen was 100 mm resulting in a length to diameter ratio of 2:1. This was selected as it is the minimum ratio required for both shear strength tests and permeability tests using triaxial methods (Evans and Fang, 1988). In addition, this corresponds with the sizes used in previous research (see Royal (2006), Ghataora and Williams (2011, and Royal et al. (2013, and 2017)).

3.2.3 PROCEDURE OF SPECIMEN PREPARATION

Specimens were prepared based on the procedure recommended by Gravin and Hayles (1999) and as followed by Royal et al. (2013, and 2017). The procedure is described as follows:

The first stage required the creation of bentonite slurry to ensure full hydration of bentonite powder used to form specimens. This was achieved by first mixing bentonite with 40 grams per litre of ultra-pure water for 45 minutes. This ensured no lumps formed in the final mix. Ultra-pure water (conductivity 0.1 µs/cm and total

organic carbon (TOC) < 5 parts per billion (ppb)) was used to avoid risk of bacterial growth during curing of the subsequently form CB specimens. Moreover, this provided batch control so ensuring the minimal variations between different batches produced. After mixing, the slurry was left a further 24 hours in sealed containers to ensure sufficient time for hydration to complete (see Gravin and Hayles, 1999).

Cement (40 grams per litre water) and GGBS (160 grams per litre water) were then added to the hydrated bentonite-water slurry and mixed for not more than 5 minutes to avoid interrupting the initial setting of the cementitious materials.

CB slurry mix was then poured in plastic moulds (50 mm internal diameter and 150 mm length). Immediately after pouring the mix, and before sealing top of the moulds, vibration was allowed for no more that 2 minutes to release any air bubbles within the mix, and avoid disturbing the initial setting of the cementitious materials. Thick plastic cover and O-rings were used to seal the top and bottom sides of the moulds.

Specimens were left to cure in the moulds for 7 days in a vertical position, then were carefully extruded and cured in the ultra-pure water in a constant temperature room of 7 ^{o}C for the different curing ages prior testing. The constant room temperature was assigned by laboratory technicians based on requests of researchers using the same room; the temperature was not too far from the expected ground temperature up to 15 m depth in the UK that ranges from 8 ^{o}C to 11 ^{o}C (BGS, 2017).

3.2.4 CUTTING EDGES OF SPECIMENS PRIOR TESTING

To form test specimens, a split mould of 50 mm diameter and 100 mm length and a wooden base support were used to hold each specimen tightly in position prior to trimming. A sharp wire saw was then used to cut away the excess length of the

hardened CB specimens, by carefully removing a small amount of material at a time. The final trimming was then completed using a sharp palette knife, this helps to minimise the effects of smear, as recommended by Olsen and Daniel (1981) and Head and Epps (2014). Following Jefferis (2012), if edges were broken off by the trimming process then the trimming was continued until a full flat face was achieved.

3.3 BASIC MATERIAL CHARACTERISTICS OF HARDENED CB SPECIMENS

The basic material characteristics of the hardened CB specimens prepared in this study (**Table 3.2**) are shown in **Table 3.3**. These were determined through; measurements of water content and size of CB specimens, and phase relationships (see Head, 2006).

Table 3.3: Basic material characteristics of hardened CB specimens in this study

Range of Bulk Density (g/cm^3)	**1.1 - 1.2**
Typical Particle Density	**2.69**
Range of Water Contents (%)	**320 - 450**
Range of Void Ratios	**9.0 - 12.0**

The bulk density varied from 1.1 g/cm^3 to 1.2 g/cm^3. The water contents were very high as expected for a fully hydrated material as CB, thus verified the fully saturation nature of the CB specimens to be tested. The water contents varied from 320% to 450%.

Furthermore, the CB material particle density and void ratio were calculated using phase relationships assuming that the specimens were fully saturated. The typical or average particle density was 2.69, this falls in the typical range of particle density of clays and many British soils that is from 2.68 to 2.72 (Head, 2006). The range of void

ratios was determined from phase relationships as well, and found to be very high indicating that the fabric of the CB material is porous. These ranged from 9.0 to 12.0.

Therefore, the hardened CB mixture used in this study had porous and fully saturated microstructure or fabric. In addition, they had slight variation in the material properties (**Table 3.3**) as being made from slurry.

3.4 CONCEPT OF THE LABORATORY TESTING METHODOLOGY

Alzayani et al. (2016) highlights that compressive deformation of rocks can results in microcracking and crack formation tends to initiate prior reaching the peak strength (**Appendix A**). The hypothesis of this thesis is that CB may also experience microcracking during deformation and if is the case it may result in an increase in hydraulic conductivity before the material reaches the peak strength. Such an increase in hydraulic conductivity could compromise the performance of a barrier in the field, even if the loading conditions were not expected to result in structural failure. Undrained conditions are deemed most susceptible to this possible failure mechanism (Alzayani et al., 2016) due to the brittle response with strain softening-post peak (**Section 2.4**).

In order to achieve the aim and objectives of this thesis (**Section 1.3**), the testing methodology should combine techniques of hydraulic conductivity measurement with TXUU shearing. The hydraulic conductivity should ideally be obtained before and after a certain period of TXUU shearing; with the peak deviator stress and the corresponding strain being the reference of analysing the effect of cracking on the hydraulic conductivity. The methodology must confirm whether the hydraulic conductivity changes with deformation before or after the peak deviator stress of the

hardened CB material under undrained shearing and the magnitude of these changes in hydraulic conductivity.

The final testing methodology took approximately 15 months of laboratory study to be established in accepted confidence. Many trials were conducted to combine the hydraulic conductivity testing with TXUU shearing. Two approaches for hydraulic conductivity testing were considered in the trails: constant head and constant flow methods (discussed in **Section 2.7**). Furthermore, two approaches to apply TXUU displacements before hydraulic conductivity testing were examined: multi-stage and single-stage shearing methods.

For clarity, the methodology is not presented as per the chronological order of the development process. It is discussed based on the two major testing variables, which are the deformation under varying TXUU displacements and the corresponding hydraulic conductivity. The term cell pressure (CP) is used in this thesis and it is same as the total minor principal stress (σ_3) used in literature (**Section 2.4**).

3.5 MEASUREMENT OF HYDRAULIC CONDUCTIVITY

The water used as a permeation fluid in all hydraulic conductivity tests was ordinary tap-water. This was de-aired through a vacuum pump to eliminate air bubbles as much as possible.

The flow direction across the test specimens was chosen to be upwards (i.e. from the bottom to top of the specimen and against the gravity). The volume change unit corresponding to the top back pressure (TBP) measured the upwards flow that was from the specimen into the TBP system. Whereas, the volume change unit corresponding to the bottom back pressure (BBP) measured the upwards flow from

the BBP system into the specimen (in constant head tests, and the pump applied the upwards flow from the bottom specimen using diffusion mode in the flow pump tests).

The saturation check prior hydraulic conductivity measurement was conducted through measuring the B-value that should be minimum 0.96. In this study, the saturated nature of CB slurry material and the curing in full hydration with water, resulted in a B-value of 1; thus saturation procedures were not required and hydraulic conductivity measurement was directly conducted.

Furthermore, in order to avoid errors in the measurement of specimen volume changes or the pore pressure changes representative of a fully saturated soil, the pore water measurement system, including drain lines, was required (Baldi et al., 1988). Therefore, it was very crucial to check that the triaxial apparatus is; free of leaks, and fully saturated and flushed using de-aired water prior every test. Also, it was important to avoid formation of trapped air bubbles during specimen installation; between membrane and specimen, and between the membrane and porous stones and top platen.

3.5.1 CONSTANT HEAD METHOD IN TRIAXIAL CELL

3.5.1.1 APPARATUS

This test was conducted in the triaxial apparatus that includes two back pressure systems to apply constant pressure heads at the top and base of the specimen to produce a flow through the specimen. The coefficient of hydraulic conductivity (k) was thus obtained through measuring the volume of water passing across the specimen in a known time under the constant hydraulic gradient applied as explained in **Section 2.7**.

The configuration of the triaxial cell is illustrated in **Figure 3.1,** and the triaxial apparatus used in this study is shown in **Figure 3.2**.

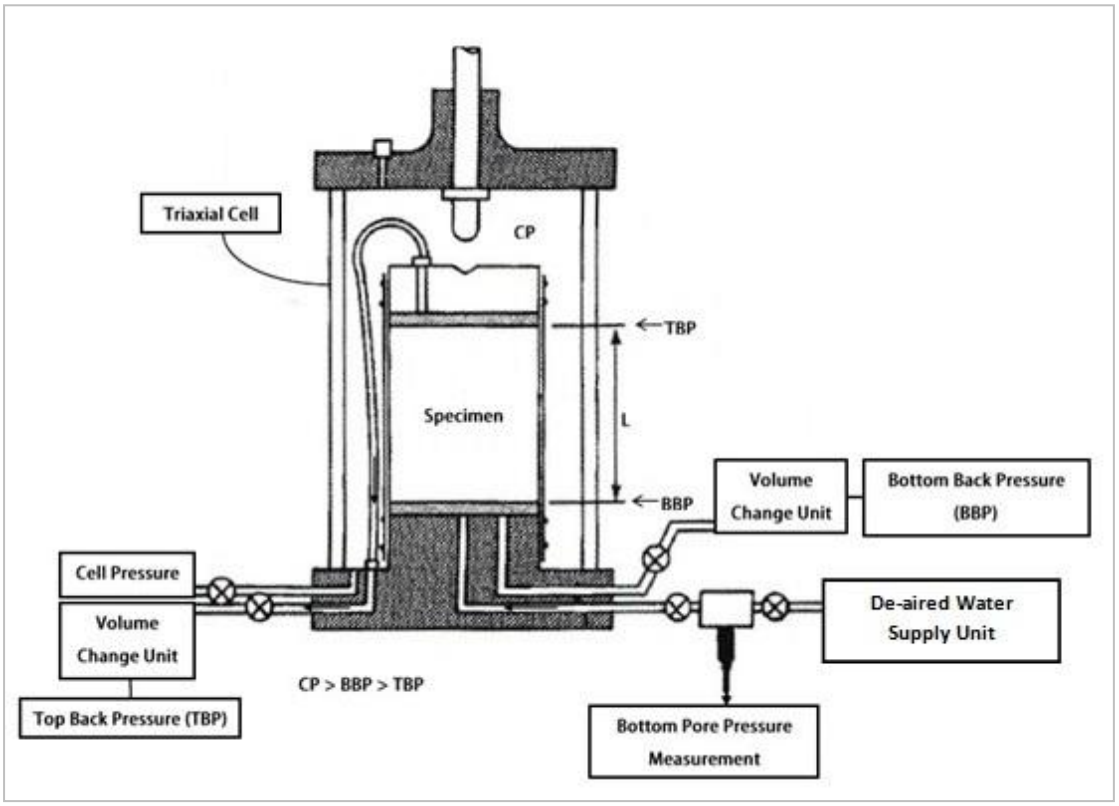

Figure 3.1: Triaxial cell configuration for hydraulic conductivity tests using constant head method with two back pressure systems in this study

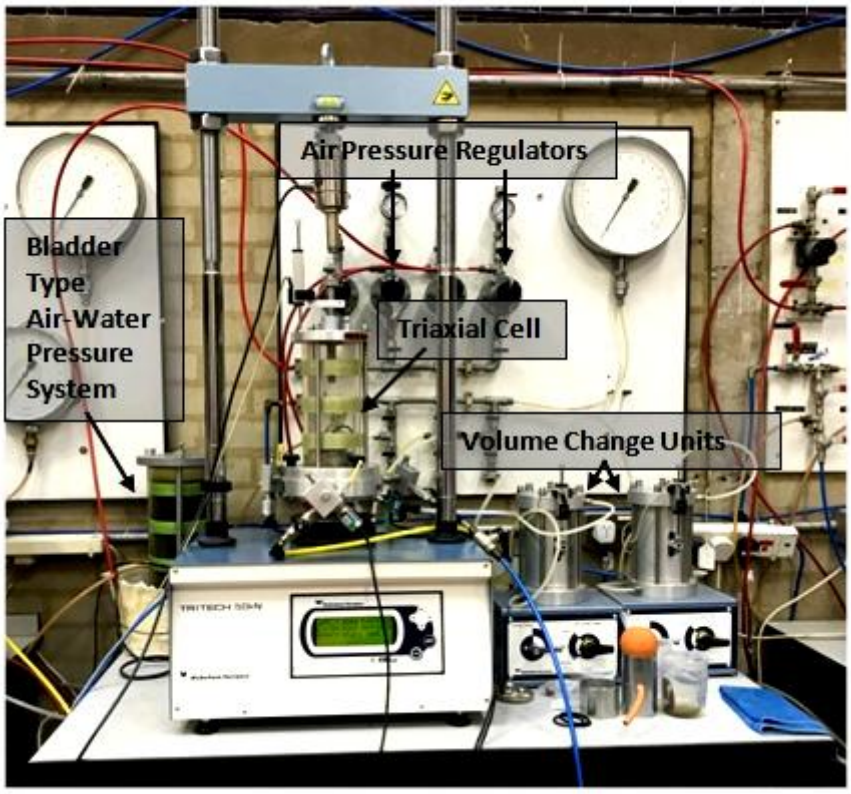

Figure 3.2: Triaxial apparatus for hydraulic conductivity tests using constant head method with two back pressure systems in this study

The CB specimens available to test were cured for 1.5 years during the preliminary practice and training on triaxial hydraulic conductivity using constant head method. This curing age was chosen as these specimens were then rejected by the time of the main testing (as they were contaminated as noted before).

3.5.1.2 PROCEDURE AND TEST CONDITIONS

The procedure of this method is covered in Clause 6 of BS 1377: Part 6: 1990, although the latter includes the use of a differential manometer with a mercury reservoir (Head and Epps, 2014). Due to the EU restrictions on the sale and transport of mercury and equipment containing mercury, a differential pressure gauge or transducer typically used as a replacement in the UK (Head and Epps, 2014).

The necessary conditions of the constant head hydraulic conductivity testing were specified as follows:

1. **The Cell and back pressures at which hydraulic conductivity was to be measured**

   The CP values were ranging from 300 kPa to 400 kPa. These values of CP must be higher than the back pressures applied across the specimen to avoid the preferred flow between the specimen and the rubber membrane. The lowest back pressure to be applied is 300 kPa (Head and Epps, 2014) as this is the minimum required to eliminate any air in the system. Therefore, the BBP should be higher than the TBP as the hydraulic head difference needs to be added to it to produce the upward direction flow across the specimen.

2. **The hydraulic gradient**

   As stated before (**Section 2.7.2.1**), low hydraulic gradients are impractical and unreliable for long term testing (Evans and Fang, 1988; Olsen et al., 1985). Therefore, for this study hydraulic gradients in the range of 25 to 30 were used. The constant hydraulic gradient applied in the trials of the constant head tests was 27, which was equivalent to 2.754 m or 27 kPa constant pressure difference. This value of hydraulic gradient was slightly lower than the maximum value (i.e. 30) recommended in ASTM D 5084 for soils having permeability less than 10^{-9} m/s (Head and Epps, 2014). A similar value was used by Opdyke and Evans (2005) that was 25.

3. **The Effective stress at which hydraulic conductivity was to be measured**

   Consolidation was not conducted before hydraulic conductivity measurement

due to the objective of analysing the behaviour at the lowest consolidation pressure possible (i.e. undrained condition). The effective stress however, would be variable across the specimen due to application of the constant hydraulic gradient, resulting in differential effective pressures ranging from 8 kPa to 37 kPa. Tevenas et al. (1983) stated that to prevent the preferred flow between the specimen and the rubber membrane, sufficient effective lateral stress must be decided and applied based on the specimen size and properties of the rubber membrane. In the experimental study of Tevenas et al. (1983), constant head tests were carried out on specimens of 50 mm diameter, and the sufficient effective lateral stress was found to be in the order of 25 kPa. Thus, the mean differential effective stress (due to the applied differential back pressures or hydraulic gradient) in the initial method trial tests was similar to the value suggested by Tevenas et al. (1983).

3.5.1.3 CALCULATIONS OF COEFFICIENT OF HYDRAULIC CONDUCTIVITY

The tests data was collected and recorded automatically through the PC data logger software. It collected the following readings:

1. **Testing time:** in terms of days:hours:minutes:seconds, and particularly in minutes in the order of 0.001.
2. **CP**: in terms of kilopascal (kPa) in the order of 0.1.
3. **TBP**: in terms of kPa in the order of 0.1.
4. **Volume change through the TBP system**: in terms of cc (cm^3) or ml in the order of 0.01.
5. **Bottom pore water pressure (BPWP)**: in terms of kPa in the order of 0.1.
6. **BBP**: in terms of kPa in the order of 0.1.

The calculation of the *k* at constant steady state flow condition is illustrated in **Figure 3.3a**. There were two flow rates to be measured: the inflow rate (Q_{In}; i.e. cumulative volume change with time from the bottom of the specimen that has the higher head) through the BBP volume change unit, and the outflow rate (Q_{Out}; i.e. cumulative volume change with time from the top of the specimen that has the lower head) through the TBP volume change unit.

Firstly, the Q_{In} and Q_{Out} are obtained from the slope of the cumulative volume change readings measured with time as follows;

Q_{Out} = |Cumulative volume change| / Time (**3.1**)

Q_{In} = |Cumulative volume change| / Time (**3.2**)

The cumulative flow from the top of the specimen into the TBP system can be graphically illustrated in a sign opposite to the sign of the flow from the BBP into the specimen. In the constant head analysis performed in this thesis, the positive sign convention corresponds to the upwards flow from the specimen into the TBP system as seen in **Figure 3.3b**.

The mean hydraulic gradient (**i**) applied throughout the test was obtained from the following;

i = ((Mean BBP- Mean TBP)) / (Gravity (**g**) x Length of specimen (**L**)) (**3.3**)

Where, the BBP and TBP would experience small cyclic variation besides the CP throughout the test (within 1 kPa) caused by fluctuation in the operation air pressure

regulators (see **Section 3.6**). Hence, the difference between the BBP and TBP was computed using their mean values during the test.

And,

Cross-sectional area of the specimen (**A**)= π (Diameter of specimen (**D**)/2)² (**3.4**)

Therefore,

Inflow or outflow coefficient of hydraulic conductivity ($\boldsymbol{k_{Inflow}}$ or $\boldsymbol{k_{Outflow}}$) =

$\boldsymbol{Q_{(In\ or\ Out)}}$/ (**A i** 60) (**3.5**)

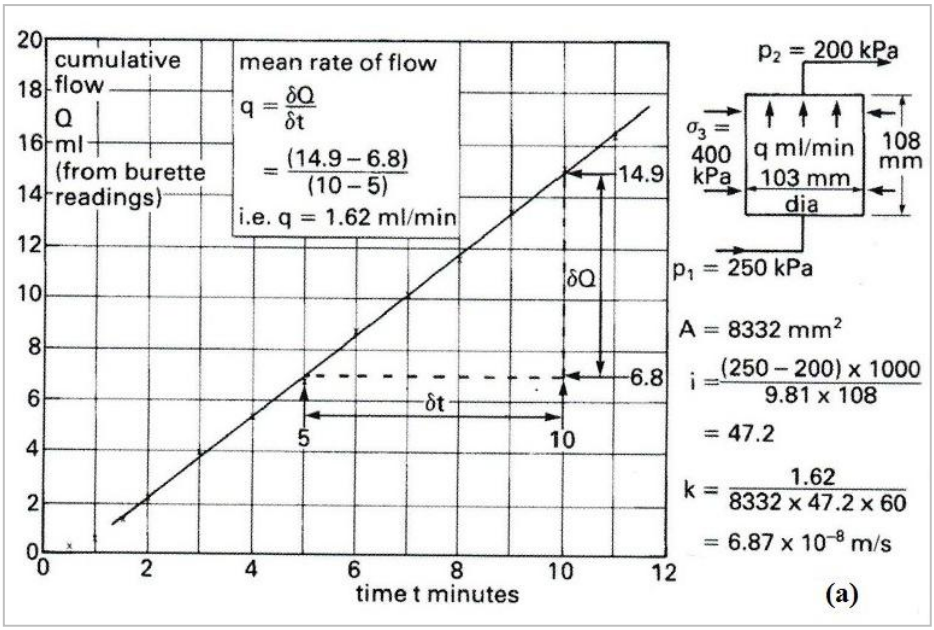

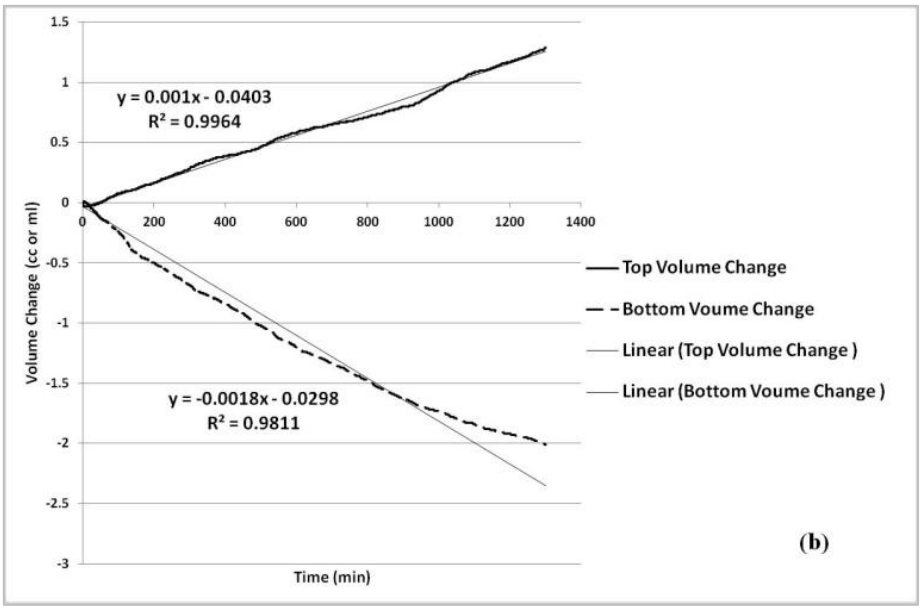

Figure 3.3: (**a**) Example of calculations of flow rate, hydraulic gradient and hydraulic conductivity for triaxial hydraulic conductivity test as graphically described by Head and Epps (2014), (**b**) Example of top and bottom volume change data of a constant head test trial in this study.

3.5.1.4 CONSTANT FLOW APPLICATION WITH CONSTANT HEAD METHOD

The constant head procedure using two back pressure systems took days to complete. In addition, top and bottom volume changes observed correspond to the initial volume loss of the specimen. The initial volume loss was found to be higher through the BBP

than the TBP as shown in the trial test data in **Figure 3.3b**, and this needed to be accounted for. Therefore, an alternative method for measuring the hydraulic conductivity was selected. This used hydraulic controlled pump to substitute the specimen volume loss detected during the standard constant head test with two back pressure systems. A suitable hydraulic controlled pump was available in the civil engineering laboratory at the University of Birmingham that is created by GDS Instruments (A division of Global Digital Systems Ltd). The addition of the GDS hydraulic controller as a pump also resulted in shorting the testing period required to measure the flow through the CB specimen. The added pressure or volume controller is a standard version that was manufactured by GDS in 2006 (**Figure 3.4**). It has a volume capacity of 200 cm^3 and its volume change resolution is 1 mm^3. It provides flow rates as low as 0.001 ml/min operating in infusion or withdrawal modes, and can be controlled by means of its keypad control panel or software programme (that can be set up in a PC server). The properties of the standard GDS controller model are specified in the **Data Sheet 1** in **Appendix C**. Unfortunately, the software files were missing, and GDS technicians were not able to retrieve the software of the model in question. Thus, they suggested operating the controller through its digital keypad, using the **Digital Set up Guide 1** in **Appendix C**. The GDS controller was then connected to the specimen through the available second bottom outlet in the triaxial cell, as the first outlet being connected to the BBP system). Hence, the variation of pore pressures could be tracked through the bottom pressure transducer connected to the triaxial data logging system. In addition, the digital keypad in the GDS controller had a monitoring screen that instantly shows the cumulative volume change (in mm^3) and pressure at the pump outlet (in kPa), which should be equal to the bottom pore water pressure and the BBP transducers measurements.

The apparatus of triaxial constant head tests was updated by the addition of the GDS hydraulic controller as illustrated in **Figures 3.5 and 3.6**. The apparatus configuration is similar to the one in the initial method (**Figure 3.1**); yet the GDS controller was connected to the bottom pore water pressure measurement transducer.

The test conditions specified in the constant head method previously (**Section 3.5.1.2**) was also valid when the GDS pump was added, yet the following update was considered:

- The constant hydraulic gradient of 27 was applied in the updated method similar to the initial method. The volume loss due to application of this gradient was expected to be compensated by the constant inflow rate provided by the GDS hydraulic controller. The flow direction to be produced across the specimen was still going to be upwards; thus the GDS controller was set up to comply with this flow direction (i.e. infusion pump mode into the specimen).
- The adequate constant pumping flow rate was the lowest possible to ensure that it did not affect the outflow from the BBP system (**Figure 3.7**).

Figure 3.4: The standard hydraulic pressure or volume controller by GDS Instruments (GDS Instruments, 2009)

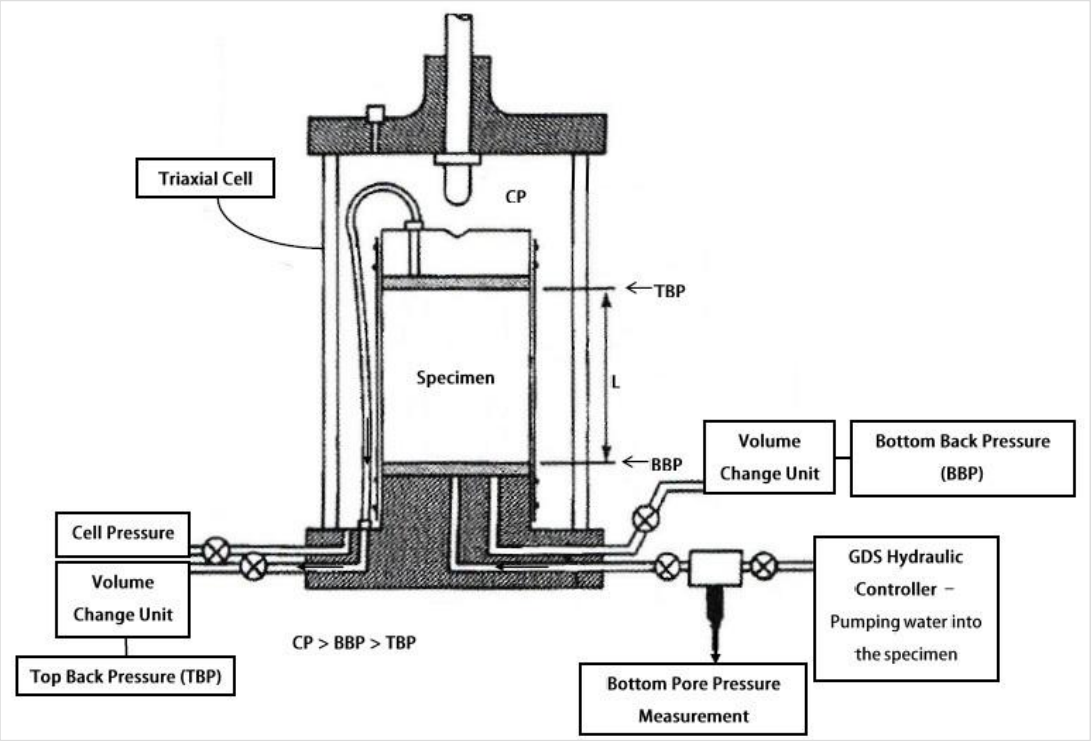

Figure 3.5: Apparatus configuration for hydraulic conductivity measurements with addition of the GDS hydraulic controller

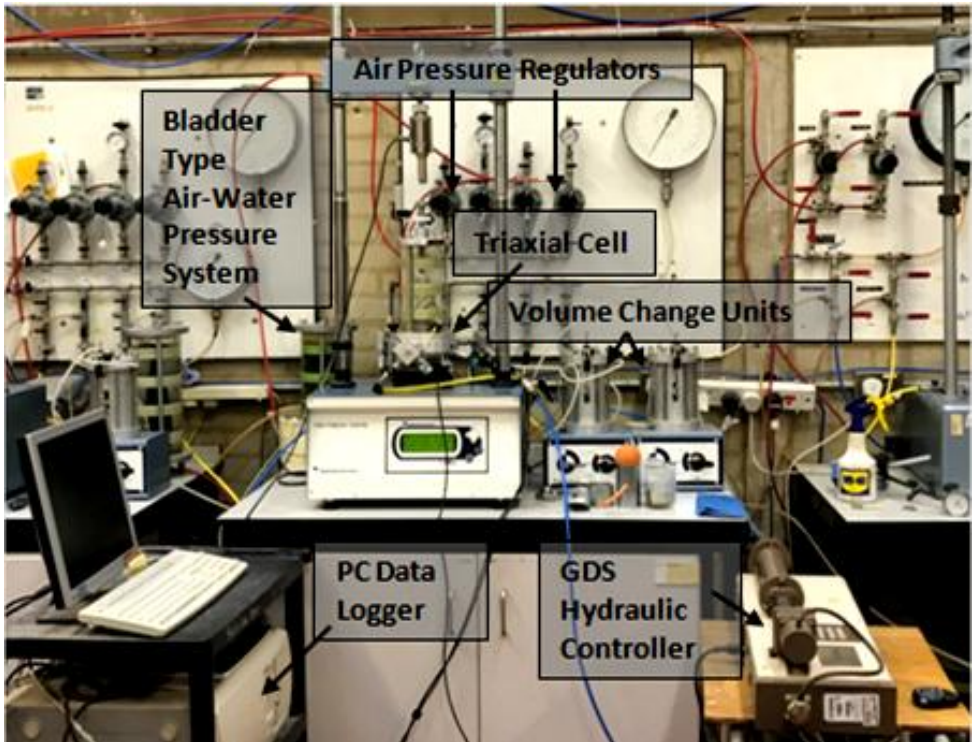

Figure 3.6: Apparatus configuration for hydraulic conductivity measurements with addition of the GDS hydraulic controller in this study

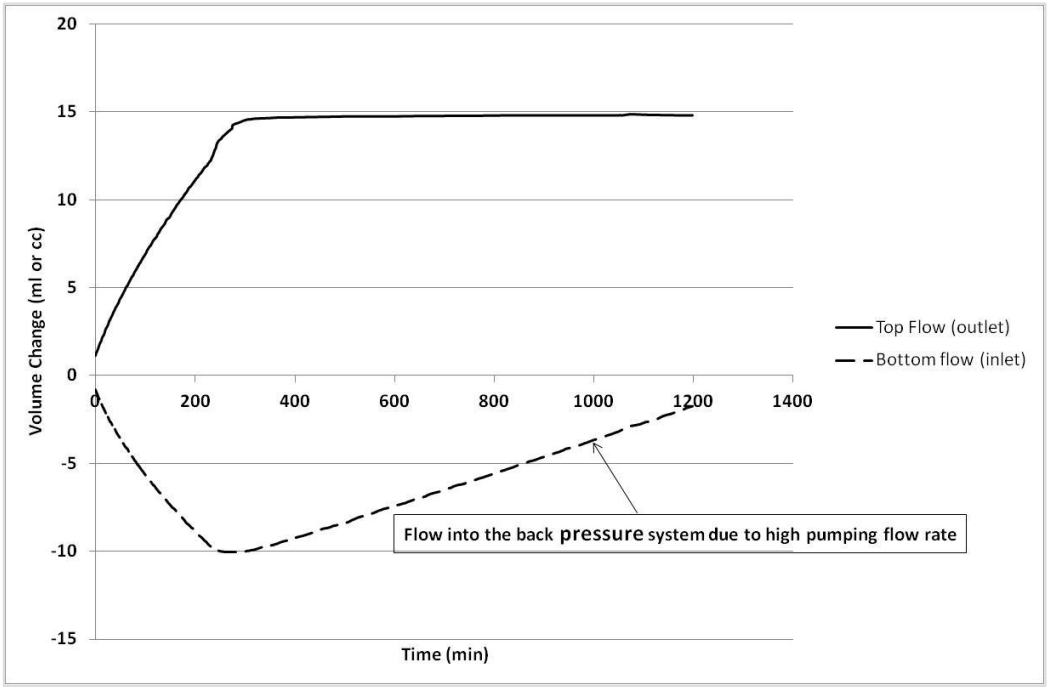

Figure 3.7: Effect of high pumping inflow rate on volume change readings

The calculation of the coefficient of hydraulic conductivity at constant steady state flow condition is explained previously in **Section 3.5.1.3**; however the bottom flow

rate calculation (**Equation 3.2**) should be adjusted to take into account the additional flow rate by the GDS pump. This is to be adjusted as follows;

$$Q_{In} = [|\Delta \text{ cumulative volume change}| / \Delta \text{ time}] + \text{Pumping flow rate} \quad (3.7)$$

Figure 3.8 shows an example of the updated graphical illustration of the flow measurement data, and calculations of the top and bottom coefficients of hydraulic conductivity considering the constant flow rate provided by the GDS pump.

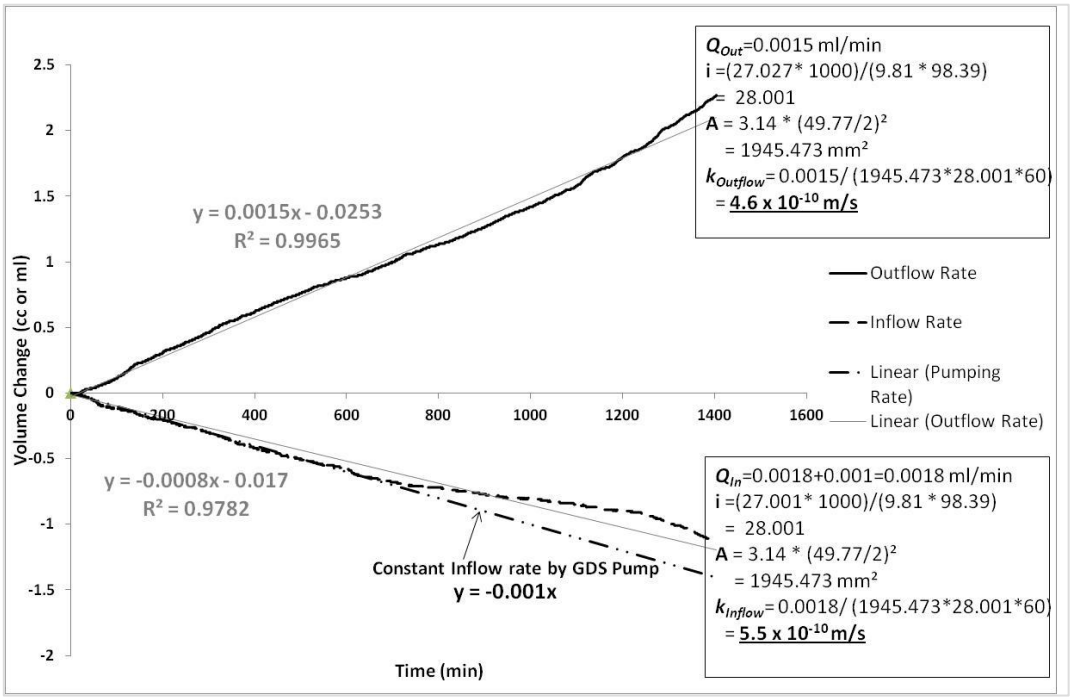

Figure 3.8: Example of flow measurement data and calculations for the second method of triaxial hydraulic conductivity testing

3.5.2 CONSTANT FLOW (FLOW PUMP) METHOD

This method was selected for measuring the hydraulic conductivity of CB specimens in the main testing in this study (as described later in **Section 3.8**) as it has favourable

advantages compared to the conventional constant head method particularly for materials of low hydraulic conductivities like CB, as reviewed in **Section 2.7.3**.

3.5.2.1 APPARATUS

The apparatus used in this method was similar to the one used previously in the constant Flow application with constant head method (**Figures 3.5** and **3.6**); except that the bottom back pressure and its volume change measurement unit were excluded. The required bottom pressure and constant inflow rate were provided by the GDS hydraulic controller (pump), which was connected to a pressure transducer (data recorded by PC data logger). The corresponding test arrangement is illustrated in **Figure 3.9** below.

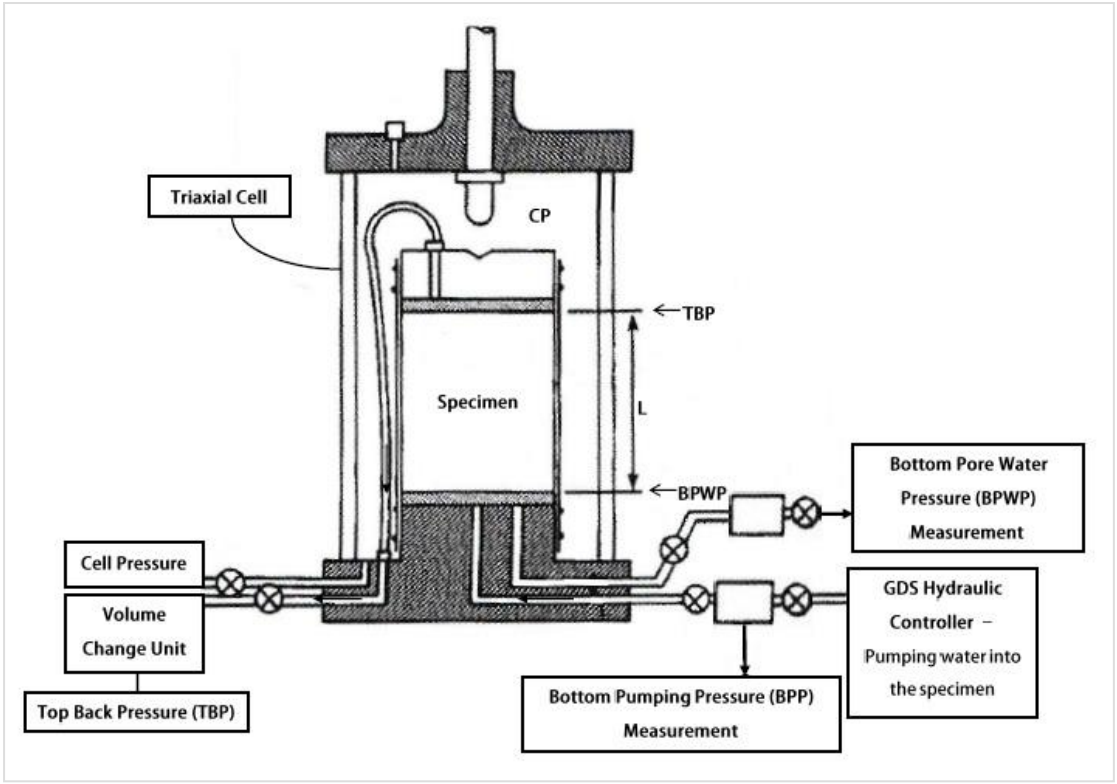

Figure 3.9: Triaxial cell configuration for hydraulic conductivity measurement through the constant flow (flow pump) method

3.5.2.2 PROCEDURE AND TEST CONDITIONS

The flow pump test was conducted through infusing flow into the specimen (by means of the GDS pump connected to the bottom of the specimen as shown in **Figure 3.9**. The infusion of flow through the specimen was more favourable over the withdraw flow test particularly for the aim of this research (i.e. to evaluate the effect of undrained loading on the low hydraulic conductivity of the CB material). This is because; the infusion of flow minimises the potential of consolidation under seepage (i.e. it does not increase the effective stress), and reduces the response time required to achieve constant flow through the specimen compared to the withdraw flow test (Olsen et al., 1988).

The procedure followed and test conditions applied were as follows:

Step 1: Prepare the test specimen

- Record the specimen batch code and curing age.
- Trim the specimen ends flat using: a sharp wire saw, spatula and split mould.
- Use some material from the trimmings to measure the water content.
- Measure the specimen dimensions (average diameter and length).
- Weigh the specimen before testing
- Smear the middle section of the saturated rubber membrane with a thin film of silicone gel while it is fitted in a suction membrane stretcher.

Step 2: Prepare and check the apparatus

- Fill the GDS controller with de-aired water
- Flush the triaxial system with de-aired water (including the pressure transducers and the TBP volume change unit).
- Check that the whole system is free from leaks.

Step 3: Set up the triaxial cell

- Place the test specimen in the triaxial cell carefully between two porous stones and filter papers (saturated with de-aired water). The saturated rubber membrane should be then fitted with two rubber O-rings at each end.

- Assemble the cell with ensuring that the cell piston is at its maximum extent and the cell sealing ring is in position. Ensure that the tie-rods are tightened down evenly and at true vertical alignment with the axis of the load frame (Head and Epps, 2014). Then, lower down the cell piston to be in contact with the ball bearing on the top cap.

- Check that the specimen is in vertical alignment with the axis of the load frame.

- Keep all the valves locked except the CP valve.

- Fill up the cell with de-aired water.

- Inflate the bladder of the TBP air-water pressure system to one third of its capacity through flushing de-aired water from its air bleed. This should provide sufficient space for collecting the outflow from the specimen's top end

- Zero the pressure transducers, displacement transducers, and the load cell which are connected to the PC data logger. Record the zero readings.

Step 4: Apply cell pressure in increments from 50 kPa until reaching 300 kPa

- Record the room temperature at the beginning of the test.

- Pressurise the cell initially by 50 kPa, and record the pore water pressure (PWP) after equalisation.

- Calculate the initial B-value; it should be a minimum of 0.95, thus indicating acceptable saturation.

- Increase the CP to 100 kPa, 200 kPa, then 300 kPa. Record the change in PWP respectively. The CP should be increased quickly after stabilisation of PWP after every increment to avoid any volume loss. Check the final B-value to be minimum 0.95.

- Check that the cell piston is in line with the ball bearing of the top cap, and the load cell does not apply any axial load on the specimen.

Step 5: Apply the TBP to be equal to the top PWP

- Record the top PWP reading after stabilisation under CP of 300 kPa.

- Open the valve to the TBP transducer and lock the valve to cell.

- Adjust the TBP to be equal to the top PWP that is usually 300 kPa indicating a B-value of 1 (full saturation of CB specimens).

- Put the TBP volume change unit in the volume change mode and at the suitable direction that measures flow collected from the specimen. In this method, negative sign convention was selected for the outflow volume collected from the top end of the specimen; this was in upwards direction.

- Open the TBP valve to the cell and start recording volume change readings.

Step 6: Increase the CP by 30 kPa (to be 330 kPa)

- Close the CP valve to the cell.

- Increase the CP to be 330 kPa. This increment is very small similar to the isotropic effective stress value (30 kPa) applied in Aiban and Znidarcic (1989) experiments. It is applied to increase the level of confinement around

the specimen to prevent circumferential flow through the membrane; yet be small enough to maintain undrained loading condition (i.e. very low effective stress). Furthermore, Tavenas et al. (1983) used similar effective lateral stress in the order of 25 kPa to also avoid circumferential preferred flow that might occur between the specimen and the membrane.

- Wait until BPWP is stable (i.e. return to be equal to TBP). This takes no more than 20 minutes for CB specimens at 90 days curing.

Step 7: Set up the GDS controller (pump)

- Close the pump valve to the cell, and adjust the pressure in the pump line to be equal to the BPWP after stabilisation (i.e. equal to the TBP).

- Set up the controller to the lowest pumping rate possible, that is 0.001 ml/min; because the CB specimen is in its intact state and higher rates were found to be producing high pressure difference across the specimen that would lead to inadequate stress and measurement conditions. The GDS pump operates in msec/mm^3, thus the lowest inflow rate to be inputted in the set up is 60,000 msec/mm^3 (corresponding to 0.001 ml/min).

- Start pumping at that rate until the pressure in the line increased sufficiently. This operation takes few minutes.

Step 8: Start pumping and measurement of the outflow from the specimen

- Re-zero the TBP volume change reading once it stabilises. The previous volume change reading indicates the amount of volume change due to application of the low effective confining pressure of 30 kPa. This was found to be negligible (less than 1 ml), and easily offset through the cumulative inflow volume by the pump.

- Open the BPP valve to the cell and start recording the corresponding TBP volume change readings and instantaneous increase in the BPWP (due to build up of pressure difference at the bottom of the specimen until it reaches a constant value).
- Check that the GDS pump operates accurately at the programmed flow rate through monitoring and recording the pump volume change with time manually for at least 10 minutes.

Step 9: Monitor the outflow volume change readings with time

- Continue measurement overnight.
- Record any change happening to the initial room temperature during the whole measurement period.
- Calculate the outflow rate after different periods of pumping from 20 hours to a maximum 2 days, to evaluate the final stable outflow rate.

Step 10: End measurement when steady state flow condition is confirmed

- The steady state flow condition is confirmed through achieving a constant outflow rate from the specimen that is approximately equal to the inflow from the pump under a constant pressure difference across the specimen. The pressure difference or hydraulic gradient and the outflow rate were found to become constant after pumping for at least 1000 minutes in case of testing CB specimens after 90 days of curing.
- Allow sufficient period of flow measurement under the constant hydraulic gradient that is at least one day (to collect constant outflow volume of at least 1 ml) as the inflow rate applied should be very slow to produce equivalent outflow rate from the intact CB specimen.

- Calculate the coefficient of hydraulic conductivity using the measured steady outflow rate and constant hydraulic gradient.

- Stop the flow pump and close the BPP valve to cell as soon as the final value of the hydraulic conductivity is achieved.

- Record the decay of the hydraulic gradient at the bottom of the specimen so that the reference readings of the BPP and BPWP transducers could be checked again (Aiban and Znidarcic, 1989).

- Take the specimen out, remove the rubber membrane gently, then observe and note if any changes happened to it.

- Weigh the specimen to obtain its final water content (after testing) to confirm that no (or negligible) volume loss has happened due to the constant flow test.

3.5.2.3 CALCULATIONS OF COEFFICIENT OF HYDRAULIC CONDUCTIVITY

The test data was collected and recorded automatically through the PC data logger software. It collected the following readings:

1. **Testing time**: in terms of days:hours:minutes:seconds, and particularly in minutes in the order of 0.001.
2. **Cell Pressure (CP)**: in terms of kilopascal (kPa) in the order of 0.1.
3. **Top pore water pressure (TPWP) and/or TBP**: in terms of kPa in the order of 0.1.
4. **Volume change through the TBP system**: in terms of cc (cm^3) or ml in the order of 0.01.
5. **Bottom pore water pressure (BPWP)**: in terms of kPa in the order of 0.1.

6. **Bottom pumping pressure (BPP)**: in terms of kPa in the order of 0.1.
7. **Axial load**: in terms of Newtons (N) in the order of 0.1.
8. **Axial displacement**: measured externally (using an external axial strain gauge), in terms of mm in order 0.001.

The coefficient of hydraulic conductivity under steady state flow condition was determined through simple calculations. This was similar to the calculations explained in **Section 3.5.1.3**; yet the constant inflow rate (from the bottom of the specimen provided by the GDS pump) was always known from the beginning of the measurements and not required to be determined.

First the **outflow rate at any time (through the TBP system)** was determined using **Equation 3.1**. Then, the mean hydraulic gradient (**i**) applied throughout the test was obtained from the following equation:

i = [Mean (BPWP and BPP) - Mean TBP] / [Gravity (**g**) x Mean length of specimen (**L**)] **(3.6)**

Where, the TBP would experience small cyclic variation throughout the test (within 1 kPa) besides the CP due to fluctuation in the operation air pressure regulators. This fluctuation in the controlled pressures affected the pore water pressure that was measured at the bottom of the specimen through the BPWP and BPP transducers (which indicates equal pressure values all the time). Hence, the difference between the bottom pore water pressures and the TBP was computed using their mean values during the test.

The $k_{Outflow}$ was determined using **Equation 3.5** (see page 79). This coefficient of hydraulic conductivity derived from the top volume change data was compared to the k_{Inflow}. The latter was calculated using the constant inflow rate applied by the GDS pump and the achieved hydraulic gradient, and then substituting similarly in **Equation 3.5**. The difference between $k_{Outflow}$ and k_{Inflow} became relatively small when the steady outflow rate under constant hydraulic gradient was achieved. This difference was also caused by the cyclic variation in the CP and TBP air regulators. A similar difference was found in flow pump measurements conducted on kaolinite specimens by Aiban and Znidarcic (1989).

Aiban and Znidarcic (1989) suggested that the difference between the inflow and outflow rates could be evaluated through calculating the accuracy in the hydraulic conductivity for the given specimen size and the imposed gradients. This was determined as follows:

The resolution of the inflow rate = Q_{In} (or the constant pumping rate) **(3.7)**

Therefore,

The accuracy in the hydraulic conductivity = k_{Inflow} **(3.8)**

The difference between the $k_{Outflow}$ and k_{Inflow} was considered to be insignificant, if it was of the same order of magnitude of the accuracy in the hydraulic conductivity.

The calculations were processed using programmed MS Excel spreadsheets that could analyse the cumulative outflow data as shown in **Figure 3.10**.

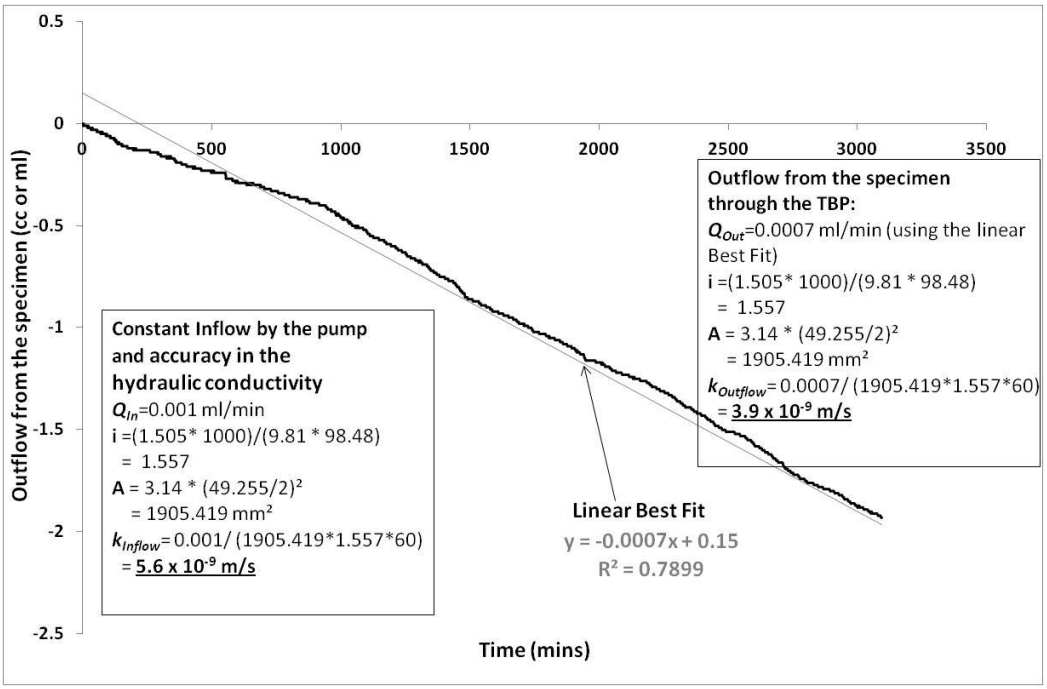

Figure 3.10: Example of the calculations and analysis of the constant flow test in this study

3.6 VARIATION IN THE PERFORMANCE OF PRESSURE REGULATORS DURING HYDRAULIC CONDUCTIVITY TESTING

The hydraulic conductivity was evaluated through the flow rate and mean hydraulic gradient (or mean hydraulic pressure difference that was between the BPP and TBP), that were possible to generate and maintain across the CB specimen under steady state conditions. The flow rates and hydraulic gradients were applied and controlled through the differential back pressure applied across the test specimen (i.e. BPP or BPWP, and TBP), besides the CP. The flow rates and hydraulic gradients were highly sensitive to any variation (fluctuation) in the cell and back pressures that were provided by means of a compressed air system and regulated through air regulators in this study, akin to the study of Aiban and Znidarcic (1989). A negligible amount of variation in the triaxial pressures was encountered, and found to insignificantly affect

the hydraulic conductivity measurements. This could be considered as an experimental error and was evaluated through conducting triaxial constant flow tests using saturated porous stones only (i.e. without test specimens). The Q_{In} values that were applied in those tests were selected based on the ones used in testing CB specimens, which varied from 0.001 ml/min to 0.1 ml/min. The results of those tests are presented in **Table 3.3** and **Figures 3.11** to **3.14**. The applied Q_{In} (using the GDS pump) was always higher than the achieved Q_{Out} (**Table 3.4**), and this agrees with what was experienced in measurements on CB specimens (as discussed later in **Chapters 5** and **6**). The difference between the Q_{In} and Q_{Out} achieved in testing with porous stones was negligible (**Table 3.4**) and similar to the difference occurred when testing CB specimens (**Chapters 5** and **6**). Therefore, these findings appear to verify the experimental error encountered when investigating the CB specimens.

The fluctuation (or hysteresis) in the hydraulic pressure difference from its mean value varied continuously and instantaneously through the complete duration of hydraulic conductivity testing by maximum $\pm$ 0.5 kPa per 0.25 a second (attributed to the performance of the compressed air system), as shown in **Figures 3.11** to **3.13**. Furthermore, the CP also fluctuated continuously and gradually from its mean value by maximum $\pm$ 1 kPa every 25 minutes (again attributed to the performance of the laboratory air compressor/compressed air system), as shown in **Figure 3.14**. The variation in hydraulic conductivity results can be avoided, if such pressure fluctuation is eliminated through using advanced pressure control system that has a constant performance. However, this was not available within the Civil Engineering laboratory in the University of Birmingham and outside the financial capabilities of this project; hence was deemed an experimental error.

Table 3.4: Flow rates measured in triaxial constant flow tests using porous stones only

Q_{In} (ml/min)	Q_{Out} (ml/min)	$Q_{In} - Q_{Out}$ (ml/min)
0.1	0.08	0.02
0.01	0.009	0.001
0.001	0.0007	0.0003

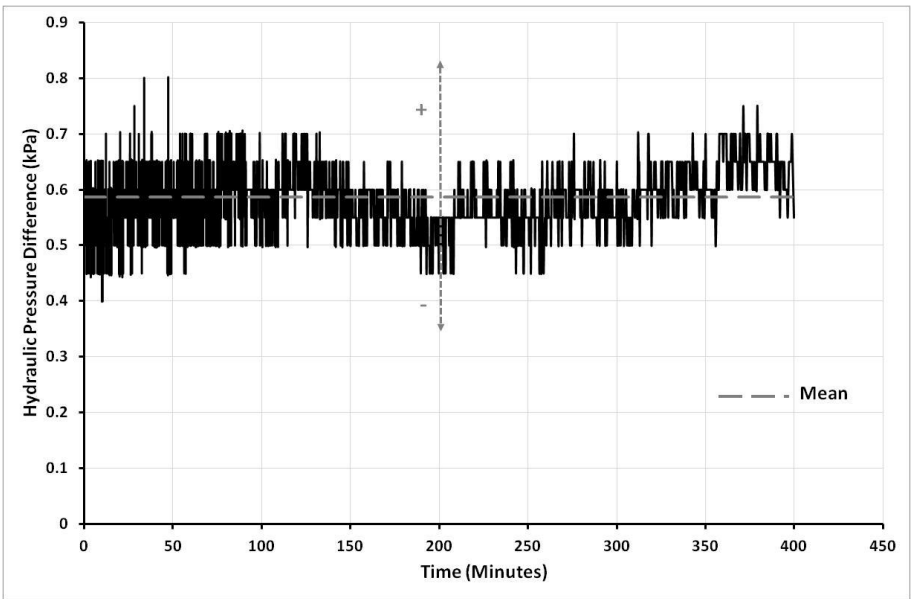

Figure 3.11: Variation of hydraulic pressure difference with time in triaxial constant flow test under Q_{In} of 0.001 ml/min

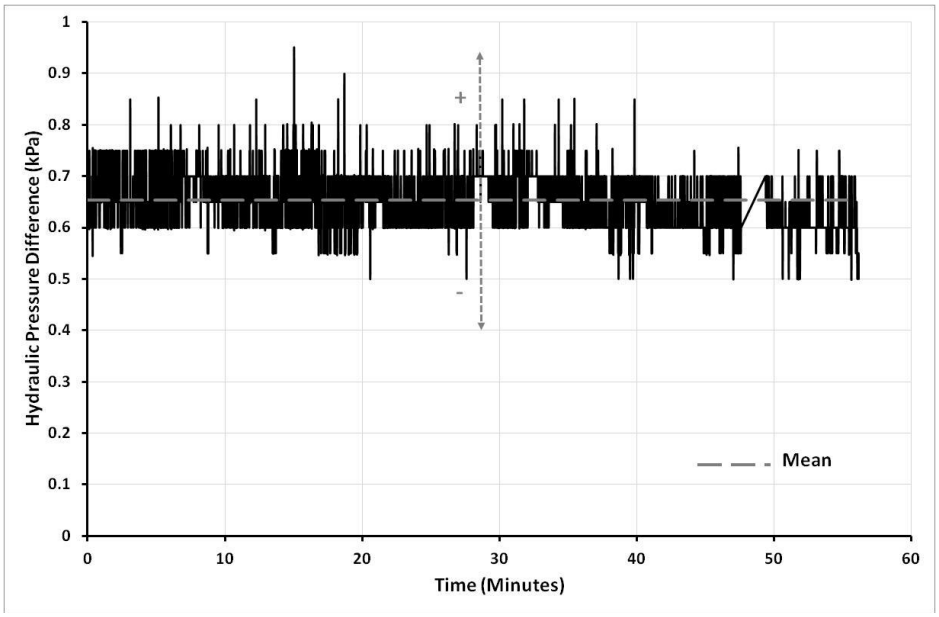

Figure 3.12: Variation of hydraulic pressure difference with time in triaxial constant flow test under Q_{In} of 0.01 ml/min

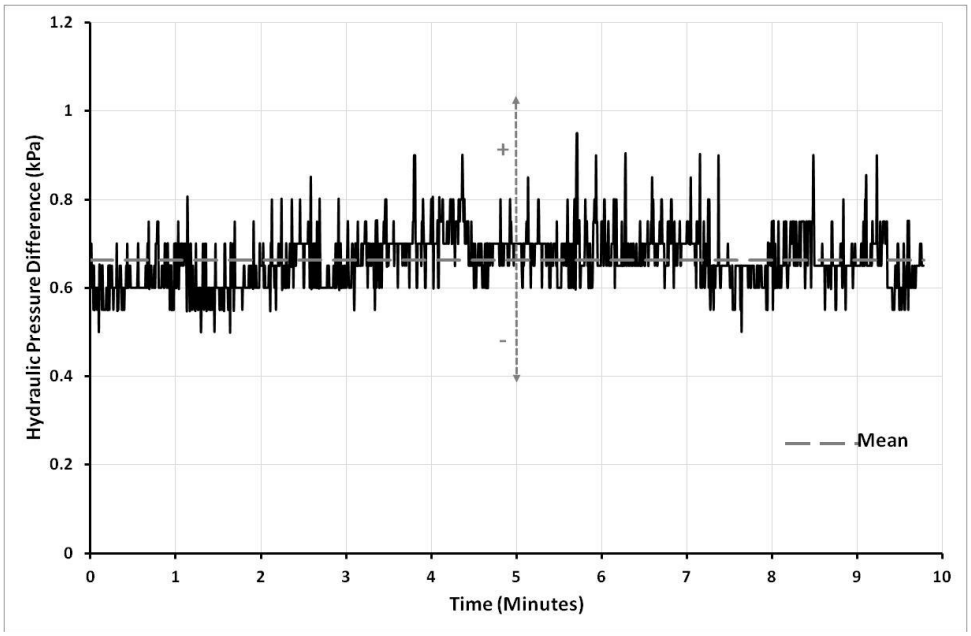

Figure 3.13: Variation of hydraulic pressure difference between with time in triaxial constant flow test under Q_{In} of 0.1 ml/min

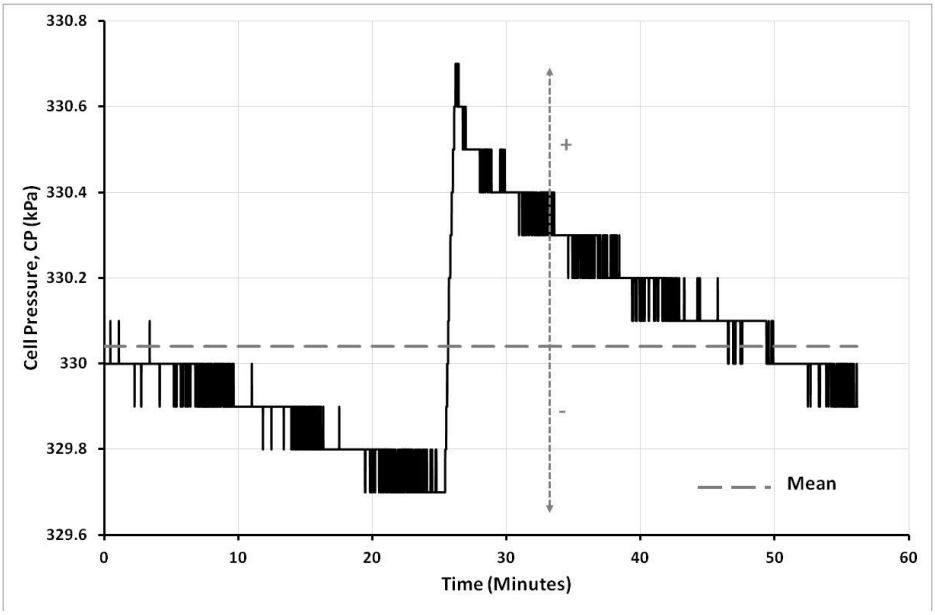

Figure 3.14: Example of variation of the cell pressure with time in triaxial tests

3.7 MULTI-STAGE TXUU SHEARING METHOD WITH HYDRAULIC CONDUCTIVITY TESTING

3.7.1 INTRODUCTION

The first attempt to assess the impact of undrained deformation on the hydraulic conductivity of CB was through the concept of multi-stage shearing triaxial tests. This

method was first investigated with the variable nature of CB material in mind. It involved measuring the hydraulic conductivity prior to deformation, then undertaking a small deformation before re-measuring the hydraulic conductivity. These cycles were repeated until the strain achieved significantly exceeded the strain corresponding to the peak strength (i.e. peak deviator stress). For the purpose of this chapter, this method is termed the 'multi-stage' method.

The idea of this procedure was to combine stages of quick undrained shearing, with hydraulic conductivity measurement stages following the method discussed in **Section 3.5.1** (i.e. measurement with two back pressure systems and the GDS controller).

The procedure was developed following the concept of multi-stage triaxial testing (BS 1377: Part 7:1990:9). The shearing stages were carried out at approximately 0.3% strain (i.e. 0.3 mm axial displacement) intervals throughout the complete stress-strain curve of a CB specimen during a TXUU test. After each shearing stage the hydraulic conductivity was measured.

The following sections explain the procedure of the developed multi-stage testing method, summary of its results, and its shortcomings.

3.7.2 PROCEDURE

The procedure of multi-stage testing is summed as follows:

1. Application of the initial test pressures that were; CP of 350 kPa, BBP of 300 kPa and TBP of 273 kPa (i.e. hydraulic gradient of 27). These pressures were kept for 24 hours to ensure that minimal effects of the initial volume change due to the application of the back pressures were not interfering with the initial

hydraulic conductivity measurement. Therefore, the top and bottom volume changes should be recorded during this step.

2. Measurement of initial hydraulic conductivity of the specimen for a permeation period that was not more than 24 hours, following the method described in **Section 3.5.1**.

3. The valves of the back pressures and the GDS pump to the specimen were closed, and the pore water pressures were checked to be stable across the specimen.

4. Undrained shearing at 0.1 mm/min up to around 0.3 mm axial displacement.

5. Monitoring of the pore water pressures after shearing until they stabilised. Pressures were considered stable whenever they were not changing as fast as 5 kPa per hour as suggested by Head and Epps (2014).

6. Checking if the back pressures (BBP and TBP) should be increased to accommodate the increase of specimen's pore pressures after the undrained shearing stage. This was required to avoid any volume loss that might happen if the initial lower back pressures were to be applied. Accordingly the CP should be increased if required to ensure that it was higher than the back pressures.

7. Measurement of the hydraulic conductivity post shearing, again for a permeation period that was not more than 24 hours, following the method described in **Section 3.5.1**.

8. Repeat the previous steps (from 1 to 6) until failure of the test specimen.

The multi-stage test conditions were as follows:

- **Initial test pressures**

  CP = 350 kPa

  BBP = 300 kPa

  TBP = 273 kPa

  i = 27

- **Test pressures post undrained shearing stages**

  The pressures varied according to the variation of pore water pressure developing after every shearing stage. The minimum pressure difference between the BBP and the CP was 10 kPa, and the hydraulic gradient was always kept 27.

- **Pumping rate**

  0.001 ml/min (through all hydraulic conductivity measurement stages)

- **Duration of a hydraulic conductivity measurement stage**

  24 hours

- **Undrained shearing axial strain rate and displacement interval**

  0.1 mm/min strain rate every 0.3 mm axial displacement (i.e. 0.3% strain)

3.7.3 SUMMARY OF OUTCOMES

Calculations of the hydraulic conductivity after each shearing stage were done as per explained in **Sections 3.5.1.3** and **3.5.1.4**. The multi-stage triaxial test procedure was practiced through one trial test on a CB specimen at 19 months curing age, and comprised of 11 stages of hydraulic conductivity measurement. This trial test lasted

for 12 days. A summary of the test conditions and the mean coefficient of hydraulic conductivity at every measurement stage are shown in **Table 3.5**.

The stress-strain curve obtained from 10 undrained shearing stages on a CB specimen at 19 months of curing using displacement rate of 0.1 mm/min is shown in **Figure 3.15**.

Table 3.5: Triaxial multi-stage test conditions and results of hydraulic conductivity measurements on a CB specimen at 19 months curing age

No. of Testing Stage	Time	Testing Stage	$k_{Outflow}$ (m/s)
0	24 hours	CP = 350 kPa, BBP = 300 kPa, TBP = 273 kPa	4.3×10^{-10}
1	24 hours ≈ 3 minutes	CP = 350 kPa, BBP = 300 kPa, TBP = 273 kPa TXUU up to 0.3% strain and deviator stress of 301 kPa	4.3×10^{-10}
2	24 hours ≈ 3 minutes	CP = 350 kPa, BBP = 327 kPa, TBP = 300 kPa TXUU up to 0.77% strain and deviator stress of 798 kPa	4.0×10^{-10}
3	24 hours ≈ 3 minutes	CP = 350 kPa, BBP = 333 kPa, TBP = 323 kPa TXUU up to 1.15% strain and deviator stress of 1084 kPa	4.4×10^{-10}
4	24 hours ≈ 3 minutes	CP = 360 kPa, BBP = 350 kPa, TBP = 323 kPa TXUU up to 1.33% strain and deviator stress of 1340 kPa	6.8×10^{-10}
5	24 hours ≈ 3 minutes	CP = 360 kPa, BBP = 355 kPa, TBP = 328 kPa TXUU up to 1.5% strain and deviator stress of 1616 kPa	5.0×10^{-10}
6	24 hours ≈ 3 minutes	CP = 360 kPa, BBP = 355 kPa, TBP = 328 kPa TXUU up to 1.74% strain and deviator stress of 2048 kPa	7.4×10^{-10}
7	24 hours ≈ 3 minutes	CP = 360 kPa, BBP = 355 kPa, TBP = 328 kPa TXUU up to 2.01% strain and deviator stress of 2564 kPa	7.7×10^{-10}
8	24 hours ≈ 3 minutes	CP = 360 kPa, BBP = 355 kPa, TBP = 328 kPa TXUU up to 2.23% strain and deviator stress of 3058 kPa	7.6×10^{-10}
9	24 hours ≈ 3 minutes	CP = 360 kPa, BBP = 355 kPa, TBP = 328 kPa TXUU up to 2.5% strain and deviator stress of 3795 kPa	1.0×10^{-9}
10	24 hours ≈ 3 minutes	CP = 360 kPa, BBP = 355 kPa, TBP = 328 kPa TXUU up to 2.78% strain and deviator stress of 4628 kPa	1.5×10^{-9}

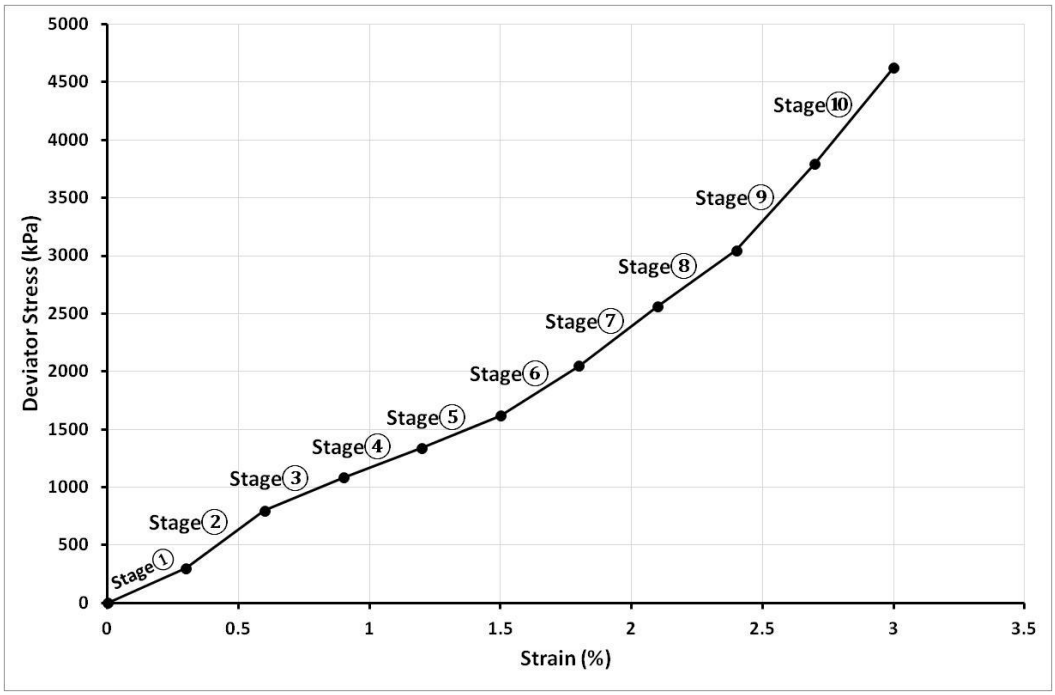

Figure 3.15: Stress-strain behaviour in a multi-stage test (consisted of 10 shearing stages) on a CB specimen at 19 months curing age

3.7.4 SHORTCOMINGS

Figure 3.15 shows that stress-strain behaviour of a CB specimen in multi-stage triaxial test was not similar to the expected behaviour of a single TXUU test (i.e. brittle strain-softening post peak). This is due to the revealed variation in the deformation behaviour between the strain-softening behaviour generally exhibited under TXUU shearing and the unexpected stain-hardening behaviour exhibited under the multi-stage triaxial shear test conducted (akin to TXCD behaviour, Alzayani et al., 2016). In addition, the hydraulic conductivity was noted to be generally constant throughout the triaxial multi-stage test (**Table 3.5**); hence justifying the strain-hardening deformation behaviour experienced. It would appear that the CB was consolidating during the measurement of the hydraulic conductivity; this reinforces the assertion that CB is most likely to be vulnerable to failure in undrained loading conditions. In addition, it verifies the unusual and variable deformation behaviour of

CB material reported in the literature: Alzayani et al., 2016; Soga et al., 2013; Manassero et al., 1995; etc). However, the multi-stage method seemed not to fit the purpose of this thesis.

The multi-stage method's perceived advantage was that it helped minimise variability in material properties that would likely be encountered between cured CB specimens; however, it is clear that this method suffers from variability in test conditions after every shearing stage that cannot be avoided (**Table 3.5**). The variation in the test conditions was necessary to: match the increasing pore water pressure building up due to undrained shearing, and avoid volume loss as much as possible in case conditions were kept constant at all stages. The developed method of hydraulic conductivity measurement using constant head (applied by two back pressure systems) and flow applied by the GDS controller (explained in **Section 3.5.1.4**) did not succeed in sustaining the required undrained condition throughout the multi-stage test. Partial drainage might be facilitated (besides the variable test conditions) through usage of two back pressure systems; thus strain-hardening behaviour would be mitigated. Therefore, the multi-stage method was decided to be abandoned without further validation or improvement due to the limited time remained for the completion of the main testing. Another method was developed to provide the most sealed (undrained) testing conditions and procedure as explained in the next section.

3.8 THE MAIN TESTING METHODOLOGY: SINGLE-STAGE TXUU SHEARING WITH HYDRAULIC CONDUCTIVITY MEASUREMENT USING CONSTANT FLOW METHOD

3.8.1 INTRODUCTION

The multi-stage method measured the hydraulic conductivity on more than one occasion for a single specimen investigated. The two problems arising from this were:

the variability in multistage test conditions, and strain-hardening behaviour of CB specimens due to seepage induced consolidation (**Section 3.7.4**).

The multi-stage methodology (that aims to evaluate the change of hydraulic conductivity through the complete stress-strain behaviour of one CB specimen) was changed to a single-stage TXUU shearing test to evaluate the hydraulic conductivity change after applying certain amount of displacement relative to the general (mean) stress-strain behaviour of CB specimens.

Unlike the multi-stage method, which exposed one specimen to cycles of deformation and measurement of hydraulic conductivity for prolong testing period, this method used multiple specimens to determine how hydraulic conductivity varies with deformation. A number of specimens would be exposed to different amounts of deformation in TXUU conditions (before and after strain corresponding to peak deviator stress) and the hydraulic conductivity would be measured for each specimen once the deformation was completed (in addition to it being measured prior to the outset of the deformation; that is at 'intact state'). Thus, for the purpose of this chapter this method was termed the 'single-stage' method. The constant flow method (**Section 3.5.2**) was selected for measuring the hydraulic conductivity at the intact state of CB specimens as well as after deformation; as it was found to be the most suitable to determine accurate and prompt results for the purpose of this study.

This methodology would, ideally, indicate if microcracking pre-peak stress is exhibited and results in increased hydraulic conductivity (as observed in rocks). In addition, to what extent it could affect the hydraulic conductivity that might be expected to change with different undrained shearing displacement amounts (including those that exceed the strain corresponding to peak stress).

The perceived advantages of the single-stage method are:

- The hydraulic conductivity of CB is not measured prior deformation; hence the specimens are not consolidated in the first instance. Additional specimens were used to measure the hydraulic conductivity of specimens that were not deformed (i.e. at intact state) to determine an approximate 'baseline' hydraulic conductivity for the CB material. Therefore, from these results changes in hydraulic conductivity with deformation could be approximated.
- The specimen was not further deformed once the hydraulic conductivity had been measured (after it had experienced the desired amount of vertical strain), thus the change in deformation response (from brittle, strain-softening under TXUU to strain-hardening with drained conditions) was avoided.

This method was not initially embraced due to potential variance in physical properties of the CB specimens cast from slurry impacting upon the ability to assess changes in hydraulic conductivity with deformation. However, it was felt that this limitation was less significant than those encountered with the multi-stage method; hence it was used during the main phase of testing and data collection. Several CB specimens (cast from different slurry batches) were required be tested in order to justify the impact of variation of physical properties on both undrained deformation and the hydraulic conductivity of the CB mixture investigated, and to check the level of results repeatability.

The following sections describe; the single-stage test constraints, curing ages to be tested for the main data collection, the strain and stress testing conditions, the procedure followed with respect to varying deformation states (i.e. intact -no

deformed, pre-peak deviator stress, and post-peak deviator stress), and the calculations required for data analysis corresponding to each of these states.

3.8.2 TEST CONSTRAINTS AND GENERAL PROCEDURE

Trials of the constant flow and TXUU tests on CB specimens (at different curing ages) were carried out to develop the single-stage testing methodology. These trials revealed the main constraints in testing CB specimens, and justified the actions required to overcome them. The main testing constraints and the corresponding solutions (procedures) and justifications are summarised in **Table 3.6**.

Table 3.6: The main testing constrains and the corresponding procedures

Testing Constraint	Procedure to follow	Justification
Meta-stable CB fabric at early curing ages (less than 90 days); due to ongoing cement hydration processes	Minimum permissible curing age to be tested is 90 days	Trials at ages from 8 days to 65 days showed that steady state flow condition at constant hydraulic gradients was not achieved even after long permeation periods (up to 7 days). Refer to Section 3.8.3.1.
Displacement rate to be applied in the TXUU stage (Slow or quick shearing?)	1 mm/min (quick UUTX shearing)	Peak deviator stresses, corresponding strains and failure modes, were similar for slow and quick displacements in TXUU tests. Refer to Section 3.8.4.
Stress conditions to simulate unconsolidated undrained situation with no or negligible specimen volume loss and air cavitations	CP to be 300 kPa to produce PWPs high enough to apply TBP of 300 kPa (i.e. B value =1). This pressure value will force any existing air bubble into solution, and prevent air cavitations in case effective confining pressure is required to be applied and/or changed.	Air cavitation in the back pressure system is prevented, if it is minimum 300 kPa, particularly in case further change in cell pressure is applied (Head and Epps, 2014). Trials of TXUU tests under different CP (100 kPa, 200 and 300 kPa) showed similar peak deviator stresses, corresponding strains and failure modes. Refer to section 3.8.4.
Strain (displacement) limits to be applied prior conducting the flow pump test	UU shearing up to the five limits: 0.6 mm, 1.1 mm, 2.2 mm, 3.3 mm, 4.4 mm, and 5.5 mm. Also, shearing up to the certain peak deviator stress of couple of specimens.	The peak deviator stress in TXUU is achieved at strains ranging from 0.8% to 1.5%. Hence, the strain limits were selected to be before and after the mean strain value corresponding to peak deviator stress that was around 1.0 mm. Undrained deformation investigation revealed that initial cracking of CB specimens happens after the peak deviator stress, thus four displacement limits out of five were selected to be after the peak point. Refer to Section 3.8.5.

3.8.3 CURING AGES TO BE TESTED

3.8.3.1 TESTING BEFORE 90 DAYS OF CURING

Constant flow test trials were conducted on the juvenile CB specimens at: 8 days, 14 days, 28 days, and 64 days (repeated twice, on separate specimens, for each curing age). Examples of the volume change measurement using the constant flow test method for CB specimens at curing age of 14 days and 28 days are shown in **Figures 3.16 and 3.17**.

It was apparent that the steady state flow condition under constant hydraulic gradient was not achieved in juvenile specimens even after 4 days of permeation. In addition, the volume change measurements on juvenile CB specimens was found to be very sensitive to the small cyclic variation of the applied CP and TBP which was caused by fluctuation in the operation air pressure regulators and air compressor as justified in **Section 3.6**. An example of the flow measurements at 14 days of curing is shown in **Figure 3.16**; the volume change measurements for two days (i.e. 2880 minutes) was not adequate to confirm the arrival of the steady state flow condition (**Figure 3.16a)**. The measurements up to seven days would allow possible approximation of the outflow rate (**Figure 3.16b)**; however the pressure difference across the CB specimen varied during the permeation period (**Figure 3.16c**), and over these times consolidation of the specimen might be an issue. Similar pattern was observed in flow measurements at 28 days of curing (**Figure 3.17)**; this justified that confident confirmation of steady state flow condition was not feasible at curing ages reflecting the short-term response of hardened CB slurry.

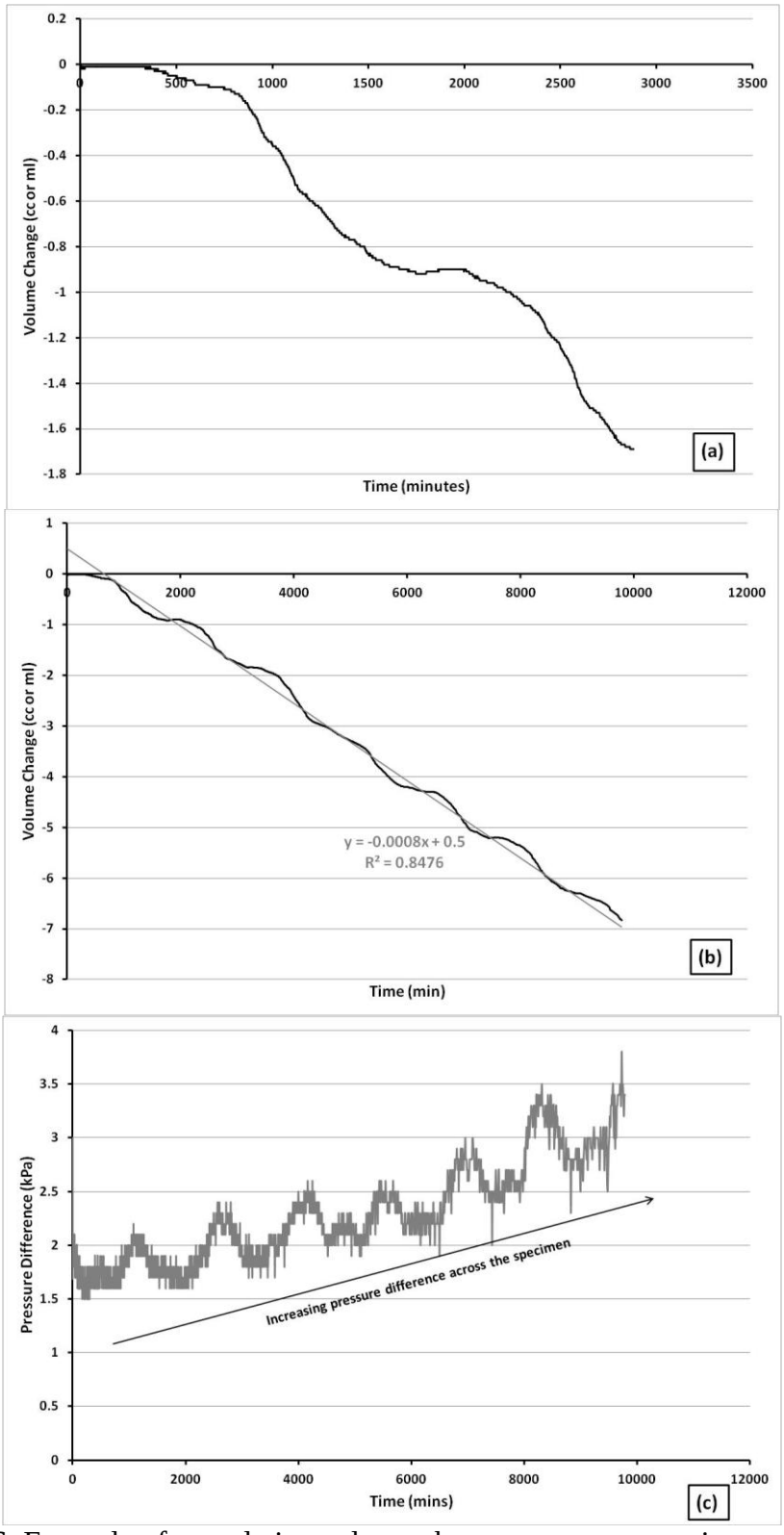

Figure 3.16: Example of cumulative volume change measurements in a constant flow test on a CB specimen at 14 days of curing. The constant inflow rate by GDS pump was 0.001 ml/min. **(a)** Cumulative outflow volume through the TBP system until 2 days of permeation. **(b)** Cumulative outflow volume through the TBP system until 7 days of permeation. **(c)** Pressure difference variation across the test specimen.

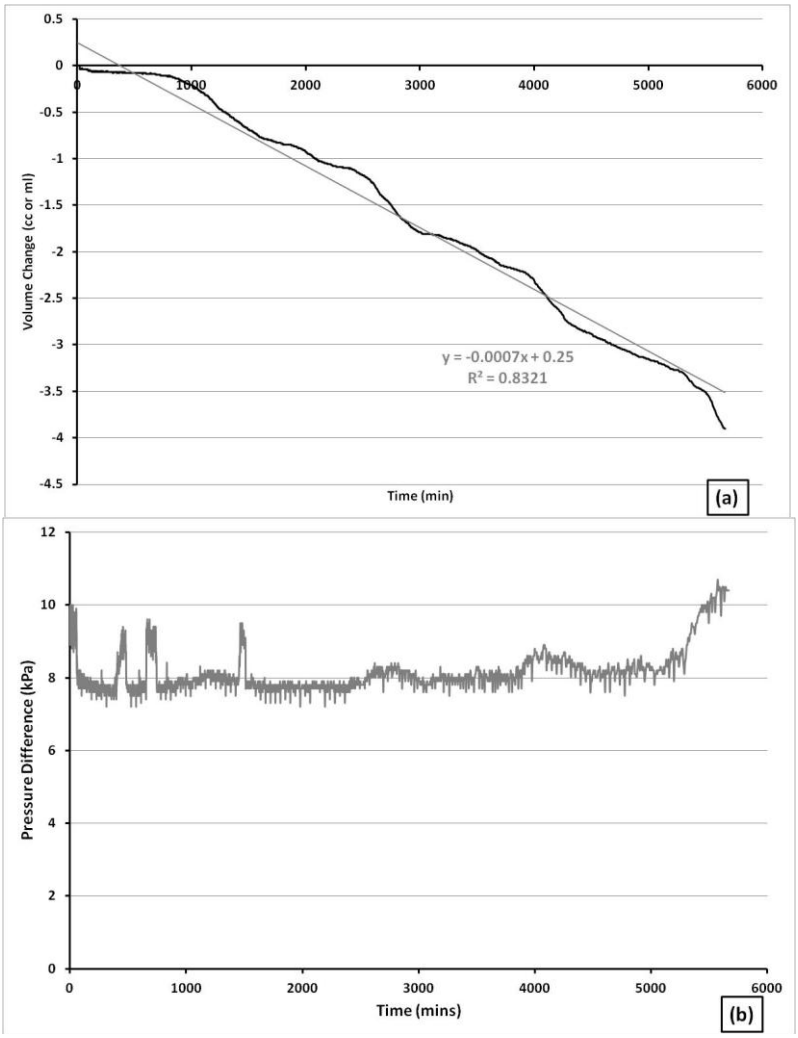

Figure 3.17: Example of cumulative volume change measurements in a constant flow test on a CB specimen at 28 days of curing. The constant inflow rate by GDS pump was 0.001 ml/min. **(a)** Cumulative outflow volume through the TBP system **(b)** Pressure difference variation across the test specimen.

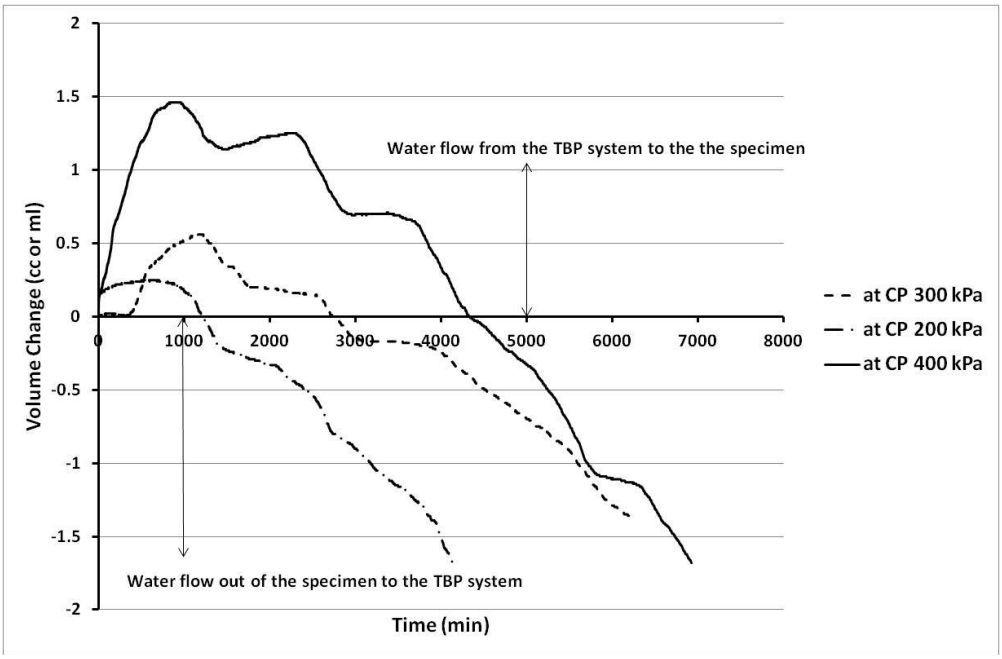

Figure 3.18: Cumulative volume change measurements in a constant flow test on CB specimen at 60 days of curing under varying confining pressures. The constant inflow rate by GDS pump was 0.001 ml/min.

CB specimens cured for 60 days were tested under different CPs (but maintained constant for a given test), which were 200 kPa, 300 kPa, and 400 kPa (**Figure 3.18**). The flow measurements appeared to be independent of the cell pressure; as measurements shows similar common patterns regardless of the applied cell pressure as the observed patterns appear similar (**Figure 3.18).** The water flow had to be produced from the bottom end of the test specimen to the top end; this was checked through the negative volume change reading (i.e. outflow from the specimen into the TBP system). However, juvenile CB specimens at curing ages less than 90 days did not show such flow response in the beginning of the permeation period (i.e. up to 4 days of permeation). In contrast, positive volume change readings were recorded indicating that water from the TBP system was taken by the test specimen as illustrated in **Figure 3.18**, and this initial positive flow response was found to increase with increasing CP. This was expected because the structure of the CB material was

still not stable and chemical reactions in the CB hardened slurry were still not completed at their early ages (i.e. less than 90 days of curing); rather than being an experimental error (as the triaxial equipment was carefully checked before every test). Hydration reactions of cementitious materials within the CB slurry (with/without GGBS) are suggested to be mostly completed by 90 days of curing (Jefferis, 2003; Evans, 2005; Jefferis, 2012). Also, bentonite hydration is suspected to continue for months after mixing (Jefferis, 1982; Jefferis, 2012).

Additional examples of results not confirming the arrival of steady state flow condition at 14 days and 28 days are shown in **Figures 3.19 and 3.20**.

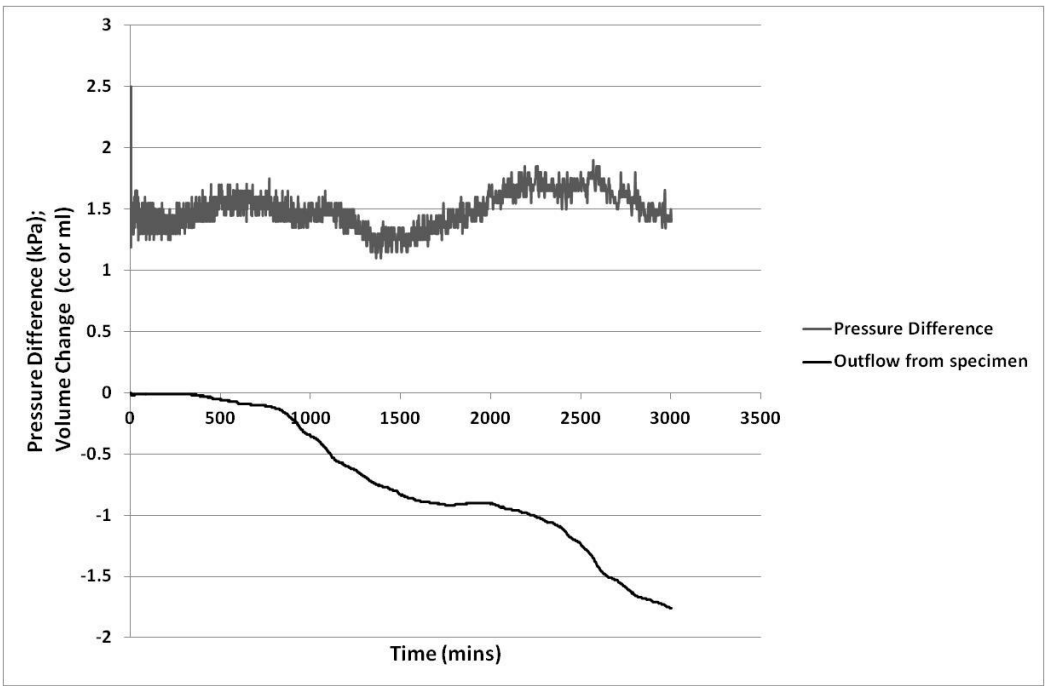

Figure 3.19: Pressure difference and outflow from the specimen at 14 days. The inflow rate by the GDS pump was 0.001 ml/min

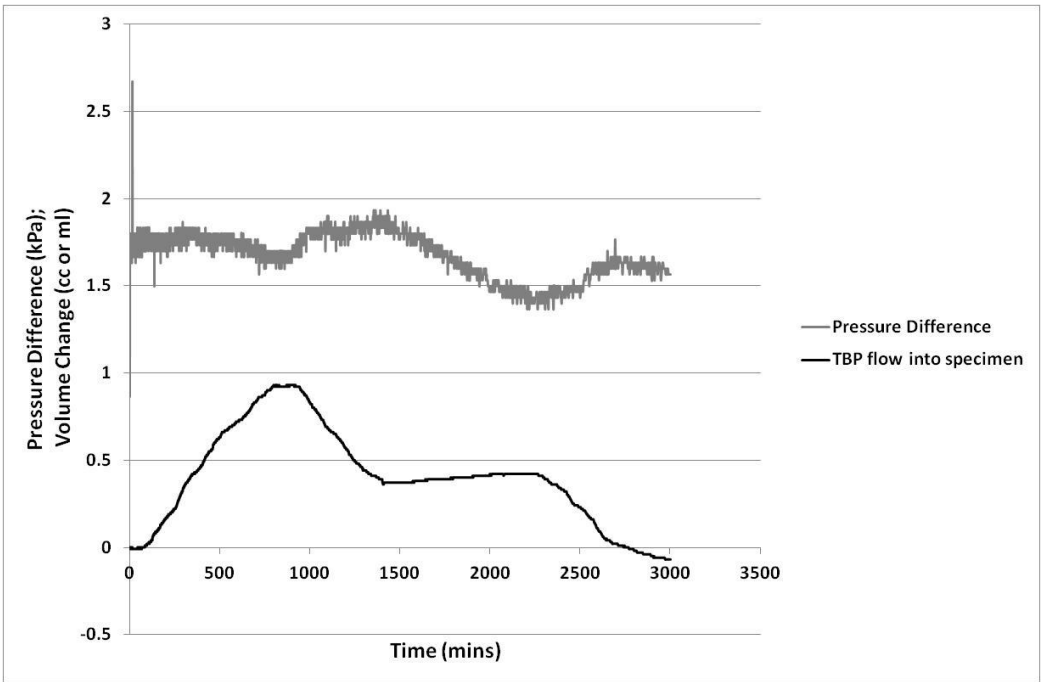

Figure 3.20: Pressure difference and outflow from the specimen at 28 days of curing. The inflow rate by the GDS pump was 0.001 ml/min

3.8.3.2 MAIN TESTING AFTER 90 DAYS OF CURING

In contrast to juvenile CB, testing at 90 days of curing showed adequate results and accepted confirmation of steady state flow condition (**Figure 3.21**). Flow measurements through constant flow tests on CB specimens at 90 days of curing were less sensitive to the fluctuation in the operation of the pressure systems, and satisfactory results could be achieved in a short period of permeation as shown in **Figure 3.21**. However, completion of the CB hydration processes after 90 days of curing could not be confirmed. Therefore, in this study, in light of issues encountered when attempting to measure the hydraulic conductivity (and when considering the changes in deformation response with curing; Alzayani et al, 2016) specimens were only considered once cured for 90 days.

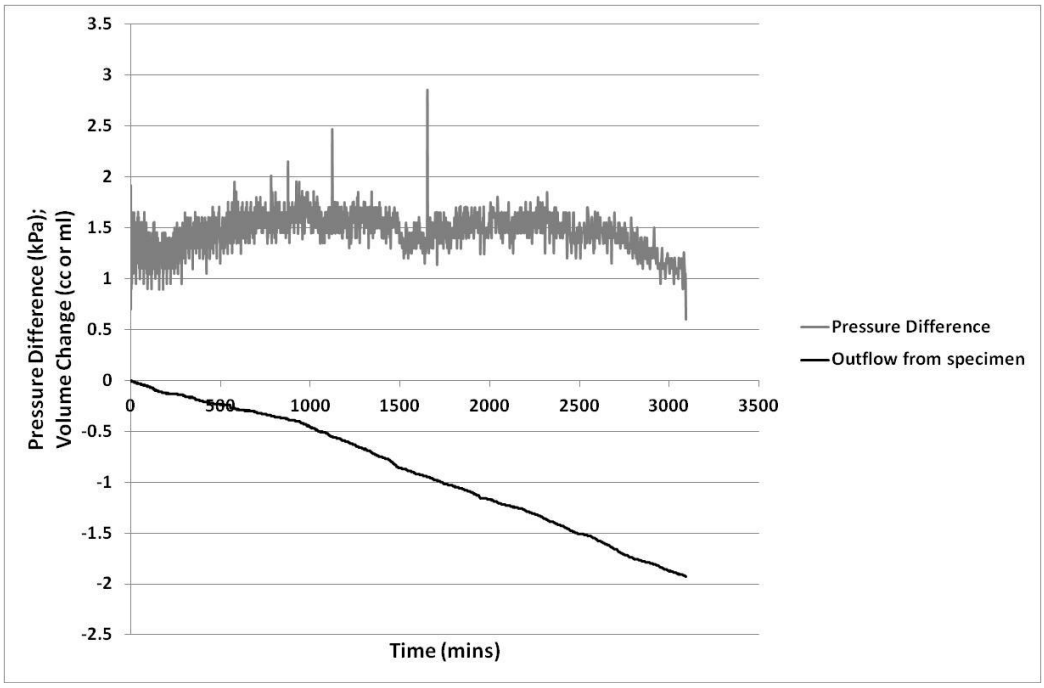

Figure 3.21: Pressure difference and outflow from the specimen at 90 days of curing. The inflow rate by the GDS pump was 0.001 ml/min

3.8.4 DISPLACEMENT RATE AND STRESS CONDITIONS

The suitable displacement rate and CP to be applied during the TXUU shearing were selected through conducting TXUU tests at different CPs and displacement rates at curing ages of 91 days and 96 days. The undrained deformation behaviour of the CB specimens was examined under; varying CPs (100 kPa, 200 kPa, and 300 kPa), and two displacement rates (slow rate 0.02 mm/min, quick rate 1 mm/min). This would indicate the level of consistency of undrained deformation behaviour of CB specimens at varying testing conditions. The rate 0.02 mm/min was selected to be checked in compliance with specification by Head and Epps (2014). The displacement rate for undrained shearing should not exceed 1.0 % per hour. Therefore, for CB specimens of 100 mm length the rate is 0.016 mm/min, which was approximated to be 0.02 mm/min. In addition, the behaviour under that slow rate was compared to the one under a fast rate which was 1 mm/min.

Table 3.7: Peak deviator stresses and corresponding strains at different CPs and displacement rates in TXUU tests after 90 days of curing

At 1 mm/min		
CP (kPa)	**ε_{peak}(%)**	**q_{peak} (kPa)**
100	1.2	648
200	1.6	714
300	1.4	672
At 0.02 mm/min		
CP (kPa)	**ε_{peak}(%)**	**q_{peak} (kPa)**
100	1.4	774
200	1.2	661
300	0.9	686

TXUU deformation behaviour of CB specimens containing GGBS in excess of 90 days of curing did not vary significantly with varied axial strain rate and CP (**Table 3.7, Figures 3.22 and 3.23**). This was also similar to the general constant undrained behaviour under variable confining pressures observed by Soga et al. (2013). However, the common variation in the peak deviator stress (q_{peak}, from 650 kPa to 770 kPa) and the corresponding strain values (ε_{peak}, from 0.9% to 1.6%) was expected due to variation in the CB slurry material properties. This was similar to the range reported by Soga et al. (2013); undrained strength (q_{peak}) ranging from 535 kPa to 745 kPa, and ε_{peak} ranging from 0.5% to 2%. The undrained deformation behaviour was found to be highly variable post-peak deviator stress as variable failure modes were exhibited; tensile failure through vertical cracks or combination of vertical and inclined cracks forming a wedge. The post-peak deformation variability was observed to be higher when using the slow displacement rate 0.02 mm/min (**Figure 3.23**). Therefore, the most convenient rate of displacement selected to be used in the main testing was 1 mm/min, as it enhanced the speed factor in testing.

Similarly, results at varying CPs (note that the highest pressure possible using the compressed air system in the laboratory was approximately 400 kPa) showed

insignificant variation (**Table 3.7, Figures 3.22 and 3.23**). However, as noted above, the measurement of hydraulic conductivity is sensitive to effective confining pressure (**Section 2.7.2.2**), and it is important to ensure that any air is dissolved into solution. Therefore, the higher cell pressure should be used. Head and Epps (2014) specify that the minimum back pressure of 300 kPa should be applied for consolidation and permeability applications and this pressure was used in the single-stage method.

When applying the CP of 300 kPa, the PWP had always increased in response to almost equalise with the CP (i.e. 300 kPa); indicating full saturation (B-value ≈1) of CB specimens and almost zero initial effective stress. Therefore, this magnitude of CP was justified to generate the PWP sufficient to apply TBP of 300 kPa that greatly assessed in preventing air cavitations during hydraulic conductivity measurements.

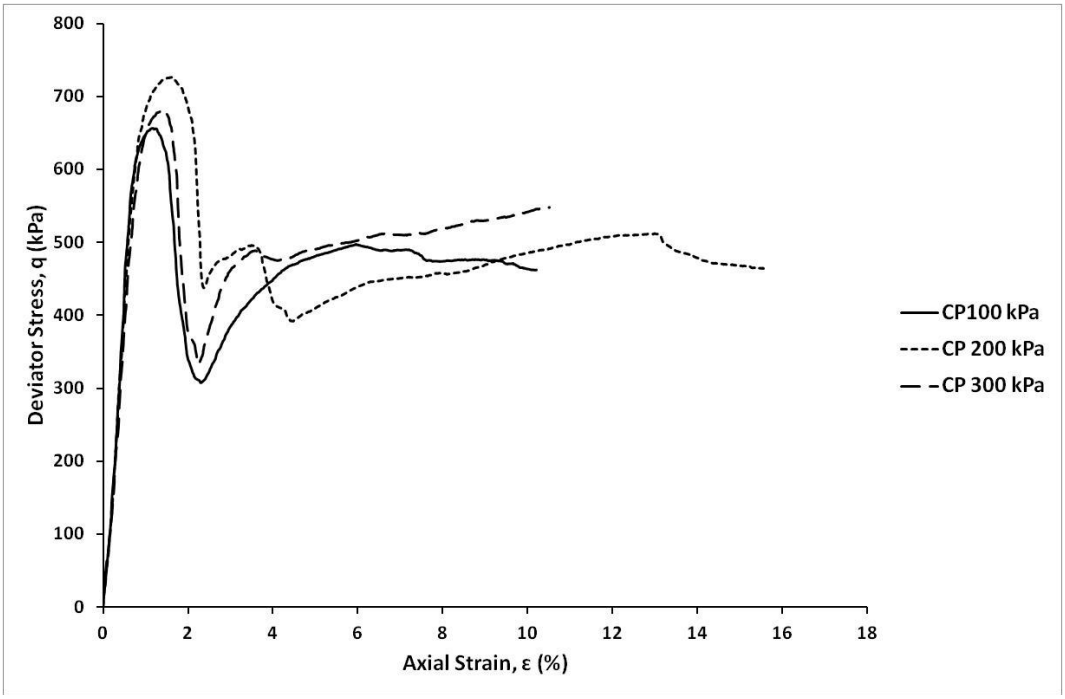

Figure 3.22: TXUU stress-strain relationships for three CB specimens at 91 days of curing tested under different CPs at 1 mm/min

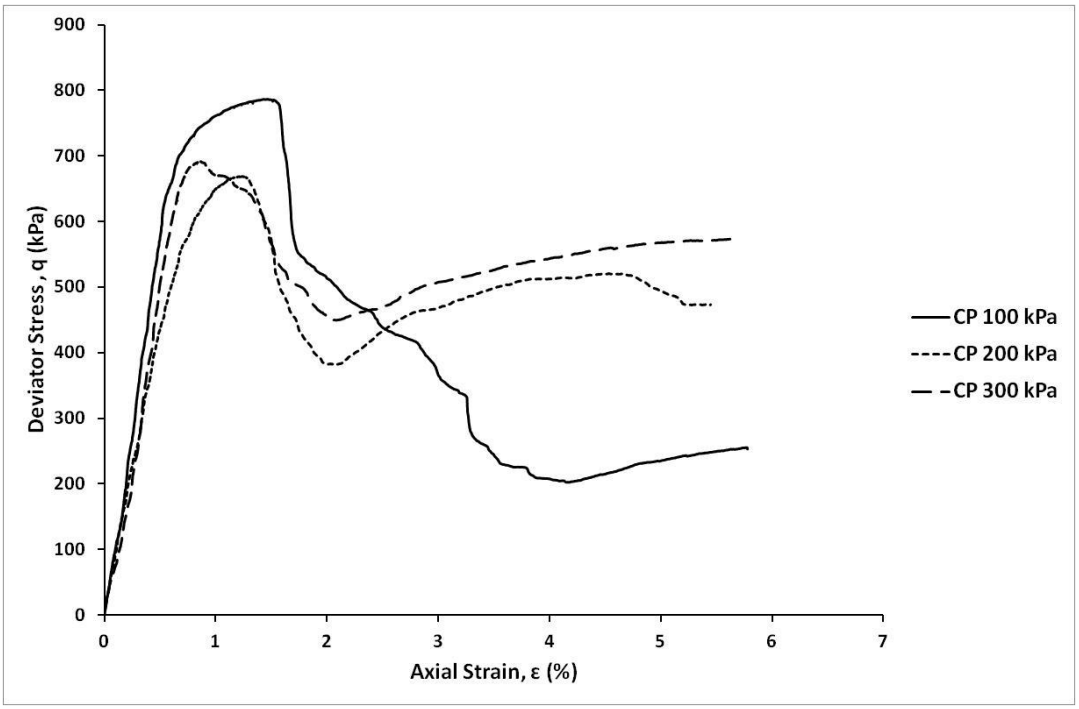

Figure 3.23: TXUU stress-strain relationships for three CB specimens 96 days of curing tested under different CPs at 0.02 mm/min

3.8.5 TXUU STRAIN LIMITS FOR ASSESSMENT OF HYDRAULIC CONDUCTIVITY CHANGE

The single-stage method required measurements of hydraulic conductivity after the specimens were deformed for a specific vertical displacement, under TXUU conditions, yet it was known that the ε_{peak} varied with specimens (and the microcracking models for rock mechanics were related to peak stress; Alzayani et al., 2016). Therefore, displacement amounts (limits) were identified.

The displacement limits should ideally be distributed along the general stress-strain relationship exhibited in the TXUU test. Hence, testing should validate the impact of undrained deformation on CB specimens, and, most importantly, should detect the increase of hydraulic conductivity due to cracking and whether it primarily happens before or after the q_{peak}.

The first approach assessed in deciding the hydraulic conductivity assessment points (displacement or strain limits), was linked to observation of the cracking process under UCS testing (in unconfined compression apparatus). Through observing and recording the deformation under unconfined compression, the initial (visible) cracking point was found to be either at or post the UCS (peak strength), regardless of the curing age of the tested CB specimen and strain rate applied.

The cracking process observed through UCS testing then had to be validated through a second approach that was observation of cracking process under TXUU testing. However, the observation of cracks initiation and growth through the latex membrane was not as clear as through the UCS testing. Therefore, several TXUU tests were conducted under CP of 300 kPa at different strain rates (0.02 mm/min and 1 mm/min) and curing ages (58 days, and 90 days), then the tests were terminated at varying displacements (before and after the peak deviator stress state; i.e. q_{peak} and ε_{peak}) to inspect the specimens for visible cracks. This inspection has validated that visible initial cracks occurs after the q_{peak} regardless of the curing age of the CB specimen and the strain rate applied (**Figure 3.24** and **3.25**). This observed cracking phenomenon was further investigated in the main testing period as discussed in **Section 6.6**. **Figures 3.24** and **3.25** shows an example of visible crack development in CB specimens sheared up to 2% strain (i.e. passing their peak deviator stress state), whereas specimens have no visible cracks when sheared up to 0.6% and 1.1% strains. This agrees with the cracking process observed under UCS testing.

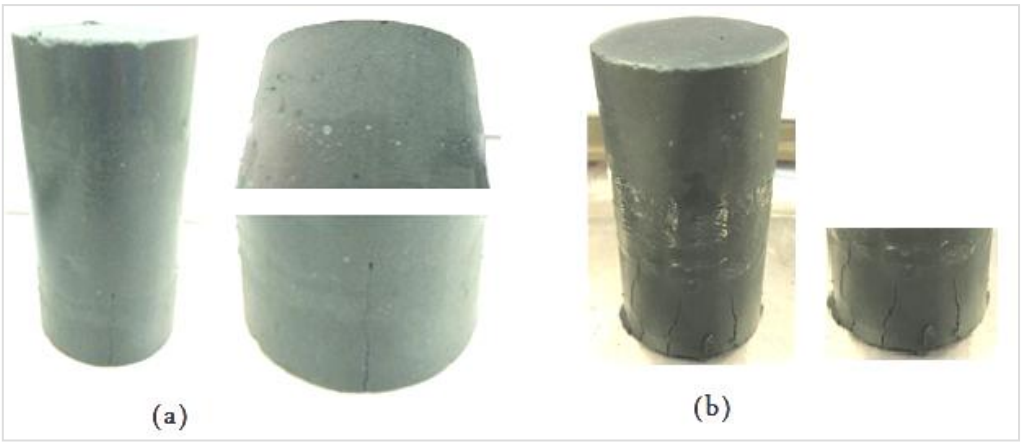

Figure 3.24: Two CB specimens showing visible crack developed at the top and bottom ends through TXUU shearing up to 2% strain at CP of 300 kPa. (**a**) CB specimen at 58 days of curing tested under 0.02mm/min strain rate, with ε_{peak} of 0.8%. (**b**) CB Specimen at 94 days of curing tested under 1 mm/min strain rate, with ε_{peak} of 1.5%). Note that the middle sections of the specimens were smeared with silicone gel, and the colours were adjusted for better visibility.

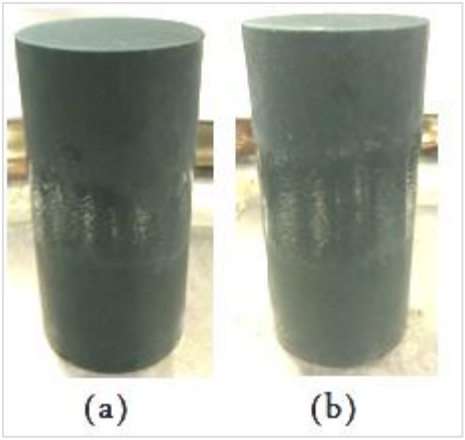

Figure 3.25: Two CB specimens showing no visible crack when sheared up to a strain not exceeding their ε_{peak}, under TXUU at 1 mm/min strain rate and CP of 300 kPa. (**a**) CB specimen at 91 days of curing sheared up to 0.6% strain. (**b**) CB specimen at 93 days of curing sheared up to 1.1% strain. Note that the middle sections of the specimens were smeared with silicone gel, and the colours were adjusted for better visibility.

Therefore, the two approaches used to evaluate the initial visual cracking point that would trigger the primary increase in the hydraulic conductivity of CB specimens, greatly helped in deciding the best TXUU strain limits for assessing the change of the hydraulic conductivity. The last step to make the decision was to determine the strain

point at which the post-peak cracking propagation was commonly expected to happen. The mean axial strain corresponding to the peak deviator stress ($\bar{\varepsilon}_{peak}$) at the decided TXUU stress conditions (i.e. strain rate of 1mm/min and CP of 300 kPa) was 1%. It was determined through conducting eight TXUU tests during the methodology development stage for CB specimens at 90 days of curing. The strain limits (hydraulic conductivity assessment points), therefore, should be mainly scattered after the $\bar{\varepsilon}_{peak}$, because the cracking process and major hydraulic conductivity changes are expected to occur after this strain limit. In addition to assessing the hydraulic conductivity after shearing; the hydraulic conductivity of intact CB specimens which should be the lowest (i.e. reference value for tracking shearing impact) need to be evaluated initially. These reference measurements would provide sufficient data for assessing the hydraulic conductivity before reaching the peak deviator stress state. Thus, the strain limits selected to be examined in the main testing are shown in **Table 3.8**.

Table 3.8: Axial strain limits and their corresponding testing states used in the single-stage method

State of Deformation	Axial Strain Limit (%)
Intact State (No Deformation)	0.0
Pre-Peak Deviator Stress State	0.6
Just after $\bar{\varepsilon}_{peak}$ at 90 Days of Curing	1.1
Post-Peak Deviator Stress State	2.2
	3.3
	4.4
	5.5

The CB specimens undergo dramatic cracking and structural collapse (fragmentation) processes after reaching 5% strain in TXUU tests. Hence, the maximum allowable

displacement limit for assessing the hydraulic conductivity post TXUU shearing was decided to be in the order of 5% (**Table 3.7**). Beyond this strain value, hydraulic conductivity measurement would not be permissible, as seepage through the failed CB specimen cannot be controlled.

3.8.6 PROCEDURE OF CONSTANT FLOW TESTS AT PRE-PEAK STATE AND JUST AFTER $\bar{\varepsilon}_{PEAK}$ AT 90 DAYS OF CURING

In order to evaluate the hydraulic conductivity at the pre-peak deviator stress state (at 0.6% strain) and just after the $\bar{\varepsilon}_{peak}$ at 90 days of curing (at 1.1% strain); the corresponding TXUU shearing displacement was firstly applied. The procedure of measuring the hydraulic conductivity after small displacement (i.e. up to 1.1% strain) for any stress state before the peak stress is the same. Also, the procedure is similar to the procedure of measurement at the intact state explained earlier (**Section 3.5.2.2**). Although operational inflow pump rates need to be usually adjusted to higher values than the ones required in the intact state measurements. This is because the PWPs significantly increases due to the applied TXUU displacement (up to 1.1% strain), thus the hydraulic conditions change within the specimen, leading to the need of higher inflow rates (than intact state) to establish the convenient pressure difference across the specimen.

The steps of the main constant flow test procedure explained in **Section 3.5.2.2** was adjusted as follows from step 5 onwards:

Step 5: Shear the specimen up to the required strain limit that is either 0.6% strain (pre-peak deviator stress state), or 1.1% strain (just after the $\bar{\varepsilon}_{peak}$ at 90 days of curing).

Step 6: Wait until the PWPs stabilise after shearing. PWPs can be considered stable when their change is less than 5 kPa per hour as suggested by Heads and Epps (2014).

Step 7: Apply the TBP to be equal to the top PWP. Check that the B-value corresponding to the stable PWPs is indicating accepted saturation (≥ 0.95); otherwise apply the convenient TBP to preserve the saturated state (≥ 0.95).

Step 8: Increase the CP by 30 kPa (to be 330 kPa)

Step 9: Set up the GDS controller (pump)

- Close the pump valve to the cell, and adjust the pressure in the pump line to be equal to the BPWP after stabilisation (i.e. equal to the TBP).
- Set up the controller to the lowest pumping rate possible, that is 0.001 ml/min (i.e. 60,000 msec/mm³).
- Start pumping at that rate until the pressure in the line increased sufficiently. This operation takes a few minutes.

Step 10: Start pumping and measurement of the outflow from the specimen

Step 11: Monitor the outflow volume change readings with time

- Check that the initial applied inflow rate (i.e. 0.001 ml/min) results in a measurable pressure difference. This was found to be between around 0.8 kPa to 2 kPa; that was similar to the range measured in the intact state, because cracks were not justified to form after applying strains less than or equal to 1.1% as discussed earlier (in **Section 3.8.5**). If a measurable pressure difference is not detected after few minutes of pumping; the pumping rate is changed to a higher value while the valve BPP to cell is

locked, after that a new flow measurement is started once the BPWP stabilises (Aiban and Znidarcic, 1989). The range of applicable inflow pump rates for adequate measurements at stress states up to 1.1% strains was found to be from 0.001 ml/min (60,000 msec/mm^3) to 0.002 ml/min (30,000 msec/mm^3).

- Continue measurement overnight.

- Record any change to the initial room temperature during the whole measurement period.

- Calculate the outflow rate after different periods of pumping from 20 hours to a maximum 2 days, to evaluate final stable outflow rate.

Step 12: End measurement when a steady state flow condition is confirmed

- The hydraulic gradient and the outflow rate were found to become constant after pumping for at least 500 minutes in the case of CB specimens tested at 90 days.

- Allow a sufficient period of flow measurement at the constant pressure difference, which is for at least one day (to collect constant outflow volume of 1 ml) as the inflow rate applied is very slow to produce an equivalent outflow rate from the intact CB specimen.

- Calculate the coefficient of hydraulic conductivity using the measured steady outflow rate and constant hydraulic gradient.

- Stop the flow pump and close the BPP valve to cell as soon as the final value of the hydraulic conductivity is achieved.

- Record the decay in the differential pressure at the bottom of the specimen so that the reference readings of the BPP and BPWP transducers could be checked again (Aiban and Znidarcic, 1989).

- Take the specimen out, remove the rubber membrane carefully, then observe and note if any visual changes happened to it.

- Weigh the specimen to obtain its final water content (after testing) to confirm that no (or negligible) volume loss has happened due to the constant flow test.

3.8.7 PROCEDURE OF CONSTANT FLOW TESTS AT POST-PEAK STATE

The procedure of measuring the hydraulic conductivity at the post-peak deviator stress state that occur after considerable TXUU shearing displacement (i.e. from 2.2% strain to 5.5% strain) was similar to the one developed earlier for measurements at strains equal or below 1.1% (**Section 3.8.6**). Although, the required inflow pump rates to establish the convenient pressure difference across the specimen, were found to be substantially higher due to propagation of cracks within the CB specimen (mostly vertical tension cracks). The hydraulic conditions within the CB specimens at 90 days of curing after shearing up to 2.2% strain and higher, was also found to be different than hydraulic conditions at lower strain limits (i.e. up to 1.1%); as cracks development resulted in decreasing the PWPs below the initial values (at the intact and pre-peak stress states). The drop in the PWPs due to air cavitations between the specimen ends and the rubber membrane was observed to increase with increasing strain under TXUU shearing particularly if the 2% strain is exceeded (See **Section 6.3**). Thus, it is important in this procedure to ensure that the CB specimens be fully

saturated before proceeding with the flow pump stage through application of high enough TBP that results in a B-value not less than 0.96.

The steps of the constant flow test procedures explained in **Sections 3.5.2.2** and **3.8.6** was adjusted as follows from step 5 onwards:

Step 5: Shear the specimen up to a certain strain limit corresponding to the post-peak deviator stress state that is; 2.2%, 3.3%, 4.4%, 5.5%, or just after the ε_{peak}.

Step 6: Wait until the PWPs stabilise after shearing (changing by less than 5 kPa per hour). Stabilisation of PWPs after TXUU shearing to post-peak deviator stress state was found to take longer time than earlier stress states.

Step 7: Apply the TBP to be equal to the top PWP. Check that the B-value corresponding to final top PWP is still indicating adequate saturation (≥ 0.95); otherwise apply TBP of minimum 280 kPa to maintain the fully saturated state.

Step 8: Increase the CP by 30 kPa (to be 330 kPa)

Step 9: Set up the GDS controller (pump)

- Close the pump valve to the cell, and adjust the pressure in the pump line to be equal to the BPWP after stabilisation (i.e. equal to the TBP).
- Set up the controller to the lowest pumping rate. This was mostly seen to be 0.01 ml/min (i.e. 600 msec/mm³) for measurements at post-peak deviator stress state of CB specimens at 90 days.

Step 10: Start pumping as soon as the BPP valve is opened to avoid excessive build up of BPWP due to this high inflow rate and measure of the outflow from the specimen.

Step 11: Monitor the outflow volume change readings with time

- Check that the initial applied inflow rate (i.e. 0.1 ml/min) results in a measurable pressure difference. This was found to be ranging from 0.8 kPa to 10 kPa. If a measurable pressure difference is not immediately detected, the pumping should be stopped (and the valve BPP to cell is locked) to adjust the inflow rate to a higher value, after that start the new measurement again once the BPWP stabilises as suggested by Aiban and Znidarcic (1989). The range of inflow pump rates for adequate measurements on CB specimens at 90 days at post-peak state was found to be from 0.01 ml/min (600 msec/mm^3) to 0.6 ml/min (99 msec/mm^3).

Step 12: End measurement when steady state flow condition is confirmed

- The hydraulic gradient and outflow rate (through the TBP) were found to become constant instantly whenever pumping was started. This was due to the higher hydraulic conductivity which was facilitated via growing cracks.
- Allow a sufficient period of flow measurement at the constant pressure difference, which was around 20 minutes in this study.
- Calculate the coefficient of hydraulic conductivity using the measured steady outflow rate and constant hydraulic gradient.
- Stop the pump and close the BPP valve to the cell as soon as the final value of the hydraulic conductivity is achieved.
- Record the decay in the differential pressure at the bottom of the specimen so that the reference readings of the BPP and BPWP transducers are checked again (Aiban and Znidarcic, 1989).

- Take the specimen out, remove the rubber membrane gently. Note any visual changes and failure modes exhibited, and measure the new dimensions of the test specimen.

- Weigh the specimen to obtain its final water content (after testing) to confirm that no (or negligible) volume loss has happened.

- Record any change to the initial room temperature during the whole measurement period.

3.8.8 CALCULATIONS OF HYDRAULIC CONDUCTIVITY AT PRE-PEAK AND POST-PEAK STATES

The calculations of the coefficient of hydraulic conductivity after a stage of TXUU shearing are same as the calculations at the intact state of the CB specimen (**Section 3.5.2.3**). However there was one adjustment; the cross-sectional area (**A**) of the test specimen should be corrected to consider the amount of axial strain applied in the shearing stage. In order to determine the corrected cross-sectional area (**A'**); the axial strain (**ε**) should be calculated as follows:

ε = Applied Axial Displacement / **L** **(3.9)**

Thus,

A' = **A** / **|** 1 – **ε |** **(3.10)**

The calculations were processed using programmed MS Excel spreadsheets that also could generate the cumulative outflow from the top of the test specimen with time as explained in previously **Section 3.5.2.3.**

3.8.9 PROCEDURE AND CALCULATIONS OF TXUU DEFORMATION

The general TXUU deformation behaviour of CB specimens at 90 days age of curing was studied through conducting individual TXUU tests. These tests were conducted at CP of 300 kPa and axial strain rate of 1 mm/min using the 'definitive' method given in Part 7 of BS 1377:1990. During the period of methodology development, four TXUU test repeats were initially conducted to assess the general TXUU deformation behaviour, and obtain the mean peak deviator stress ($\bar{q}_{peak}$) and its corresponding mean axial strain ($\bar{\varepsilon}_{peak}$) of CB specimens at 90 days of curing. Furthermore during the main testing period, several TXUU tests at different curing ages (15 days, 30 days, 60 days, and 90 days) and under different CPs (50 kPa, 150 kPa, and 300 kPa) were conducted to inspect the undrained behaviour of CB in more detail. These tests were repeated three times only at every curing age and CP due to the limited number of moulds available for casting the specimens.

The following parameters should be calculated accordingly using data collected from a TXUU test:

- The strain at any time (**ε**)

  ε = Applied Axial Displacement / **L**

- The deviator stress at any time (**q** or **q'**)

  A = π (**D** / 2)²

  A' = **A** / | 1 – **ε** |

  q = **q'** = Axial Load / **A'**

- The total minor and major principal stresses at any time ($\boldsymbol{\sigma_3}$, and $\boldsymbol{\sigma_1}$ respectively)

$\boldsymbol{\sigma_3}$ = **CP**

$\boldsymbol{\sigma_1}$ = **CP** + **q**

- The effective minor and major principal stresses at any time ($\boldsymbol{\sigma'_3}$, and $\boldsymbol{\sigma'_1}$ respectively)

  Mean pore water pressure across the specimen (**MPWP**) = 0.5(TPWP+ BPWP)

  Where; TPWP is the top pore water pressure measured by the TBP transducer, and BPWP is the bottom pore water pressure measured by the BBP or the BPP transducers

  $\boldsymbol{\sigma'_3}$ = $\boldsymbol{\sigma_3}$ **- MPWP**

  $\boldsymbol{\sigma'_1}$ = $\boldsymbol{\sigma_1}$ **- MPWP**

- The total and effective mean principal stress at any time (**p** , and **p'** respectively)

  p = $(\boldsymbol{\sigma_1} + 2\boldsymbol{\sigma_3})/3$

  p' = $(\boldsymbol{\sigma'_1} + 2\boldsymbol{\sigma'_3})/3$

- The **A-value** at any time

  A-value =

  Change in mean pore water pressure across the specimen (**ΔMPWP**) / **q**

All of those calculations were processed using programmed MS Excel spreadsheets that also generate the following results plots as presented in **Chapter 4**.

3.8.10 TESTING PROCEDURE AT CURING AGES GREATER THAN 90 DAYS

For testing CB specimens at curing ages over 90 days, the single-stage testing procedures explained in **Section 3.8** can be followed to assess the impact of undrained deformation on the hydraulic conductivity. The step of applying low effective confining pressure of 30 kPa before measuring the hydraulic conductivity of intact and sheared specimens is very important to prevent preferred circumferential flow between the test specimen and the rubber membrane as stated earlier. However, this step might take longer time (in the order of days) when testing CB specimens at curing ages greater than 90 days comparative to the time required for testing younger specimens. In addition, the effective pressure of 30 kPa might be insufficient to consolidate the CB specimens at curing ages greater than 190 days. The structure of the CB material at this age of curing was found to be very stiff and well developed. This structure could not be compressed at low effective confinement as 30 kPa. Philip (2001) and Joshi (2009) used an effective stress of 100 kPa to consolidate CB specimens at an age of 3 years or older. Therefore, the hydraulic conductivity testing procedures explained herein could be followed but using higher confining pressures for testing mature CB specimen. Unfortunately, the remained time in the PhD programme (at the time this matter was discovered) was not enough to investigate the CB long-term behaviour. However, the short-term behaviour of CB material has been evaluated and could be considered as a reference to forecast the long-term behaviour. The short-term properties of CB specimens are more critical than the long-term ones, because the structure development processes is not yet completed. Hence, mature CB material was found to be stronger and stiffer due to the full developed structure. Also, it showed higher strength due to progressed consolidation in case further or extra

loads were applied for considerable time with adequate drainage. Not to mention that the TXUU deformation behaviour of CB material was justified to be insensitive to the change in: curing age, CP, and shearing rate (as shown in **Section 3.8.4** and **Chapter 4**). Therefore, the single-stage test time would be mainly affected by the dissipation of excess of PWP of 30 kPa. The convenient B-value indicating full saturation of the test specimen should be achieved through applying the required back pressure prior measuring the hydraulic conductivity to ensure the production of accurate test results using the constant flow method. For stiff soils a B-value of 0.95 is theoretically impossible to achieve even at full saturation state, hence a value of 0.90 is acceptable according to Black and Lee (1973) and BS 1377.

3.9 SUMMARY

This chapter has explained the methodology followed in specimen preparation, which includes the selection of the CB mixture composition and specimen size, and the procedure of casting and preparation prior testing. In addition, this chapter has discussed the development of the testing methodology required to achieve the aim of this thesis through combining TXUU shearing with hydraulic conductivity measurement. Firstly, different hydraulic conductivity measurement methods have been discussed in detail (in terms of apparatus, procedure, test conditions, and calculations). Secondly, the variation in the performance of the pressure regulators during the hydraulic conductivity testing that affected the results (presented in **Chapter 5** and discussed in **Chapter 6**) has been evaluated. Thirdly, different combinations of shearing and hydraulic conductivity testing methods have been evaluated. These are the multi-stage TXUU shearing with hydraulic conductivity

testing, and the single stage TXUU shearing with hydraulic conductivity testing. As a result of this evaluation, the single-stage testing methodology was favoured over the multi-stage methodology to be used in the main testing. This was because the tested CB specimen did not fail and did not show significant changes of the hydraulic conductivity with increasing axial strain under multi-stage shearing. However, it seemed to undergo ductile-strain hardening behaviour through multi-stage seepage. In addition, the multi-stage testing methodology did not show the ability of imitating the critical scenario of cracking under undrained loading during a relatively short testing time (i.e. a week or less per test) as required for completing the main testing in time.

Finally, this chapter has explained and justified the procedure and testing constrains of the single-stage testing methodology, which enabled the assessment of the relationship between CB hydraulic conductivity and undrained deformation in a period convenient for this thesis. Various specimens were used to determine how the CB hydraulic conductivity changes with the varying strain limits. The selection of the strain limits of TXUU shearing is explained. These were selected based on the typical stress-strain relationship of CB specimens at the different curing ages, which is characterised in **Chapter 6**. The CB hydraulic conductivity was measured using the constant flow method in the main testing. This was because it can determine low hydraulic conductivities in relatively short periods comparative to the conventional constant head method. Also, the constant flow method can provide more control of small flow rates and hydraulic gradients that are convenient for materials of low hydraulic conductivities (as reviewed in **Chapter 2** and justified in this chapter).

CHAPTER 4
RESULTS (PART A)

TXUU DEFORMATION OF CB SPECIMENS AT DIFFERENT CURING AGES

4.1 INTRODUCTION

In this chapter, the results of TXUU tests are presented, and commentary is provided with the data to aid understanding.

The TXUU behaviour of CB specimens is presented in an order that is with respect to duration of curing; increasing curing ages from 15 days to 90 days. Within each curing period, the data is presented with respect to CP applied (from 50 kPa to 300 kPa). The data presented is from the data logger connected to the triaxial equipment (no modifications have been made, unless stated otherwise, i.e. in the case of mean behaviour). In addition, the mean TXUU behaviour at every curing age and CP is presented. This was determined using selected (or filtered) data points corresponding to specific axial strains. As TXUU tests were repeated at least twice per different CP at a given curing age; data filtering was required to produce an appropriate average behaviour at each CP and/or age. The ‘filtered data’ consists of 21 deviator stress points corresponding to the following axial strains; 0%, 0.25%, 0.50%, 0.75%, 1.00%, 1.25%, 1.5%, 1.75%, 2.00%, 2.25%, 2.50%, 2.75%, 3.00%, 3.50%, 4.00%, 4.50%, 5.00%, 5.50%, 6.50%, and 7.00%.

Table 4.1 shows the count of TXUU tests conducted in this study at every curing age investigated.

Table 4.1: The count of TXUU tests conducted in the main testing period at different curing ages

Curing Age (Days)	Count of Test Repeats
15	9
30	9
60	8
90	13
Total Number of TXUU Tests at all Curing ages	**39**

4.2 TXUU BEHAVIOUR AFTER 15 DAYS OF CURING

4.2.1 BEHAVIOUR UNDER A CP OF 50 KPA

Figures 4.1, **4.2** and **4.3**, show the stress-strain relationships, MPWP-strain relationships, and effective stress paths in q-p′ field at 15 days of curing under a CP of 50 kPa, respectively. Three repeated tests were undertaken for these conditions using TXUU.

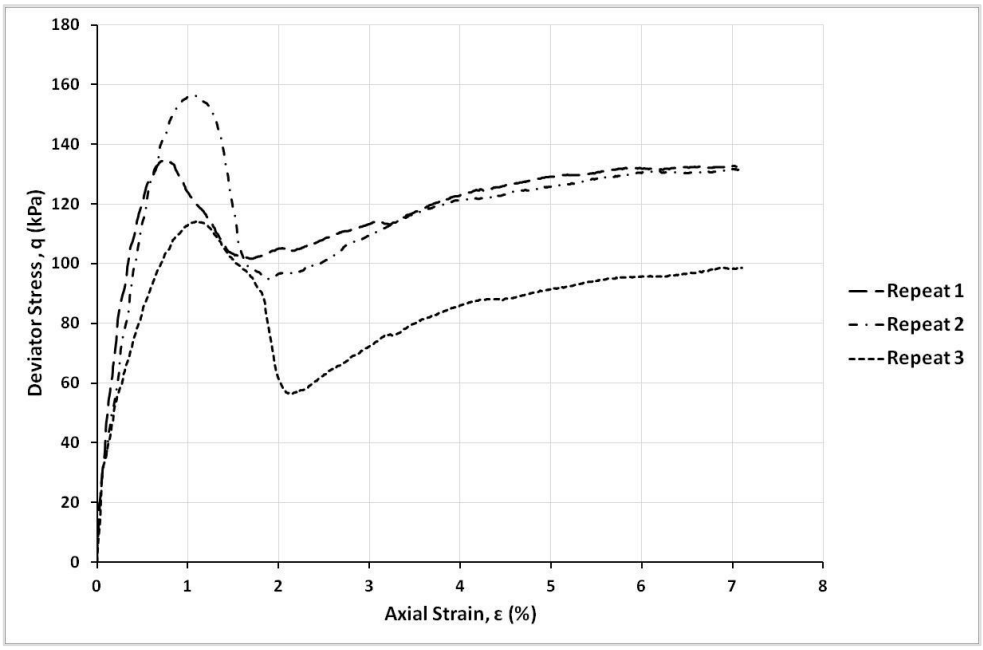

Figure 4.1: Stress-strain behaviour at 15 days of curing under a CP of 50 kPa

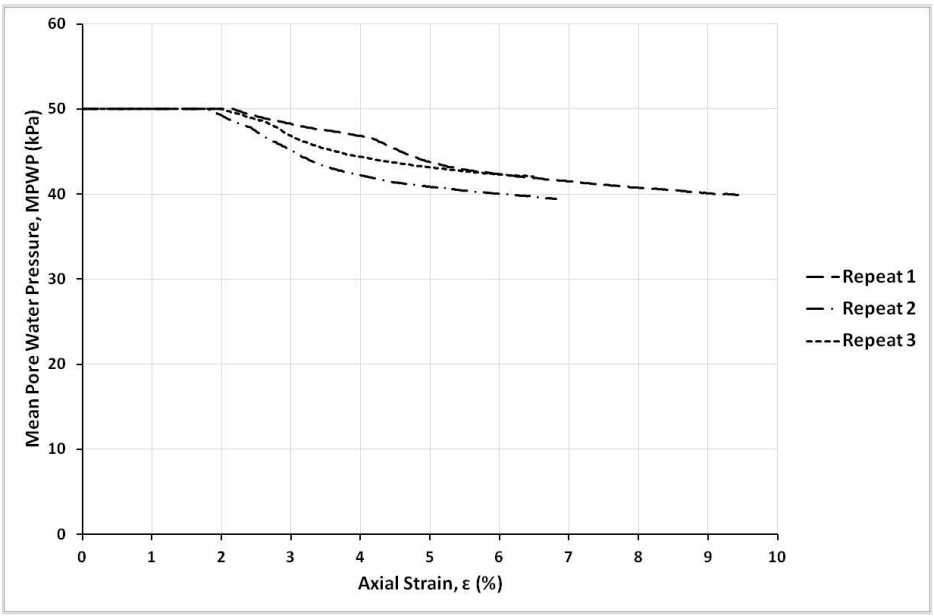

Figure 4.2: MPWP and axial strain relationships at 15 days of curing under a CP of 50 kPa

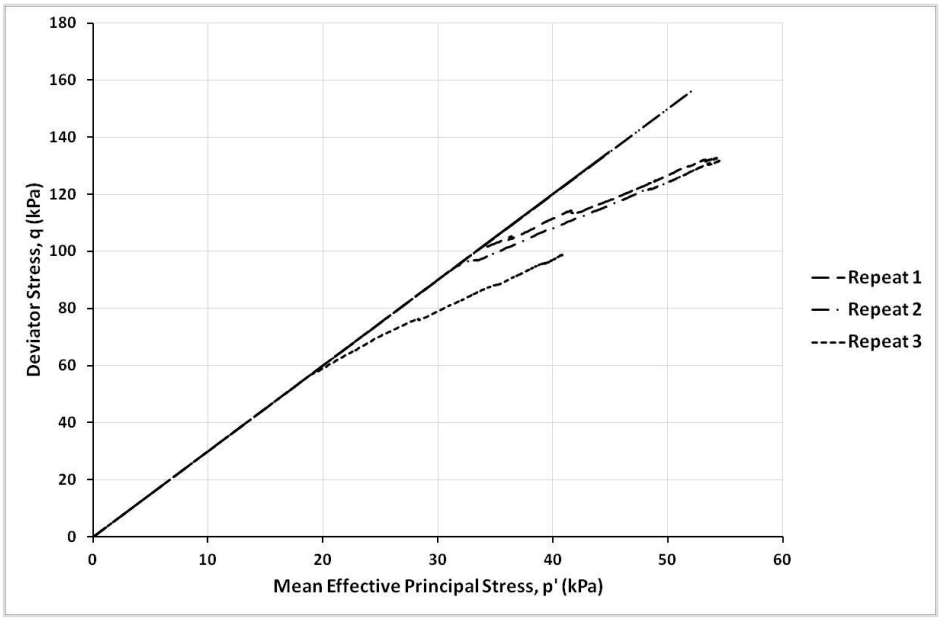

Figure 4.3: Effective stress paths at 15 days of curing under a CP of 50 kPa

4.2.2 BEHAVIOUR UNDER A CP OF 150 KPA

Figures 4.4, **4.5** and **4.6**, show the stress-strain relationships, MPWP-strain relationships, and effective stress paths in q-p′ field at 15 days of curing under a CP of

150 kPa, respectively. Three repeated tests were undertaken for these conditions using TXUU.

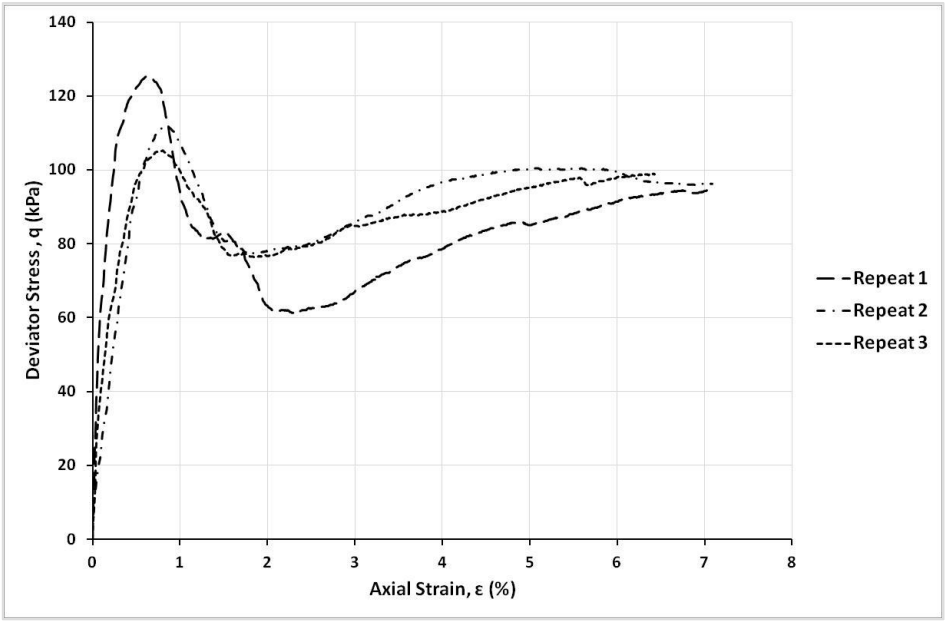

Figure 4.4: Stress-strain behaviour at 15 days of curing under a CP of 150 kPa

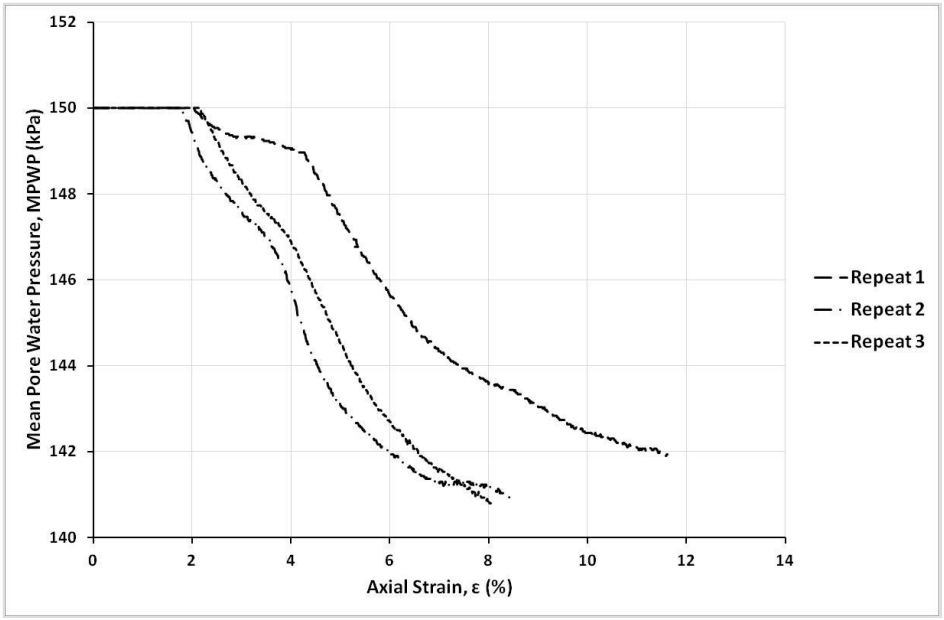

Figure 4.5: MPWP and axial strain relationships at 15 days of curing under a CP of 150 kPa

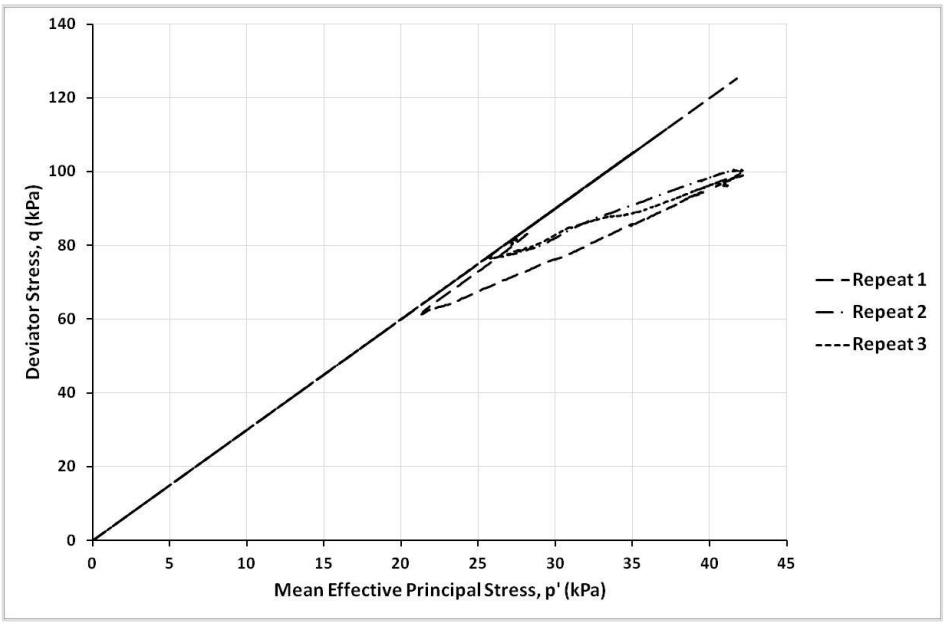

Figure 4.6: Effective stress paths at 15 days of curing under a CP of 150 kPa

4.2.3 BEHAVIOUR UNDER A CP OF 300 KPA

Figures 4.7, **4.8** and **4.9**, show the stress-strain relationships, MPWP-strain relationships, and effective stress paths in q-p′ field at 15 days of curing under a CP of 300 kPa, respectively. Three repeated tests were undertaken for these conditions using TXUU.

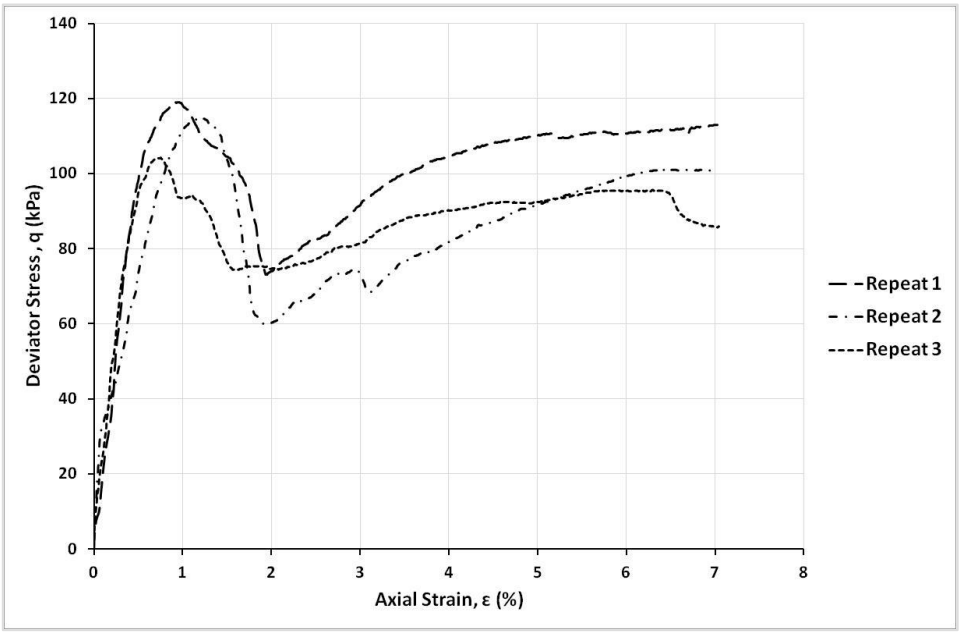

Figure 4.7: Stress-strain behaviour at 15 days of curing under a CP of 300 kPa

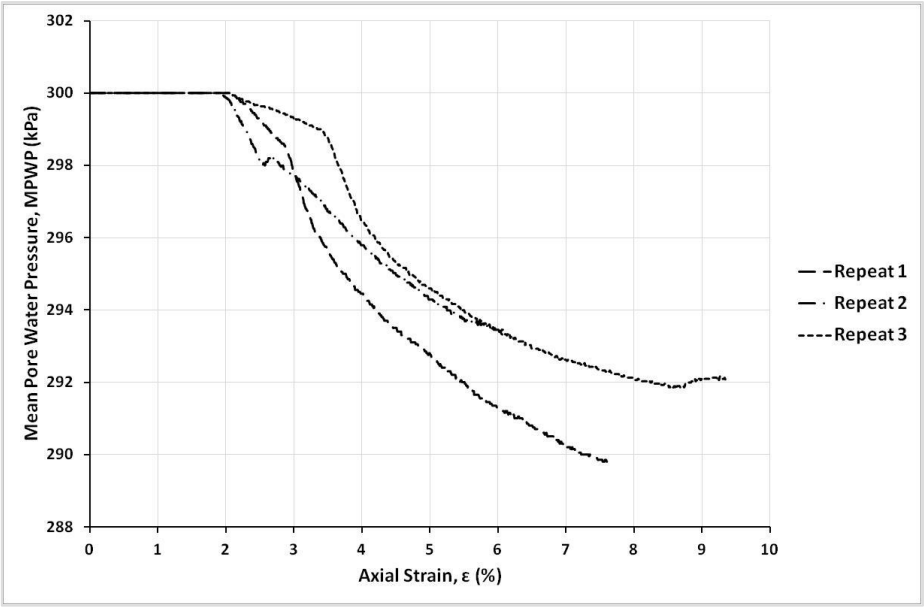

Figure 4.8: MPWP and axial strain relationships at 15 days of curing under a CP of 300 kPa

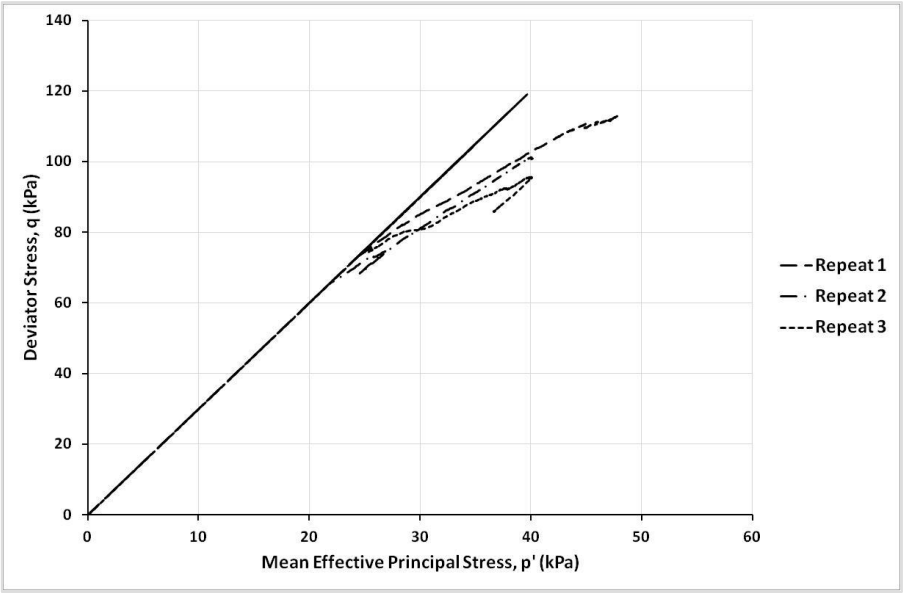

Figure 4.9: Effective stress paths at 15 days of curing under a CP of 300 kPa

4.2.4 VARIATION AT 15 DAYS OF CURING

The q_{peak} and ε_{peak} of the complete data of all TXUU test repeats at 15 days under the different CPs are presented in **Table 4.2**. The q_{peak} at 15 days under TXUU deformation was independent of the CP or σ_3, as it typically varied from 104 kPa to

156 kPa (**Table 4.2**). Similarly, the ε_{peak} varied from 0.6% to 1.2% regardless of the CP (**Table 4.2**).

Table 4.2: Variation of q_{peak} and ε_{peak} at 15 days of curing in TXUU tests

CP (kPa)	No. of Test Repeat	q_{peak}(kPa)	ε_{peak} (%)
50	1	135	0.7
	2	156	1.0
	3	114	1.1
150	1	125	0.6
	2	112	0.8
	3	105	0.8
300	1	119	0.9
	2	115	1.2
	3	104	0.8

4.2.5 MEAN BEHAVIOUR AND VARIATION AT 15 DAYS OF CURING USING THE FILTERED DATA

The mean stress-strain relationships at 15 days of curing under different CPs using the averaged filtered data (presenting a mean stress of the three test repeats at each CP corresponding to the 21 strain points stated earlier) are shown in **Figure 4.10**. These have similar patterns, indicating that the TXUU behaviour at 15 days was independent of CP. Also in **Figure 4.10**, the overall mean stress-strain curve at 15 days of curing is plotted (using the filtered data of all test repeats under different CPs at this age of curing; i.e. 9 test repeats). Note that the 'variation bars' presented are added to illustrate the maximum, minimum and mean deviator stress behaviour observed with each CP.

In addition, the relationships of mean change of MPWP ($\bar{\Delta}$MPWP) with axial strain at 15 days of curing (of the filtered data for all test repeats under different CPs), and the overall mean relationship are plotted in **Figure 4.11**. These show similar patterns for all CPs with dramatic drop of MPWPs at axial strains ranging from 1.3% to 1.7%.

The q_{peak} and ε_{peak} of the filtered data of all TXUU test repeats and their means at 15 days are presented in **Table 4.3**. Their variation (**Table 4.3**) was similar to the variation of the ones of the complete data (**Table 4.2**). The mean peak deviator stress ($\bar{q}_{peak}$) per CP ranged from 108 kPa to 131 kPa, and the overall mean at 15 days was 115 kPa. The mean strain at peak deviator stress ($\bar{\varepsilon}_{peak}$) per CP ranged from 0.7% to 1.0%, and the overall mean at 15 days was 0.7%.

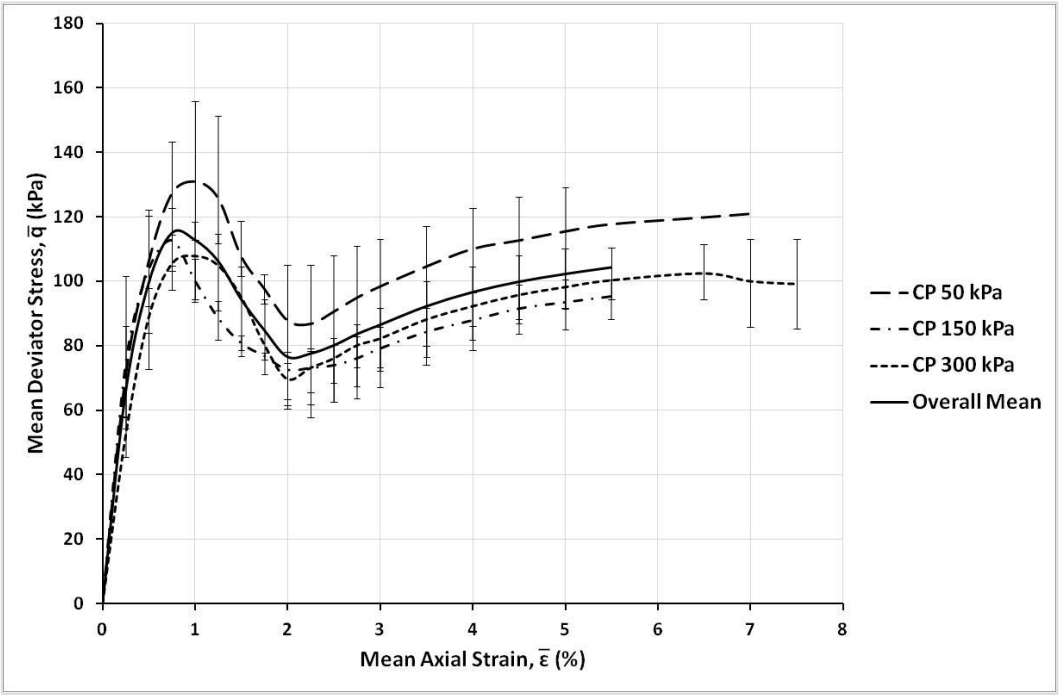

Figure 4.10: Mean stress-strain curves at 15 days of curing under different CPs, using filtered data

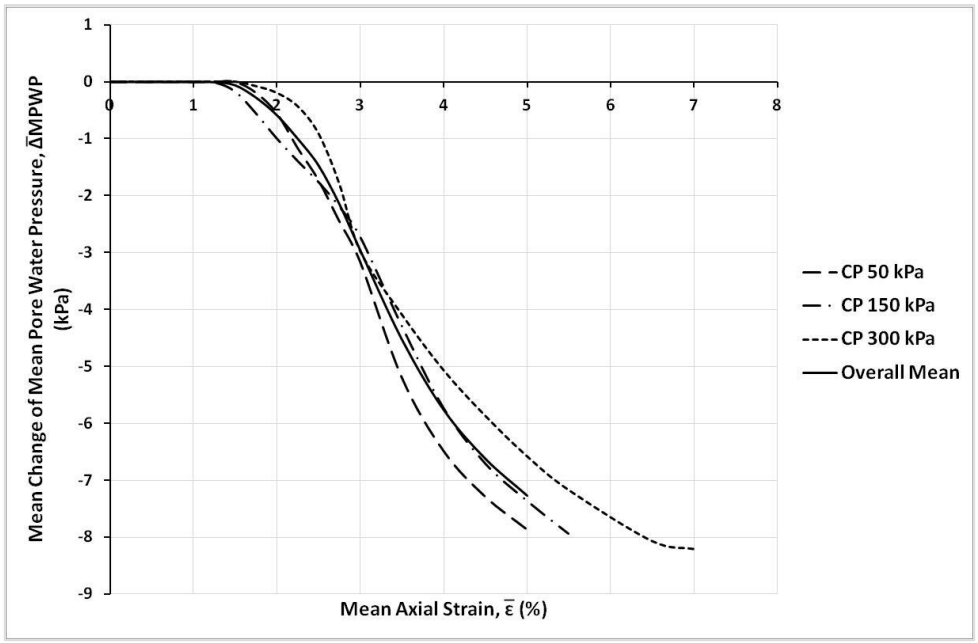

Figure 4.11: Mean Change of MPWP with axial strain at 15 days of curing under different CPs, using filtered data

Table 4.3: Variation of q_{peak} and ε_{peak} of filtered data (i.e. mean trends) at 15 days of curing in TXUU tests under different CPs

CP (kPa)	No. of Test Repeat	q_{peak}(kPa)	ε_{peak} (%)
50	1	135	0.8
	2	156	1.0
	3	113	1.0
	Mean	**131**	**1.0**
150	1	123	0.8
	2	111	0.8
	3	105	1
	Mean	**113**	**0.7**
300	1	118	1.0
	2	115	1.2
	3	104	0.7
	Mean	**108**	**1.0**
Overall Mean at 15 Days		**115**	**0.7**

4.2.6 FAILURE MODES AT 15 DAYS OF CURING

Figure 4.12 shows photos of common failure modes in TXUU tests at 15 days of curing. Cone and vertical cracking, synonymous with concrete behaviour, appear to dominate, with no specimens failing via the classic angled shear plane synonymous with clayey soil specimen failure under TXUU conditions.

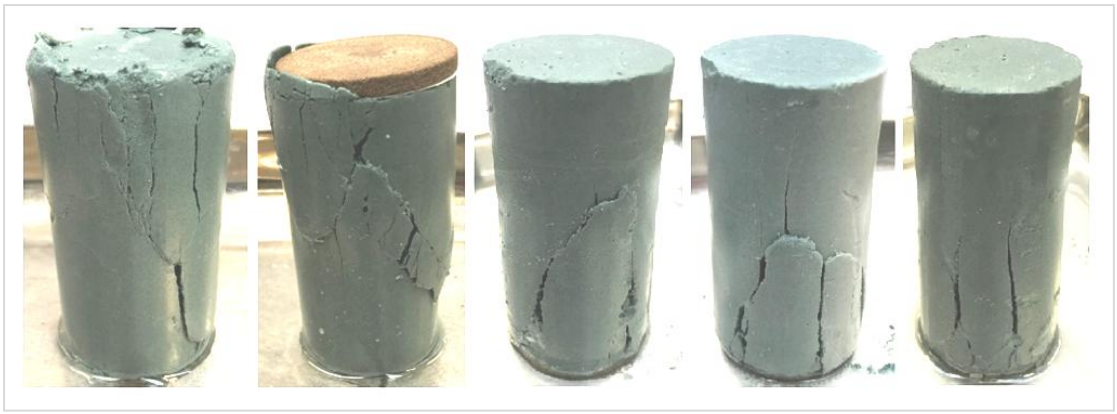

Figure 4.12: Failure modes at 15 days of curing in TXUU tests. Note that the colours were adjusted for better visibility.

4.3 TXUU BEHAVIOUR AFTER 30 DAYS OF CURING

4.3.1 BEHAVIOUR UNDER A CP OF 50 KPA

Figures 4.13, **4.14** and **4.15**, show the stress-strain relationships, MPWP-strain relationships, and effective stress paths in q-p′ field at 30 days of curing under a CP of 50 kPa, respectively. Three repeated tests were undertaken for these conditions using TXUU.

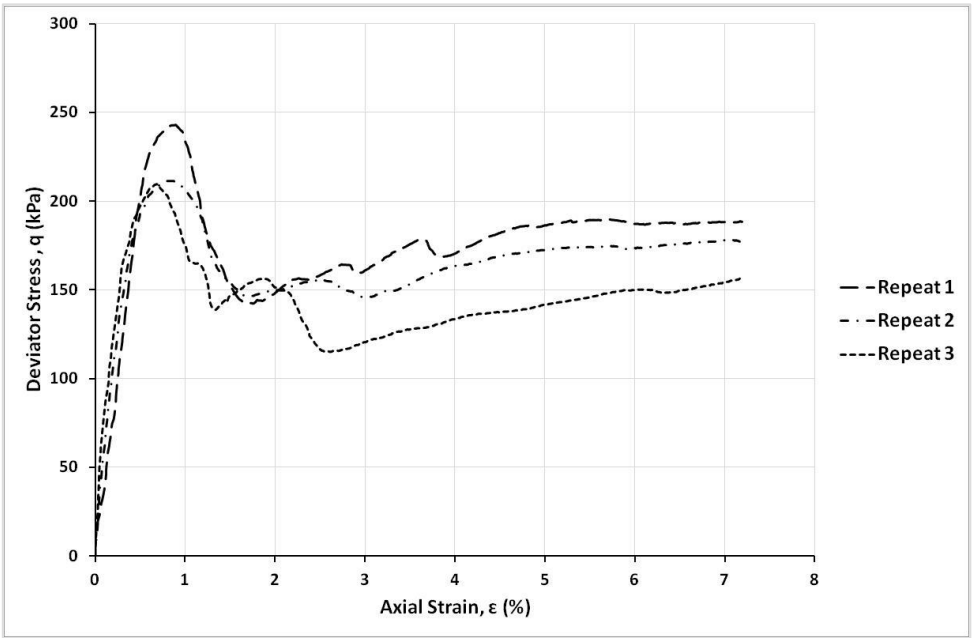

Figure 4.13: Stress-strain behaviour at 30 days of curing under a CP of 50 kPa

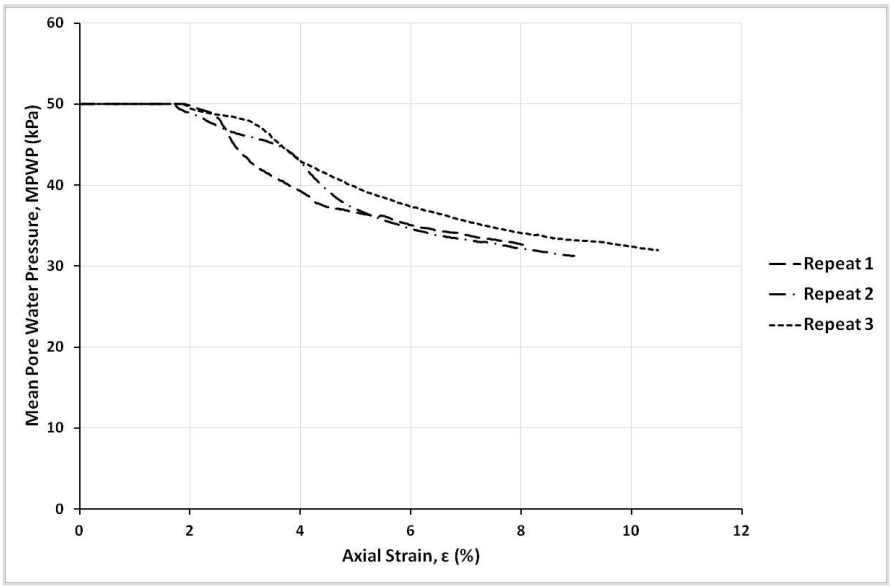

Figure 4.14: MPWP and axial strain relationships at 30 days of curing under a CP of 50 kPa

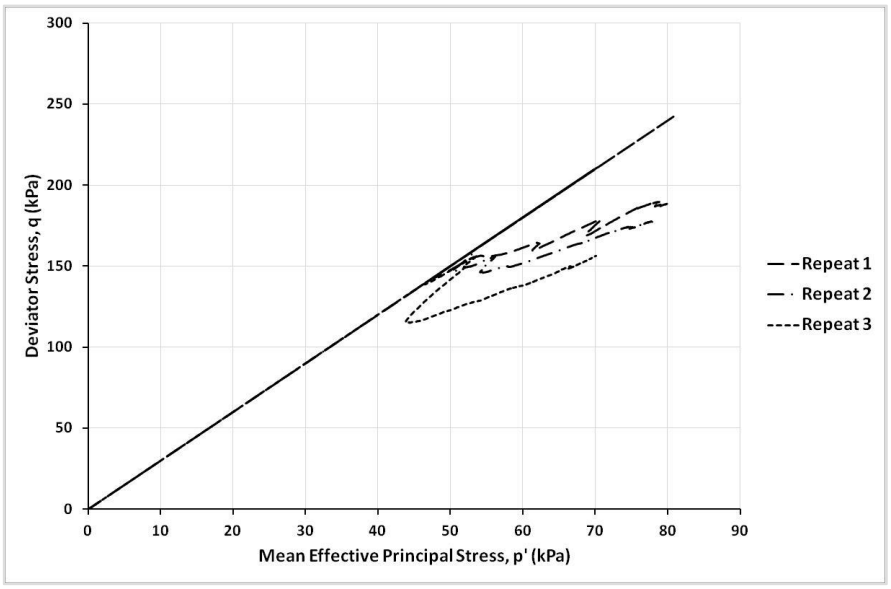

Figure 4.15: Effective stress paths at 30 days of curing under a CP of 50 kPa

4.3.2 BEHAVIOUR UNDER A CP OF 150 KPA

Figures 4.16, **4.17** and **4.18**, show the stress-strain relationships, MPWP-strain relationships, and effective stress paths in q-p′ field at 30 days of curing under a CP of 150 kPa, respectively. Three repeated tests were undertaken for these conditions using TXUU.

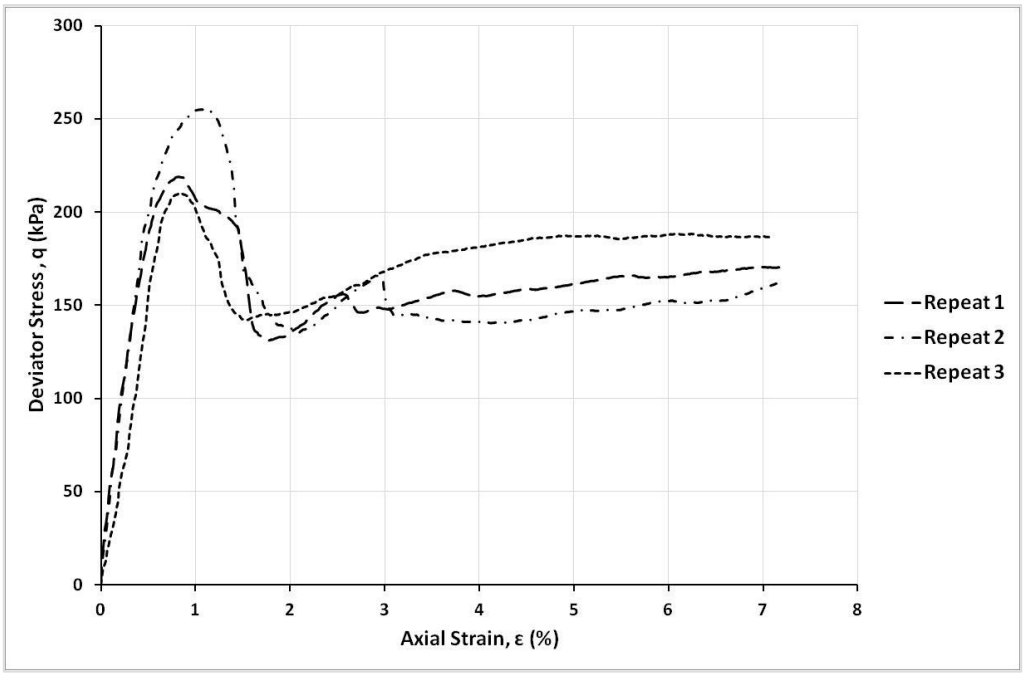

Figure 4.16: Stress-strain behaviour at 30 days of curing under a CP of 150 kPa

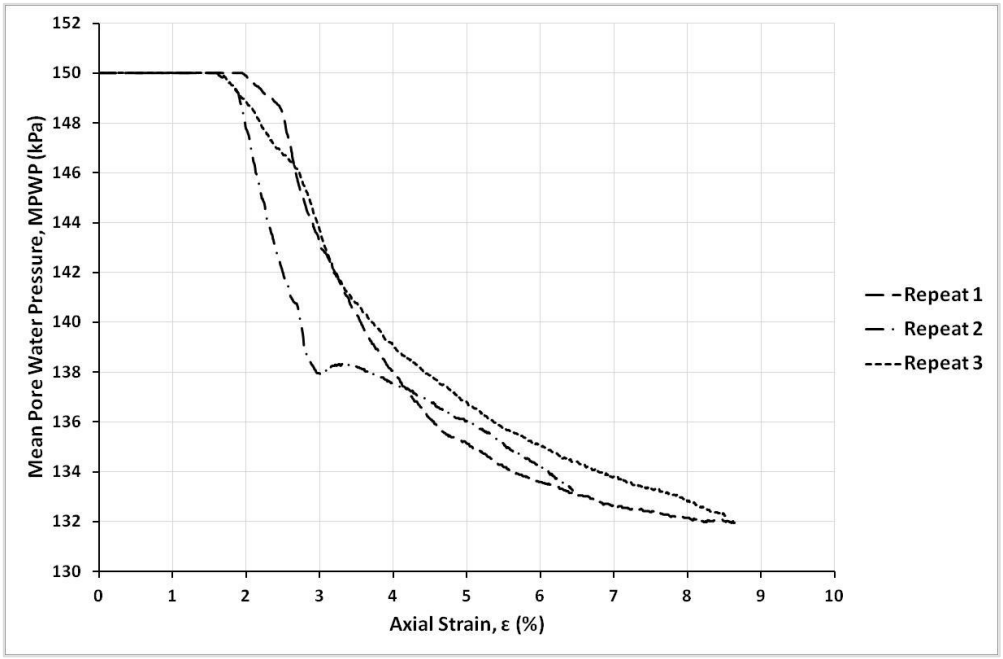

Figure 4.17: MPWP and axial strain relationships at 30 days of curing under a CP of 150 kPa

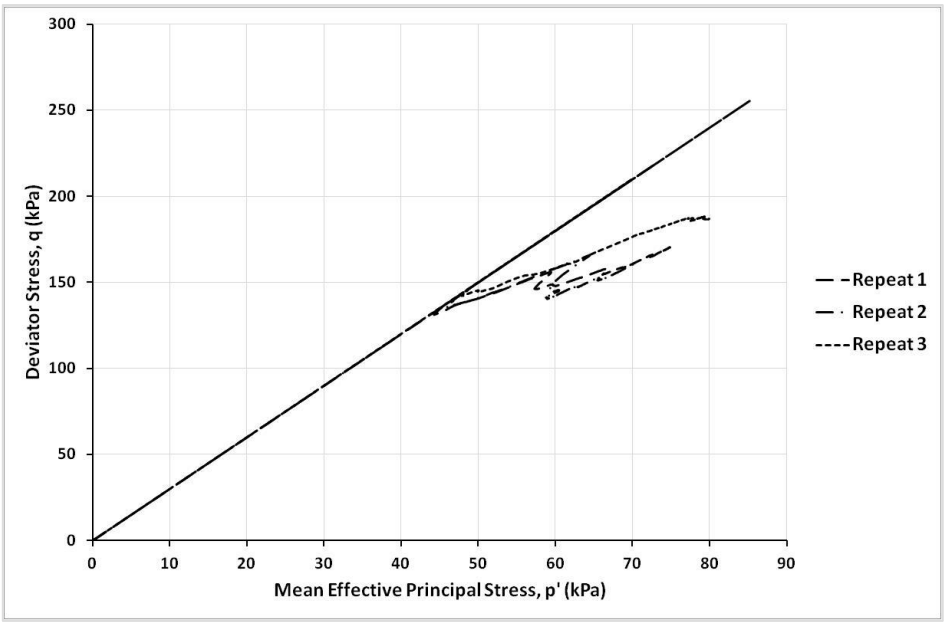

Figure 4.18: Effective stress paths at 30 days of curing under a CP of 150 kPa

4.3.3 BEHAVIOUR UNDER CP OF 300 KPA

Figures 4.19, **4.20** and **4.21**, show the stress-strain relationships, MPWP-strain relationships, and effective stress paths in q-p′ field at 30 days under CP of 300 kPa, respectively. Three repeated tests were undertaken for these conditions using TXUU.

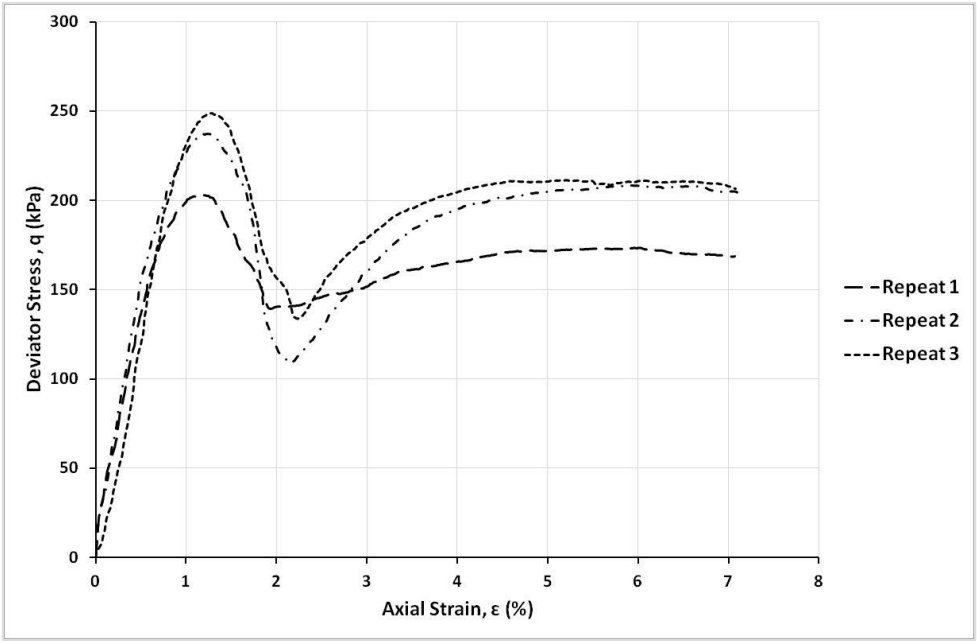

Figure 4.19: Stress-strain behaviour at 30 days of curing under a CP of 300 kPa

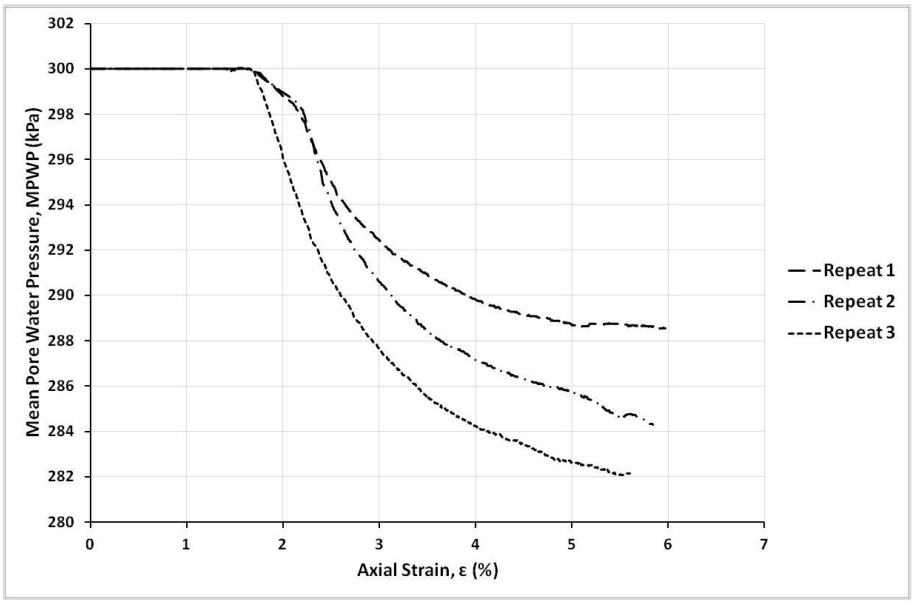

Figure 4.20: MPWP and axial strain relationships at 30 days of curing under a CP of 300 kPa

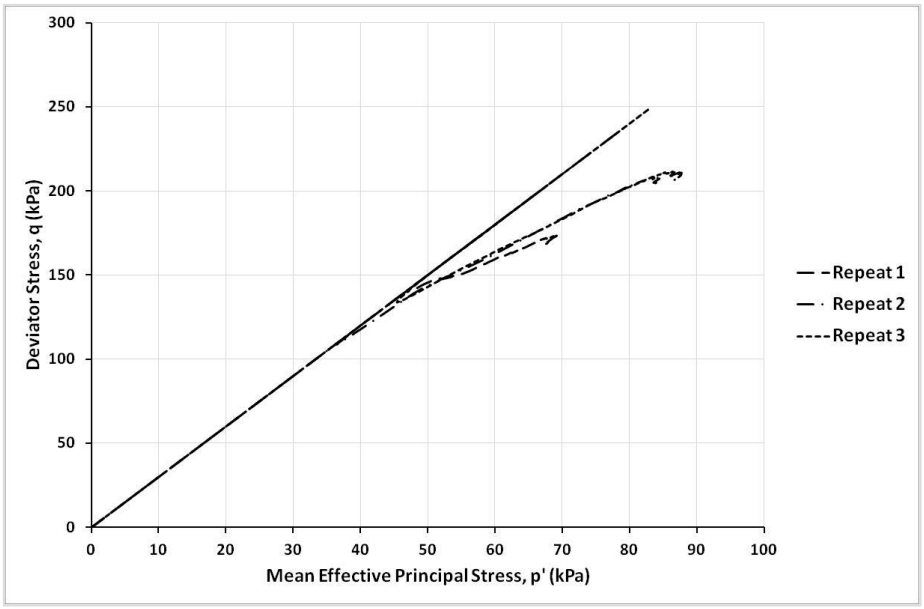

Figure 4.21: Effective stress paths at 30 days of curing under a CP of 300 kPa

4.3.4 VARIATION AT 30 DAYS OF CURING

The q_{peak} and ε_{peak} of the complete data of all TXUU test repeats at 30 days under the different CPs are presented in **Table 4.4**. The q_{peak} at 30 days under TXUU deformation was independent of the CP, as it typically varied from 203 kPa to 256

kPa (**Table 4.4**). Similarly, the ε_{peak} varied from 0.7% to 1.3% regardless of the CP (**Table 4.4**).

Table 4.4: Variation of q_{peak} and ε_{peak} at 30 days of curing in TXUU tests

CP (kPa)	No. of Test Repeat	q_{peak}(kPa)	ε_{peak} (%)
50	1	243	0.9
	2	211	0.8
	3	210	0.7
150	1	219	0.8
	2	256	1.1
	3	210	0.8
300	1	203	1.2
	2	237	1.2
	3	249	1.3

4.3.5 MEAN BEHAVIOUR AND VARIATION AT 30 DAYS OF CURING USING THE FILTERED DATA

The mean stress-strain relationships at 30 days of curing at different CPs using the averaged filtered data (presenting a mean stress of the three test repeats at each CP corresponding to the 21 strain points stated earlier) are shown in **Figure 4.22**. These have similar patterns, indicating that the TXUU behaviour at 30 days was independent of CP. Also in **Figure 4.22**, the overall mean stress-strain curve at 30 days is plotted (using the filtered data of all test repeats under different CPs at this age of curing; i.e. 9 test repeats), and variation bars are outlined to show ranges of deviator stress variation (from maximum to minimum) around the mean stress-strain curve of every CP.

In addition, the relationships of the $\bar{\Delta}$MPWP with axial strain at 30 days of curing (of the filtered data for all test repeats under different CPs), and the overall meanrelationship at 30 days, are plotted in **Figure 4.23**. These show similar patterns for all CPs with dramatic drop of MPWPs at axial strains ranging from 1.5% to 2%.

The q_{peak} and ε_{peak} of the filtered data of all TXUU test repeats and their means at 30 days are presented in **Table 4.5**. Their variation (**Table 4.5**) was similar to the variation of the ones of the complete data (**Table 4.4**). The $\bar{q}_{peak}$ per CP ranged from 218 kPa to 229 kPa, and the overall mean at 30 days was 215 kPa. The $\bar{\varepsilon}_{peak}$ per CP ranged from 0.8% to 1.2%, and the overall mean at 30 days was 1%.

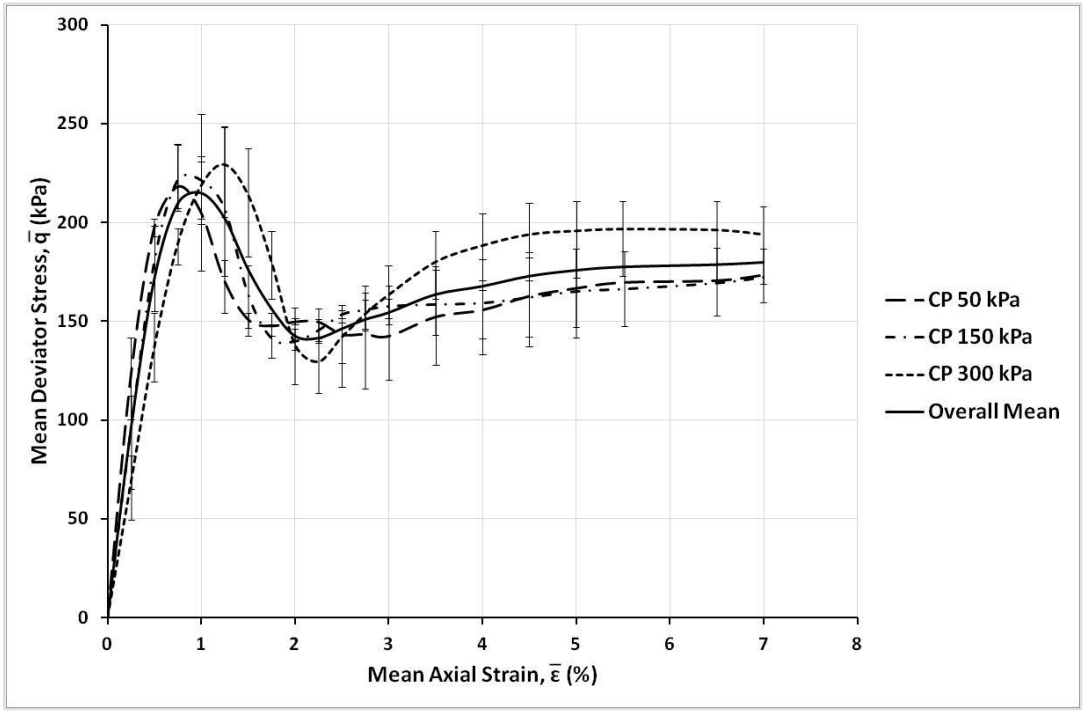

Figure 4.22: Mean stress-strain curves at 30 days of curing under different CPs, using the filtered data

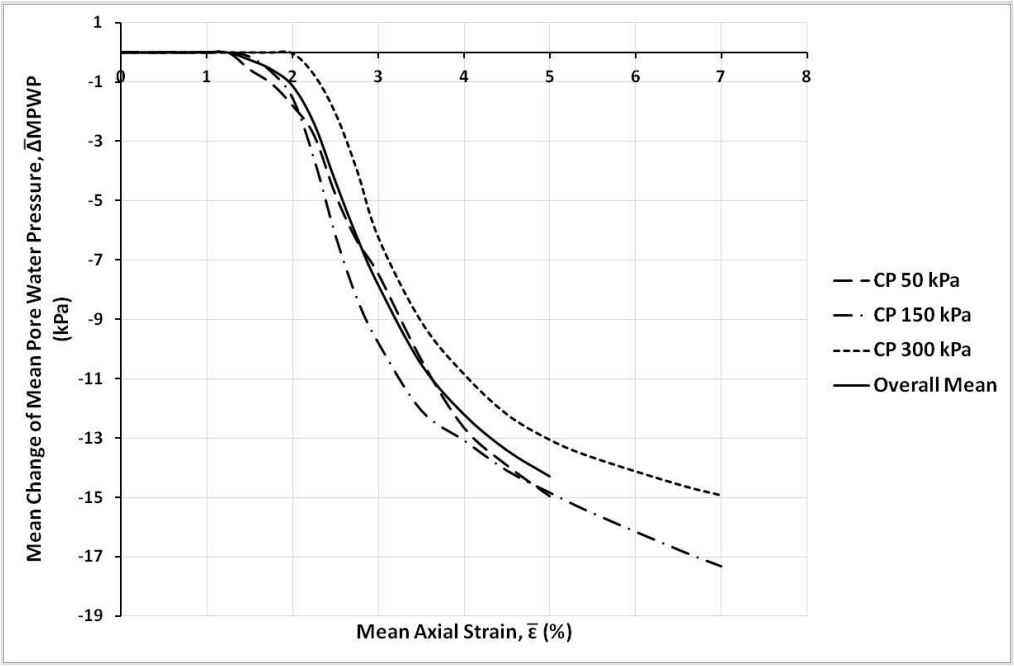

Figure 4.23: Mean Change of MPWP with axial strain at 30 days of curing under different CPs, using filtered data

Table 4.5: Variation of q_{peak} and ε_{peak} of filtered data (i.e. mean trends) at 30 days of curing in TXUU tests under different CPs

CP (kPa)	No. of Test Repeat	q_{peak}(kPa)	ε_{peak} (%)
50	1	239	0.9
	2	210	0.8
	3	206	0.7
	Mean	**218**	**0.8**
150	1	217	0.7
	2	255	1.0
	3	207	0.7
	Mean	**221**	**1.0**
300	1	203	1.2
	2	237	1.2
	3	249	1.2
	Mean	**229**	**1.2**
Overall Mean at 30 Days		**215**	**1.0**

4.3.6 FAILURE MODES AT 30 DAYS OF CURING

Figure 4.24 shows photos of common failure modes in TXUU tests at 30 days of curing. These were similar to the ones occurred at 15 days of curing; i.e. cone and vertical cracking.

Figure 4.24: Failure modes at 30 days of curing in TXUU tests. Note that the colours were adjusted for better visibility.

4.4 TXUU BEHAVIOUR AFTER 60 DAYS OF CURING

4.4.1 BEHAVIOUR UNDER A CP OF 50 KPA

Figures 4.25, **4.26** and **4.27**, show the stress-strain relationships, MPWP-strain relationships, and effective stress paths in q-p′ field at 60 days of curing under a CP of 50 kPa, respectively. Three repeated tests were undertaken for these conditions using TXUU.

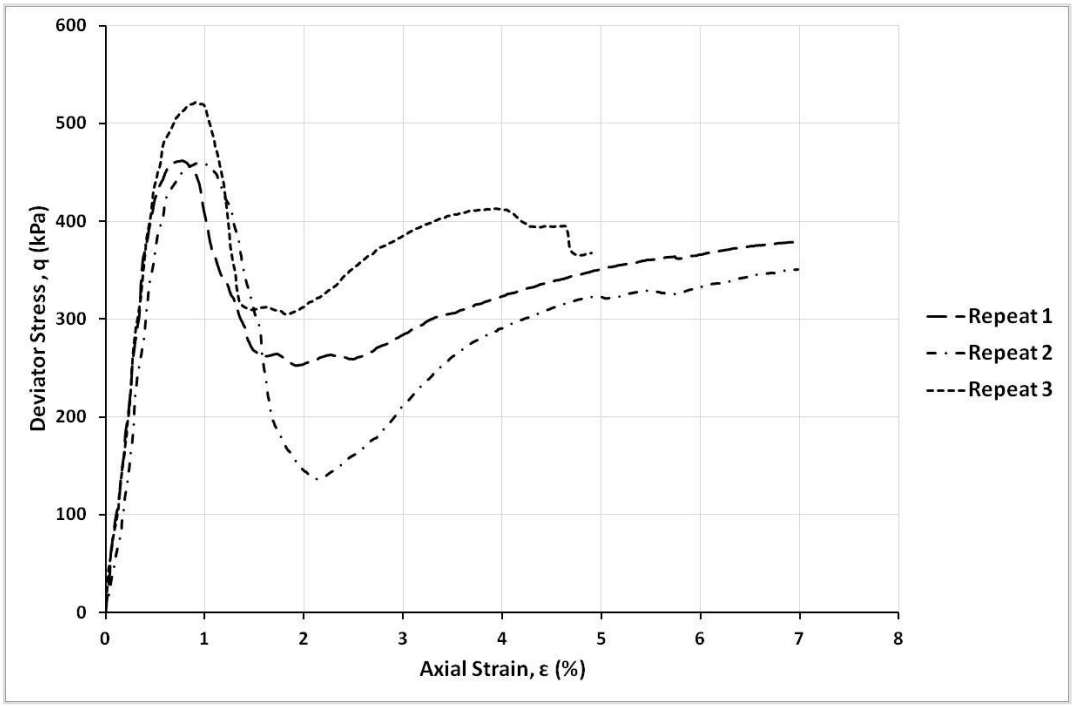

Figure 4.25: Stress-strain behaviour at 60 days of curing under a CP of 50 kPa

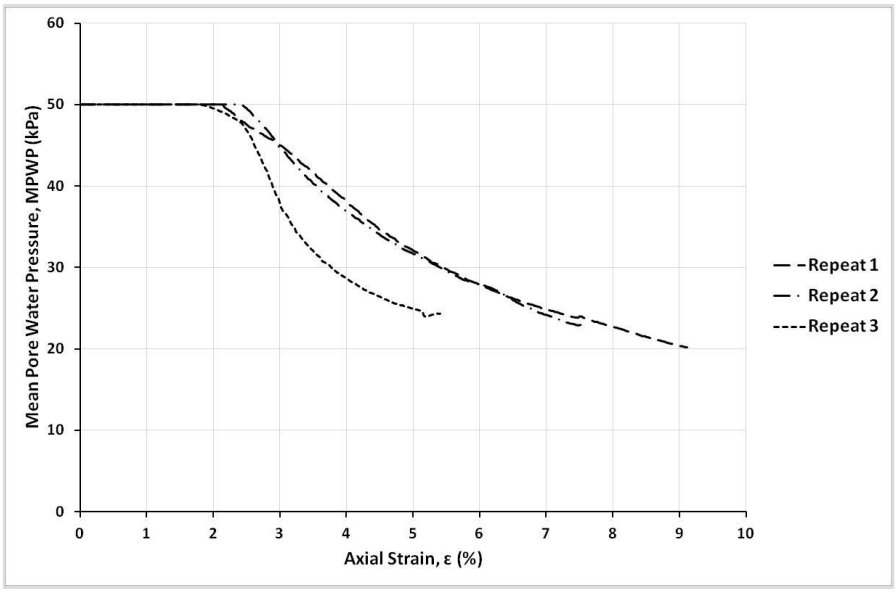

Figure 4.26: MPWP and axial strain relationships at 60 days of curing under a CP of 50 kPa

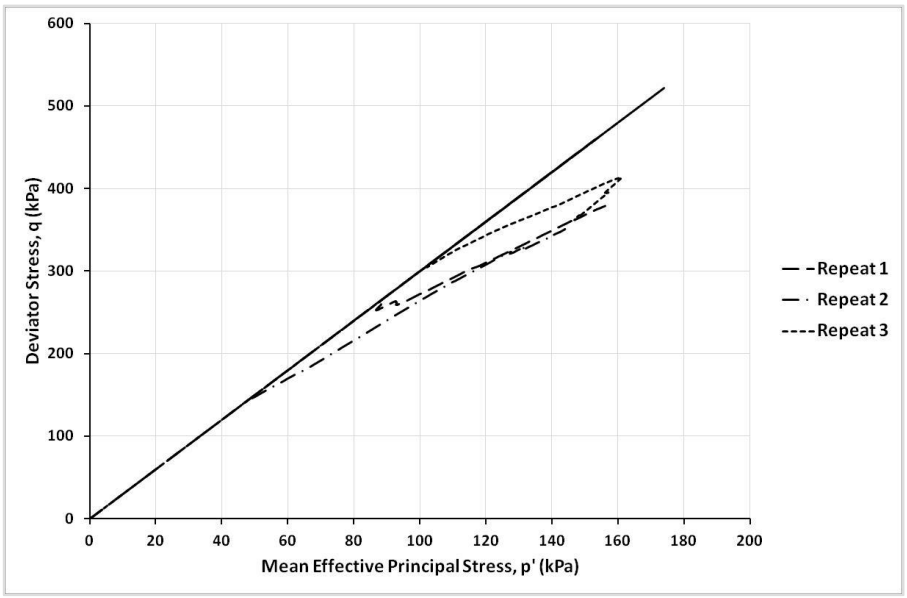

Figure 4.27: Effective stress paths at 60 days of curing under a CP of 50 kPa

4.4.2 BEHAVIOUR UNDER A CP OF 150 KPA

Figures 4.28, **4.29**, and **4.30**, show the stress-strain relationships, MPWP-strain relationships, and effective stress paths in q-p′ field at 60 days of curing under a CP of 150 kPa, respectively. Two repeated tests were undertaken for these conditions using TXUU.

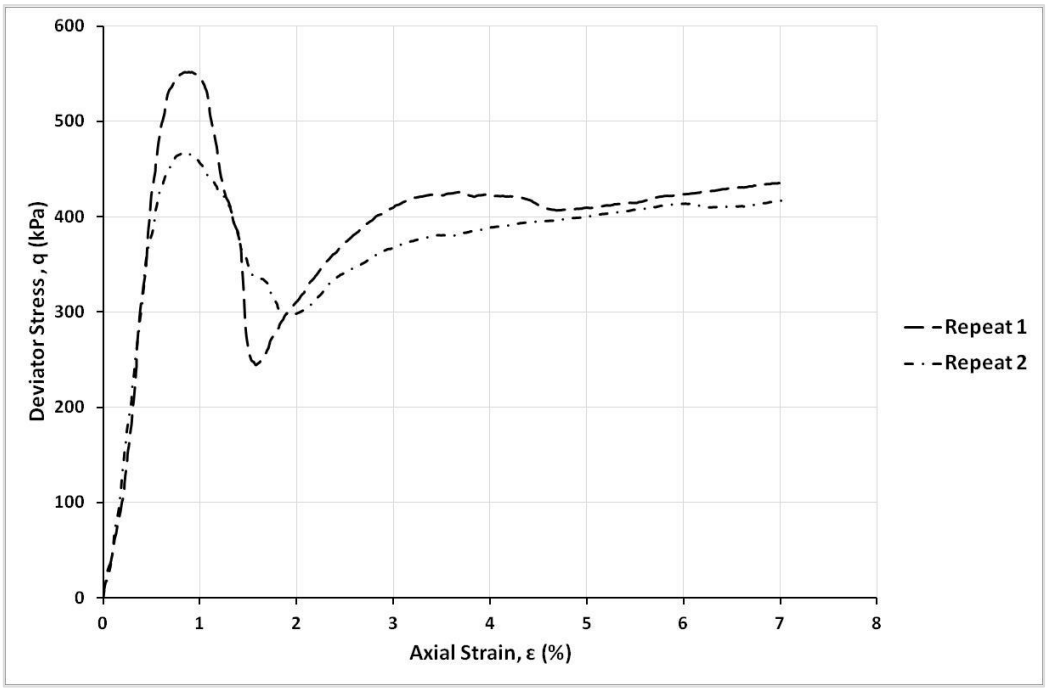

Figure 4.28: Stress-strain behaviour at 60 days of curing under a CP of 150 kPa

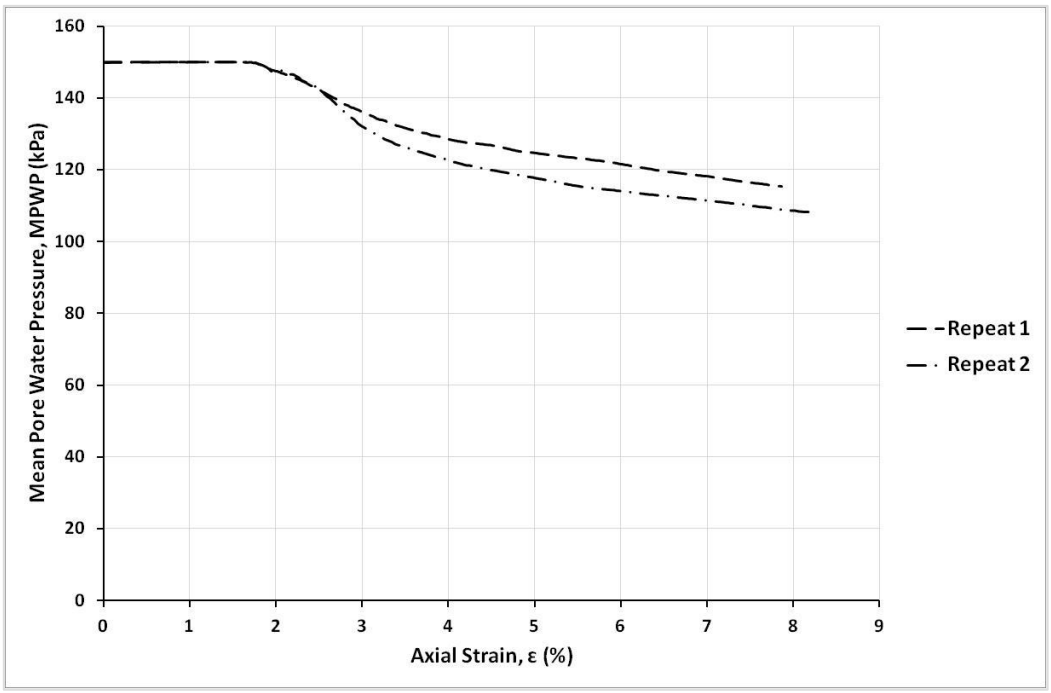

Figure 4.29: MPWP and axial strain relationships at 60 days of curing under a CP of 150 kPa

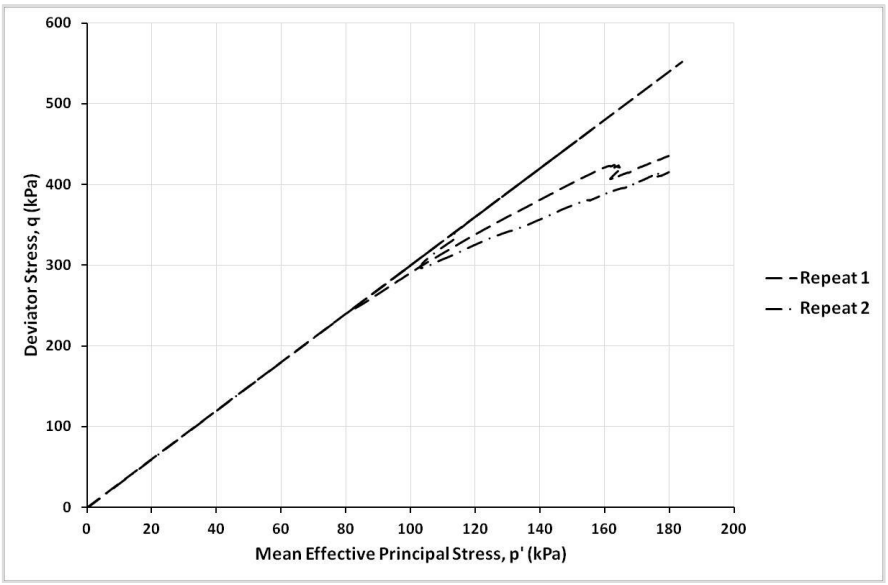

Figure 4.30: Effective stress paths at 60 days of curing under a CP of 150 kPa

4.4.3 BEHAVIOUR UNDER A CP OF 300 KPA

Figures 4.31, **4.32** and **4.33**, show the stress-strain relationships, MPWP-strain relationships, and effective stress paths in q-p′ field at 60 days of curing under a CP of 300 kPa, respectively. Three repeated tests were undertaken for these conditions using TXUU.

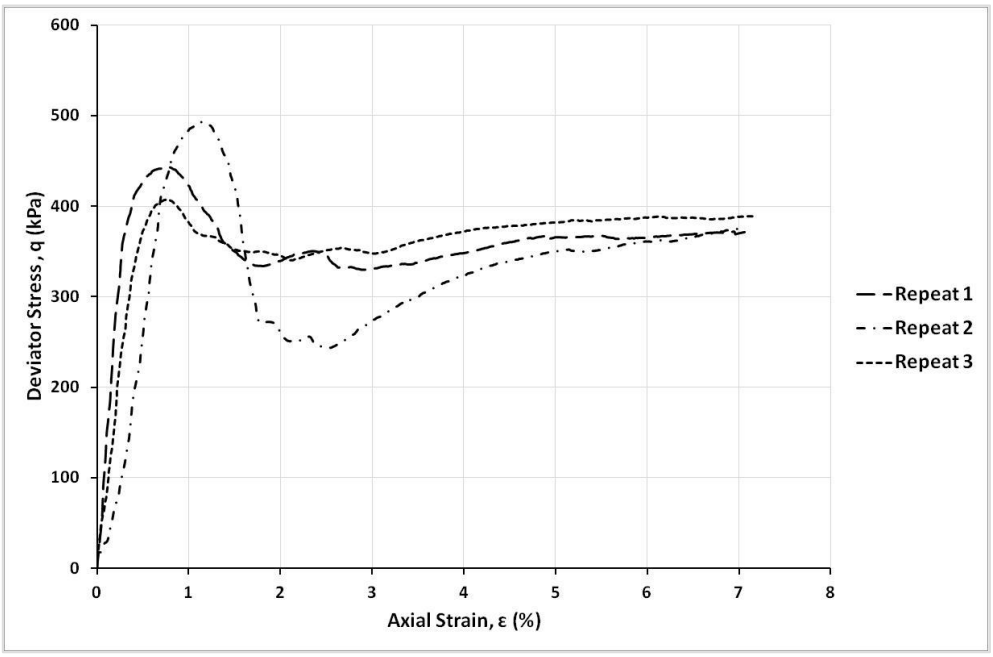

Figure 4.31: Stress-strain behaviour at 60 days of curing under a CP of 300 kPa

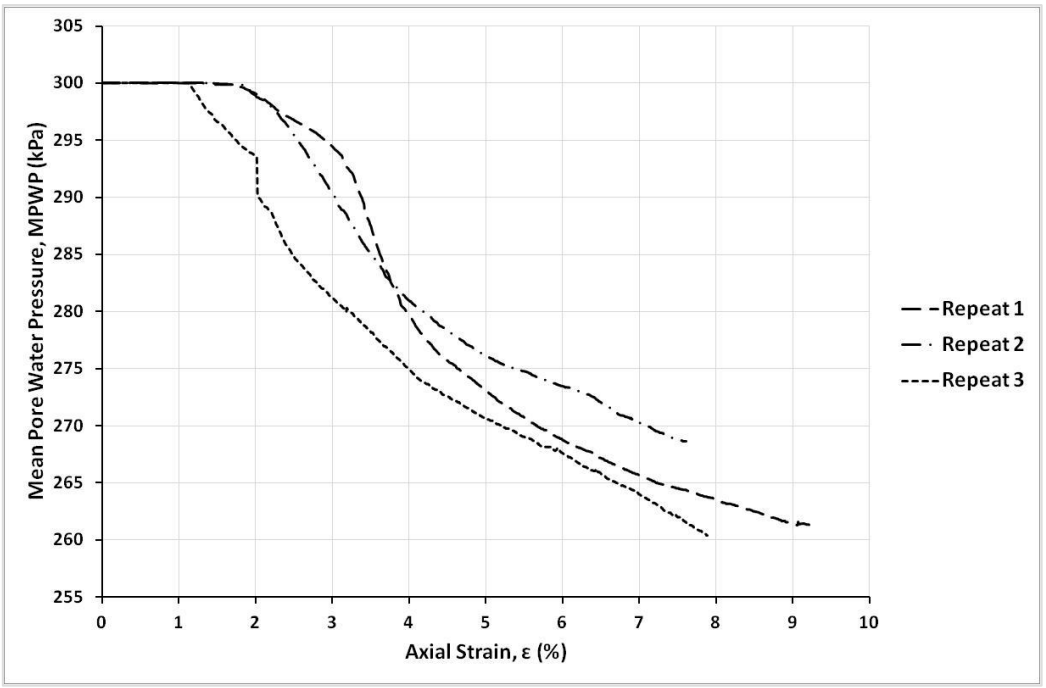

Figure 4.32: MPWP and axial strain relationships at 60 days of curing under a CP of 300 kPa

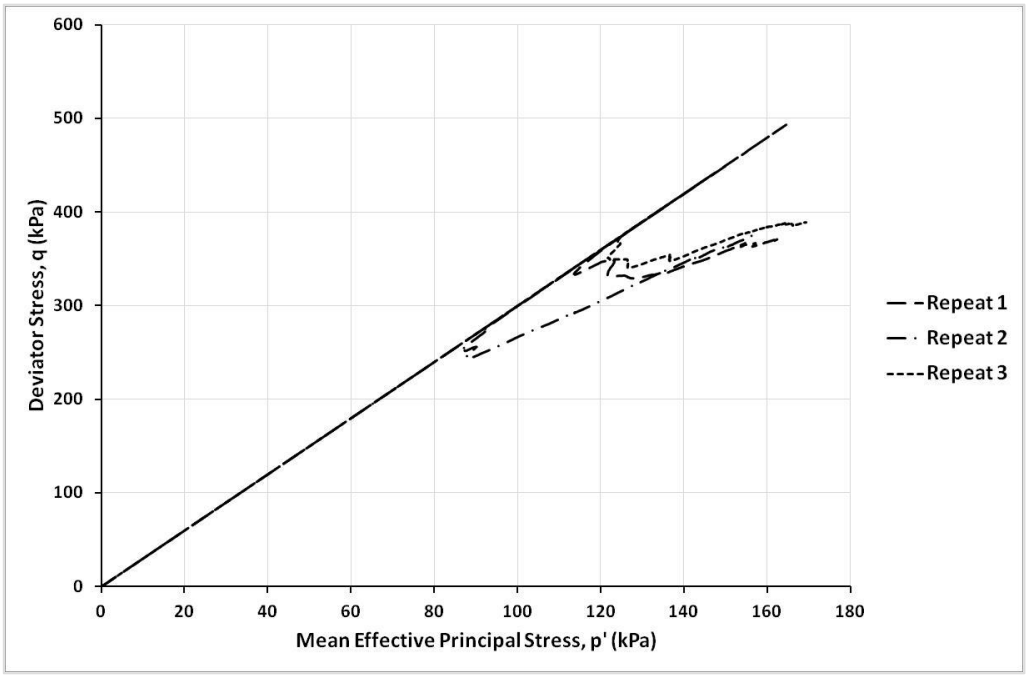

Figure 4.33: Effective stress paths at 60 days of curing under a CP of 300 kPa

4.4.4 VARIATION AT 60 DAYS OF CURING

The q_{peak} and ε_{peak} of the complete data of all TXUU test repeats at 60 days under the different CPs are presented in **Table 4.6**. The q_{peak} at 60 days under TXUU deformation was independent of the CP, as it typically varied from 408 kPa to 552 kPa (**Table 4.6**). Similarly, the ε_{peak} varied from 0.7% to 1.1% regardless of the CP (**Table 4.6**).

Table 4.6: Variation of q_{peak} and ε_{peak} at 60 days of curing in TXUU tests

CP (kPa)	No. of Test Repeat	q_{peak}(kPa)	ε_{peak} (%)
50	1	462	0.8
	2	459	0.9
	3	522	0.9
150	1	552	0.9
	2	467	0.9
300	1	443	0.7
	2	493	1.1
	3	408	0.8

4.4.5 MEAN BEHAVIOUR AND VARIATION AT 60 DAYS OF CURING USING FILTERED DATA

The mean stress-strain relationships at 60 days of curing at the different CPs using the averaged filtered data (presenting a mean stress of the test repeats at each CP corresponding to the 21 strain points stated earlier) are shown in **Figure 4.34**. These have similar patterns, indicating that the TXUU behaviour at 60 days was independent of CP. Also in **Figure 4.34**, the overall mean stress-strain curve at 60 days is plotted (using the filtered data of all test repeats under different CPs at this age of curing; i.e. 8 test repeats), and variation bars are outlined to show ranges of deviator stress variation (from maximum to minimum) around the average stress-strain curve of every CP.

In addition, the relationships of the $\bar{\Delta}$MPWP with axial strain at 60 days of curing (of the filtered data for all test repeats under the different CPs), and the overall mean relationship at 60 days, are plotted in **Figure 4.35**.These show similar patterns for all CPs with dramatic drop of MPWPs at axial strains ranging from 1.3% to 1.8%.

The $\boldsymbol{q_{peak}}$ and $\boldsymbol{\varepsilon_{peak}}$ of the filtered data of all TXUU test repeats and their means at 60 days are presented in **Table 4.7**. Their variation (**Table 4.7**) was similar to the variation of the ones of the complete data (**Table 4.6**). The $\boldsymbol{\bar{q}_{peak}}$ per CP ranged from 430 kPa to 503 kPa, and the overall mean at 60 days was 467 kPa. The $\boldsymbol{\bar{\varepsilon}_{peak}}$ per CP ranged from 0.8% to 1%, and the overall mean at 60 days was 0.8%.

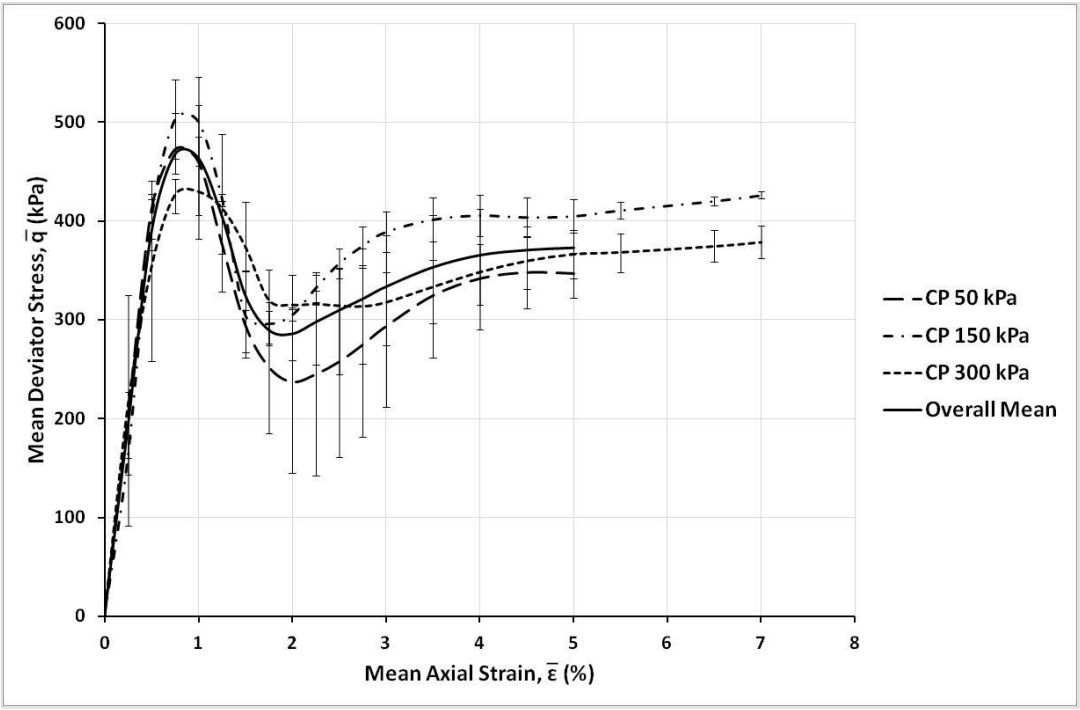

Figure 4.34: Mean stress-strain curves at 60 days of curing under different CPs, using filtered data

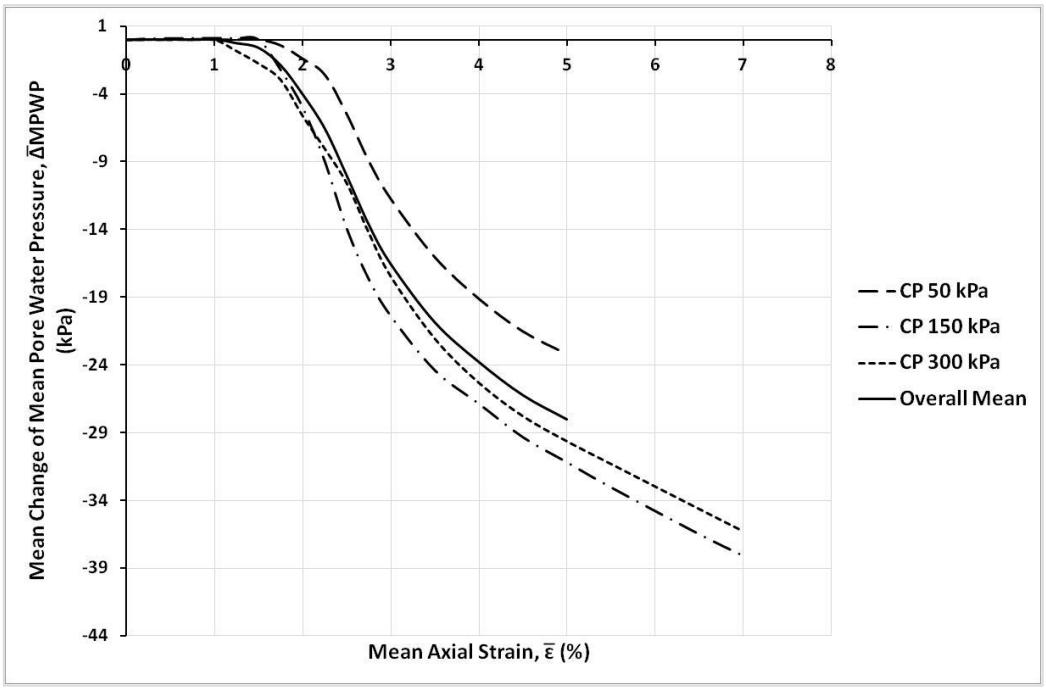

Figure 4.35: Mean Change of MPWP with axial strain at 60 days of curing under different CPs, using filtered data

Table 4.7: Variation of q_{peak} and ε_{peak} of filtered data (i.e. mean trends) at 60 days of curing in TXUU tests under different CPs

CP (kPa)	No. of Test Repeat	q_{peak}(kPa)	ε_{peak} (%)
50	1	462	0.8
	2	458	1.0
	3	517	1.0
	Mean	**473**	**0.8**
150	1	546	1.0
	2	463	0.8
	Mean	**503**	**0.8**
300	1	442	0.7
	2	488	1.1
	3	407	0.8
	Mean	**430**	**1.0**
Overall Mean at 60 Days		**467**	**0.8**

4.4.6 FAILURE MODES AT 60 DAYS

Figure 4.36 shows photos of common failure modes in TXUU tests at 60 days of curing. These were similar to the ones occurred at previous curing ages (15 days and 30 days); i.e. cone and vertical cracking.

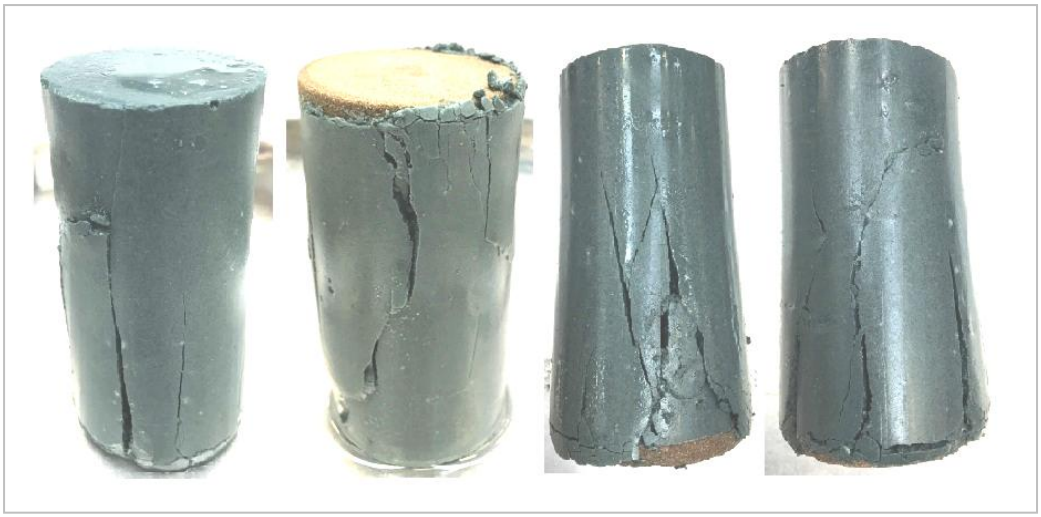

Figure 4.36: Failure modes at 60 days of curing in TXUU tests. Note that the colours were adjusted for better visibility.

4.5 TXUU BEHAVIOUR AFTER 90 DAYS OF CURING

4.5.1 BEHAVIOUR UNDER A CP OF 50 KPA

Figures 4.37, **4.38** and **4.39**, show the stress-strain relationships, MPWP-strain relationships, and effective stress paths in q-p′ field at 90 days of curing under a CP of 50 kPa, respectively. Three repeated tests were undertaken for these conditions using TXUU.

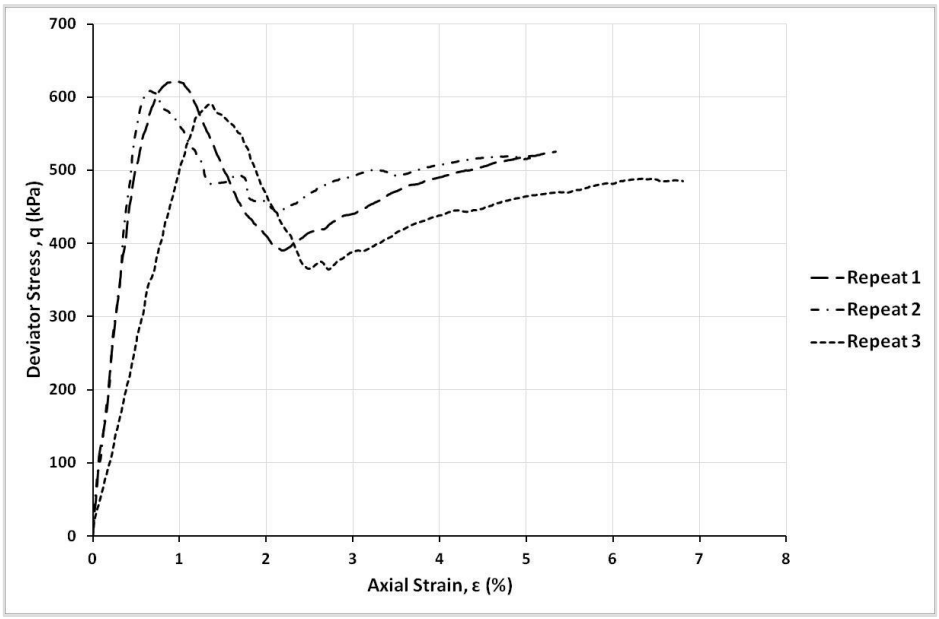

Figure 4.37: Stress-strain behaviour at 90 days of curing under a CP of 50 kPa

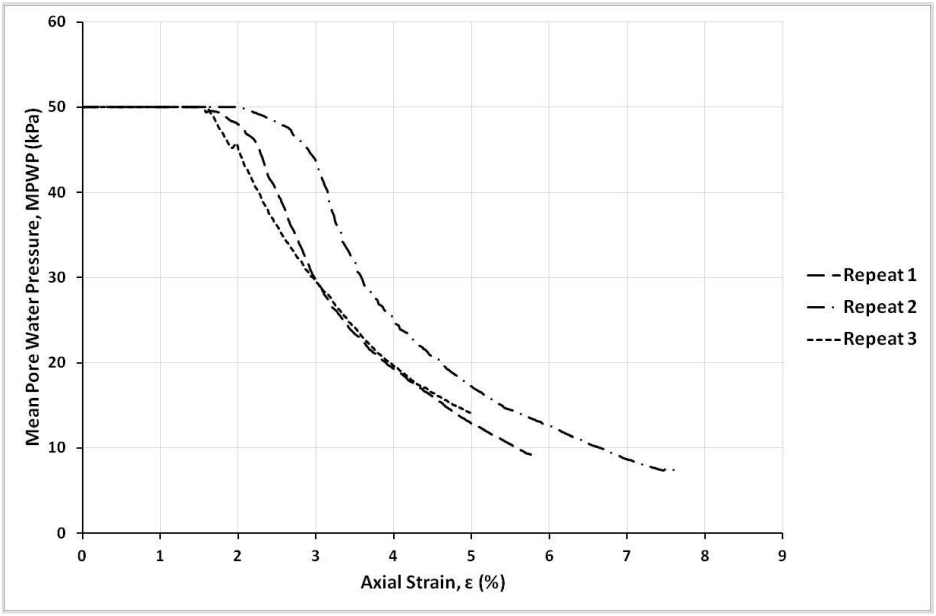

Figure 4.38: MPWP and axial strain relationships at 90 days of curing under a CP of 50 kPa

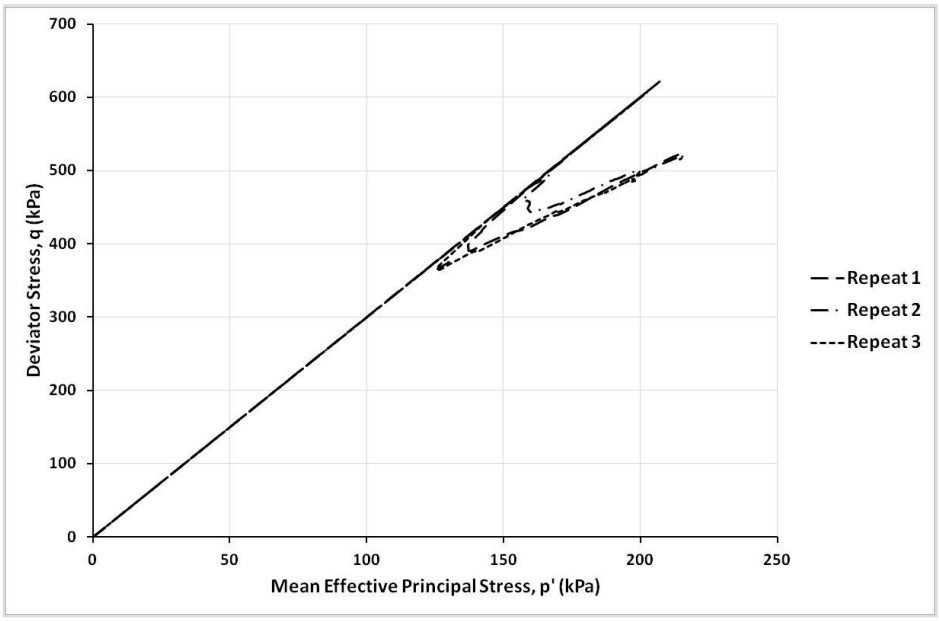

Figure 4.39: Effective stress paths at 90 days of curing under a CP of 50 kPa

4.5.2 BEHAVIOUR UNDER A CP OF 150 KPA

Figures 4.40, **4.41** and **4.42**, show the stress-strain relationships, MPWP-strain relationships, and effective stress paths in q-p′ field at 90 days of curing under a CP of 150 kPa, respectively. Two repeated tests were undertaken for these conditions using TXUU.

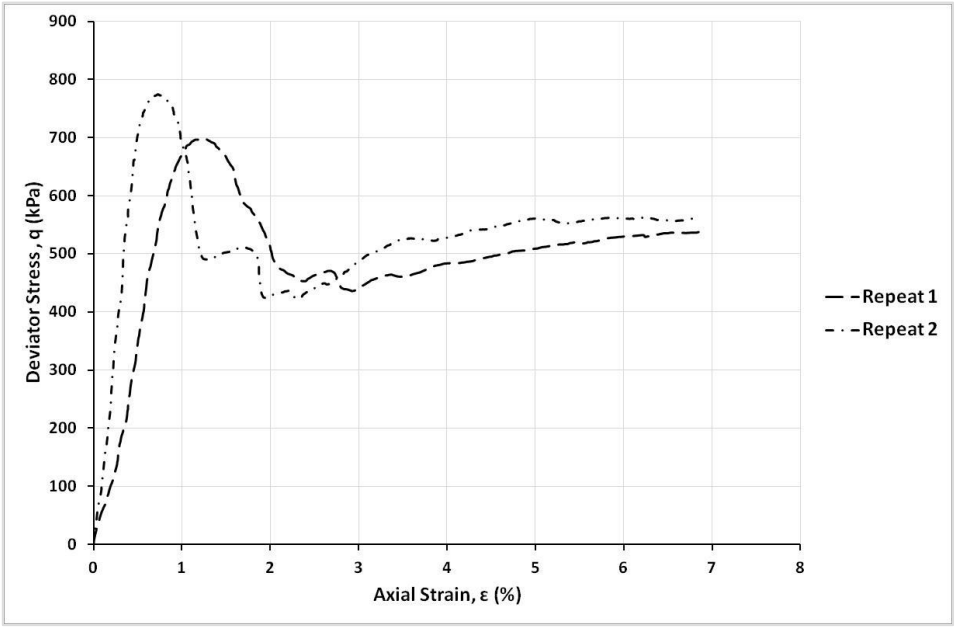

Figure 4.40: Stress-strain behaviour at 90 days of curing under a CP of 150 kPa

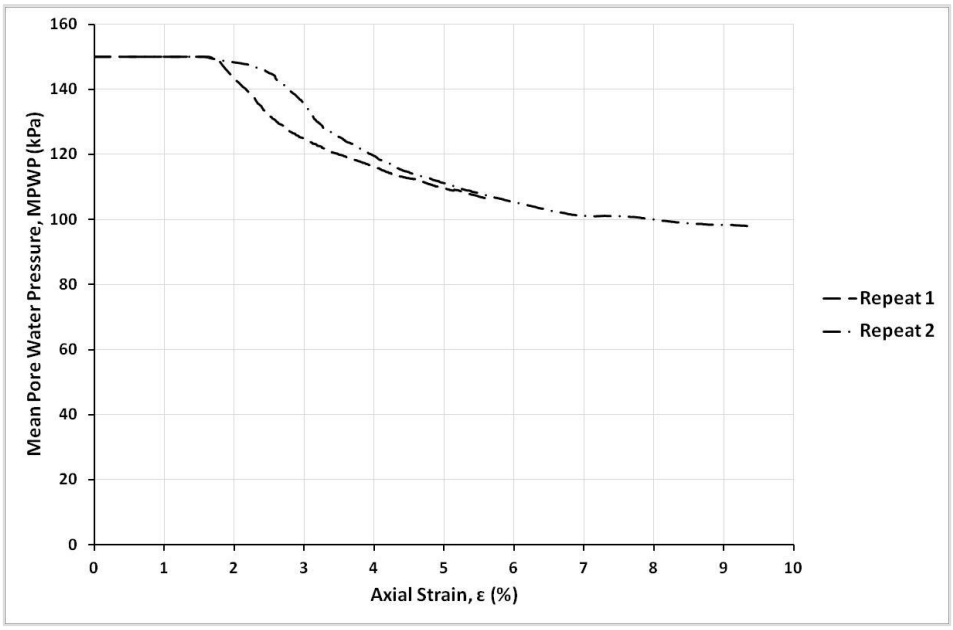

Figure 4.41: MPWP and axial strain relationships at 90 days of curing under a CP of 150 kPa

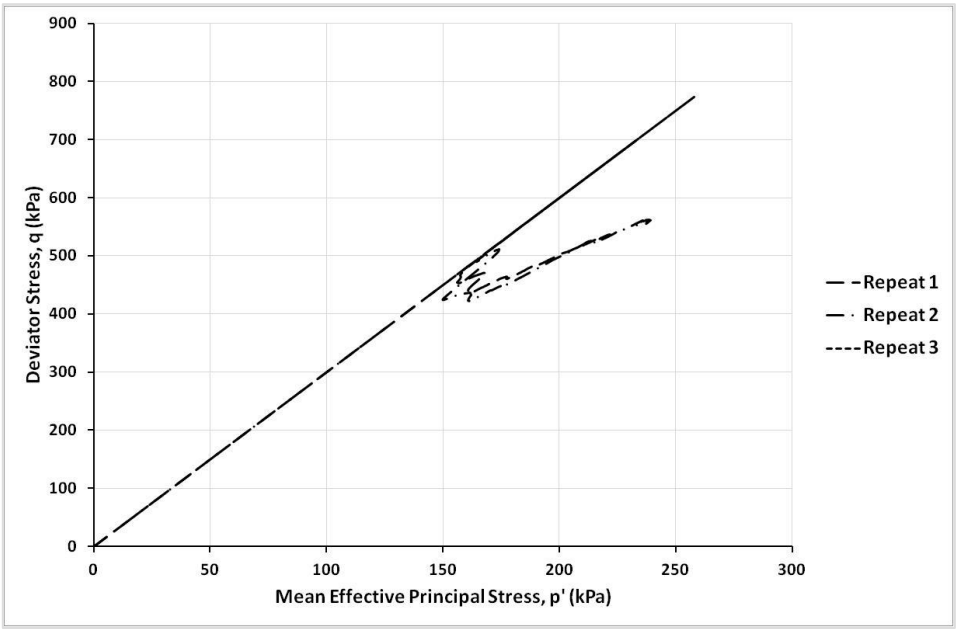

Figure 4.42: Effective stress paths at 90 days of curing under a CP of 150 kPa

4.5.3 BEHAVIOUR UNDER A CP OF 300 KPA

Figures 4.43, **4.44** and **4.45**, show the stress-strain relationships, MPWP-strain relationships, and effective stress paths in q-p′ field at 90 days of curing under a CP of

300 kPa, respectively. Eight repeated tests were undertaken for these conditions using TXUU.

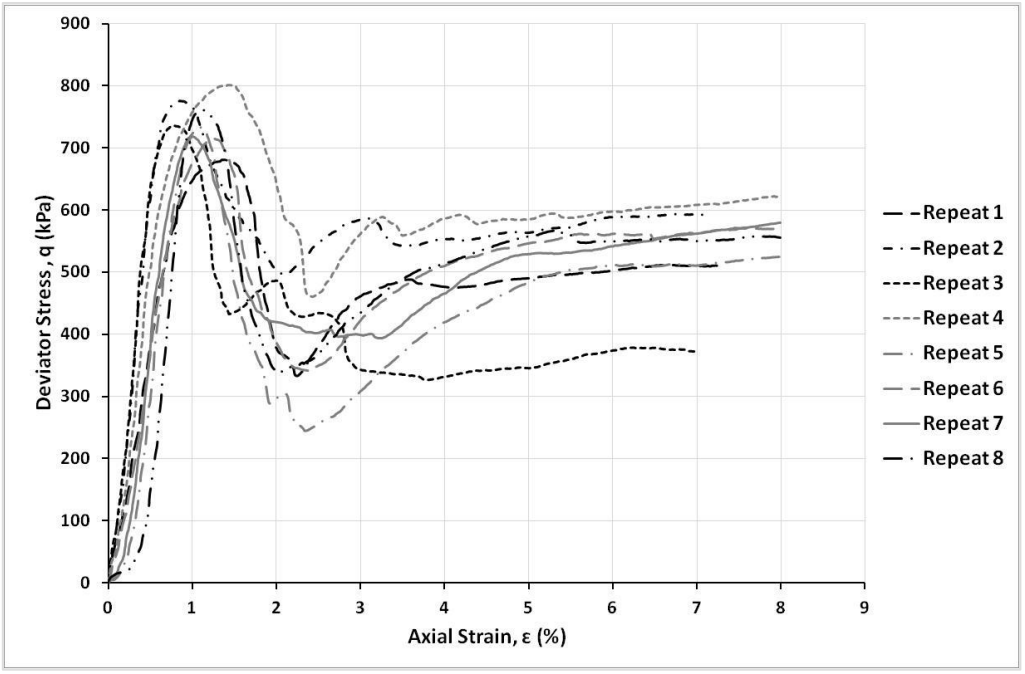

Figure 4.43: Stress-strain behaviour at 90 days of curing under a CP of 300 kPa

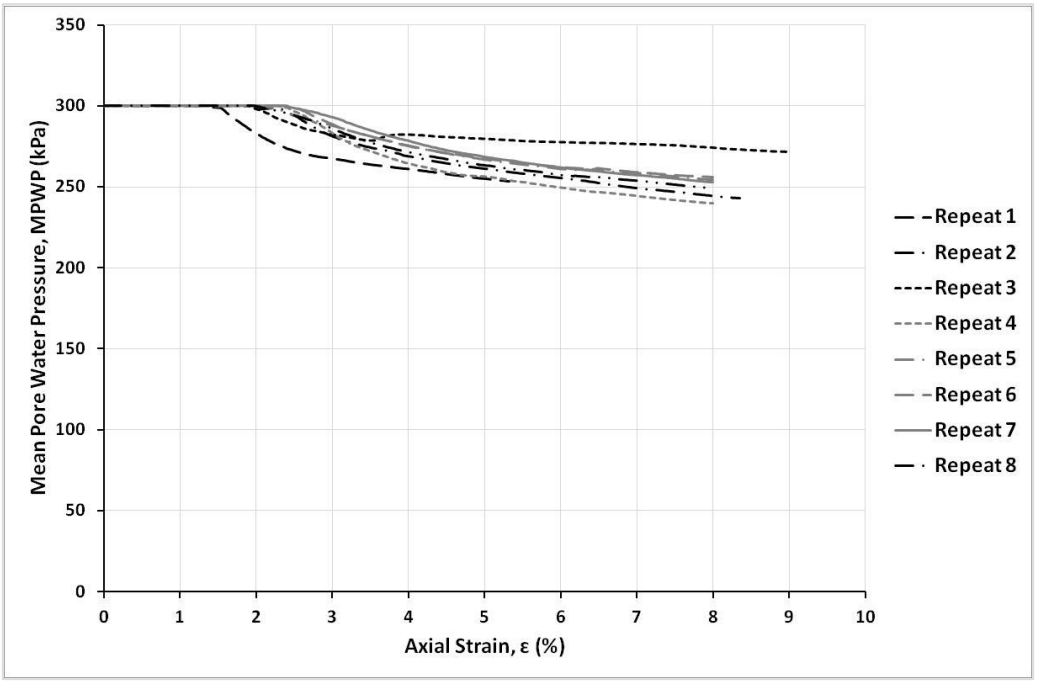

Figure 4.44: MPWP and axial strain relationships at 90 days of curing under a CP of 300 kPa

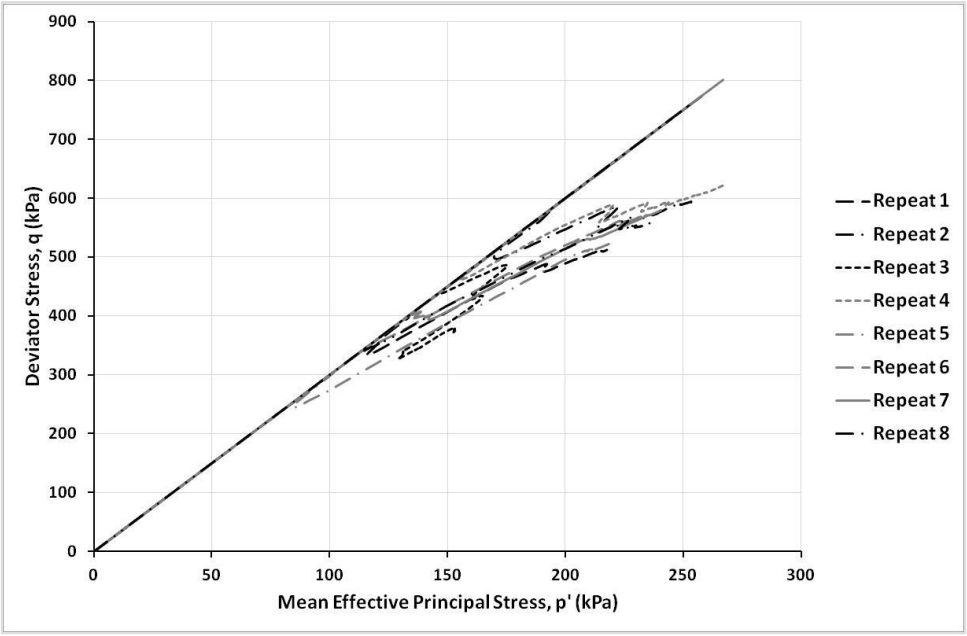

Figure 4.45: Effective stress paths at 90 days of curing under a CP of 300 kPa

4.5.4 VARIATION AT 90 DAYS OF CURING

The q_{peak} and ε_{peak} of the complete data of all TXUU test repeats at 90 days under the different CPs are presented in **Table 4.8**. The q_{peak} at 90 days under TXUU deformation was independent of the CP, as it typically varied from 591 kPa to 801 kPa (**Table 4.8**). Similarly, the ε_{peak} varied from 0.7% to 1.4% regardless of the CP (**Table 4.8**).

Table 4.8: Variation of q_{peak} and ε_{peak} at 90 days of curing in TXUU tests

CP (kPa)	No. of Test Repeat	q_{peak}(kPa)	ε_{peak} (%)
50	1	622	0.9
	2	609	0.7
	3	591	1.4
150	1	698	1.2
	2	775	0.7
300	1	681	1.4
	2	775	0.9
	3	736	0.8
	4	801	1.4
	5	733	1.1
	6	716	1.2
	7	718	1.0
	8	761	1.1

4.5.5 MEAN BEHAVIOUR AND VARIATION AT 90 DAYS OF CURING USING THE FILTERED DATA

The mean stress-strain relationships at 90 days of curing at different CPs using the averaged filtered data (presenting a mean stress of the test repeats at each CP corresponding to the 21 strain points stated earlier) are shown in **Figure 4.46**. These have similar patterns, indicating that the TXUU behaviour at 90 days was independent of CP. Also in **Figure 4.46**, the overall mean stress-strain curve at 90 days is plotted (using the the filtered data of all test repeats under different CPs at this age; i.e. 13 test repeats), and variation bars are outlined to show ranges of deviator stress variation (from maximum to minimum) around the mean stress-strain curve of every CP.

In addition, the relationships of $\bar{\Delta}$MPWP with axial strain at 90 days (of the filtered data for all test repeats under different CPs), and the overall mean relationship at 90 days, are plotted in **Figure 4.47**. These show similar patterns for all CPs with dramatic drop of MPWPs at axial strains ranging from 1.3% to 1.5%.

The q_{peak} and ε_{peak} of the filtered data of all TXUU test repeats and their means at 90 days are presented in **Table 4.9**. Their variation (**Table 4.9**) was similar to the variation of the ones of the complete data (**Table 4.8**). The $\bar{q}_{peak}$ per CP ranged from 560 kPa to 716 kPa, and the overall mean at 90 days was 653 kPa. The $\bar{\varepsilon}_{peak}$ per CP was 1%, and the overall mean at 90 days was also 1%.

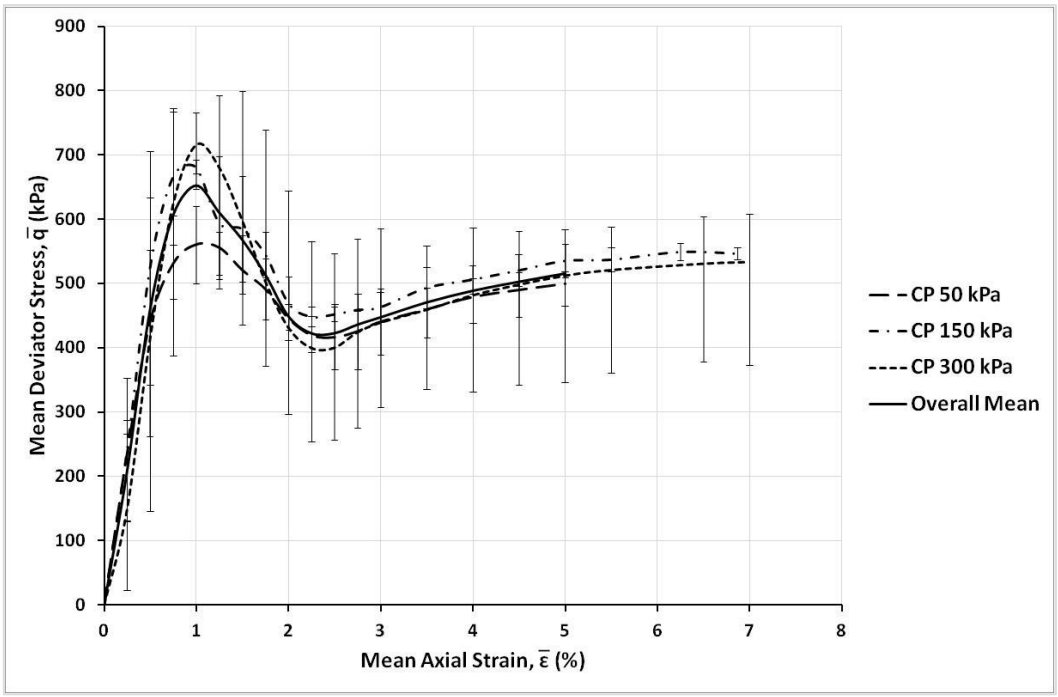

Figure 4.46: Average stress-strain curves at 90 days of curing under different CPs, using filtered data

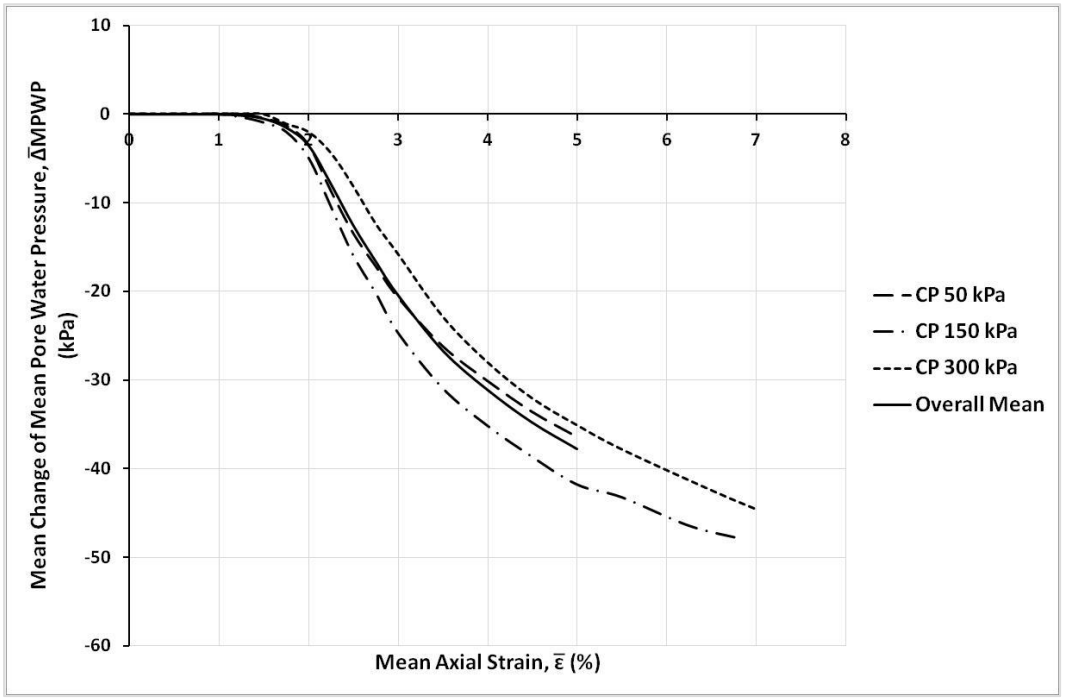

Figure 4.47: Mean Change of MPWP with axial strain at 90 days of curing under different CPs, using filtered data

Table 4.9: Variation of q_{peak} and ε_{peak} of filtered data (i.e. mean trends) at 90 days of curing in TXUU tests

CP (kPa)	No. of Test Repeat	q_{peak}(kPa)	ε_{peak} (%)
50	1	621	1.0
	2	601	0.7
	3	581	1.3
	Mean	**560**	**1.0**
150	1	697	1.2
	2	773	0.8
	Mean	**681**	**1.0**
300	1	676	1.3
	2	767	0.7
	3	735	0.8
	4	800	1.5
	5	723	1.0
	6	716	1.2
	7	718	1.0
	8	747	1.2
	Mean	**716**	**1.0**
Overall Mean at 90 Days		**653**	**1.0**

4.5.6 FAILURE MODES AT 90 DAYS OF CURING

Figure 4.48 shows photos of common failure modes in TXUU tests at days of curing. These were similar to the ones occurred at previous curing ages (15 days to 60 days); i.e. cone and vertical cracking.

Figure 4.48: Failure modes at 90 days of curing in TXUU tests. Note that the colours were adjusted for better visibility.

4.6 SUMMARY

The results of TXUU deformation are presented in this chapter. The undrained behaviour of CB material in TXUU tests was examined under different cell pressures (i.e. 50 kPa, 150 kPa, and 300 kPa). The TXUU behaviour has been justified to be independent of CP, strain rate, and curing age. Furthermore, the TXUU behaviour (i.e. brittle strain-softening) has been justified to be broadly similar to the behaviour exhibited in TXCU tests (reported in previous research as reviewed in **Chapter 2**). The general TXUU behaviour that was exhibited at the different curing ages (as presented in this chapter) is characterised in **Chapter 6**.

The undrained peak strength of CB specimens (q_{peak}) has been justified to increase with increasing curing ages from 15 days to 90 days. The mean undrained peak strength ($\bar{q}_{peak}$) increased from 115 kPa after 15 days of curing to 607 kPa after 90 days of curing. However, the mean axial strain at undrained peak strength ($\bar{\varepsilon}_{peak}$) did not appear to have a clear relationship with curing age, as it insignificantly varied from 0.7% after 15 days of curing to 1% after 90 days of curing. Further discussion on the TXUU behaviour is given in **Chapter 6**.

The failure modes experienced by CB specimens in TXUU tests was observed to be similar regardless of the CP, strain rate, and curing age. The failure modes observed (post-peak strength) were either through propagation of vertical tension cracks, or combination of vertical and inclined cracks forming single or multiple wedges at the top or bottom of the test specimens.

As the hardened CB material is known to be physically variable by its nature as being made from slurry, the undrained mechanical properties of the CB material was found to vary due to variation in its material properties (e.g. water content and void ratio).

This variation has been justified to fall within a relatively narrow range in this study (based on at least seven TXUU test repeats per curing age) as further evaluated in **Chapter 6**.

CHAPTER 5
RESULTS (PART B)

HYDRAULIC CONDUCTIVITY OF CB SPECIMENS AFTER 90 DAYS OF CURING USING CONSTANT FLOW METHOD IN FLEXIBLE-WALL TRIAXIAL CELL AND SINGLE-STAGE TXUU TESTING METHOD

5.1 INTRODUCTION

The hydraulic conductivity results of intact and deformed CB specimens at 90 days of curing using constant flow method in flexible-wall triaxial cell under σ'_3 of 30 kPa, are presented in this chapter. The combined response of deformation and hydraulic conductivity are not considered together herein. This is considered in the Discussion chapter (**Chapter 6**), as is the implications of the observed behaviour during testing.

As noted in **Section 3.8.3**, the main testing of CB hydraulic conductivity was chosen to be at 90 days of curing, as steady state flow condition could not be confirmed before reaching this curing duration. Also, the σ'_3 was chosen to be as low as 30 kPa to avoid considerable consolidation that would alter the structure of CB material; yet provide the required sealed conditions for triaxial hydraulic conductivity measurement in the flexible-wall cell (i.e. prevent circumferential seepage between the membrane and specimen, see **Section 3.5.1.2**).

The CB hydraulic conductivity at an intact state (i.e. specimens were not exposed to any deformation) was determined using the constant flow method as explained in

Section 3.5.2. Also, it was measured after exposing the CB specimens to different amounts of TXUU deformation using single-stage TXUU with constant flow method (explained in **Section 3.8**). The tested states of deformation corresponds to certain axial strain limits that were chosen to ensure that the hydraulic conductivity of the CB specimens was assessed either prior to/or after the $\bar{\varepsilon}_{peak}$ at 90 days of curing (determined through TXUU testing), as previously explained in **Section 3.8.5**). Furthermore, at the end of the main testing period, the hydraulic conductivity was also measured just after the particular q_{peak} and ε_{peak} (i.e. peak state parameters) following the same testing procedure for hydraulic conductivity measured just after the $\bar{\varepsilon}_{peak}$ at 90 days of curing explained in **Section 3.8.6**. This was additional to the measurements conducted at the primary strain limits (described previously in **Section 3.8.5**) to provide specific information about the change of the hydraulic conductivity just after exceeding the particular peak state of a given CB specimen (i.e. after their particular ε_{peak} by 0.2% strain). This was possible to be measured for two CB specimens only as being the remaining number of specimens at 90 days of curing after completing the main tests scheduled during the methodology development period.

Table 5.1 shows the count of hydraulic conductivity tests undertaken in this study at 90 days of curing and different states of deformation.

Table 5.1: The count of hydraulic conductivity tests undertaken at 90 days of curing and different states of deformation

Testing of Hydraulic Conductivity		
State of Deformation	**Axial Strain Limit (%)**	**Count of Test Repeats**
Intact State (No Deformation)	0.0	5
Pre-Peak Deviator Stress State	0.6	4
Just after $\bar{\varepsilon}_{peak}$ at 90 Days of Curing	1.1	4
Just after Peak Deviator Stress State	Varied from 1 to 1.3	2
Post-Peak Deviator Stress State	2.2	4
	3.3	5
	4.4	5
	5.5	5
Total Number of Hydraulic Conductivity Tests at all States		**34**

5.2 HYDRAULIC CONDUCTIVITY AT INTACT STATE (NO DEFORMATION) AFTER 90 DAYS OF CURING

The results of hydraulic conductivity testing on intact CB specimens are shown in **Tables 5.2** and **5.3**. Note that five repeat tests were undertaken under these conditions. The mean hydraulic pressure difference (between the BPWP and BPP, and the TBP) varied from 0.9 kPa to 1.5 kPa, and the resulting mean hydraulic gradients under steady state flow condition varied from 1.0 to 1.6 (**Table 5.2**).

The applied Q_{In} at the intact state (for all test repeats) was 0.001 ml/min, and the Q_{Out} ranged between 0.0006 ml/min and 0.0007 ml/min (**Table 5.2**). The Q_{In} and Q_{Out} clearly supposed to be equal under steady state flow condition. However, due to the variation in the performance of CP and TBP air regulators, a negligible difference between the Q_{In} and Q_{Out} had occurred (as explained by Aiban and Znidarcic, 1989; **Section 3.5.2.3**). This difference might be also due to the unconfirmed completion of the CB hydration processes after 90 days of curing. Thus, this resulted in an insignificant difference between k_{Inflow} and $k_{Outflow}$ (**Table 5.3**), as it was found to be always of the same order of magnitude of the accuracy of the hydraulic conductivity

(i.e. k_{Inflow}). The k_{Inflow} varied from 5.6 x 10^{-9} m/s to 9.3 x 10^{-9} m/s, and the $k_{Outflow}$ ranged between 3.6 x 10^{-9} m/s and 6.5 x 10^{-9} m/s.

Table 5.2: Flow rates and mean hydraulic gradient at steady state of intact CB specimens

No. of Test Repeat	Q_{In} (ml/min)	Q_{Out} (ml/min)	Mean Hydraulic Pressure Difference (kPa)	Mean Hydraulic Gradient at Steady State
1	0.001	0.0007	1.5	1.6
2	0.001	0.0007	0.9	1.0
3	0.001	0.0006	1.4	1.4
4	0.001	0.0006	1.1	1.1
5	0.001	0.0006	1.2	1.2

Table 5.3: Hydraulic conductivity results at steady state of intact CB specimens

No. of Test Repeat	$k_{Outflow}$ (x 10^{-9} m/s)	$k_{Intflow}$ (x 10^{-9} m/s)	$k_{Intflow}$ - $k_{Outflow}$ (x 10^{-9} m/s)
1	3.9	5.6	1.7
2	6.5	9.3	2.8
3	3.6	6.0	2.4
4	4.7	7.8	3.1
5	4.3	7.2	2.9

5.3 HYDRAULIC CONDUCTIVITY AT PRE-PEAK STATE OF DEFORMATION AFTER 90 DAYS OF CURING

The results of hydraulic conductivity after 0.6% axial strain deformation (i.e. pre-peak state); for the four test repeats using single-stage TXUU with constant flow method for CB specimens after 90 days of curing, are shown in **Tables 5.4** and **5.5**. The mean hydraulic pressure difference varied from 0.8 kPa to 1.9 kPa, and the resulting mean hydraulic gradient at steady state flow condition varied from 0.8 to 2.0 (**Table 5.4**). These were similar to the ranges of mean hydraulic pressure difference and hydraulic gradient measured at the intact state (**Section 5.2**).

The applied Q_{In} varied from 0.0006 ml/min to 0.002 ml/min that was two times higher than the one applied at the intact state (**Section 5.2**), and the Q_{Out} ranged between 0.0005 ml/min and 0.00017 ml/min (note that the correlating pairs are presented in **Table 5.4**). The variation in the performance of CP and TBP air regulators resulted in observed negligible difference between the Q_{In} and Q_{Out} (**Table 5.4**). This difference might be also due to the unconfirmed completion of the CB hydration processes after 90 days of curing. Thus, this yielded an insignificant difference between k_{Inflow} and $k_{Outflow}$ (**Table 5.5**), as it was found to be of lower or same order of magnitude of the accuracy of the hydraulic conductivity (i.e. k_{Inflow}). The k_{Inflow} varied from 6.5 x 10^{-9} m/s to 1.1 x 10^{-8} m/s, and the $k_{Outflow}$ ranged between 5.4 x 10^{-9} m/s and 9.5 x 10^{-9} m/s.

Table 5.4: Flow rates and mean hydraulic gradient at steady state of deformed CB specimens up to 0.6% axial strain

No. of Test Repeat	Q_{In} (ml/min)	Q_{Out} (ml/min)	Mean Hydraulic Pressure Difference (kPa)	Mean Hydraulic Gradient at Steady State
1	0.0006	0.0005	0.8	0.8
2	0.002	0.0017	1.5	1.6
3	0.002	0.0017	1.9	2.0
4	0.002	0.0017	1.6	1.6

Table 5.5: Hydraulic conductivity results at steady state of deformed CB specimens up to 0.6% axial strain

No. of Test Repeat	$k_{Outflow}$ (x 10^{-9} m/s)	$k_{Intflow}$ (x 10^{-9} m/s)	$k_{Intflow}$ - $k_{Outflow}$ (x 10^{-9} m/s)
1	5.4	6.5	1.1
2	9.5	11.2	1.7
3	7.6	9.0	1.3
4	9.4	11.1	1.7

5.4 HYDRAULIC CONDUCTIVITY JUST AFTER THE $\bar{\varepsilon}_{PEAK}$ AT 90 DAYS OF CURING

The mean axial strain corresponding to the peak deviator stress ($\bar{\varepsilon}_{peak}$) at 90 days of curing was 1%, as shown in **Table 4.9** in **Section 4.5.5**. Therefore, the hydraulic conductivity was measured at 1.1% axial strain; this was just after $\bar{\varepsilon}_{peak}$ at 90 days as explained previously in **Section 3.8.5**. The results of hydraulic conductivity after 1.1% axial strain, for four repeat tests using single-stage TXUU with constant flow method for CB specimens at 90 days, are shown in **Tables 5.6** and **5.7**.

The mean hydraulic pressure difference varied from 0.9 kPa to 2.3 kPa, and the mean hydraulic gradient at steady state flow condition varied from 0.9 to 2.3 (**Table 5.6**). These were similar to the ranges encountered at the pre-peak states (**Sections 5.2 and 5.3**).

The applied Q_{In} varied from 0.0006 ml/min to 0.002 ml/min that was two times higher than the ones applied at the intact state (**Section 5.2**); although, this was similar to Q_{In} range applied in the pre-peak state (**Section 5.3**). The Q_{Out} ranged between 0.0005 ml/min and 0.00017 ml/min (**Table 5.6**). This Q_{Out} range was also similar to the one obtained at the pre-peak state (i.e. 0.6% axial strain). Similarly, as experienced in the measurements of the previous states, the variation in the performance of CP and TBP air regulators and the unconfirmed completion of the CB hydration processes after 90 days of curing might be the reasons of the negligible difference between the Q_{In} and Q_{Out}.

The difference between k_{Inflow} and $k_{Outflow}$ (**Table 5.7**) is insignificant, as it was found to be of lower or the same order of magnitude as the accuracy of the hydraulic

conductivity (i.e. k_{Inflow}). The k_{Inflow} varied from 5.6 x 10^{-9} m/s to 1.1 x 10^{-8} m/s, and the $k_{Outflow}$ ranged between 4.7 x 10^{-9} m/s and 8.5 x 10^{-9} m/s. These ranges were similar to the ones occurred in the previous states (i.e. intact and pre-peak states); although the axial strain limit tested was approximately equivalent to the particular ε_{peak} of three test specimens (i.e. test repeats no. 1, 2, and 4) as shown in **Table 5.7**. This implies that the change of hydraulic conductivity due to cracking was not exhibited before and just at the ε_{peak} of CB specimens at 90 days.

Table 5.6: Flow rates and mean hydraulic gradient at steady state of deformed CB specimens up to 1.1% axial strain

No. of Test Repeat	Q_{In} (ml/min)	Q_{Out} (ml/min)	Mean Hydraulic Pressure Difference (kPa)	Mean Hydraulic Gradient at Steady State
1	0.0006	0.0005	0.9	0.9
2	0.002	0.0015	1.5	1.6
3	0.001	0.0008	1.2	1.2
4	0.002	0.0017	2.3	2.3

Table 5.7: Hydraulic conductivity results at steady state of deformed CB specimens up to 1.1% axial strain

No. of Test Repeat	ε_{peak} (%)	$k_{Outflow}$ (x 10^{-9} m/s)	$k_{Intflow}$ (x 10^{-9} m/s)	$k_{Intflow}$ - $k_{Outflow}$ (x 10^{-9} m/s)
1	1.0	4.7	5.6	0.9
2	1.1	8.5	11.3	2.8
3	Not Reached	5.8	7.3	1.4
4	1.0	6.4	7.5	1.1

5.5 HYDRAULIC CONDUCTIVITY JUST AFTER THE POST-PEAK DEVIATOR STRESS STATE AFTER 90 DAYS CURING

The results of hydraulic conductivity just after the actual post-peak state after 90 days of curing; i.e. after exceeding their particular ε_{peak} by approximately 0.2% strain (rather than the imposed strain value at 1.1%, as described in the previous section), using single-stage TXUU with constant flow method, are shown in **Tables 5.8** and

5.9. As noted earlier, this was decided to be conducted at end of the main testing period (additional to the primary strain limits described in previously, and in **Section 3.8.5**), to provide specific information about the change of the hydraulic conductivity just after exceeding the particular q_{peak} and ε_{peak} (i.e. peak state) of a given CB specimen. Therefore, only two CB specimens were available to be tested for this specific state at that time of testing.

The ε_{peak} of the first specimen was 0.8%; thus the hydraulic conductivity was measured at 1% axial strain. The ε_{peak} of the second specimen was 1.2%; hence the hydraulic conductivity was measured at 1.3% axial strain.

The mean hydraulic pressure difference varied from 5.9 kPa to 11.8 kPa, and the resulting mean hydraulic gradient at steady state flow condition varied from 6.2 to 12.2 (**Table 5.8**). These were higher than the ranges of mean hydraulic pressure difference and hydraulic gradient occurred at the previous stress states (from the intact state to state just after $\bar{\varepsilon}_{peak}$ at 90 days; **Sections 5.2** to **5.4**); indicating that a notable change of CB structure had happened at this state of deformation, which requires a higher hydraulic gradient to generate a measurable flow through the deformed specimen.

The applied Q_{In} varied from 0.01 ml/min to 0.02 ml/min that is approximately ten times higher than the ones applied at the previous states (**Sections 5.2** to **5.4**). As experienced in the measurements of the previous states, the variation in the performance of CP and TBP air regulators resulted in negligible difference between the Q_{In} and Q_{Out}, as Q_{Out} ranged between 0.009 ml/min and 0.018 ml/min (**Table 5.9**).

The difference between k_{Inflow} and $k_{Outflow}$ (**Table 5.9**) is insignificant, as it was found to be of lower order of magnitude than the accuracy of the hydraulic conductivity (i.e. k_{Inflow}). The k_{Inflow} and $k_{Outflow}$ values, was approximately equal for the two test repeats that were 1.4 x 10^{-8} m/s and 1.3 x 10^{-8} m/s, respectively. These were higher than the k_{Inflow} and $k_{Outflow}$ values obtained at the earlier states by approximately one order of magnitude. Despite no cracks being visible when tested specimens were investigated after testing, the results implies that the negative impact of microcracking under undrained deformation is most critical after exceeding the ε_{peak} by 0.2%.

Table 5.8: Flow rates and mean hydraulic gradient at steady state of deformed CB specimens up to just post-peak deviator stress

No. of Test Repeat	Q_{In} (ml/min)	Q_{Out} (ml/min)	Mean Hydraulic Pressure Difference (kPa)	Mean Hydraulic Gradient at Steady State
1	0.01	0.009	5.9	6.2
2	0.02	0.018	11.8	12.2

Table 5.9: Hydraulic conductivity results at steady state of deformed CB specimens up to just post-peak deviator stress

No. of Test Repeat	ε_{peak} (%)	$k_{Outflow}$ (x 10^{-9} m/s)	$k_{Intflow}$ (x 10^{-9} m/s)	$k_{Intflow}$ - $k_{Outflow}$ (x 10^{-9} m/s)
1	0.8	13.2	14.5	1.3
2	1.2	13.0	14.1	1.1

5.6 HYDRAULIC CONDUCTIVITY AT POST-PEAK DEVIATOR STRESS STATE AFTER 90 DAYS OF CURING

The results of hydraulic conductivity that was measured at strains considered to clearly exceed the peak deviator stress state of CB specimens after 90 days are shown in **Tables 5.10** to **5.17**. Axial strains of 2.2%, 3.3%, 4.4%, and 5.5% were investigated. Four to five repeat tests were undertaken at each axial strain limit using single-stage TXUU with constant flow method.

The mean hydraulic pressure difference generally varied from 0.8 kPa to 13.6 kPa, and the mean hydraulic gradient at steady state flow condition varied from 0.8 to 13.9 (**Tables 5.10, 5.12, 5.14,** and **5.16**). The highest values of the mean hydraulic gradient were encountered in tests at 2.2% axial strain (**Table 5.10**), and ranged from 6.2 to 13.3. However, the lowest values of the mean hydraulic gradient were encountered in tests at 3.3% axial strain (**Table 5.12**), and ranged from 0.9 to 3.0. For tests at axial strains of 4.4% and 5.5%; the mean hydraulic gradients varied from 0.8 to 13.9 and from 1.7 to 8, respectively (**Tables 5.14** and **5.16**).

The applied Q_{In} varied from 0.10 ml/min to 0.61 ml/min that was approximately ten times higher than the ones applied at the state just post-peak deviator stress (**Section 5.5**). As experienced in the measurements of the previous states, the variation in the performance of CP and TBP air regulators resulted in negligible difference between the Q_{In} and Q_{Out} , as Q_{Out} ranged between 0.085 ml/min and 0.55 ml/min (**Tables 5.10, 5.12, 5.14,** and **5.16**).

The difference between k_{Inflow} and $k_{Outflow}$ (**Tables 5.11, 5.13, 5.15,** and **5.17**) was insignificant for all the tests, as it was found to be of lower order of magnitude of the accuracy of the hydraulic conductivity (i.e. k_{Inflow}). In general, at the post-peak state, the k_{Inflow} varied from 6.5 x 10^{-8} m/s to 3.1 x 10^{-6} m/s, and the $k_{Outflow}$ ranged between 6.3 x 10^{-8} m/s and 2.8 x 10^{-6} m/s. These results were notably higher than the ones determined in the previous states; indicating that the CB specimens had failed to maintain the recommended hydraulic conductivity for CB barriers (i.e. 1 x 10^{-9} m/s) due to propagation of major failure planes that facilitates the passage of higher flow rates.

Table 5.10: Flow rates and mean hydraulic gradient at steady state of deformed CB specimens up to 2.2% axial strain

No. of Test Repeat	Q_{In} (ml/min)	Q_{Out} (ml/min)	Mean Hydraulic Pressure Difference (kPa)	Mean Hydraulic Gradient at Steady State
1	0.61	0.59	10.7	11.1
2	0.61	0.60	6.5	6.7
3	0.1	0.096	13.0	13.3
4	0.1	0.097	6.0	6.2

Table 5.11: Hydraulic conductivity results at steady state of deformed CB specimens up to 2.2% axial strain

No. of Test Repeat	$k_{Outflow}$ ($\times 10^{-7}$ m/s)	$k_{Intflow}$ ($\times 10^{-7}$ m/s)	$k_{Intflow} - k_{Outflow}$ ($\times 10^{-9}$ m/s)
1	4.7	4.8	16.7
2	7.8	7.9	6.6
3	0.6	0.6	2.6
4	1.4	1.4	4.0

Table 5.12: Flow rates and mean hydraulic gradient at steady state of deformed CB specimens up to 3.3% axial strain

No. of Test Repeat	Q_{In} (ml/min)	Q_{Out} (ml/min)	Mean Hydraulic Pressure Difference (kPa)	Mean Hydraulic Gradient at Steady State
1	0.61	0.60	1.8	1.9
2	0.61	0.59	2.9	3.0
3	0.1	0.094	2.3	2.3
4	0.1	0.098	0.9	0.9
5	0.1	0.095	1.6	1.7

Table 5.13: Hydraulic conductivity results at steady state of deformed CB specimens up to 3.3% axial strain

No. of Test Repeat	$k_{Outflow}$ ($\times 10^{-7}$ m/s)	$k_{Intflow}$ ($\times 10^{-7}$ m/s)	$k_{Intflow} - k_{Outflow}$ ($\times 10^{-8}$ m/s)
1	28.0	28.1	0.9
2	17.1	17.5	4.0
3	3.6	3.8	2.4
4	8.9	9.2	2.3
5	5.0	5.3	2.8

Table 5.14: Flow rates and mean hydraulic gradient at steady state of deformed CB specimens up to 4.4% axial strain

No. of Test Repeat	Q_{In} (ml/min)	Q_{Out} (ml/min)	Mean Hydraulic Pressure Difference (kPa)	Mean Hydraulic Gradient at Steady State
1	0.61	0.58	13.6	13.9
2	0.61	0.56	5.9	6.0
3	0.1	0.099	0.8	0.8
4	0.1	0.098	3.9	4.0
5	0.1	0.096	6.2	6.5

Table 5.15: Hydraulic conductivity results at steady state of deformed CB specimens up to 4.4% axial strain

No. of Test Repeat	$k_{Outflow}$ ($\times 10^{-7}$ m/s)	$k_{Intflow}$ ($\times 10^{-7}$ m/s)	$k_{Intflow} - k_{Outflow}$ ($\times 10^{-8}$ m/s)
1	3.6	3.8	1.6
2	8.3	8.9	6.3
3	10.6	10.8	1.6
4	2.1	2.2	0.4
5	1.3	1.3	0.5

Table 5.16: Flow rates and mean hydraulic gradient at steady state of deformed CB specimens up to 5.5% axial strain

No. of Test Repeat	Q_{In} (ml/min)	Q_{Out} (ml/min)	Mean Hydraulic Pressure Difference (kPa)	Mean Hydraulic Gradient at Steady State
1	0.61	0.55	1.6	1.7
2	0.1	0.099	3.7	3.8
3	0.1	0.085	2.9	2.9
4	0.1	0.098	5.5	5.7
5	0.6	0.59	7.8	8.0

Table 5.17: Hydraulic conductivity results at steady state of deformed CB specimens up to 5.5% axial strain

No. of Test Repeat	$k_{Outflow}$ ($\times 10^{-7}$ m/s)	$k_{Intflow}$ ($\times 10^{-7}$ m/s)	$k_{Intflow} - k_{Outflow}$ ($\times 10^{-9}$ m/s)
1	28.0	31.1	307.7
2	2.3	2.3	2.3
3	2.5	3.0	44.1
4	1.5	1.5	3.5
5	6.6	6.7	7.8

5.7 SUMMARY

This chapter presents the results of the hydraulic conductivity testing of the CB specimens cured for at least 90 days using the constant flow method in the flexible-wall triaxial cell. As explained in **Chapter 3**, the CB hydraulic conductivity was not evaluated for curing ages younger than 90 days, because the testing was significantly affected by the ongoing major CB hydration processes.

The outflow hydraulic conductivity ($k_{Outflow}$) of the intact (i.e. not deformed) specimens after 90 days of curing ranged from 3.6 x 10^{-9} m/s to 6.5 x 10^{-9} m/s (with a mean value of 4.6 x 10^{-9} m/s). This was found to be slightly higher than the recommended value by ICE (1999) that is 1 x 10^{-9} m/s and broadly similar to values determined by the previous studies for CB mixtures of similar compositions using the flexible-wall triaxial cell (as reviewed in **Chapter 2** and compared in **Chapter 6**).

At the pre-peak deviator stress state (taken at 0.6% strain) and just after the $\bar{\varepsilon}_{peak}$ at 90 days of curing (taken at approximately 1.1% strain), the $k_{Outflow}$ ranged between 5.4 x 10^{-9} m/s and 9.5 x 10^{-9} m/s, respectively (with a mean value of 8.0 x 10^{-9} m/s at 0.6% strain and 6.3 x 10^{-9} m/s at 1.1% strain). These results did not show a notable change of the CB hydraulic conductivity from the ones at the intact state. However, the slight variation encountered at those states (including the intact state) has been suggested to occur due to variation in the CB material properties (reflecting the variation in the CB microstructure as being created from slurry), variation in the performance of the pressure air regulators, and the unconfirmed completion of the CB hydration processes after 90 days of curing. Further discussion of the effect of TXUU deformation on the CB hydraulic conductivity is given in **Chapter 6**.

At post-peak deviator stress state (or strain limits higher than the ε_{peak}), failure planes facilitating higher seepage through the CB macrostructure were observed to form. The $k_{Outflow,}$ therefore, ranged from 1.3 x 10^{-8} m/s (just after the ε_{peak}) to 2.8 x 10^{-6} m/s (at strains higher than 2.2%). The initial increase of the minimum mean hydraulic conductivity that was 4.6 x 10^{-9} m/s ($\bar{k}_{Outflow}$ at the intact state) was confirmed to happen immediately after exceeding the particular ε_{peak} of the test specimens by approximately 0.2% strain.

A considerable variation in the CB hydraulic conductivity at the post-peak state was experienced and suggested to occur due to variation in the formed cracks patterns and their intensity in every test repeat. This is evaluated and discussed in **Chapter 6**.

The impact of the change of the CB hydraulic conductivity due to the TXUU deformation and its implications on the CB performance is comprehensively discussed in **Chapter 6**.

CHAPTER 6
DISCUSSION OF RESULTS

THE IMPACT OF UNDRAINED DEFORMATION ON THE HYDRAULIC CONDUCTIVITY OF CB SPECIMENS

6.1 INTRODUCTION

This chapter considers the implications of the observed trends previously presented in the Results chapters (**Chapters 4** and **5**). In order to do so, the TXUU and hydraulic conductivity behaviour observed in this study will be considered separately and in combination.

Initially, the deformation characteristics of TXUU behaviour of CB specimens experiencing relatively short durations of curing (15 days to 90 days) are discussed. This is considered in conjunction with the MPWP response in the TXUU tests and the effect of increasing curing age on the TXUU behaviour. Variations in stress-strain response are also reviewed. Furthermore, the observed cracking phenomenon under TXUU shearing is described.

This is followed by consideration of the hydraulic conductivity measurements for the specimens cured for 90 days. The impacts of increasing axial strain of CB specimens are discussed, as is the accuracy, repeatability, and variability of these results.

Finally, the impact of undrained loading on CB (of various ages), with respect to both deformation response and hydraulic conductivity (refereeing to specimen behaviour cured for 90 days but postulated for earlier ages) is considered.

6.2 CHARACTERISTICS OF THE GENERAL TXUU BEHAVIOUR

The CB specimens tested in TXUU conditions after 15 days to 90 days curing (**Chapter 4**) showed common undrained deformation behaviour that was independent of the CP (or σ_3). An idealised stress-strain behaviour for the CB (that is based on the trends presented in **Chapter 4**), exposed to unconsolidated, undrained deformation, is illustrated in **Figure 6.1**; this is presented to permit a generalised discussion of the material behaviour. Upon TXUU loading, a rapid increase of deviator stress up to a well-defined peak deviator stress (q_{peak}) at small axial strain (ε_{peak}) is observed. Once the peak strength (q_{peak}) is exceeded, strain softening is (almost) immediately exhibited and this is attributed to failure of the CB structure (shearing of the cementing bonds). The deviator stress rapidly drops to a value that is typically found to be the minimum of the complete stress-strain curve (q_{min}) and corresponds to a certain axial strain (ε_{min}) as shown in **Figure 6.1**. However, typically after reaching the q_{min}, the deviator stress increases gradually to a higher value that is still lower than the q_{peak}.

TXUU tests were typically terminated at axial strains ranging from 5% to 8% depending on the performance of the tested CB specimen. The final deviator stress achieved at the end of the TXUU test (q_{end}) that is typically higher than the q_{min}. It is suggested that this apparent constant strength (q_{end}) is a function of frictional contacts between the disintegrated parts of the failed specimen with increasing axial strain

(**Figure 6.1**). However, the reason of the q_{end} being higher than the q_{min} is discussed next in **Section 6.3**.

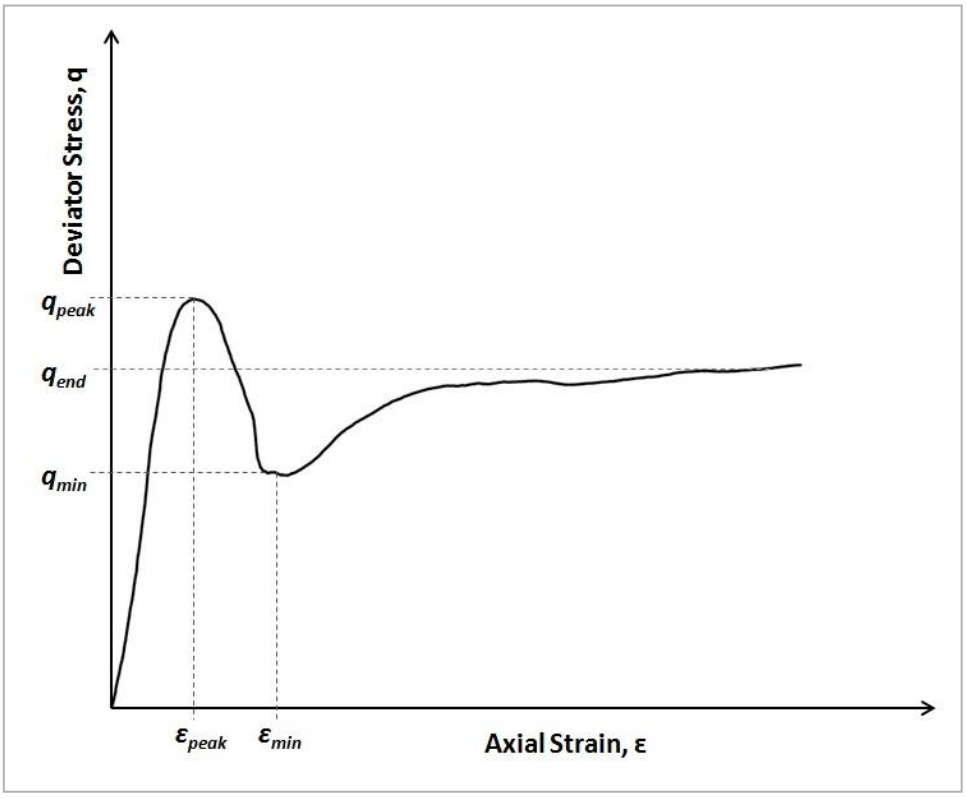

Figure 6.1: Idealised model of stress-strain relationship, modelled on behaviour exhibited by CB specimens in TXUU tests

The application of the CP (or σ_3) during TXUU tests (on CB specimens of all the curing ages investigated), produced equivalent MPWP (as shown in **Sections 4.2** to **4.5**) within the specimens initially. This initial MPWP response confirmed that the CB specimens cast in the laboratory were fully saturated and the B-value was higher than 0.96. This was expected because the water contents of the CB specimens exceeded 320%, as previously reported in **Table 3.3** (**Section 3.3**). Once again, an idealised trend (based on those observed during testing, for the various curing periods) has been presented for discussion; the idealised MPWP response during TXUU tests on CB specimens is illustrated in **Figure 6.2**. Once a certain axial strain was exceeded ($\varepsilon_{\Delta MPWP}$), which occurs after the ε_{peak}, the MPWP was observed to decrease (non-

linearly) with increasing axial strain (**Figure 6.2**). The reason of the decrease of MPWP is discussed next in **Section 6.3**.

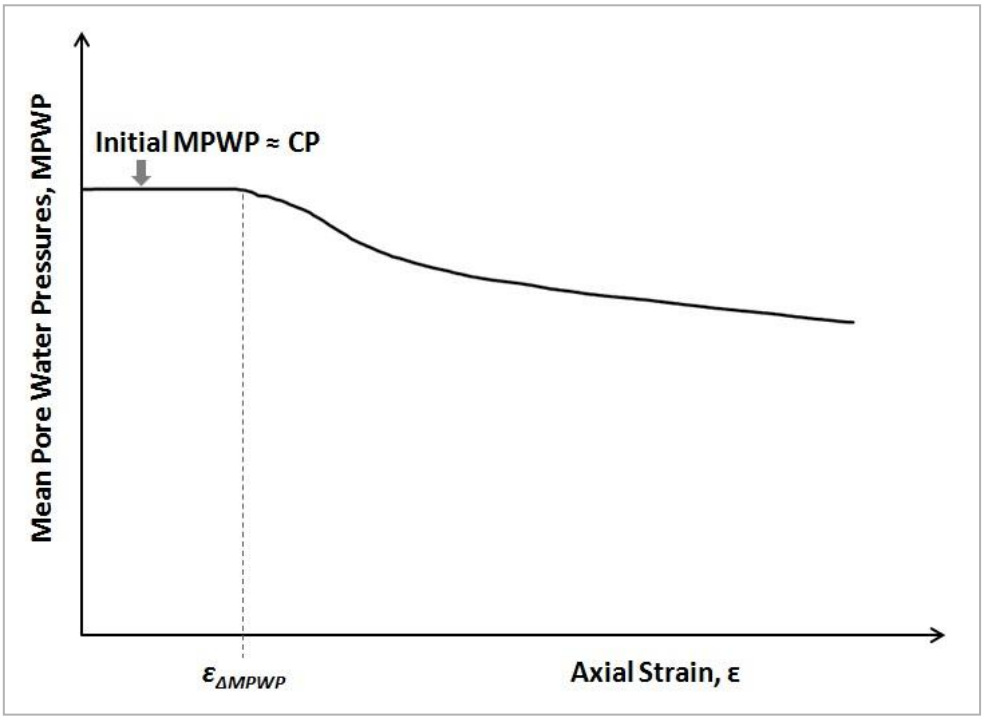

Figure 6.2: The idealised MPWP-strain response, modelled on behaviour exhibited by CB specimens in TXUU tests

The effective stress paths (in q-p′ stress field) followed in TXUU tests (presented in **Chapter 4**), and the idealised stress-strain and MWPW models, allows for the development of a model of the typical effective stress path in TXUU tests as shown in (**Figure 6.3**). This model appears to be followed by all of the CB specimens (for all curing ages) investigated in TXUU tests herein. Effective stress paths were plotted using the effective stresses developed from the change of MPWP after exceeding the peak state (**Figure 6.2**). The stress path begins to move along the $\sigma'_3 = 0$ line, or the tension cut-off line (q=3p′), until the q_{peak} is reached (**Figure 6.3**). This is expected for fully saturated specimens in TXUU testing. After exceeding the q_{peak}, the path travels

back along the $\sigma'_3=0$ line until the q_{min} is achieved (**Figure 6.3**), whereupon the stress path deviates from the tension cut-off line. As observed in TXUU tests, the specimens typically exhibited tension cracks once the q_{peak} was exceeded. It is suggested that the change in the modelled effective stress path (after exceeding the q_{min}) is a function of the change (reduction) in MPWP behaviour (**Figure 6.2**). Furthermore, in some tests the path ends with a tendency to tilt again to the left towards the $\sigma'_3=0$ line (**Chapter 4**, and **Figure 6.3**). However, conclusions could not be drawn for this final behaviour as the tests were usually terminated at this stage to avoid damage of the triaxial equipment.

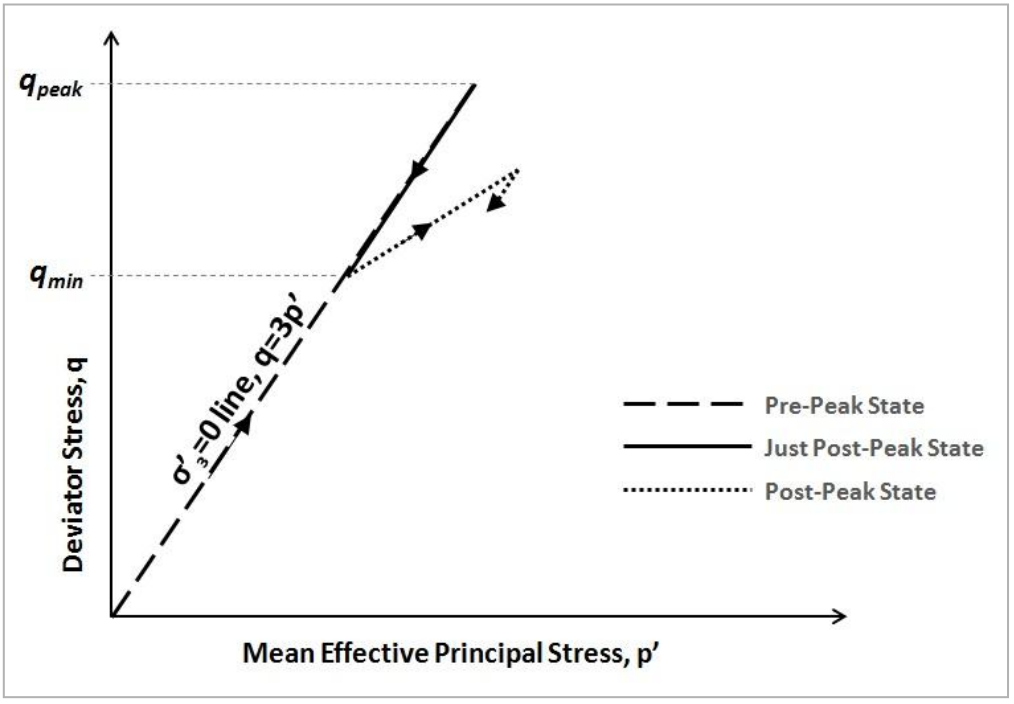

Figure 6.3: Proposed model of typical effective stress path of CB specimens in TXUU tests

The common or general TXUU behaviour that is characterised in **Figures 6.1** to **6.3** was also observed by Joshi (2009) for CB specimens cast in the laboratory and tested at varying curing ages from 35 days to 3.25 years (**Section 2.4.1; Figures 2.4** to **2.6**).

However, Joshi (2009) did not explain the occurrence of such behaviour. The interpretation of that behaviour is presented in the following section.

6.3 INTERPRETATION OF COMMON MPWP AND DEVIATOR STRESS RESPONSES OF CB SPECIMENS AT POST-PEAK STATE IN THE TXUU TEST

When slip occurs along a failure plane, the 'wedging' effect of the relative movement of the multiple portions of the failed specimen theoretically stretches the rubber membrane (**Figure 6.4**), tending to increase the volume between the specimen and membrane (Head and Epps, 2014). Thus, development of a cavity between specimen and membrane is likely to result in negative pore pressure; induced by the uneven distortion of the rubber membrane in an undrained test and in turn may increase the effective stress and deviator stress after the appearance of failure planes (Head and Epps, 2014; Chandler, 1968). Whilst the failure of the CB specimens does not follow the mechanism depicted in **Figure 6.4**; the mechanisms observed in this study are illustrated in **Figure 6.5** (also similar to ones observed by Royal et al., 2013 and Royal et al., 2017). Examples of failed CB specimens surrounded by unevenly distorted membranes are shown in **Figure 6.5**. The phenomenon of uneven stretching of the membrane was exhibited as seen in **Figure 6.5**, thus this explains the TXUU behaviour exhibited after exceeding the peak state and the drop of MPWP characterised in **Section 6.2**.

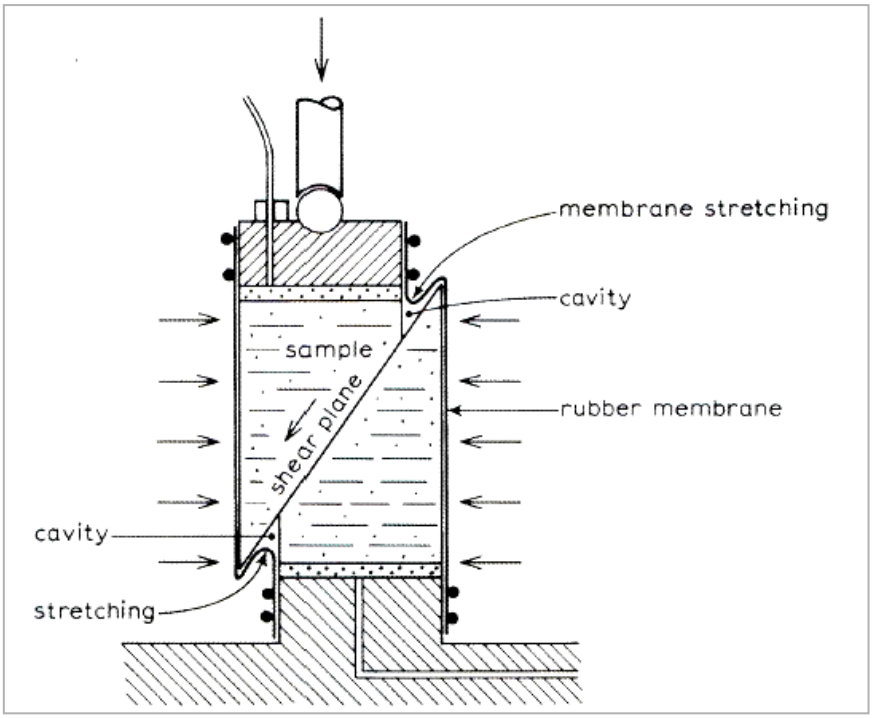

Figure 6.4: Stretching of rubber membrane due to single plane slip (Head and Epps, 2014)

The failure modes exhibited by CB specimens in TXUU tests conditions were similar for all of short-term curing ages investigated; via development of vertical tension cracks, or combination of vertical and inclined cracks forming single or multiple wedges (**Chapter 4**).

Figure 6.5: Examples of failed CB specimens showing the uneven stretching of the rubber membranes in TXUU tests

Therefore, as suggested above by Chandler (1968) and Head and Epps (2014), the distortion of the membrane post q_{min} results in the increase of the **p'** and hence change in the effective stress path to move to the right, away from the $\sigma'_3=0$ line, as shown in **Figure 6.3**. Therefore, the TXUU behaviour exhibited after exceeding the q_{min} does not represent the actual undrained behaviour of the CB material expected to occur in the field. Hence, this could be considered as a limitation of UU testing in the laboratory. The idealised models for deformation response and MPWP (**Figures 6.1 and 6.2**) are therefore modified to take account of this limitation as shown in **Figures 6.6 and 6.7**).

The modified models (dotted lines; **Figures 6.6 and 6.7**) suggests that q_{min} should ideally remain constant (i.e. equal to q_{end}), and the MPWP should remain constant during TXUU loading.

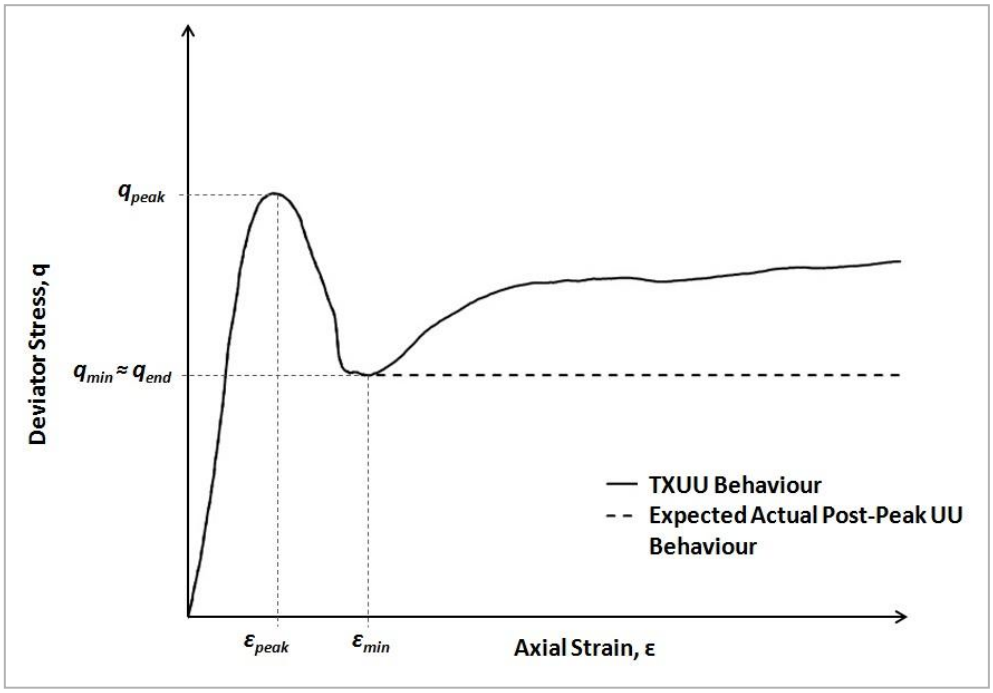

Figure 6.6: Refined idealised modelled stress-strain behaviour that redefines (dotted line) the stress-strain behaviour post-peak strength under TXUU loading

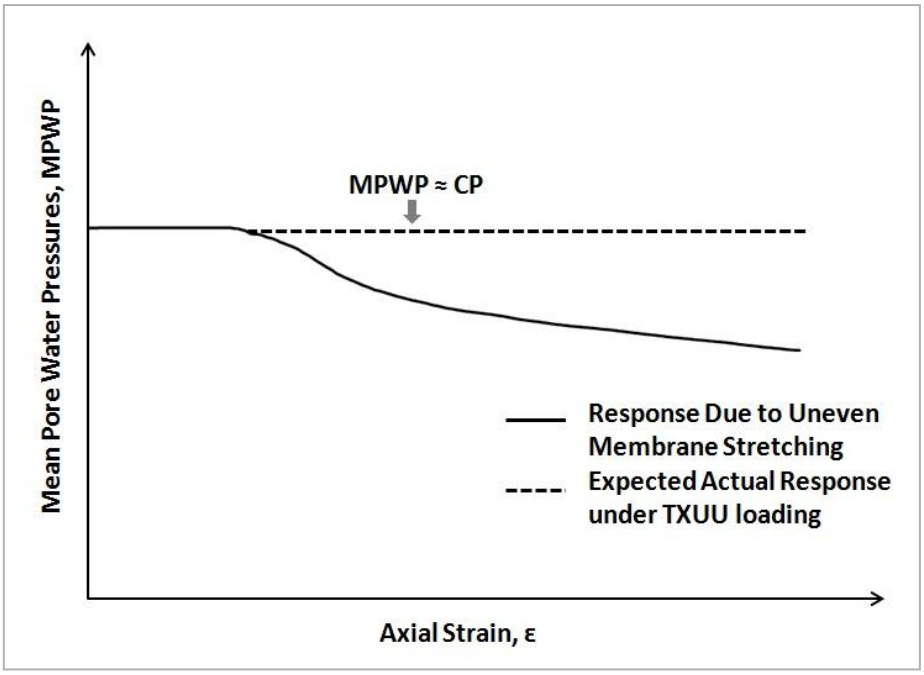

Figure 6.7: Refined idealised MPWP response (dotted line) expected to be exhibited under TXUU loading

The distortion of the membrane with deformation of the specimen in TXUU conditions is considered to have an impact on undrained behaviour. However, Chandler (1968) and Head and Epps (2014) suggest that this limitation has a large impact on highly permeable materials, whereas it is less pronounced in case of less permeable materials such as overconsolidated clays (i.e. akin to CB material). It was only possible to measure the pore water pressure at the top and bottom ends of the test specimens, hence the exact or actual pore water pressures within the microfabric that led to failure were unknown. Therefore, this is a source of uncertainty within this body of work and merits additional research.

The drop of MPWPs after failure or formation of failure planes in the CB specimens might also be attributed to the deformation response of the material post peak strength. An idealised model of the observed failure mechanism is presented in **Figure 6.8**. This proposed model illustrates the development of a cone and vertical cracking of the specimens with increasing compressive axial strain in the TXUU tests.

Formation of cone and vertical cracks results in disintegration of the specimen into multiple elements that moves individually (yet relatively) in relation to the applied compression force (**Figure 6.8**). The relative displacement of the discrete elements of a failed specimen increases the dilation response (i.e. drop of pore water pressures) within the cracks against the CP. **Figure 6.3** shows the typical path followed at post-peak state due to that dilation behaviour which is mainly exhibited within the expanding cracks (at the vicinity of the PWP measurement transducers).

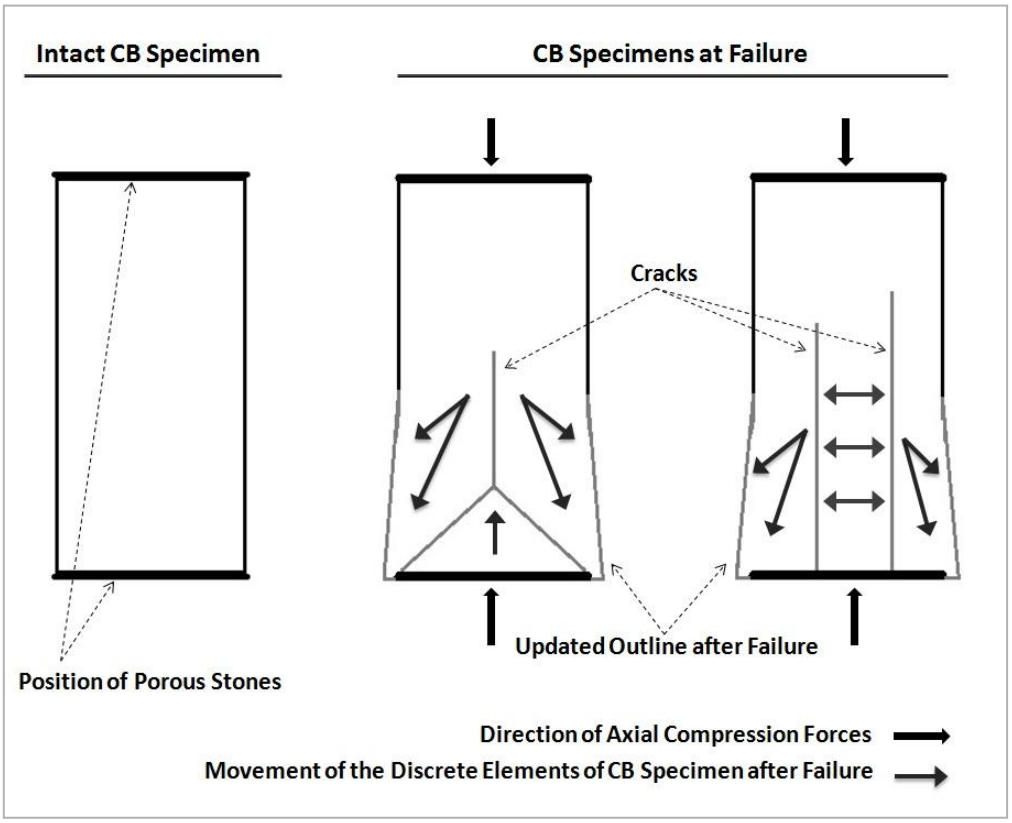

Figure 6.8: Proposed model of relative displacements within the fragmented CB specimen in TXUU tests with increasing axial compressive strain post undrained peak strength

6.4 EFFECT OF CURING AGE ON THE TXUU BEHAVIOUR

The TXUU deformation behaviour (brittle with strain softening post the q_{peak}) of CB specimens was found broadly similar (the physical and mechanical parameters

changed with curing but the brittle nature was constant), and independent of CP and curing age (for those considered herein) (**Chapter 4**, and **Section 6.2**). **Figures 6.1** to **6.3** shows that, the (idealised) TXUU behaviour of CB specimens was characterised by specific parameters that vary under TXUU shearing in this study. These parameters are:

- the undrained peak strength (q_{peak}) and its corresponding axial strain (ε_{peak}),
- and the undrained elastic stiffness (Undrained Young's Modulus, E_u; Undrained Shear Modulus, G_u).

Clearly, whilst the deformation response is the same for the CB specimens cured for different durations, the mechanical properties (characterised by parameters stated above) are not. Curing results in a non-linear increase in properties such as peak strength and elastic stiffness, but does not appear to significantly change the strain corresponding to the peak strength, as shown in **Figure 6.9** and **Table 6.1**.

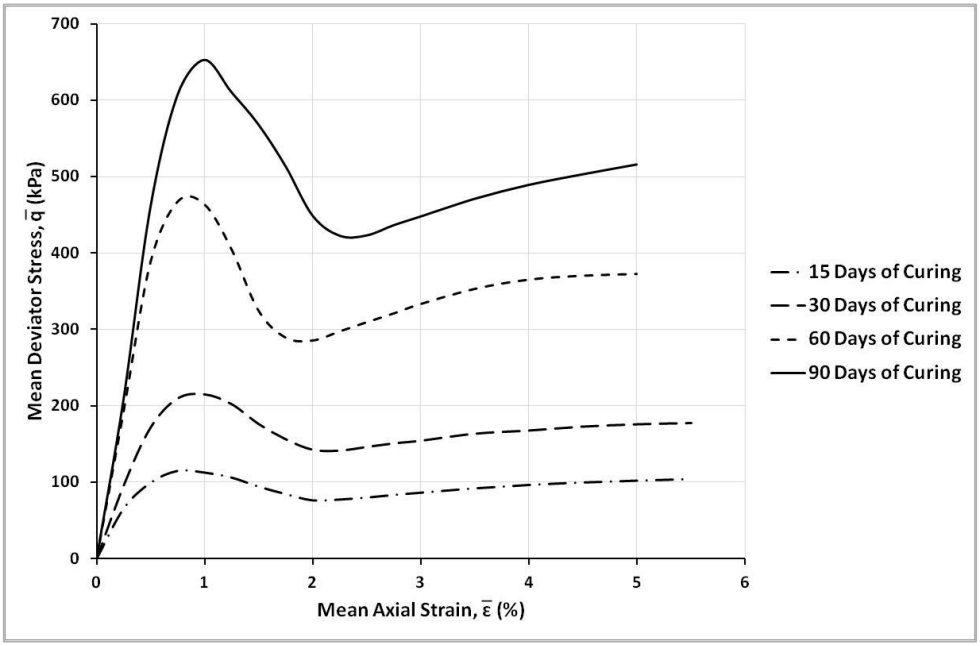

Figure 6.9: Mean stress-strain relationships in TXUU tests for CB specimens at varying curing ages

In addition, the TXUU behaviour was further characterised by other variable parameters that were encountered due to TXUU testing limitations (explained in **Section 6.3**), these are; q_{min}, ε_{min}, $\varepsilon_{\Delta MPWP}$, and q_{end}. For the purpose of comparing those parameters with varying curing ages, their means (i.e. $\bar{q}_{peak}$, $\bar{\varepsilon}_{peak}$, $\bar{E}_u$, $\bar{G}_u$, $\bar{q}_{min}$, $\bar{\varepsilon}_{min}$, $\bar{\varepsilon}_{\Delta MPWP}$, and $\bar{q}_{end}$) at each tested curing age were obtained as listed in **Table 6.1**. These means were obtained from the filtered data of TXUU tests as presented in **Chapter 4**.

Table 6.1: Comparison of TXUU results of CB specimens at different curing ages

Average Parameters	Curing Age (Days)			
	15	30	60	90
$\bar{q}_{peak}$ (kPa)	115	215	467	653
$\bar{\varepsilon}_{peak}$ (%)	0.7	1	0.8	1
$\bar{E}_u$ (kPa)	200	344	777	923
$\bar{G}_u$ (kPa)	67	115	259	308
$\bar{q}_{min}$ (kPa)	77	142	286	423
$\bar{\varepsilon}_{min}$ (%)	2	2.2	2	2.3
$\bar{\varepsilon}_{\Delta MPWP}$ (%)	1.5	1.5	1.3	1.3
$\bar{q}_{end}$ (kPa)	104	180	373	516
$\bar{q}_{peak}$ - $\bar{q}_{min}$ (%)	33	34	39	35
ΔMPWP at $\bar{\varepsilon}_{min}$ (kPa)	-0.6	-2.4	-4	-8
Final ΔMPWP (kPa)	-8	-17	-28	-38
$\bar{q}_{end}$ - $\bar{q}_{min}$ (%)	26	21	23	18

The mean undrained peak strength, or $\bar{q}_{peak}$, was observed to increase with increasing curing age from 115 kPa at 15 days to 653 kPa at 90 days of curing (**Table 6.1**). This agrees with findings by Joshi (2009), Soga et al. (2013), and Royal et al., (2017) (as reviewed in **Section 2.4**). Similarly, the elastic stiffness parameters, $\bar{E}_u$ and $\bar{G}_u$, were found to increase with increasing curing age; from 200 kPa and 67 kPa at 15 days of

curing, to 923 kPa and 308 kPa at 90 days of curing, respectively. However, the $\bar{\varepsilon}_{peak}$ at which the undrained peak strength occurred did not appear to have a clear relationship with the curing age and peak strength, as it typically varied from 0.7% at 15 days to 1% at 90 days of curing.

The variation of TXUU behaviour at the post-peak state was mainly characterised by q_{min}, and q_{end} (**Figure 6.1**). These were found to increase with the increasing curing ages similar to $\bar{q}_{peak}$ (**Table 6.1**). The $\bar{q}_{min}$ increased from 77 kPa at 15 days to 423 kPa at 90 days of curing, indicating the increase of brittle strain-softening behaviour at the post-peak state with increasing curing age. Also, the $\bar{q}_{end}$ increased from 104 kPa at 15 days to 516 kPa at 90 days of curing.

The percentage difference between $\bar{q}_{peak}$ and $\bar{q}_{min}$ was found to be almost constant with increasing curing age, as it was 33% at 15 days and 35% at 90 days of curing (**Table 6.1**). However, the percentage difference between $\bar{q}_{end}$ and $\bar{q}_{min}$ was observed to slightly decrease with increasing curing age from 26% at 15 days to 18% at 90 days (**Table 6.1**).

The $\bar{\varepsilon}_{min}$ and $\bar{\varepsilon}_{\Delta MPWP}$ did not show a certain relationship with increasing curing age (i.e. similar to $\bar{\varepsilon}_{peak}$), as they were approximately constant (**Table 6.1**). The $\bar{\varepsilon}_{min}$ was 2% at 15 days and 2.3% at 90 days of curing. The $\bar{\varepsilon}_{\Delta MPWP}$ was lower than $\bar{\varepsilon}_{min}$; as it was 1.5% at 15 days, and 1.3% at 90 days of curing. The $\bar{\Delta}$MPWP at $\bar{\varepsilon}_{min}$ was found to increase with increasing curing age from -0.6 kPa at 15 days to -8 kPa at 90 days of curing (**Table 6.1**). Furthermore, this justifies that the actual drop of MPWP due to cracking might happen immediately after exceeding the undrained peak strength that occurred at a lower strain (i.e. just after exceeding the ε_{peak}), and somewhere at the middle of

the test specimen where the pore water pressure could not be measured. The final $\bar{\Delta}MPWP$ that was measured at the end of TXUU tests increased from -8 kPa at 15 days to -38 kPa at 90 days of curing (**Table 6.1**). This also justifies the increase of brittle strain-softening behaviour, and dilation within the formed cracks post-peak state, with increasing curing age.

6.5 VARIATION OF TXUU DEFORMATION RESULTS

The ranges of the parameters controlling the mechanical behaviour of CB specimens in TXUU tests at different curing ages are shown in **Table 6.2**, and **Figures 6.10** to **6.16**. These were found to be independent of the CP (but not curing, as described in the previous section) as seen in **Chapter 4**, as they did not show a noticeable relationship with increasing CP. This is shown in **Figure 6.10** for q_{peak} and q_{end} parameters- as an example. In general (regardless of the curing age), the q_{peak} varied by 21% to 33%; showing the least variation (**Table 6.2**, and **Figure 6.11**). The q_{min} varied by 26% to 60% (**Table 6.2**, and **Figure 6.12**). The q_{end} varied by19% to 40% (**Table 6.2**, and **Figure 6.13**). The ε_{peak} varied by 36% to 50% (**Table 6.2**, and **Figure 6.14**). The ε_{min} varied by 30% to 48% (**Table 6.2**, and **Figure 6.15**). The $\varepsilon_{\Delta MPWP}$ varied by 27% to 55% (**Table 6.2**, and **Figure 6.16**).

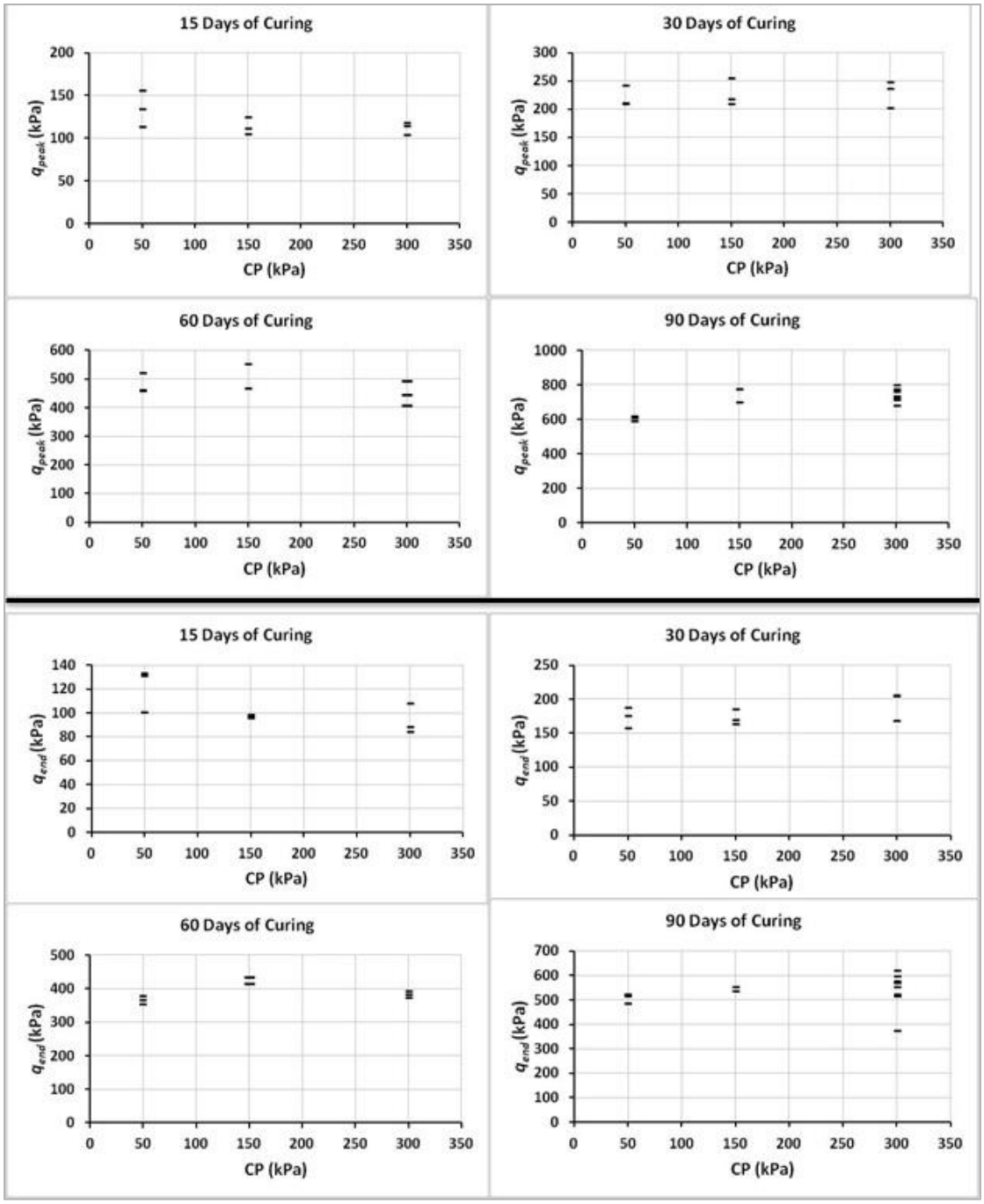

Figure 6.10: Variation of strength parameters (q_{peak} and q_{end}) showing their independence of variation of CP in TXUU tests at the different curing ages

Table 6.2: Variation of TXUU results of CB specimens at different curing ages

Range of Parameters	Curing Age (Days)			
	15	30	60	90
q_{peak} (kPa)	104 - 156	203 - 256	408 - 552	591 - 801
q_{min} (kPa)	57 - 102	109 - 147	137 - 341	245 - 496
q_{end} (kPa)	84 - 133	164 - 207	354 - 436	375 - 621
ε_{peak} (%)	0.6 - 1.2	0.7 - 1.3	0.7 - 1.1	0.7 - 1.4
ε_{min} (%)	1.6 - 2.3	1.3 - 2.2	1.6 - 2.5	1.3 - 2.5
$\varepsilon_{\Delta MPWP}$ (%)	1.6 - 2.2	1.3 - 2.1	1 - 2.2	1.3 - 2.4
Total Number of Tests	9	9	8	13

A major source of the variation in stress-strain parameters is expected to be due to the variation of the hardened CB material properties (as being made from mixed slurry) such as the water content and void ratio (**Table 3.3**; **Section 3.3**), as recalled below.

Table 3.3: Basic material characteristics of CB specimens in this study

Range of Bulk Density (g/cm^3)	**1.1 - 1.2**
Typical Particle Density	**2.69**
Range of Water Contents (%)	**320 - 450**
Range of Void Ratios	**9.0 - 12.0**

The water content of CB specimens varied from 320% to 450%, and the void ratio also varied from 9.0 to 12.0. Therefore, the water content and void ratio of hardened CB specimens of the different curing ages tested varied by around 29% and 25%, respectively. These magnitudes of variation in the material properties overlap with the variation magnitudes encountered in the parameters of the mechanical behaviour (stated earlier). Hence, the variation observed in the physical and mechanical properties (**Figures 6.10 to 6.16**) could be attributed to the casting of the specimens from slurry; this is a well-known issue that has been reported previously in the literature (Joshi, 2009; Soga et al, 2013; Royal et al. 2013). The percentages of variation experienced herein (with respect to the q_{peak} and ε_{peak}) agrees with those

encountered previously in the literature for UCS, TXUU, TXCU tests on CB specimens of different curing ages and mixture compositions (Deschênes et al., 1995; Manassero et al.,1995; Philip, 2001; Opdyke and Evans, 2005; Joshi, 2009; Williams and Ghataora, 2011; Jefferis, 2012; Royal et al., 2013; Soga et al., 2013; Royal et al., 2017), as reviewed by Alzayani et al. (2016).

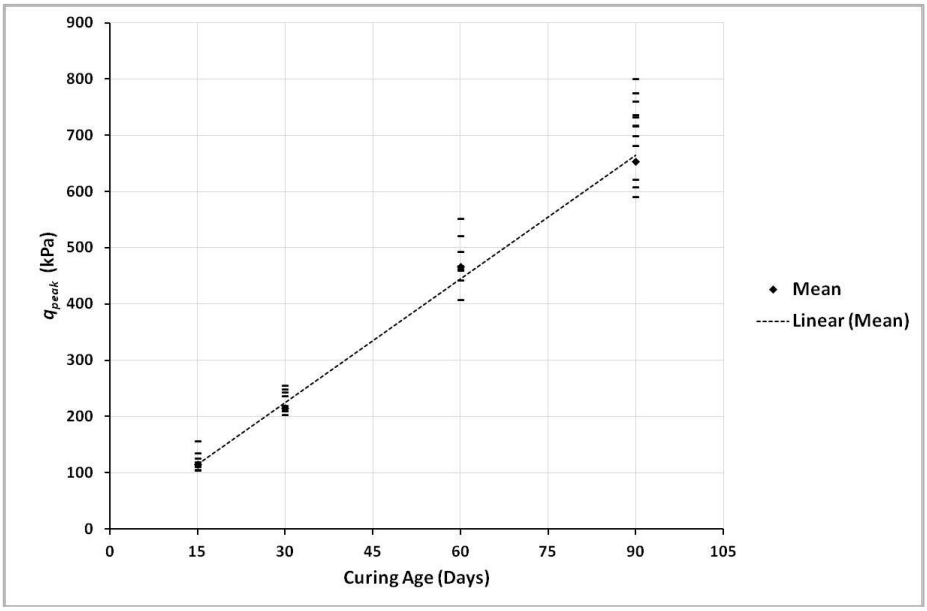

Figure 6.11: Variation of q_{peak} with curing age in TXUU tests, where total count of tests per curing age is presented in **Table 6.2**

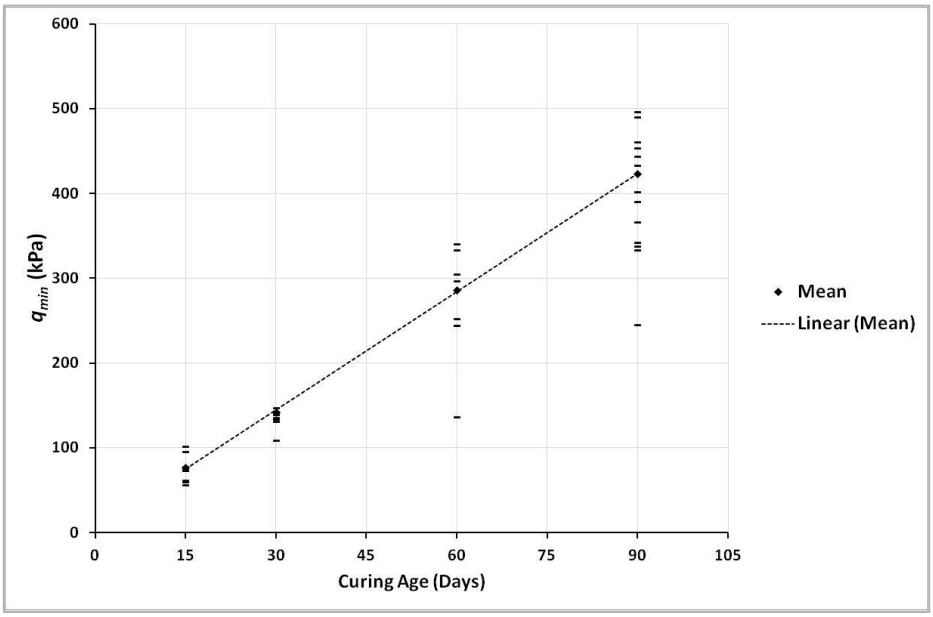

Figure 6.12: Variation of q_{min} with curing age in TXUU tests, where total count of tests per curing age is presented in **Table 6.2**

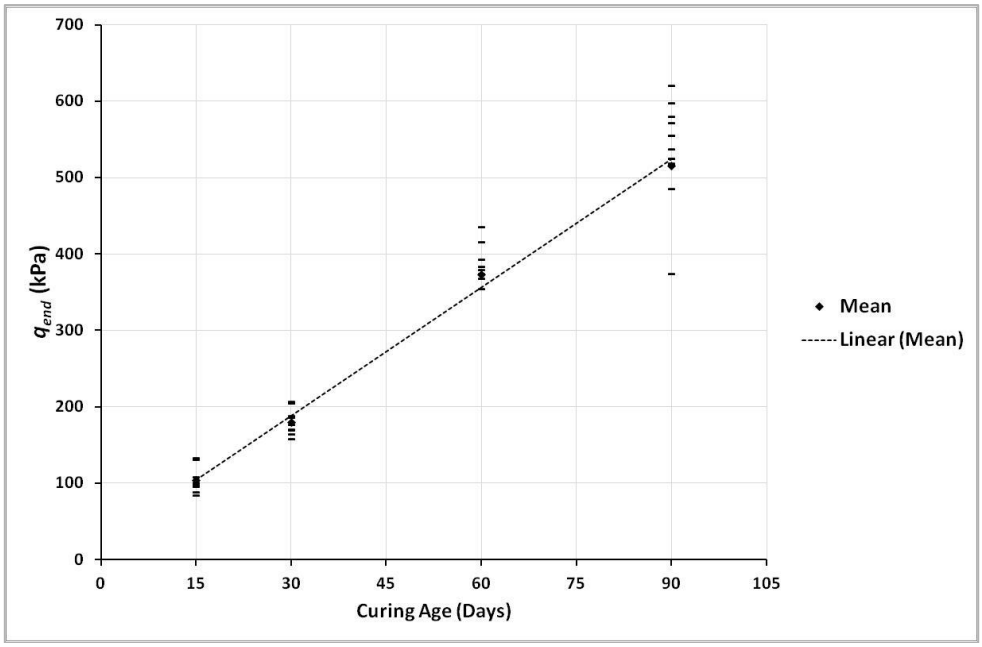

Figure 6.13: Variation of q_{end} with curing age in TXUU tests, where total count of tests per curing age is presented in **Table 6.2**

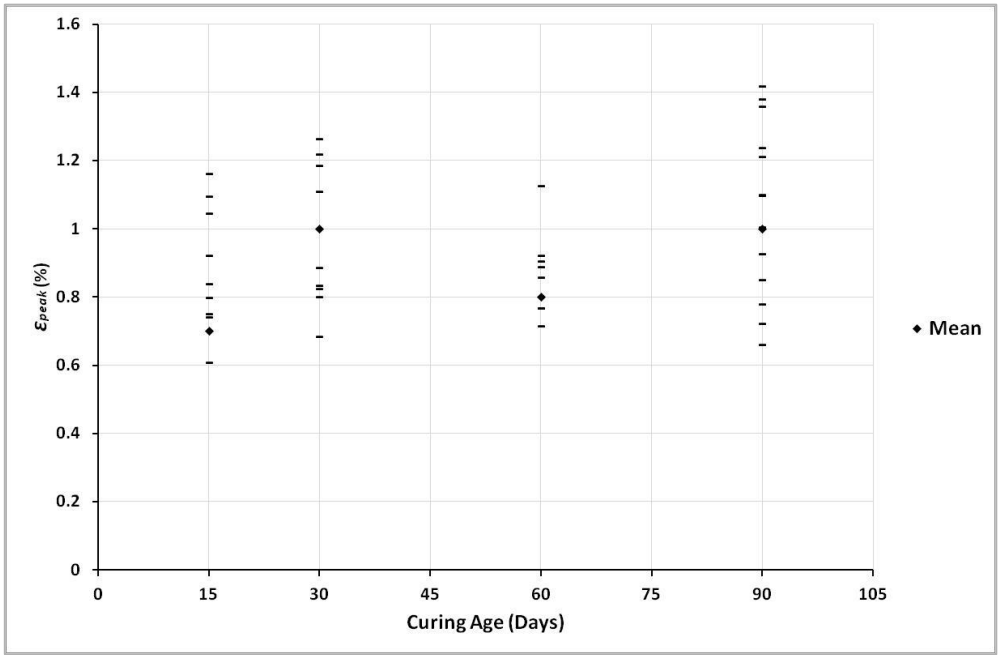

Figure 6.14: Variation of ε_{peak} with curing age in TXUU tests, where total count of tests per curing age is presented in **Table 6.2**

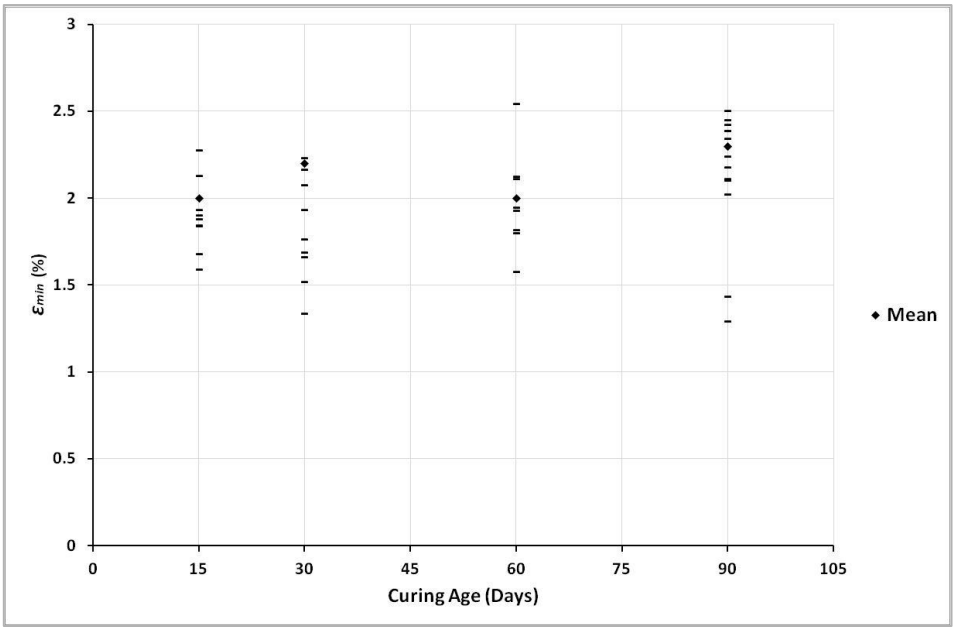

Figure 6.15: Variation of ε_{min} with curing age in TXUU tests, where total count of tests per curing age is presented in **Table 6.2**

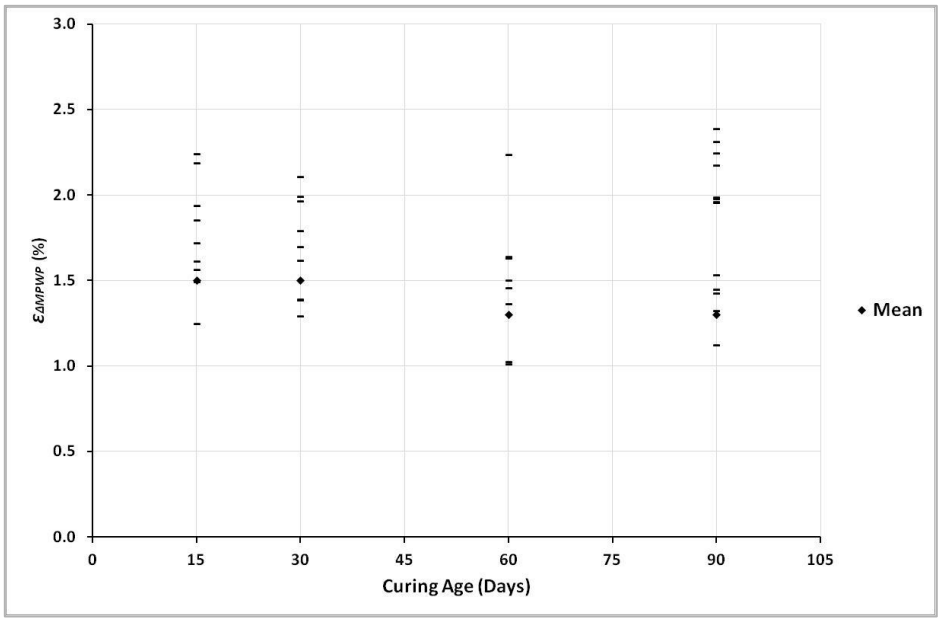

Figure 6.16: Variation of $\varepsilon_{\Delta MPWP}$ with curing age in TXUU tests, where total count of tests per curing age is presented in **Table 6.2**

6.6 CRACKING PHENOMENON OF CB SPECIMENS UNDER TXUU DEFORMATION

The idealised stress-strain relationship of CB specimens of varying curing ages (that is modelled in **Figure 6.1)** is used to herein to explain the typical process of crack

development observed within the CB specimens in TXUU tests, shown in **Figure 6.17**. **Table 6.3** indicates the selected axial strain values at which the TXUU tests were terminated and CB specimens were carefully taken out for visible inspection for cracks. The selected axial strains were labelled by letters from ***A*** to ***E*** and called cracking visualisation points as shown in **Figure 6.17** and **Table 6.3**. The first point of inspection (i.e. ***A***) was selected at 1.4% strain, as no cracks were visible before this point of deformation. The following inspection points (i.e. ***B*** to ***E***) were selected to be similar to the strain limits used to evaluate the hydraulic conductivity after TXUU deformation post the peak deviator stress state; these were 2.2%, 3.3%, 4.4%, and 5.5%.

Furthermore, examples of investigated CB specimens showing the growth of visible cracks with respect to the selected visualisation points (***A*** to ***E***) are shown in **Figure 6.18**.

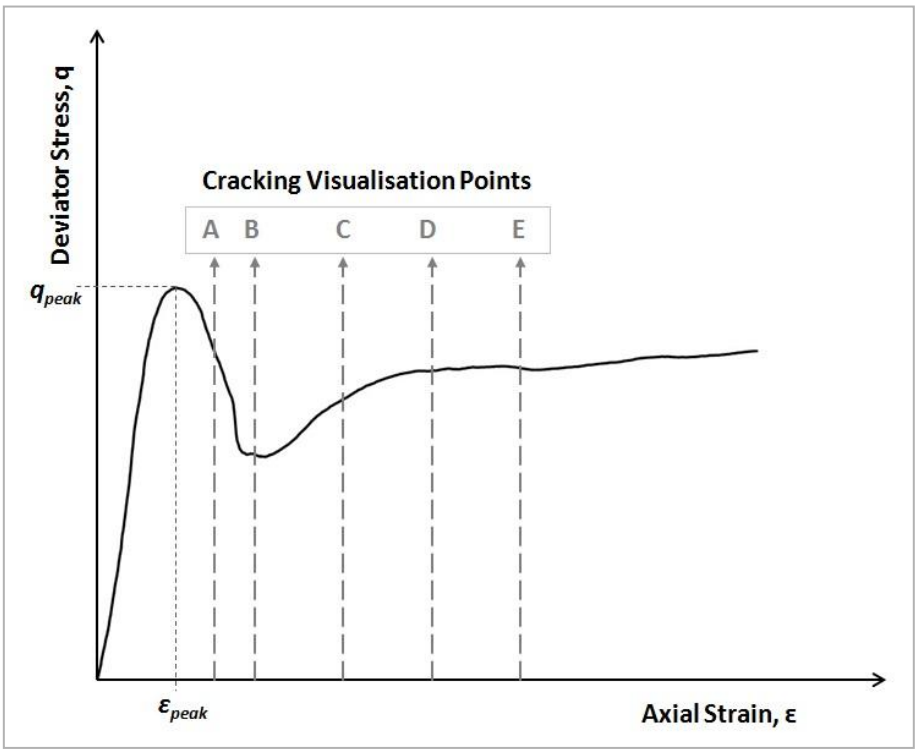

Figure 6.17: Idealised stress-strain relationship of CB specimens in TXUU tests with mapping of cracking visualisation points (***A*** **–** ***E***)

Table 6.3: Description of the cracking visualisation points with respect to axial strain

Cracking Visualisation Points	ε (%)
A	1.4
B	2.2
C	3.3
D	4.4
E	5.5

t

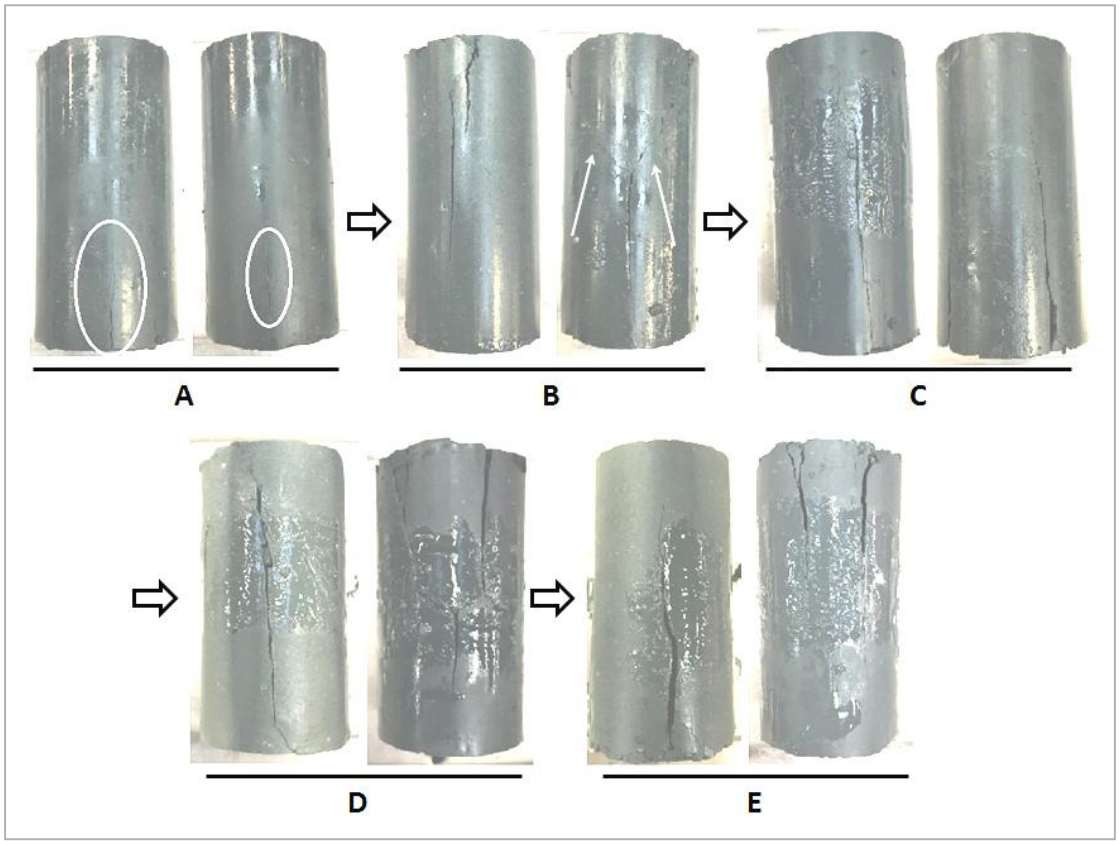

Figure 6.18: Growth of visible cracks of some CB specimens in TXUU tests with respect to the cracking visualisation points described in **Table 6.3**. Note that the colour of images was adjusted to capture the cracks in a clearer vision, and the middle section of some of the specimens was coated with silicone gel. Cracks at points A and B are annotated with white circles and arrows.

The first minor tension cracks were visible at point ***A*** that is just after exceeding the undrained peak strength, (**Figures 6.17 and 6.18**). At point B (at which the strain-softening behaviour usually commences) the cracks had propagated, and widened, to form either multiple major tension cracks or a combination of tension and inclined

cracks (**Figures 6.17 and 6.18**). From point ***C*** onwards, the cracks were observed to extend and widen with increasing axial strain (**Figures 6.17 and 6.18**). The final inspection point was point ***E*** (**Figures 6.17 and 6.18**), because after it the failed specimens had split into multiple fragments.

This inspection of visible cracking process of CB specimens under TXUU loading confirmed that the impact of cracking and loss of intact structure takes place just after exceeding the peak state (q_{peak}, ε_{peak}). Prior to this visible cracking was not evident, although the impact of microcracking could not be determined using the equipment available. The development of microcracking experienced by weak sedimentary rocks, such as sandstones has been observed to initiate well before reaching the peak strength (Alzayani et al, 2016). The impact of deformation on the hydraulic conductivity of CB under TXUU conditions is considered in **Section 6.9**.

6.7 THE HYDRAULIC CONDUCTIVITY OF INTACT (NOT DEFORMED) CB SPECIMENS AT 90 DAYS OF CURING AND COMPARISON WITH RESULTS PREVIOUSLY PUBLISHED IN LITERATURE

In this study, the hydraulic conductivity of CB specimens cured for at least 90 days was measured through the constant flow method in the flexible-wall triaxial cell (described in **Sections 3.5.2** and **3.8**); developed because of the advantages it offers when measuring low hydraulic conductivities (**Section 2.7.3**). The curing period of 90 days was used as the testing associated with the development of the methodology illustrated that accurate measurement of the CB hydraulic conductivity was only permissible when the curing age reached 90 days (**Section 3.8.3**). Prior to this curing period, steady state conditions were not reached after 2 days of permeation, the outflow rates were considerably lower than the inflow rates, and the mean hydraulic

gradients were not constant. This phenomena was also experienced by Williams and Ghataora (2011) (previously reviewed in **Section 2.6.9**). This was attributed to ongoing major CB hydration processes during early curing ages (i.e. less than 90 days). However, the completion of the CB hydration processes is still unconfirmed even after 90 days of curing.

The CB specimens in the intact state (i.e. not deformed prior to measurement of the hydraulic conductivity), experienced the lowest inflow and outflow rates of water at steady state flow condition (**Section 5.2**); thus the lowest values of $k_{Intflow}$ and $k_{Outflow}$ that conformed to expectation. The hydraulic conductivity results considered in this discussion is based on the mean outflow coefficient of hydraulic conductivity ($\bar{k}_{Outflow}$), which could be determined through averaging results of multiple test repeats. The $\bar{k}_{Outflow}$ represents the hydraulic conductivity that could be determined through measurement of the outflow collected from the test specimen (i.e. Q_{Out}) using different methods (conventional or advanced) in the triaxial cell. Therefore, it is considered to be the best parameter to compare the CB hydraulic conductivity of different studies.

The comparison of the hydraulic conductivities measured herein with those previously published in literature was not as straight forward as first perceived and much of this is down to the nature of the material. CB is created from slurry and there is no single slurry mixture used in geotechnical applications, therefore multiple materials are effectively being reported. This is additional to the inherent variation in the physical properties of CB specimens casted from the same mixture, which results in a slight variation of the hydraulic conductivity as seen experienced in this study (to be discussed in **Section 6.9**).

The CB is designed to have low hydraulic conductivities, and measuring low hydraulic conductivities in the triaxial laboratory setting was found to be complex and difficult, particularly at very low effective stress (Daniel and Koerner, 2007). Although, the flexible-wall triaxial cell provides full control over stresses (Daniel and Koerner, 2007), the hydraulic conductivity measurement is likely to be affected by the boundary conditions of the testing method employed (i.e. effective confining pressure and hydraulic gradient, as reviewed in **Section 2.7.2**). This is additional to the effect of size of test specimens used, as it was found to have a considerable influence on the measured hydraulic conductivity as reviewed in **Section 2.7.2**. The hydraulic conductivity results of intact CB specimens at 90 days in this study (**Section 5.2**) were found to be broadly similar to the ones (determined in the flexible-wall triaxial cell) of similar compositions published in literature (**Section 2.7**). **Table 6.4** presents a comparison of; the $\bar{k}_{Outflow}$ obtained in this study with other studies that used almost similar CB mixture compositions with respect to their triaxial testing conditions and specimen sizes.

Table 6.4: Comparison of $\bar{k}_{Outflow}$ at the intact state of this study with other studies with respect to their; mixture composition, triaxial testing conditions, and specimen size

Study	Mixture Composition (by Total Weight)	Triaxial Testing Conditions	Curing age	$\bar{k}_{outflow}$ (m/s)	Specimen Size
Current Study (Section 5.2)	4% Bentonite 20% Cement with 80% GGBS Replacement 76% Water	Constant Flow Method Q_{in} = 0.001 ml/min σ'_3 = 30 kPa i= 1 - 1.6	90 Days	4.6×10^{-9}	Dia = 50 mm Length = 100 mm
Gill and Christpher (1985) (Section 2.6.1)	Mix 4 and Mix 6 See Table 2.1	Falling Head Method σ'_3 = 13 kPa i= 8 - 10	90 Days	6.0×10^{-9} (Mix 4) 9.0×10^{-8} (Mix 6)	Dia = 51 mm Length = 102 mm
Khera and Tirumala (1992) (Section 2.6.2)	Mix ACL3-W 12% Bentonite 15% Cement:Slag (1:3)	Constant Head Method σ'_3 = 55 kPa i= 20 - 60	Not Stated	3.8×10^{-9}	Dia = 70 mm Length = 25 mm - 60 mm
Deschênes et al. (1995) (Section 2.6.4)	Mixes: BJ-1, BJ-2, and BJ-4 See Table 2.3	Constant Head Method σ'_3 = 100 kPa i= 12 - 24	90 Days and 98 Days	4.4×10^{-9} (BJ-1) 1.9×10^{-8} (BJ-2) 6.2×10^{-9} (BJ-4)	Dia = 51 mm Length = 127 mm
Manassero et al. (1995) (Section 2.6.5)	4% Bentonite 19.2% Cement Containing 60% GGBS 76.8% Water	Constant Head Method p' = 0.08 MPa i= 12	5 to 7 Months	$\approx 1.0 \times 10^{-8}$	Not Stated
Tedd et al. (1997) (Section 2.6.6)	Not Described (It was in Accordance to Specification used in the UK)	Not Described (It was in Accordance with ICE 1996)	90 Days	$\approx 1.0 \times 10^{-10}$	Dia = 100 mm
Philip (2001) (Section 2.6.7)	3.5% Bentonite 16.5% Cement with 79% GGBS Replacement 76% Water	Constant Flow Method Q_{in} = 0.001 - 0.01 ml/min σ'_3 = 100 kPa i= 3 - 70	3 Years	5.9×10^{-9}	Dia = 50 mm
Joshi et al. (2010) and Soga et al. (2013) (Section 2.6.8)	3.4% Bentonite 12.6% Cement with 80% GGBS Replacement 84% Water	Constant Flow Method Q_{in} Not Stated σ'_3 = 100 kPa i= 5 - 30	90 Days	2.0×10^{-10}	Dia = 100 mm Length = 100 mm
Williams and Ghataora (2011) (Section 2.6.9)	3% Bentonite 13.5% Cement with 80% GGBS Replacement 83.5% Water	Constant Head Method σ'_3 = 60 kPa i= 27	90 Days	0.2×10^{-9}	Dia = 38 mm
Carreto (2014) and Carreto et al. (2015, 2016) (Section 2.6.10)	4% Bentonite 16.2% Cement (Without GGBS) 79.8% Water	Constant Head Method σ'_3 = 50 kPa i= 10	60 Days	6.0×10^{-8}	Dia = 97 mm Length = 200 mm

Table 6.4 shows that, the CB hydraulic conductivity varies up to around two orders of magnitude from 10^{-8} m/s to 10^{-10}m/s, with comparatively small variations in: mixture composition, specimen size, and triaxial testing conditions (particularly the effective confining pressure ($\boldsymbol{\sigma'_3}$) and the hydraulic gradient (**i**), as reviewed in **Section 2.7.2**).

The lowest $\bar{k}_{Outflow}$ values were found by Tedd et al. (1997) that was 1.0×10^{-10} m/s, Joshi et al. (2010) and Soga et al. (2013) that was 2.0×10^{-10} m/s, and Williams and Ghataora (2011) that was 0.2×10^{-9} m/s (**Table 6.4**). Tedd et al. (1997), Joshi et al. (2010) and Soga et al. (2013) used the largest size of specimen (100 mm diameter). This assessed in achieving a lower hydraulic conductivity in short-term testing. This

was justified by Carpenter and Stephenson (1986) and shown in **Figures 2.24** and **2.25** (**Sections 2.7.2.1 and 2.7.2.2**), particularly when using low effective confining pressures (i.e. σ'_3 less than 80 kPa) and relatively low hydraulic gradients (i.e. less than 100).

The highest $\bar{k}_{Outflow}$ values were obtained by Gill and Christopher (1985): 9.0 x 10^{-8} m/s for Mix 6, Manassero et al. (1995): 1.0 x 10^{-8} m/s, and Carreto (2014) and Carreto et al. (2015 and 2016): 6.0 x 10^{-8}m/s. These $\bar{k}_{Outflow}$ values are higher than the value recommended by ICE (1999) that is 1.0 x 10^{-9} m/s. This is expected to be mainly due to the CB mixture compositions used; as Gill and Christopher (1985) and Carreto (2014) and Carreto et al. (2015, 2016) did not contain GGBS cement replacement which has a great effect on the performance of CB material.

The other studies presented in **Table 6.4**, including this study, showed $\bar{k}_{Outflow}$ values in the order of 10^{-9}m/s, which is slightly higher than the recommendation of ICE (1999). These ranged between 1.9 x 10^{-8} m/s to 6.2 x 10^{-9} m/s, thus fall between the ranges of lowest and highest $\bar{k}_{Outflow}$ values stated above.

The results of hydraulic conductivity determined through the flexible-wall triaxial cell (**Table 6.4**) were higher than ones determined through the oedometer (indirect method) and falling head permeameter, as reviewed in **Section 2.5**. In the oedometer, the CB hydraulic conductivity varied from 10^{-9} m/s under effective stress of 1000 kPa to 10^{-11} m/s under effective stress of 2500 kPa (Manassero et al., 1995; Philip, 2001; and Royal et al., 2017). This is because the effective stresses applied in the oedometer were very high. Similarly in the falling head permeameter, the CB hydraulic conductivity varied from 10^{-10} m/s to 10^{-11} m/s (Royal, 2006).

In general, the σ'_3 used in the various studies reviewed in **Table 6.4** (including this study) were not high enough to exceed the yield stress of the tested CB specimens, as it mainly ranged from 13 kPa to 100 kPa; thus it did not alter or significantly reduce the initial void ratio. This might be the reason of not achieving $\bar{k}_{Outflow}$ values of orders lower than 10^{-10}m/s even after 3 years of curing as investigated by Philip (2001). However, the hydraulic conductivity measured under such low σ'_3 seems to be more realistic to reflect the expected underground stress conditions around a CB barrier as suggested by Grube (1992) and Philip (2001). This also applies on the range of hydraulic gradients used that ranged from 1 to 70 (**Table 6.4**), which do not seem to have a deteriorating impact or decreasing effect on the hydraulic conductivity of CB (reviewed in **Section 2.7.2.1)**.

Finally, the results of the hydraulic conductivity, which are presented in **Table 6.4,** do not seem to vary with respect to the variation of the testing methods in flexible-wall triaxial cell, i.e. conventional as constant and falling head, to more advanced (and quicker tests) such as constant flow.

6.8 CHANGE OF HYDRAULIC CONDUCTIVITY WITH TXUU DEFORMATION AT 90 DAYS OF CURING

The change of hydraulic conductivity with TXUU deformation of CB specimens after 90 days of curing was measured using the single-stage with constant flow method (**Section 3.8**), that was developed for this purpose. This method aimed to evaluate the hydraulic conductivity after applying certain amount of axial displacement or strain relative to the general stress-strain behaviour that was characterised through repeated TXUU tests as shown in **Figure 6.1**. The results of CB hydraulic conductivity after TXUU deformation were detailed in **Sections 5.3** to **5.6**, and compared with each

other herein with respect to the $\bar{k}_{Outflow}$ determined at each deformation state as shown in **Table 6.5**, and **Figure 6.19**.

The variation in hydraulic conductivity with strain is illustrated as an idealised model in **Figure 6.19**. This model depicts the minimum $\bar{k}_{Outflow}$ occurred before failure (i.e. before exceeding the undrained peak strength). Also, this model shows the upper and lower bounds of $k_{Outflow}$ values occurred once the undrained peak strength is exceeded, based on the repeated tests with increasing strain. Details of the variation of $k_{Outflow}$ values encountered in this study (that were used to draw those upper and lower bounds) are discussed in the next section (**Section 6.9**).

Table 6.5: The change of $\bar{k}_{Outflow}$ at 90 days with increasing axial strain

State of Deformation	Axial Strain Limit (%)	Count of Test Repeats	$\bar{k}_{Outflow}$ (x 10^{-9} m/s)
Intact State	0.0	5	4.6
Pre-Peak Deviator Stress State	0.6	4	8.0
Just after $\bar{\varepsilon}_{peak}$ at 90 Days of Curing	1.1	4	6.3
Just after Peak Deviator Stress State	Varied from 1 to 1.3	2	13.1
Post-Peak Deviator Stress State	2.2	4	363.9
	3.3	5	1252.9
	4.4	5	519.3
	5.5	5	819.0

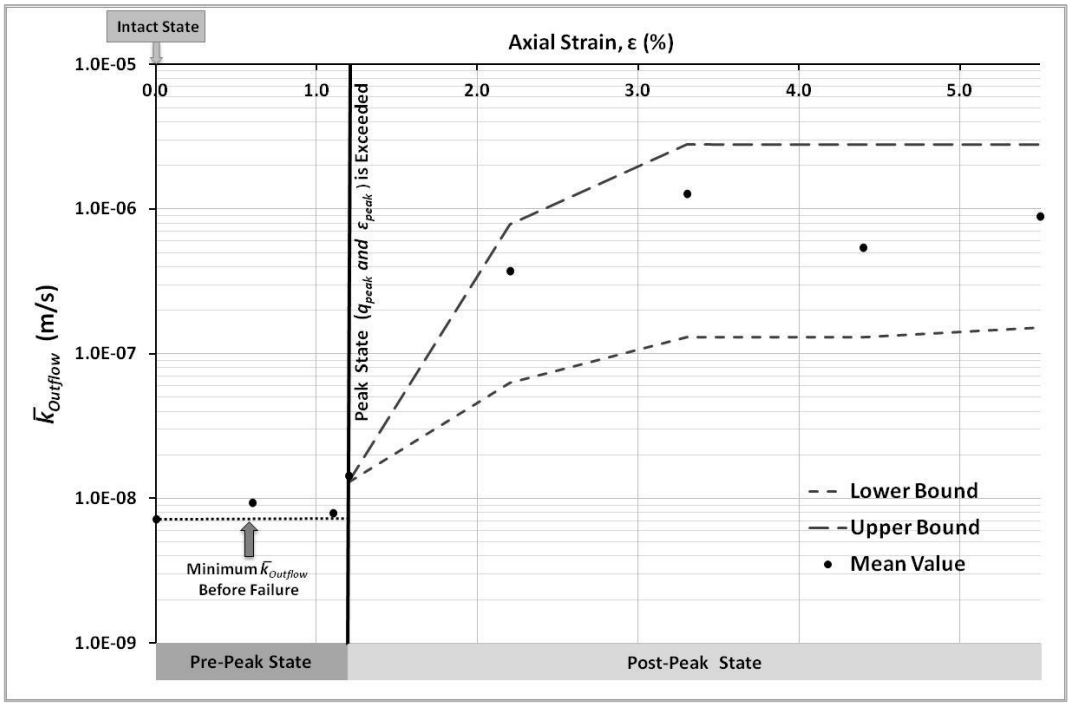

Figure 6.19: Idealised model of the impact of TXUU loading on the CB hydraulic conductivity at 90 days of curing

The $\bar{k}_{Outflow}$ was the lowest at the intact state, i.e. 4.6 x 10^{-9} m/s (**Table 6.5**, and **Figure 6.19**). This did not notably change, when TXUU deformation were performed up to 1.1% axial strain (i.e. just after the $\bar{\varepsilon}_{peak}$ at 90 days), as the $\bar{k}_{Outflow}$ of pre-peak states were overlapping within the same order of magnitude (i.e. 10^{-9} m/s), as shown in **Table 6.5** and **Figure 6.19**. This implies that if microcracking took place due to undrained loading before achieving the peak state (q_{peak}, ε_{peak}) that was not possible to be justified herein, this does not appear to have a significant impact upon the hydraulic conductivity of the material. Therefore, the minimum $\bar{k}_{Outflow}$ occurred before failure can be considered to be equivalent to the $\bar{k}_{Outflow}$ achieved at the intact state that was 4.6 x 10^{-9} m/s (**Figure 6.19**).

The $\bar{k}_{Outflow}$ immediately increases once the peak state was exceeded (by 0.2% axial strain) to be 1.3 x 10^{-8} m/s (**Table 6.5**, and **Figure 6.19**), although an evaluation of

potential variation of hydraulic conductivity at the state just post-peak strength was not possible, due to the limited number of test specimens available at that testing time. Thus, **Figure 6.19** does not present the expected upper and lower bound of $k_{Outflow}$ at this state. The hydraulic conductivity parameter is effectively a measure of microstructure properties. The sudden increase in $\bar{k}_{Outflow}$ immediately after the peak state indicates that potential negative impact of TXUU loading on the performance of CB material initiates with the shearing of the cementitious bonds. This coincides with the observed cracking phenomenon in TXUU tests, as minor cracks were visible on CB specimens just after exceeding the peak state, as seen at an axial strain of 1.4% (Point ***A***, **Figure 6.18**; **Section 6.6**).

The $\bar{k}_{Outflow}$ values were the highest at post-peak state after exceeding 2.2% axial strain; they were of 10^{-6} m/s and 10^{-7} m/s order of magnitudes (**Table 6.5**, and **Figure 6.19**). The range of $k_{Outflow}$ at post-peak state (illustrated by the upper and lower bounds in **Figure 6.19**) was the widest comparative to ranges at pre-peak states. This agrees with the higher variation of TXUU behaviour exhibited after exceeding the peak state that is independent of curing age and CP, as presented in **Section 6.5**. At post-peak state; the CB specimens fail through propagation of major failure planes of different patterns, as observed in **Figure 6.18** (from point ***B*** onwards). Thus, facilitating higher seepage through the variable macrostructure of failed CB specimens and compromising the low hydraulic conductivity of the CB material.

6.9 VARIATION OF HYDRAULIC CONDUCTIVITY RESULTS

The hydraulic conductivity parameter is well known as being an extremely variable parameter, possibly the most variable in geotechnical engineering (Dunn and Mitchell, 1984). This is evident from the data developed in this study (reviewed in

Section 2.6 and shown in **Section 6.7**). The major sources of the variation seen in the hydraulic conductivity results in this study were identified as being a variation in the performance of the CP and TBP air regulators (i.e. the performance of triaxial testing equipment, **Section 3.6**), and variation in the material properties of the various CB specimens tested using the single-stage method (**Section 3.3**). Another source of variation was encountered after failure of the CB specimens (i.e. at the post-peak state), which was the variation in development and propagation of major multiple failure planes of varying lengths and widths (**Figure 6.18**) affecting the flow paths and flow rates possible to achieve through each tested specimen.

Table 6.6 presents the mean hydraulic conductivity results of CB specimens at 90 days at all testing states. As observed in results of all the hydraulic conductivity test repeats at every testing state, as detailed in **Chapter 5**, the Q_{Out} was always smaller than the Q_{In}. In addition, the difference between the Q_{In} and Q_{Out} was negligible and similar in magnitude to the control testing (using only porous stones, **Section 3.6**). This, therefore, yielded to the $k_{Outflow}$ being always smaller than the k_{Inflow}, and produces a relatively negligible difference in hydraulic conductivity (as illustrated by $\bar{k}_{Inflow} - \bar{k}_{Outflow}$ in **Table 6.6**).

Table 6.6: Variation of mean hydraulic conductivity results at 90 days with increasing axial strain

State of Deformation	Axial Strain Limit (%)	Count of Test Repeats	$\bar{k}_{Inflow}$ (x 10^{-9} m/s)	$\bar{k}_{Outflow}$ (x 10^{-9} m/s)	$\bar{k}_{Inflow} - \bar{k}_{Outflow}$ (x 10^{-9} m/s)
Intact State	0.0	5	7.2	4.6	3.6
Pre-Peak Deviator Stress State	0.6	4	9.4	8.0	5.4
Just after $\bar{\varepsilon}_{peak}$ at 90 Days of Curing	1.1	4	7.9	6.3	4.7
Just after Peak Deviator Stress State	Varied from 1 to 1.3	2	14.3	13.1	13.0
Post-Peak Deviator Stress State	2.2	4	371.4	363.9	62.8
	3.3	5	1277.9	1252.9	356.4
	4.4	5	540.3	519.3	129.6
	5.5	5	892.1	819.0	150.9

The negligible difference between $\bar{k}_{Inflow}$ and $\bar{k}_{Outflow}$ (**Chapter 5, Table 6.6**), was mainly encountered due to the experimental error detailed in the Methodology Chapter (**Section 3.6**) as suggested and justified by Aiban and Znidarcic (1989). This difference was noticed to relatively reduce at post peak state (i.e. when cracks form after exceeding the peak state). This indicates that the hydraulic conductivity is more sensitive to the variations in triaxial equipment performance and CB material properties before exceeding the peak state. In other words, the hydraulic conductivity reflects the CB microstructure before exceeding the peak state (or before failure); whereas it reflects the CB macrostructure (i.e. characterised by discontinuities) once the peak state is exceed. Yet, the difference between k_{Inflow} and $k_{Outflow}$ (or, $\bar{k}_{Inflow}$ and $\bar{k}_{Outflow}$) at all deformation states could be considered acceptable, as being always of the same order of magnitude of the accuracy of the hydraulic conductivity (i.e. k_{Inflow} or $\bar{k}_{Inflow}$) as suggested and justified by Aiban and Znidarcic (1989).

In addition, the variation in hydraulic conductivity results can be assessed by considering the range of hydraulic gradients required to establish steady state flow condition. The mean hydraulic gradients were found to considerably increase and widen in range once the peak state was exceeded (**Chapter 5**). This increased from a range of; 0.8 to 2.0 at the intact and pre-peak states, to 0.8 to 13.9 at the post-peak states. This also suggests that CB hydraulic conductivity is controlled by the macrostructure once the peak state is exceeded; as higher hydraulic gradients are required for generating a measurable flow through discontinuities forming after failure (or peak state).

Furthermore, to illustrate the variability of hydraulic conductivity of CB specimens with increasing TXUU deformation, the variation of $k_{Outflow}$ and $\bar{k}_{Outflow}$ values are

illustrated in **Figure 6.20** and **Table 6.7**. The variation of $k_{Outflow}$ and $\bar{k}_{Outflow}$ from intact state to state just after $\bar{\varepsilon}_{peak}$ at 90 days was negligible. The ranges of difference between the maximum $k_{Outflow}$ and minimum $k_{Outflow}$ were narrow and overlapped at these states, as they were in the same order of magnitude (i.e. 10^{-9} m/s). This negligible variation is believed to have occurred mainly due to variation of material properties (i.e. function of microstructure) and triaxial equipment performance justified in **Section 3.6**.

The potential variation of $k_{Outflow}$ and $\bar{k}_{Outflow}$ just after peak state, could not be evaluated as a limited number of specimens (two only) were available to investigate at this state (**Figure 6.20** and **Table 6.7**). The results of the conducted two test repeats did not show any variation at this state, as $k_{Outflow}$ was 1.3 x 10^{-8} m/s in both tests.

For the post-peak state, the major source of variation of $k_{Outflow}$ and $\bar{k}_{Outflow}$ was the variability in the formed cracks patterns after exceeding the peak state (i.e. function of macrostructure) as justified earlier. The ranges of difference between the maximum $k_{Outflow}$ and minimum $k_{Outflow}$ at this state was higher and wider than the ones occurred at earlier states, as it varied from an order of 10^{-8} m/s to 10^{-6} m/s (**Figure 6.20** and **Table 6.7**).

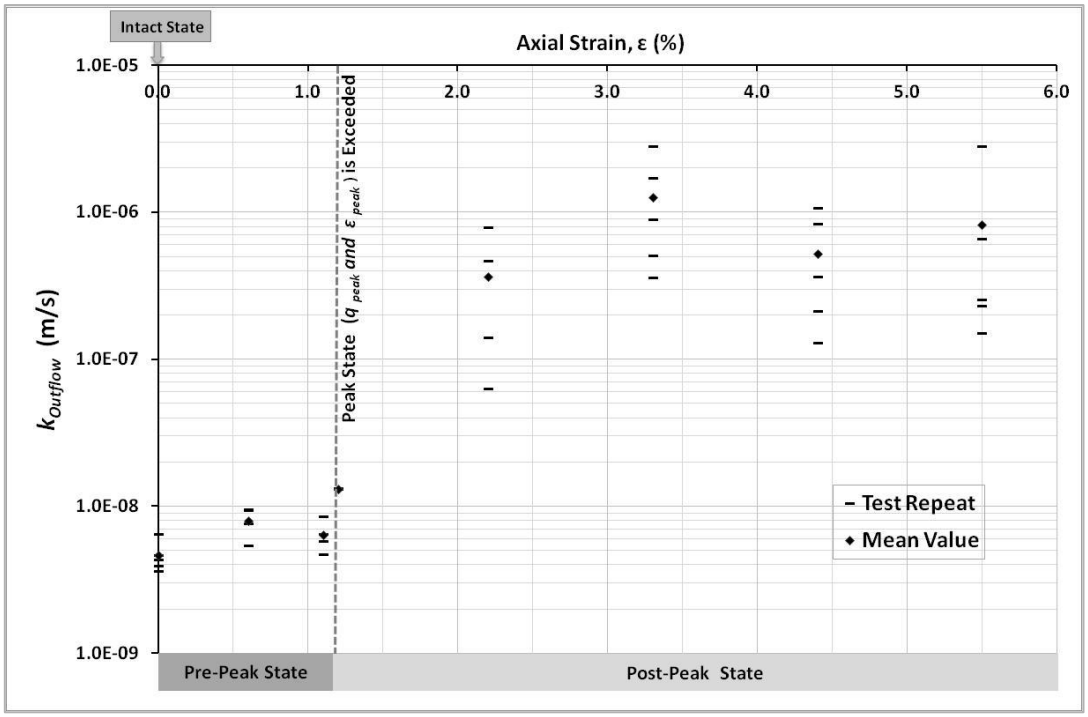

Figure 6.20: Variation of $k_{Outflow}$ and $\bar{k}_{Outflow}$ of CB specimens at 90 days with increasing axial strain in repeated single-stage TXUU and constant flow tests

Table 6.7: Variation of hydraulic conductivity of CB specimens at 90 days with increasing axial strain in repeated single-stage TXUU and constant flow tests

State of Deformation	Axial Strain Limit (%)	Count of Test Repeats	$\bar{k}_{Outflow}$ (x 10^{-9} m/s)	Maximum $k_{Outflow}$ (x 10^{-9} m/s)	Minimum $k_{Outflow}$ (x 10^{-9} m/s)
Intact State	0.0	5	4.6	6.5	3.6
Pre-Peak Deviator Stress State	0.6	4	8.0	9.5	5.4
Just after $\bar{\varepsilon}_{peak}$ at 90 Days of Curing	1.1	4	6.3	8.5	4.7
Just after Peak Deviator Stress State	Varied from 1 to 1.3	2	13.1	13.2	13.0
Post-Peak Deviator Stress State	2.2	4	363.9	785.2	62.8
	3.3	5	1252.9	2802.2	356.5
	4.4	5	519.3	1062.1	129.6
	5.5	5	819.0	2800.2	150.9

6.10 IMPLICATIONS FOR CB PERFORMANCE WHEN EXPOSED TO UNDRAINED DEFORMATION

From the results obtained in this study (presented in **Chapters 4 and 5**, and discussed in this chapter), it is evident that the CB stress-strain behaviour under TXUU loading is broadly similar to the behaviour under TXCU loading (reported in the literature, **Section 2.4**), that is brittle strain softening-post peak with formation of multiple

failure planes. This behaviour is independent of the curing age as seen in this study, and independent of effective stress achieved prior to undrained shearing as reported by Joshi (2009) and Soga et al. (2013). The only difference seen between TXCU and TXUU is the failure modes; that is tensile or wedge failure under zero or low effective stresses ($\leq$ 200 kPa), and shear failure under higher effective stresses (Alzayani et al., 2016). Therefore, regardless of the effective stress achieved prior to undrained loading, cracking of CB material happens (either through formation of vertical or inclined discontinuities), which impacts the performance of CB. In contrast, strain-hardening behaviour is exhibited by CB material under TXCD shearing (Alzayani et al., 2016). Hence, deformation under undrained condition yields the most critical behaviour that risks the performance of CB (Alzayani et al., 2016), as it triggers the increase of pore water pressures (that might overcome the total stresses at small strains) within the low hydraulic conductivity fabric if effective drainage is not provided. When sufficient drainage is provided prior and during loading of CB, the pore water pressures will not rapidly increase above hydrostatic (or exceed the total stress); thus shearing and cracking of CB will not occur.

Furthermore, through results of the multi-stage TXUU shearing method with constant head hydraulic conductivity testing (**Section 3.7.3**), failure of CB material was not justified as it exhibited strain-hardening behaviour (akin to behaviour under TXCD loading). This implies that even if the CB material experiences a phase of small and quick undrained loading (i.e. around 0.3 mm displacement at a rate of 1 mm/min, as applied in this study) that is followed by a sufficient drainage phase; cracking might not occur and the performance criteria would still be satisfied. This is worth investigating thoroughly in future research as it was not covered in the published literature. In addition, the effect of such treatment (i.e. drainage after a phase of

undrained loading) on the CB microstructure need to be evaluated to confirm whether healing (or beneficial alteration) of the hardened CB fabric happens through drainage and further curing in relation to varying curing ages and total stresses.

As a result of this study, the undrained peak strength (i.e. q_{peak}) and the undrained elastic stiffness (i.e. E_u and G_u) were justified to be greatly governed by the curing age (**Sections 6.4** and **6.5**). Whereas, the axial strain at which the undrained peak strength occurs (i.e. ε_{peak}) was not observed to greatly vary with curing age as it normally ranged between 0.6% and 1.4% (**Sections 6.4** and **6.5**). This confirms that the brittle nature of hardened CB (i.e. failure under small axial strains) is key when undrained loading is exhibited regardless of the curing age achieved.

The triaxial testing equipment used in this study was not sufficient to validate if microcracking (not visible to the naked eye) is experienced before reaching the q_{peak} or $\varepsilon_{peak.}$ Although, as the hydraulic conductivity is a measure of a material microstructure, the CB hydraulic conductivity remained approximately constant (in the order of 10^{-9} m/s) with increasing strain until the q_{peak} or ε_{peak} was mobilised (**Figures 6.19 and 6.20**). This, therefore, does not confirm if microcracking is experienced before reaching the ε_{peak}; particularly as the hydraulic conductivity measured before failure is highly sensitive to variations in material properties and performance of triaxial equipment as seen in this study. This implies that future research using advanced equipment is required to validate the microcracking phenomenon of CB material, as it has a brittle nature akin to sedimentary rocks that were confirmed to undergo microcracking prior exceeding their peak compressive strength (Alzayani et al., 2016).

Through visible crack investigation of cracking process of CB specimens of various curing ages in this study (**Section 6.6**), the first (visible) minor crack appeared to the naked eye just after exceeding the $\boldsymbol{\varepsilon_{peak}}$ (generally at 1.4% strain). This seemed to corroborate the findings of hydraulic conductivity measurement just after exceeding the particular $\boldsymbol{\varepsilon_{peak}}$ of CB specimens after 90 days of curing by around 0.2% strain, which indicated the initial increase of the hydraulic conductivity from being in the order of 10^{-9} m/s to 10^{-8} m/s. Unfortunately, such findings were not possible to be determined for CB specimens of curing ages less than 90 day in the triaxial cell, as steady state flow condition was never confirmed, thus the hydraulic conductivity could not be calculated (**Section 3.8.3.1**). However, the negative impact of undrained deformation on the performance of hardened CB of curing ages less than 90 days is postulated to be broadly similar to the one after 90 days, because the brittle deformation behaviour and cracking post undrained peak strength in TXUU tests (i.e. failure under small axial strains ranging from 0.6% to 1.4%) was exhibited at all curing ages from 15 days to 90 days. Hence, as the $\boldsymbol{\varepsilon_{peak}}$ does not seem to vary considerably with varying undrained peak strength or curing age, it is suggested to be the most significant parameter affecting the CB performance at any curing age, and must not to be mobilised under undrained loading. In other words, even if the CB mixture is designed to satisfy the required undrained strength specification; mobilising this strength (at any curing age or effective stress) under undrained loading likely results in fracturing the hardened CB material and hence loss of its low hydraulic conductivity (i.e. fail the performance criteria to retard underground seepage), even at small stain values (i.e. $\boldsymbol{\varepsilon_{peak}} \leq 1.4\%$).

Furthermore, when considering a CB barrier, it is important to acknowledge that the CB material and the surrounding ground are not similar in nature; thus they are likely to undergo different deformation responses. In this case the CB barrier should be designed to maintain its stability and withstand any ground loads without experiencing a strain that approaches failure (i.e. not be the weakest component). Hence, provision of underground drainage and monitoring facilities is very important to optimise the performance of a CB barrier in the field (i.e. maintain stable pore water pressure conditions within the CB material). Controlled drainage is essential in case any increase in overburden load or underground seepage is expected to occur due to superstructure construction work or increase in hydraulic head across an adjacent embankment or waste control system. Also, drainage might help in case a change in both strain and stress conditions occurs (generating horizontal or vertical movement of the ground) due to; adjacent excavation and backfilling works, vegetation, or seismic activities.

Finally, as a result of this study it is recommended to characterise the undrained deformation behaviour of any CB mixture aimed to be used in designing a CB barrier, particularly in the short term and under TXUU conditions. This is because it is not certain under what stress and drainage conditions the CB material will begin to consolidate or exhibit strain hardening behaviour. As the CB material is found to be far weaker in undrained conditions at any age and effective stress post hardening (i.e. after 7 days of curing), the ground conditions must be monitored and optimised to ensure the best performance throughout the complete service terms of a CB barrier.

6.11 SUMMARY

This chapter discusses the findings from the TXUU shearing (**Chapter 4**) and the hydraulic conductivity testing (**Chapter 5**) and establishes the relationship between them.

The general TXUU behaviour of CB specimens has been characterised with explanation of the pore water pressure response experienced. The effect of the curing age on the TXUU behaviour and the mechanical properties is discussed. The drop in the deviator stress from q_{peak} to q_{min} (after failure) was observed to increase with the increase of the curing age. Thus, this confirmed the increase of the brittleness and stiffness of the CB material with the increase of the curing age. In addition, the variation in TXUU deformation results has been evaluated and discussed. The major source of variation in the CB mechanical properties has been attributed to variation in the CB material properties as being casted from slurry. Furthermore, the findings from the visible investigation of cracks development process under the UCS and TXUU testing have been discussed. The first minor tension crack was observed to form just after exceeding the peak deviator stress state (q_{peak} and ε_{peak}).

The CB hydraulic conductivity results of the intact CB specimens (i.e. not deformed) have been compared with similar ones published in the literature (reviewed in **Chapter 2**). The results did not seem to vary with respect to variation in the testing methods in the flexible-wall triaxial cell. However, they seemed to vary due to variations in the specimen size, hydraulic gradient, and effective confining pressure. The variation in the hydraulic conductivity results has been evaluated and discussed.

Finally, an idealised model illustrating the relationship between the TXUU deformation and hydraulic conductivity of the CB specimens after 90 days of curing

has been proposed based on the single-stage methodology results. The implications for CB performance when exposed to undrained deformation have been suggested and discussed.

CHAPTER 7
CONCLUSIONS AND RECOMMENDED FURTHER WORK

7.1 INTRODUCTION

Hardened CB material is demonstrably most vulnerable to fail in the short-term, if loaded under undrained conditions as consolidation might still not commenced (Alzayani et al., 2016); thus understanding undrained deformation response is believed to be key if the low hydraulic conductivity is to be maintained. This study aimed to assess the relationship between CB hydraulic conductivity and undrained deformation response (i.e. under worst case TXUU loading conditions expected to occur in the short-term of a CB barrier).

A mixture design (based on recommendations of ICE 1999 and Gravin and Hayles, 1999) was selected to be examined in this study, and evaluate its performance under TXUU loading. This mixture comprised (by total weight); 4% bentonite, 4% cement, 16% GGBS (80% cement-replacement), and 76% water.

The brittle TXUU behaviour at curing ages less than 90 days was found to be broadly similar to that after 90 days of curing (but of a lower magnitude of strength). Therefore, the relationship between the undrained deformation and hydraulic conductivity has been predicted to be similar for CB specimens during a shorter curing term less than 90 days. This relationship was identified through developing the

single-stage triaxial testing methodology, through which a predefined strain was applied before measuring the hydraulic conductivity using the constant flow technique. The brittle strain-softening deformation response in undrained conditions was maintained through applying the single-stage triaxial testing methodology and the main testing was completed in relatively short period. The repeatability testing has justified that the inherent variability of the CB specimens batched from slurry did not have a negative influence on the hydraulic conductivity results determined using the single-stage triaxial method.

In this chapter, the conclusions of this study are summarised, and recommendations for future research are suggested.

7.2 CONCLUSIONS

This thesis has identified the unknown relationship between the undrained deformation and hydraulic conductivity of the CB specimens containing GGBS in the triaxial cell. This relationship was justified to be controlled by the peak deviator stress state parameters; q_{peak} and ε_{peak}.

The CB hydraulic conductivity did not appear to be adversely affected if the undrained peak strength (q_{peak}) was not mobilised regardless of the curing age and effective stress achieved. It was initially in the order of 10^{-9} m/s and increased up to 10^{-6} m/s order of magnitude through propagation of multiple major cracks under TXUU shearing. This key finding has confirmed the detrimental impact of undrained deformation on the CB performance (i.e. hydraulic conductivity).

The CB hydraulic conductivity after 90 days of curing experienced insignificant variation at axial strains smaller than the ε_{peak}. This variation was within the same

order of magnitude (i.e. 10^{-9} m/s) and occurred due to the CB material variation rather than the microstructure changes. The formation of unfavourable minor visible cracks was observed to happen suddenly and immediately after exceeding the ε_{peak} by approximately 0.2% as inspected in the TXUU and UCS tests. This resulted in the failure of the CB performance, because the hydraulic conductivity suddenly increased to 1.3 x 10^{-8} m/s. After exceeding the ε_{peak}, the CB hydraulic conductivity showed significant variation as it ranged from the order of 10^{-7} m/s to 10^{-6} m/s due to variation in the cracking patterns and intensity. This has confirmed that the CB performance is directly influenced by the brittle strain-softening behaviour that is experienced under undrained loading regardless of the curing age and the effective stress achieved.

Furthermore, this thesis has concluded the following:

- The multi-stage triaxial testing methodology has confirmed the variable deformation behaviour of the CB material that is presented in the previous research. Ductile strain-hardening behaviour was exhibited when multiple cycles of triaxial undrained shearing and hydraulic conductivity testing were applied to a single CB specimen.

- The measurement of CB hydraulic conductivity was affected by the CB hydration processes. The effect of these processes was most significant when CB specimens at curing ages less than 90 days were tested. The outflow rates were found to be insignificantly lower than the inflow rates (even after 90 days of curing), and the hydraulic gradients were not constant when testing CB specimens of curing ages less than 90 days.

- The CB hydraulic conductivity was controlled by the CB material properties and its strength and elastic stiffness before reaching the undrained peak strength. However, the fissured macrostructure controlled the CB hydraulic conductivity after exceeding the undrained peak strength.

- The stability of the pore water pressure within the CBB is important to maintain its performance requirement. The increase of the pore water pressure might mobilise the brittle nature of the hardened CB material. The effective stress and curing age achieved are less important comparative to the pore water pressure control.

- The q_{peak} was justified to increase with the increase of the curing age and the effective stress achieved. Whereas, the ε_{peak} was relatively constant (with a mean of 1%) and independent of the curing age and effective stress. Therefore, it is critical that the ε_{peak} and elastic stiffness of the CB material is not mobilised, if cracking is to be avoided and the low hydraulic conductivity is to be maintained.

- Unconsolidated or consolidated (under low effective confining conditions associated with shallow CBB projects) undrained loading on the CB material should be used when investigating its performance, as it is the most vulnerable loading condition in the short and long term.

Finally, considerable care is advised to be taken not to expose the CBB to relatively large loads (i.e. including temporary loading from the construction processes and plant) particularly during the short term as the consolidation might not be established. In addition, controlled drainage is highly recommended to be installed around the CBB in order to encourage the ductile strain-hardening behaviour, which might

optimisie the performance in case changes in the total stress occurs (for example due to an increase in the overburden load, groundwater seepage, or ground movements caused by seismic or rapid drawndown of reservoir water level).

7.3 RECOMMENDATIONS FOR FURTHER WORK

The aim and objectives developed for this study were successfully accomplished through the findings achieved as discussed in this thesis. Although, these findings revealed that implications for CB barrier performance if experiencing loading of various drainage scenarios before and after exceeding the peak strength is not completely known. Hence, further research in this area is highly recommended. Some of these revealed unknowns are microcracking phenomenon pre-peak strength, effect of drainage or consolidation in healing fissured CB fabric at varying curing ages, and possible ways of optimising the performance of CB barrier material in the field (e.g. through controlled drainage) if loading or movement is experienced. As seen in this study, limitations of equipment and time prevented investigation of those revealed unknowns.

In addition, as explained in this thesis, the scope of work undertaken in this project has been limited to relatively small number of parameters as a function of time required to develop the bespoke method that required considerable research and experimental effort. These parameters were: development of single mixture design, investigation of curing ages up to 90 days, and permeation with tap water for hydraulic conductivity measurement. Therefore, it is recommended that variation of these parameters is to be studied in future research using the developed methodology herein.

Furthermore, the usage of advanced pressure control system that provides stable performance is highly recommended to avoid the experimental error that might be encountered in the hydraulic conductivity results as seen in this study when using conventional pressure air regulators for controlling the cell and back pressures.

Further work is recommended to complement what was achieved in this study as summarised below, based on the limitations of time and testing equipments that prevented identification of the unknowns revealed in this study.

7.3.1 STUDY OF MICROCRACKING PROCESS USING ADVANCED LABORATORY TESTING EQUIPMENTS

As the CB material has a brittle nature akin to sedimentary rocks; and these rocks exhibits microcracking prior to mobilisation of the peak strength, it would be worthy to determine if CB also undergoes microcracking before undrained peak strength and what impacts this has on long-term performance (durability, deformation response, etc.).

Therefore, the microcracking behaviour of the CB material at small strains (less than 1%) should be investigated using advanced testing equipment such as acoustic emission (AE) monitoring (in UCS tests) and bender elements (in triaxial shear tests). A complex and comprehensive laboratory study combining advanced uniaxial and triaxial compression techniques should be undertaken to validate the microcracking phenomenon of CB specimens of varying curing ages. Such findings would justify if the CB is a durable material and have adequate performance in case undrained loading phases were experienced at very small strains.

7.3.2 STUDY OF EFFECT OF CONSOLIDATION (DRAINED LOADING) ON THE PERFORMANCE OF JUVENILE FISSURED CB SPECIMENS IN THE TRIAXIAL CELL

A study to confirm if microcracks or minor cracks that might form during the short-term due to undrained loading could be modified through continued curing of cementitious components and drained loading is required.

In such study, CB specimens of varying curing ages up to 90 days could be deformed using the single-stage TXUU shearing until minor cracks form. Different drained loading scenarios are suggested to be applied on the fissured specimens to evaluate their implications. This should validate if the fissured CB material is positively affected or recovered by; increase of effective stress (i.e. closure of cracks through consolidation under drained loading), and the ongoing CB hydration processes (under continuous seepage) in the short-term (i.e. up to 90 days of curing).

Triaxial pressure control equipment with very high resolution and stable performance should be used to avoid limitations of conventional air regulators.

CB specimens of various sizes and different crack patterns and intensity are suggested to be tested to assess their influence on potential variations of results.

7.3.3 STUDY OF DRAINAGE IMPLICATIONS ON PERFORMANCE OF SMALL SCALE CB SLURRY WALL IN THE LABORATORY

The size of the test specimens in the laboratory potentially has an effect on the results of hydraulic conductivity (highlighted in the literature review); the larger the specimen size, the lower the hydraulic conductivity. Therefore, it is recommended to investigate the implications of drainage on the performance of a small scale CB slurry wall in the laboratory using the multi-stage or single-stage loading and flow pump methods (presented in this study). It is recommended to first simulate the behaviour of

the small scale wall under different loading scenarios using numerical analysis such as Finite Element Modelling (FEM), and then use the numerical findings to tailor the laboratory loading scenarios and testing methodology and stress-strain conditions. Furthermore, the CB performance would be evaluated through the comparison of the numerical behaviour with the one exhibited in the laboratory.

Such a study would aid in specifying the convenient drainage and stress-strain conditions that could speed up the consolidation process within the CB barrier. Furthermore, such study might validate the CB behaviour in a larger scale in case the hydraulic conductivity has increased due to cracking, and whether it has the ability to recover through further curing and/or consolidation.

Finally, such study is suggested to be undertaken after drawing conclusions from the two studies recommended earlier (**Sections 7.3.1**, and **7.3.2**) besides the study discussed in this thesis. This will therefore, justify the advantages and disadvantages of using CB barriers in waste and underground seepage control systems, and set great references to develop a comprehensive specification for controlling and monitoring CB barriers in the field.

REFERENCES

Aiban SA and Znidarčić D (1989) Evaluation of the flow pump and constant head techniques for permeability measurements. *Geotechnique*, *39*(4), pp.655-666. https://doi.org/10.1680/geot.1989.39.4.655.

Alam MS, Chakraborty T, Matsagar V, Rao KS, Sharma P, Singh M (2014) Characterization of Kota Sandstone under different strain rates in uniaxial loading. *Geotech Geol Eng*. DOI 10.1007/s10706-014-9810-3.

Alzayani NJ, Royal ACD, Ghataora GS, Jefferson IN (2016) A review of cement–bentonite in comparison with concrete, rocks and cemented soils. *Environmental Geotechnics* (October 2017, EG5), pp.353–372. https://doi.org/10.1680/jenge.14.00050.

Anderson DC, Crawley W and Zabcik JD (1985) Effects of various liquids on clay soil: bentonite slurry mixtures. In *Hydraulic Barriers in Soil and Rock* (pp. 93-103). ASTM International. DOI: 10.1520/STP34571S.

ASTM Designation D 5084-11 (2011) Standard Test Method for Measurment of Hydraulic Conductivity of Porous Materials Using a Flexible Wall Permeameter. American Society for Testing and Materials, Philadelphia.

Baldi G, Hight DW and Thomas GE (1988) State-of-the-art paper: a reevaluation of conventional triaxial test methods. In *Advanced triaxial testing of soil and rock* (pp. 219-263). ASTM International. DOI: 10.1520/STP29080S.

Banthia N and Mindess S (1989) Water permeability of cement paste. *Cement and concrete research*, *19*(5), pp.727-736. https://doi.org/10.1016/0008-8846(89)90043-4.

Barker P, Esnault A and Braithwaite P (1997) Containment barrier at pride park, Derby, England. *Land Contamination & Reclamation*, 6(1), pp.51-58.

Barvenik MJ (1992) Design Options Using Vertical Barriers Systems, *Environmental Geotech Symposium*, New York, September 1992. ASCE International Convention and Symposium, pp. 14-17.

Benson CH, Gunter JA, Boutwell GP, Trautwein SJ and Berzanskis PH (1997) Comparison of four methods to assess hydraulic conductivity. *J. of Geotech. and Geoenviron. Eng.*, *123*(10), pp.929-937. https://doi.org/10.1061/(ASCE)1090-0241(1997)123:10(929).

Boscardin M, Patterson C, Landis M, Younan JC and Aghjayan D (2006) Evaluation of Permeability of Containment Slurry Walls. In *GeoCongress 2006: Geotech. Eng. in the Information Technology Age* (pp. 1-6). https://doi.org/10.1061/40803(187)8.

Boyes RGH (1972) Uses of bentonite in civil engineering. In *Institution of Civil Engineers, Proceedings*, May 1972 (Vol. 52, No. 7461 Proc Paper), pp. 25-37.

British Geological Survey(BGS) (2017) Ground source heat pumps. Available at: http://www.bgs.ac.uk/reference/gshp/gshp_report.htmlb (Accessed: 29 April 2018).

British Standards Institution (BSi) (1990) Consolidation and permeability tests in hydraulic cells and with pore pressure measurements. BS 1377-6, London, UK.

British Standards Institution (BSi) (1990) Methods of test for Soils for civil engineering purposes-Part 7: Shear strength tests (total stress). BS 1377-7, London, UK.

British Standards Institution (BSi) (1990) Methods of test for Soils for civil engineering purposes-Part 8: Shear strength tests (effective stress). BS 1377-8, London, UK.

British Standards Institution (BSi) (1990) Multi-stage triaxial tests. BS 1377-7:1990:9, London, UK.

Britton JP, Filz GM and Herring WE (2004) Measuring the hydraulic conductivity of soil–bentonite backfill. *J. of geotech. and geoenviron. Eng.*, *130*(12), pp.1250-1258. https://doi.org/10.1061/(ASCE)1090-0241(2004)130:12(1250).

Building Research Establishment (BRE) (1994). *Slurry trench cut-off walls to contain contamination*. Digest 395.

Carpenter GW and Stephenson RW (1986). Permeability testing in the triaxial cell. *Geotech. testing J.*, *9*(1), pp.3-9. https://doi.org/10.1520/GTJ10605J. ISSN 0149-6115.

Carreto J (2014) Self-hardening slurry walls: A contribution for design, quality control and performance monitoring. PhD thesis. Lisbon University, Portugal.

Carreto J, Caldeira L and Maranha das Neves E (2016) Processes Involved in the Formation and Performance of Self-Hardening Slurry Walls: Santa Clara-a-Velha Monastery Cutoff Wall. *J. of geotech. and geoenviron. Eng.*, *142*(7), pp. 04016019(1-12). https://doi.org/10.1061/(ASCE)GT.1943-5606.0001483.

Carreto JMR, Caldeira LMMS and Neves EJLMD (2015) Hydromechanical Characterization of Cement-Bentonite Slurries in the Context of Cutoff Wall Applications. *Journal of Materials in Civil Engineering*, *28*(2), pp. 04015093(1-13). https://doi.org/10.1061/(ASCE)MT.1943-5533.0001365.

Chandler RJ (1968) A note on the measurement of strength in the undrained triaxial compression test. *Géotechnique*, *18*(2), pp.261-266. https://doi.org/10.1680/geot.1968.18.2.261.

Chew SH, Kamruzzaman AHM and Lee FH (2004) Physicochemical and engineering behavior of cement treated clays. *J. of geotech. and geoenviron. Eng.*, *130*(7), pp.696-706. https://doi.org/10.1061/(ASCE)1090-0241(2004)130:7(696).

Craig RF (1998) *Soil Mechanics*, 6th Ed. E & FN Spon. ISBN: 0-419-22450-5.

Daniel D and Koerner R (2007, February) *Waste containment facilities: Guidance for construction quality assurance and construction quality control of liner and cover systems*. ASCE. https://doi.org/10.1061/9780784408599.

Daniel DE, Anderson DC and Boynton SS (1985) Fixed-wall versus flexible-wall permeameters. In *Hydraulic barriers in soil and rock* (pp. 107-126). ASTM International. DOI: 10.1520/STP34573S.

Das BM (2010) *Principles of geotechnical engineering*. 7th Ed. Cengage Learning. ISBN: 0-495-41132-9.

Dendani H, Flavigny E and Fry JJ (1988) Triaxial test for embankment dams: interpretation and validity. In *Advanced triaxial testing of soil and rock* (pp. 486-500). ASTM International. DOI: 10.1520/STP29094S.

Deschênes J-H, Massiéra M, Tournier J-P (1995) Testing of a cement-bentonite mix for a low-permeability plastic barrier. Dredging, remediation, and contaminated sediments. Demars KR, Richardson GN, Yong RN, Chaney RC (eds). ASTM STP 1293, Philadelphia, pp. 252-270.

Dunn RJ and Mitchell JK (1984). Fluid conductivity testing of fine-grained soils. *J. of Geotech. Eng.*, 110(11), pp.1648-1665. https://doi.org/10.1061/(ASCE)0733-9410(1984)110:11(1648).

Dunstan S, Zdinak AP and Lodman D (1997) Considerations in the development of subsurface containment barrier performance standards. *Land Contamination & Reclamation*, 5(3), pp.177-181.

Evans J (1996) Soil and cement-based vertical barriers with focus on materials. *Assessment of barrier containment technologies. A comprehensive treatment for environmental remedial application*, R. R. Rumer and J. K. Mitchell, eds., International Containment Technology Workshop, National Technical Information Service, Alexandria, VA, pp. 5–43.

Evans JC (1994) Hydraulic conductivity of vertical cutoff walls. In *Hydraulic conductivity and waste contaminant transport in soil* (pp. 79-94). ASTM International. DOI: 10.1520/STP23885S.

Evans JC (1991) Geotechnics of hazardous waste control systems. In *Foundation Eng. Handbook* (pp.750-777). Springer, Boston, MA. https://doi.org/10.1007/978-1-4757-5271-7_20.

Evans JC (1993) Vertical cutoff walls. Daniel DE (eds) *Geotechnical practice for waste disposal*. 1st edn. Chapman & Hall, London. ISBN 0 412 35170 6.

Evans JC and Dawson AR (1999) Slurry walls for control of contaminant migration: A comparison of U.K. and U.S. practices. *ASCE Specialty Conference on Geo-Engineering for Underground Facilities*, ASCE Geotechnical Special Publication No. 90., Reston, Va., pp. 105–120.

Evans JC and Fang HY (1988) Triaxial permeability and strength testing of contaminated soils. In *Advanced Triaxial Testing of Soil and Rock* (pp. 387-404). ASTM International. DOI: 10.1520/STP29089S.

Evans JC and Huang H (2016) Hydraulic Conductivity of Soil-Bentonite Slurry Walls. In *Geo-Chicago 2016* (pp. 548-557). https://doi.org/10.1061/9780784480144.054.

Farmer I (1983) Engineering behaviour of rocks,2nd edn. Chapman and Hall, London. ISBN 0 412 25280 5.

Fratalocchi E, Brianzoni V, Di Sante M, Mazzieri F, Pasqualini E (2013) Migration of aggressive solutions through cement-bentonite slurry walls. Manassero et al. (eds) Coupled Phenomena in Environmental Geotechnics , pp. 243-252.

Fratalocchi E, Pasqualini E (2007) Vertical barriers for side containment. Proc. XXI Geotechnical Conference , Geosythetics and Environment, Torino, Italy.

Fratalocchi E, Pasqualini E, Balboni P (2006) Performance of a cement-bentonite cut-off wall in an acidic sulphate environment. Proc. 5 ICEG, International Congress on Environmental Geotechnics, Cardiff (UK), pp.133-139.

Garvin SL, Hayles CS (1999) Chemical compatibility of cement–bentonite cut-off wall material. Constr. Build. Mater. 13, pp. 329–341.

Georgiannou VN, Burland JB (2006) A laboratory study of slip surface formation in an intact natural stiff clay. Geotèchnique 56(8), pp. 551-559.

Germaine JT and Ladd CC (1988) State-of-the-art paper: Triaxial testing of saturated cohesive soils. In *Advanced triaxial testing of soil and rock* (pp. 421-459). ASTM International. DOI: 10.1520/STP29091S.

Gill SA and Christopher BR (1985) Laboratory Testing of Cement-Bentonite Mix for Proposed Plastic Diaphragm Wall for Complexe LaGrande Reservoir Caniapiscau, James Bay, Canada. In *Hydraulic Barriers in Soil and Rock* (pp. 75-92). ASTM International. DOI: 10.1520/STP34569S.

Graham MD, Xiao M and Owaidat LM (2012) Seismic Performance of Slurry Walls. In *GeoCongress 2012: State of the Art and Practice in Geotechnical Engineering* (pp. 1879-1887). https://doi.org/10.1061/9780784412121.193.

Grube WE (1992) Slurry trench cut-off walls for environmental pollution control. In *Slurry Walls: Design, Construction, and Quality Control* (pp.69-77). ASTM International. DOI: 10.1520/STP19723S.

Guner A (1978) Properties and behaviour of bentonite-cement slurries. PhD thesis. University of London, UK.

Head KH (2006) *Manual of soil laboratory testing* (Vol. 1: Soil Classification and Compaction tests). 3rd Ed. Whittles Publishing. ISBN: 1-904445-36-5.

Head KH and Epps RJ (2011) *Manual of soil laboratory testing* (Vol. 2: Permeability, Shear Strength and Compressibility tests). 3rd Ed. Whittles Publishing. ISBN: 978-1904445-69-2.

Head KH and Epps RJ (2014) *Manual of soil laboratory testing* (Vol. 3: Effective Stress Tests). 3rd Ed. Whittles Publishing. ISBN: 978-184995-054-1.

Hewlett PC (1998) *Lea's Chemistry of Cement and Concret*, 4th Ed. Oxford, UK. Elsevier Ltd. ISBN-10: 0-7506-6256-5.

Hill J and Sharp JH (2002) The mineralogy and microstructure of three composite cements with high replacement levels. *Cement and Concrete Composites, 24*(2), pp.191-199. https://doi.org/10.1016/S0958-9465(01)00041-5.

Hinchberger S, Wech J, Newson T (2010) Mechanical and hydraulic characterization of plastic concrete for seepage cut-off walls. Can. Geotech. J. 47, pp. 461-471.

ICE (1999) Specification for the construction of slurry trench cut-off walls as barriers to pollution migration, Thomas Telford Publishing, London, ISBN: 0 7277 2625 0.

Indraratna B, Balasubramaniam AS, Khan MJ (1995) Effect of fly ash with lime and cement on the behaviour of a soft clay. Quarterly J. Eng. Geo. 28, pp. 131-142.

Jefferis SA (1981) Bentonite-cement slurries for hydraulic cut-offs. Proc. 10thICSMFE, A.A. Balkema, Rotterdam, pp. 435–440.

Jefferis SA (1997) The origins of the slurry trench cut-off and a review of cement-bentonite cut-off walls in the UK. Land Contamination and Reclamation. Vol. 5, n3, p239-245.

Jefferis SA (2012) Cement-bentonite slurry systems. ASCE Proceedings of the 4th International Conference on Grouting and Deep Mixing GSP 228, pp. 1–24.

Jia L, Chen M, Zhang W, Xu T, Zhou Y, Hou B, Jin Y (2013) Experimental study and numerical modeling of brittle fracture of carbonate rock under uniaxial compression. Mechanics Research Communications 50, pp. 58-62.

Jones ME, Bedford J, Clayton C (2013) On natural deformation mechanisms in the chalk. J. Geo. Soc. 141, pp. 675-683.

Joshi K (2009) Long-term engineering performance and in-situ Assessment of cement-bentonite cut-off walls. PhD thesis. University of Cambridge, UK.

Joshi K, Kechavarzi C, Sutherland K, Ng MYA, Soga K, Tedd P (2010) Laboratory and in situ tests for long-term hydraulic conductivity of a cement-bentonite cut-off wall. J. Geotech. Geoenviron. Eng. 136, pp. 562-572.

Joshi K, Soga K, Ng MYA and Kechavarzi C (2008) Durability Study of Eleven Years Old Cement-Bentonite Cut-Off Wall Material. In *GeoCongress 2008: Geotechnics of Waste Management and Remediation* (pp.620-627). https://doi.org/10.1061/40970(309)78.

Khera RP and Tirumala RK (1992) Materials for slurry walls in waste chemicals. In *Slurry Walls: Design, Construction, and Quality Control* (pp.172-180). ASTM International. DOI: 10.1520/STP19732S.

La Rochelle P, Leroueil S, Trak B, Blais-Leroux L and Tavenas F (1988) Observational approach to membrane and area corrections in triaxial tests. In *Advanced triaxial testing of soil and rock* (pp. 715-731). ASTM International. DOI: 10.1520/STP29110S.

Lade PV and Wasif U (1988) Effects of height-to-diameter ratio in triaxial specimens on the behavior of cross-anisotropic sand. In *Advanced triaxial testing of soil and rock* (pp. 706-714). ASTM International. DOI: 10.1520/STP29109S.

Lentz RW, Horst WD and Uppot JO (1985) The permeability of clay to acidic and caustic permeants. In *Hydraulic barriers in soil and rock* (pp.127-139). ASTM International. DOI: 10.1520/STP34574S.

Leroueil S, Tavenas F, La Rochelle P and Tremblay M (1988) Influence of filter paper and leakage on triaxial testing. In *Advanced triaxial testing of soil and rock* (pp. 189-201). ASTM International. DOI: 10.1520/STP29078S.

Manassero M and Viola C (1992) Innovative aspects of leachate containment with composite slurry walls: A case history. In *Slurry Walls: Design, Construction, and Quality Control* (pp. 181-193). ASTM International. DOI: 10.1520/STP19733S.

Manassero M, Benson CH and Bouazza A (2000) Solid waste containment systems. In *ISRM International Symposium*, November 2000, International Society for Rock Mechanics.

Manassero M, Fratalocchi E, Pasqualini E, Claudia S, and Verga F (1995) Containment with vertical cutoff walls. Proc. Geoenviron. – 2000, Geotechnical special publication 46, ASCE, New Orleans, pp. 1142–1172.

Manassero M, Roccato M, Spanna C (1994) Collaudo e certificazione degli impianti di smaltimento rifiuti. Proc., *La geotecnica nella progettazione e costruzione delle discariche controllate*, Milazzo, Messina, Associazione Poligeotecnici Riuniti.

Menzies BK (1988) A computer controlled hydraulic triaxial testing system. In *Advanced triaxial testing of soil and rock* (pp. 82-94). ASTM International. DOI: 10.1520/STP29070S.

Mesri G and Olson RE (1971) Mechanisms Controlling Permeability of Clays. *Clays and Clay Minerals*, Clay Mineral Society, 19(3), pp. 151-158.

Millet RA, Perez JY and Davidson RR (1992) USA practice slurry wall specifications 10 years later. In *Slurry walls: Design, construction, and quality control* (pp. 42-66). ASTM International. DOI: 10.1520/STP19722S.

Mitchell J K, Soga K (2005) *Fundamentals of soil behaviour.* 3rd edn. Wiley, USA. ISBN-10: 0-471-46302-7.

Mitchell JK (1986) Hazardous waste containment. *Geological Society, London, Eng. Geology Special Publications, 3*(1), pp. 145-157. https://doi.org/10.1144/GSL.ENG.1986.003.01.17.

Morin RH and Olsen HW (1987) Theoretical analysis of the transient pressure response from a constant flow rate hydraulic conductivity test. *Water Resources Research, 23*(8), pp. 1461-1470. https://doi.org/10.1029/WR023i008p01461.

Murray EJ, Davis J, Keeton P and Hill RG (2001) Laboratory permeability measurements with Mercia Mudstone. *Geoenvironmental engineering geoenvironmental impact management. London (UK): Thomas Telford Ltd*, pp.455-463. ISBN: 0727730339, 9780727730336.

National Research Council (NRC) (2007) *Assessment of the performance of engineered waste containment barriers*. National Academies Press. ISBN: 0-309-10810-1.

Olsen HW (1966) Darcy's law in saturated kaolinite. *Water Resources Research*, *2*(2), pp.287-295. https://doi.org/10.1029/WR002i002p00287.

Olsen HW, Gill JD, Wilden AT and Nelson KR (1991) Innovations in hydraulic-conductivity measurements. *Transportation Research Record* (1309), pp. 9-17.

Olsen HW, Morin RH and Nichols RW (1988) Flow pump applications in triaxial testing. In *Advanced triaxial testing of soil and rock*. ASTM International. DOI: 10.1520/STP29069S.

Olsen HW, Nichols RW and Rice TL (1985) Low gradient permeability measurements in a triaxial system. *Geotechnique, 35*(2),pp.145-157. https://doi.org/10.1680/geot.1985.35.2.145.

Olson RE and Daniel DE (1981) Measurement of the hydraulic conductivity of fine-grained soils. In *Permeability and groundwater contaminant transport*. ASTM International. DOI: 10.1520/STP28316S.

Opdyke SM, Evans JC (2005) Slag-cement–bentonite slurry walls. J. Geotech Geoenviron. Eng. 131, pp. 673–681.

Pane V, Croce P , Znidarcic D, Ko HY, Olsen HW and Schiffman RL(1983) Effects of consolidation on permeability measurements for soft clay. *Geotechnique*. 33(1), pp. 67-72. https://doi.org/10.1680/geot.1983.33.1.67.

Peters JF, Lade PV and Bro A (1988) Shear band formation in triaxial and plane strain tests. In *Advanced triaxial testing of soil and rock* (pp. 604-627). ASTM International. DOI: 10.1520/STP29102S.

Peterson RW (1988) Interpretation of triaxial compression test results on partially saturated soils. In *Advanced Triaxial Testing of Soil and Rock* (pp. 512-538). ASTM International. DOI: 10.1520/STP29096S.

Philip LK (2001) An investigation into contaminant transport processes through single-phase cement-bentonite slurry walls. *Eng. Geol*. 60, pp. 209-221. https://doi.org/10.1016/S0013-7952(00)00102-2.

Plee D, Lebedenko F, Obrecht F, Letellier M, Van Damme H (1990) Microstructure, permeability and rheology of bentonite-cement slurries. *Cement and Concrete Research* 20, pp. 45-61.

Ressi A and Cavalli N (1985) Bentonite slurry trenches. *Eng. Geo.*, *21*(3-4), pp. 333-339.

Richardson IG and Groves GW (1992) Microstructure and microanalysis of hardened cement pastes involving ground granulated blast-furnace slag. *Journal of Materials Science*, *27*(22), pp.6204-6212. https://doi.org/10.1007/BF01133772.

Roscoe KH, Schofield AN, Wroth CP (1958) On The Yielding of Soils. Géotechnique 8(1), pp. 22 –53.

Royal ACD (2006) Hydraulic retardation of contaminant transport through cement - bentonite walls. PhD thesis. University of Birmingham, UK.

Royal ACD, Makhover Y, Moshirian S, Hesami D (2013) Investigation of Cement–Bentonite Slurry Samples Containing PFA in the UCS and Triaxial Apparatus. *Geotech. Geol. Eng*. 31(1), pp. 767-781. https://doi.org/10.1007/s10706-013-9626-6.

Royal ACD, Opukumo AW, Qadr CS, Perkins LM and Walenna MA (2017) Deformation and Compression Behaviour of a Cement–Bentonite Slurry for Groundwater Control Applications. *Geotech. and Geo. Eng.*, April 2018, *36*(2), pp.835-853. https://doi.org/10.1007/s10706-017-0359-9.

Ryan CR (1985) Slurry cutoff walls: Applications in the control of hazardous wastes. In *Hydraulic barriers in soil and rock* (pp.9-23). ASTM International. DOI: 10.1520/STP34562S.

Scholz C, Rosenberg M and Stahlmann J (2004) State of the art in permeability tests of single-phased cut-off walls. *Land Contamination & Reclamation*, *12*(1), pp.1-8.

Schweitzer F (1989) Strength and permeability of single phase diaphragm walls. *Proc., 12th ICSMFE*, Rio de Janeiro, A.A. Balkema, Rotterdam, The Netherlands, Vol. 3, pp.1515-1518.

Soga K, Joshi K, Evans JC (2013) Cement bentonite cutoff walls for polluted sites, Manassero et al (eds), *Coupled phenomena in environmental geotechnics*. 1st edn. Taylor & Francis, London, ISBN 978 1 138 00060 5.

Talefirouz D, Çokça E and Omer J (2016) Use of granulated blast furnace slag and lime in cement-bentonite slurry wall construction. *Int. J. of Geotech. Eng. 10*(1), pp.81-85. https://doi.org/10.1179/1939787915Y.0000000005.

Tavenas F, Leblond P, Jean P and Leroueil S (1983) The permeability of natural soft clays. Part I: Methods of laboratory measurement. *Canadian Geotechnical Journal*, *20*(4), pp.629-644. https://doi.org/10.1139/t83-072.

Taylor HF (1997) *Cement chemistry*, 2nd Ed. London, UK. Thomas Telford. ISBN: 0 7277 2592 0.

Taylor R, Richardson IG and Brydson RMD (2007) Nature of C–S–H in 20 year old neat ordinary Portland cement and 10% Portland cement–90% ground granulated blast furnace slag pastes. *Advances in Applied Ceramics*, 106(6), pp.294-301. https://doi.org/10.1179/174367607X228106.

Tedd P, Holton IR, Butcher AP and Wallace S (1997) Investigation of the performance of cement-bentonite cut-off walls in aggressive ground at a disused gasworks site. *Land Contamination and Reclamation*, 5(3), pp. 217-223.

Tirumala RK (1989) Calcium Bentonite in Containment Structure, Master's Thesis, NJIT, Newark, NJ.

US EPA (1984) *Slurry trench construction for pollution migration control*. US Environmental Protection Agency, Cincinnati, Ohio, EPA-540/2-84-001.

Wang H, Xu W (2013) Relationship between permeability and strain of sandstone during the process of deformation and failure. *Geotech. Geol. Eng.* 31, pp. 347-353.

Williams M, Ghataora GS (2011) Effect of fibre reinforcement on the properties of ground granulated blast furnace slagcement–bentonite slurry. *Stud. Geotech. Mech.* 33, pp. 63–83.

Xanthakos PP (1979) *Slurry Walls*. McGraw Hill Publishers. ISBN: 0-07-072215-3.

Xiao M, Ledezma M and Wang J (2015) Reduced-Scale Shake Table Testing of Seismic Behaviors of Slurry Cutoff Walls. *Journal of Performance of Constructed Facilities, 30*(3), pp.04015057 (1-10). DOI: 10.1061/(ASCE)CF.1943-5509.0000795.

Yang DS, Luscher U, Kimoto I and Takeshima S (1993) SMW Wall for Seepage Control in Levee Reconstructio. INTERNATIONAL CONFERENCE ON CASE HISTORIES IN GEOTECHNICAL ENGINEERING. *PAPER 28* (pp. 487-492).

Yang SQ, Jing HW (2011) Strength failure and crack coalescence behaviour of brittle sandstone samples containing a single fissure under uniaxial compression. *Int. J. Fract.* 168, pp. 227-250.

Yang SQ, Jing HW, Wang SY (2011) Experimental investigation on the strength, deformability, failure behaviour and acoustic emission locations of red sandstone under triaxial compression. *Rock Mech. Rock Eng.*168, pp. 227–250.

Zhao H, Zhou K, Zhao C, Gong BW and Liu J (2016) A long-term investigation on microstructure of cement-stabilized Handan clay. *Euro. J. of Enviro. and Civil Eng., 20*(2), pp.199-214. https://doi.org/10.1080/19648189.2015.1030087.

Appendix A

Environmental Geotechnics
Volume 4 Issue EG5

Cement-bentonite in comparison with other cemented materials
Alzayani, Royal, Ghataora and Jefferson

Environmental Geotechnics October 2017 Issue EG5
Pages 353–372 http://dx.doi.org/10.1680/jenge.14.00050
Paper 14.00050
Received 12/12/2014; accepted 21/12/2015
Published online 18/04/2016
Keywords: geoenvironment/geomaterial characterisation/waste containment & disposal system

ice
Institution of Civil Engineers
publishing

Cement-bentonite in comparison with other cemented materials

Nuha J. Alzayani MSc, DIC, BSc
Doctoral Research Student, School of Civil Engineering, University of Birmingham, Birmingham, UK (corresponding author: axn325@bham.ac.uk; nuha.alzayani@gmail.com)

Alexander C. D. Royal MEng, PhD
Lecturer, School of Civil Engineering, University of Birmingham, Birmingham, UK

Gurmel S. Ghataora BEng, PhD, MIMM, MILT
Senior Lecturer, School of Civil Engineering, University of Birmingham, Birmingham, UK

Ian Jefferson BEng, DIS, PhD, FGS
Professor, School of Civil Engineering, University of Birmingham, Birmingham, UK

The deformation behaviour of cement-bentonite (CB) materials used in low-permeability cut-off walls is critical to the performance of these barriers on site. While a number of investigations have focused on the deformation behaviour of CB materials, it is suggested that insufficient knowledge has been generated to allow for the determination of the behaviour of a CB wall on site with confidence. This paper reviews the deformation behaviour of other cemented particulate systems commonly encountered in civil engineering, concrete, rock, clays and cemented soils, and compares it with CB response to determine if the greater research effort associated with these materials could be used to improve understanding of CB. It is concluded that a direct comparison of physical behaviour between these materials is problematic due to the differences observed. Furthermore, formation of microcracks before the peak strength in cemented materials (rocks, etc.) is an area that does not appear to have been studied previously with CB materials; yet it could have a significant impact on the ability of a CB barrier to retard groundwater migration. Therefore, additional research is required on CB behaviour, prior to the achievement of the peak strength, to determine whether microcracking in CB is a significant hazard.

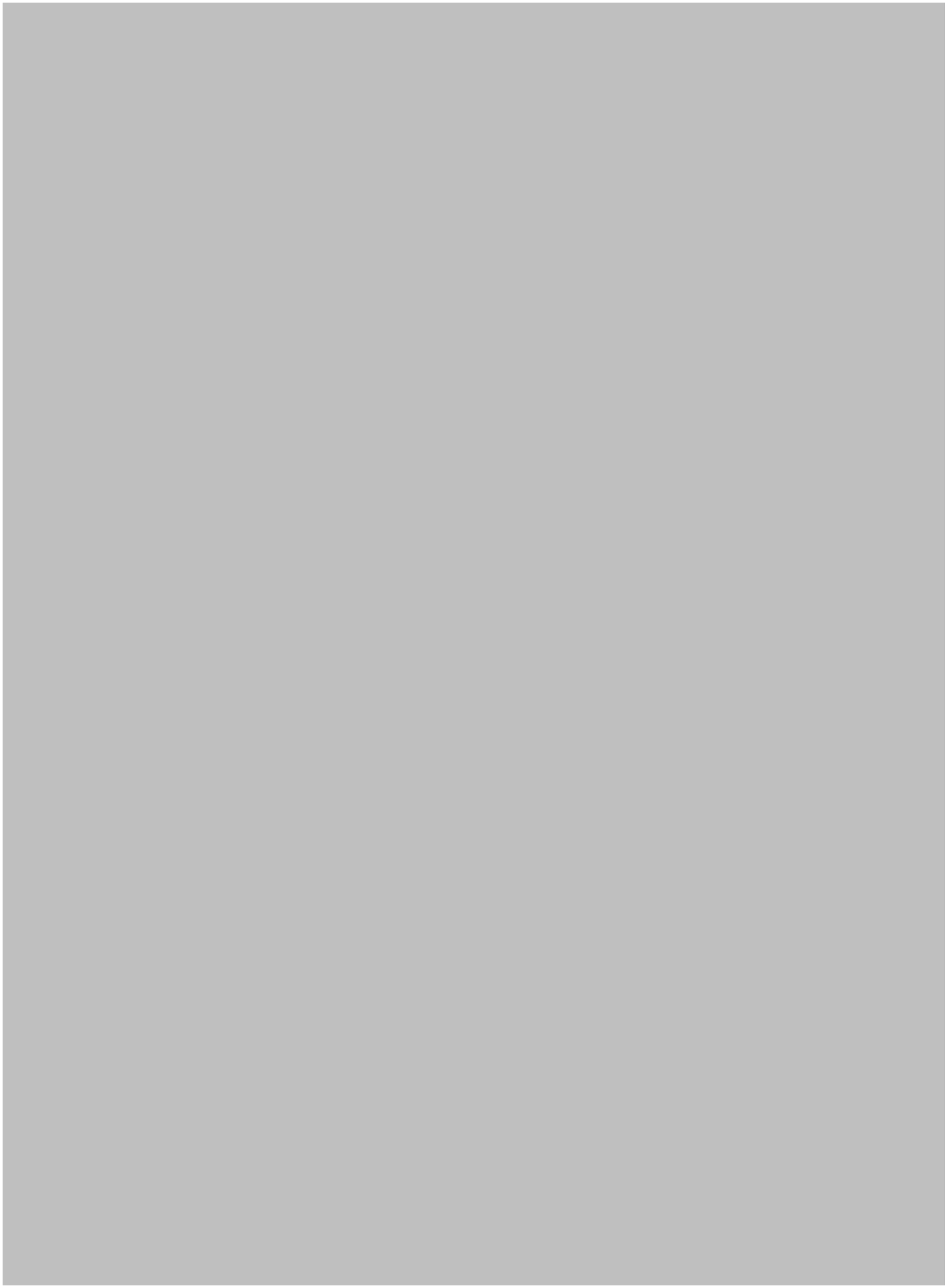

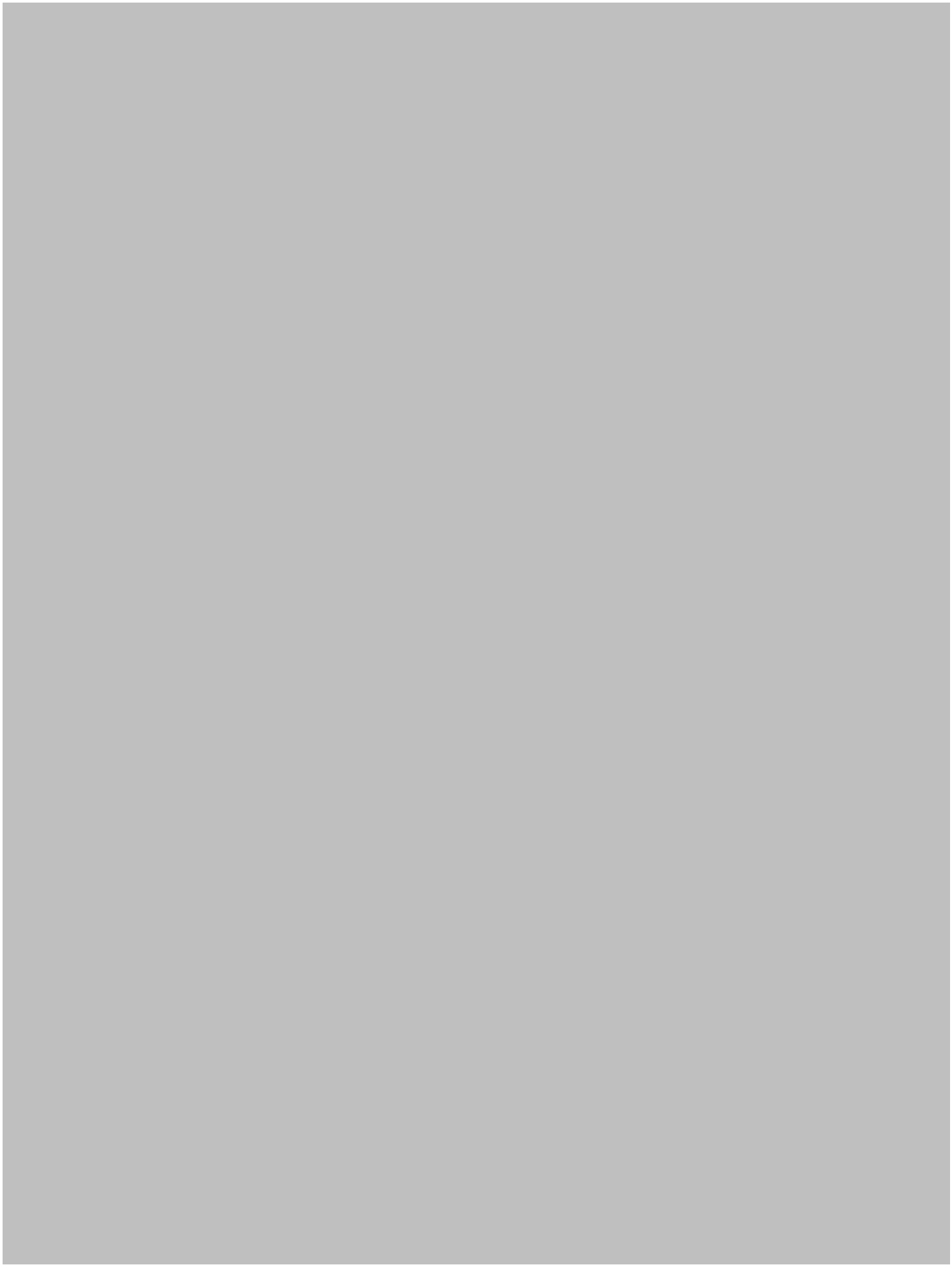

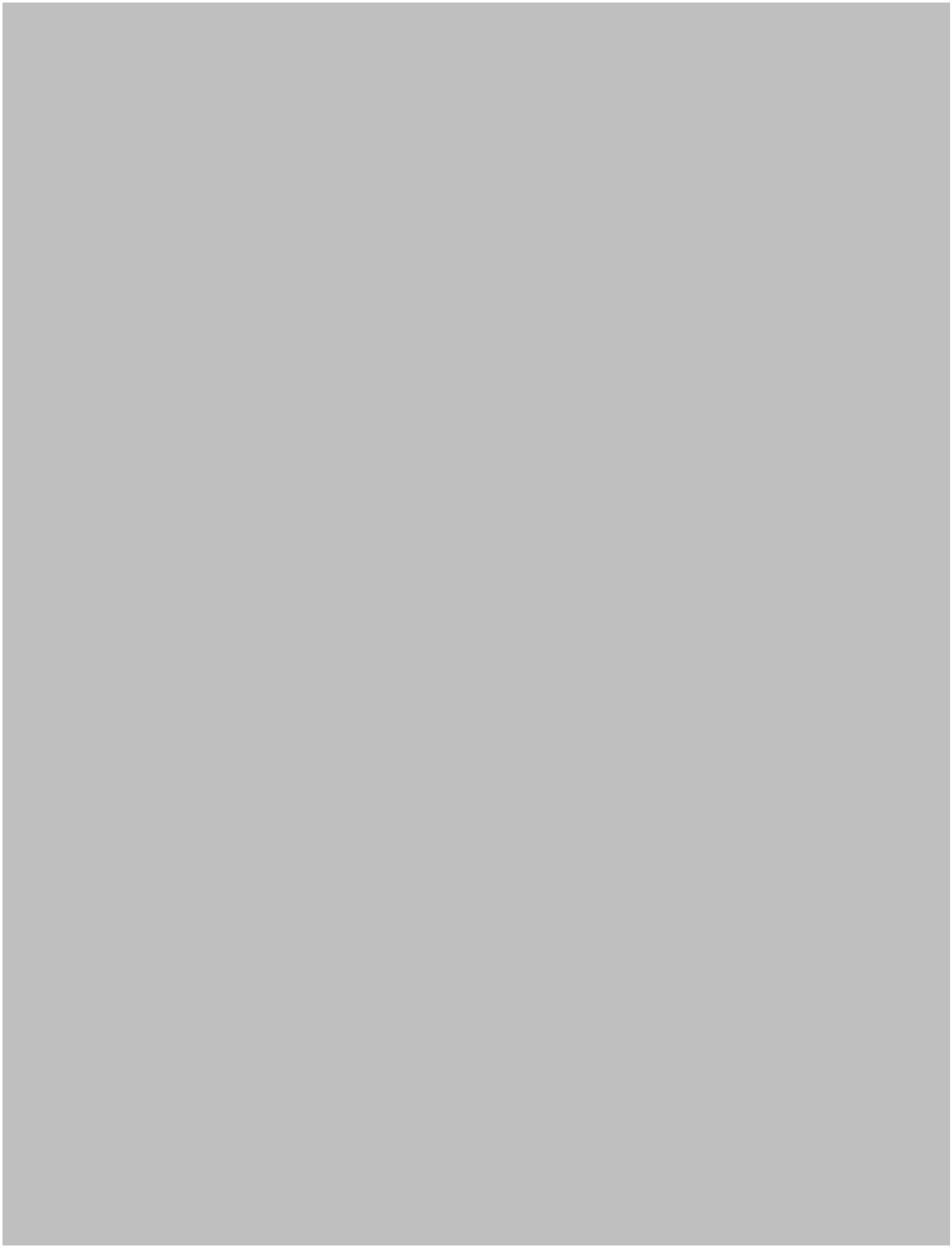

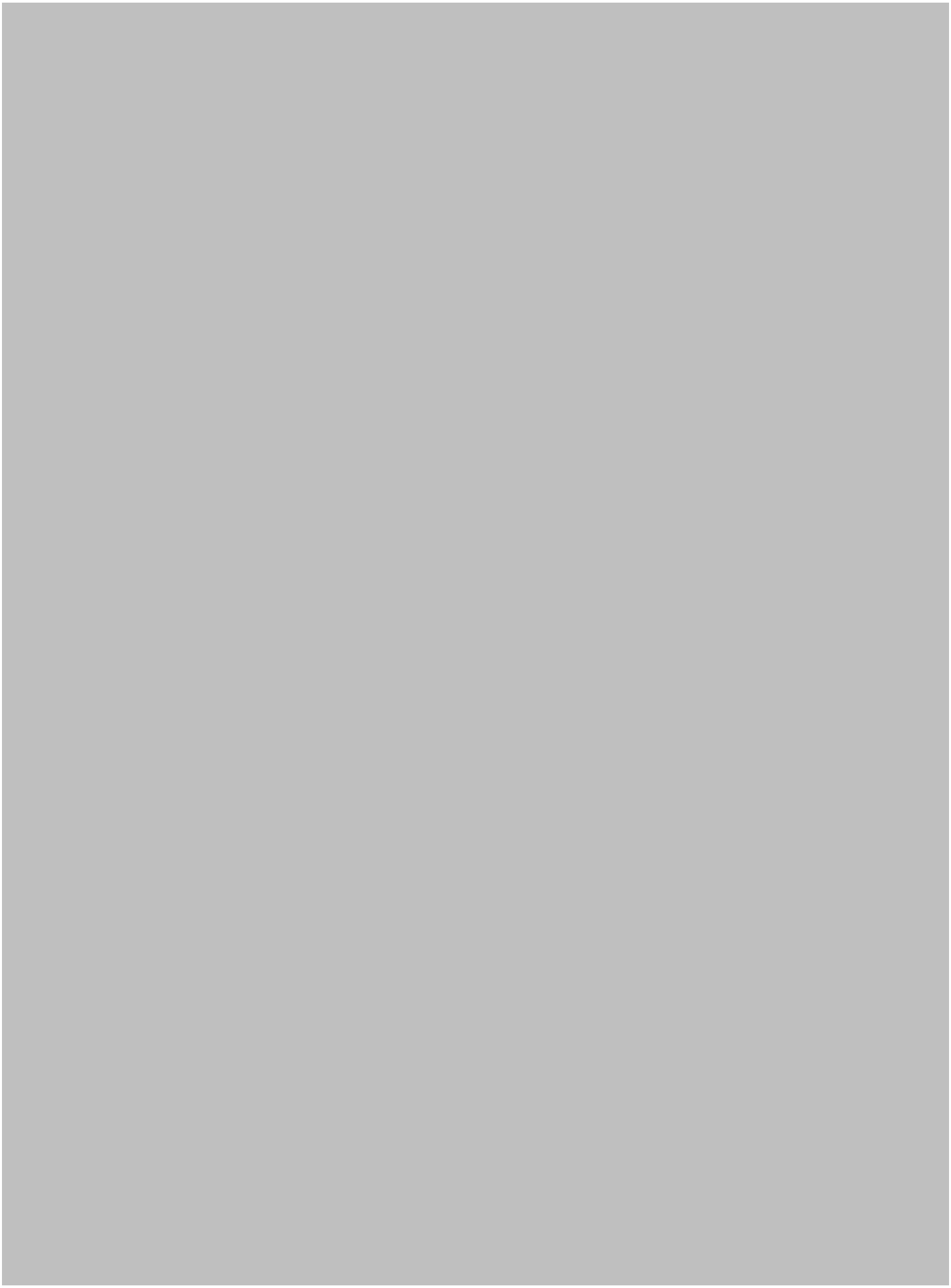

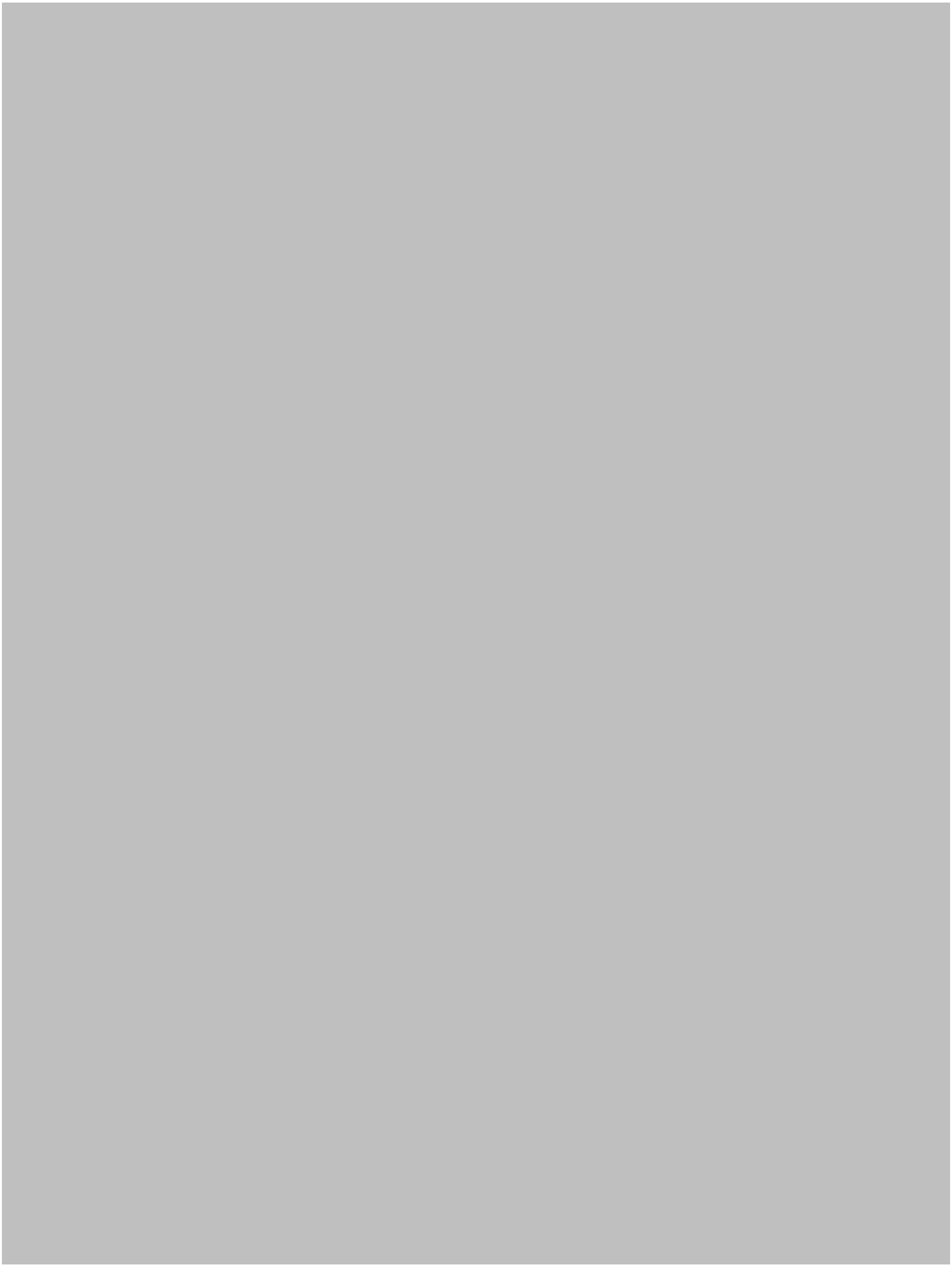

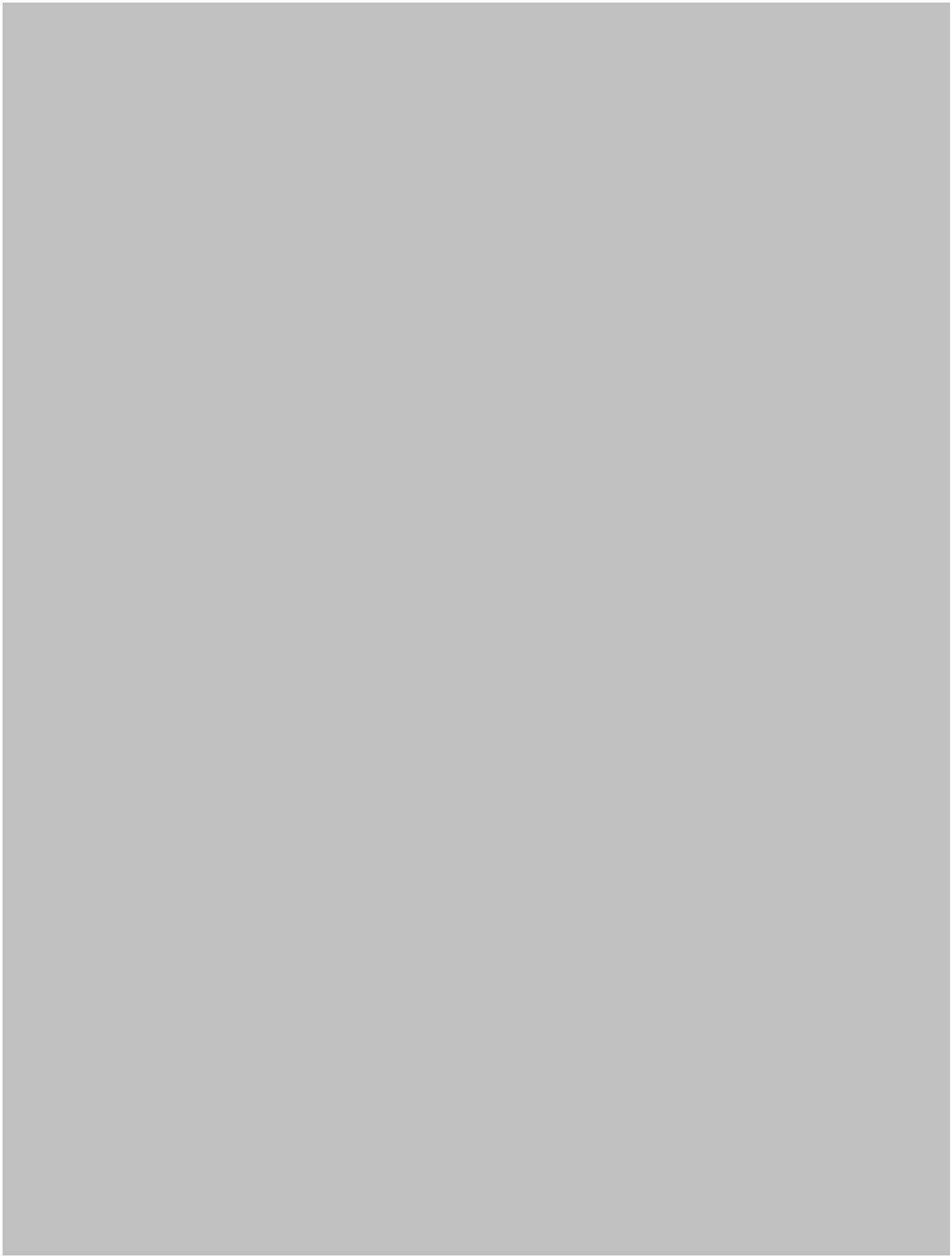

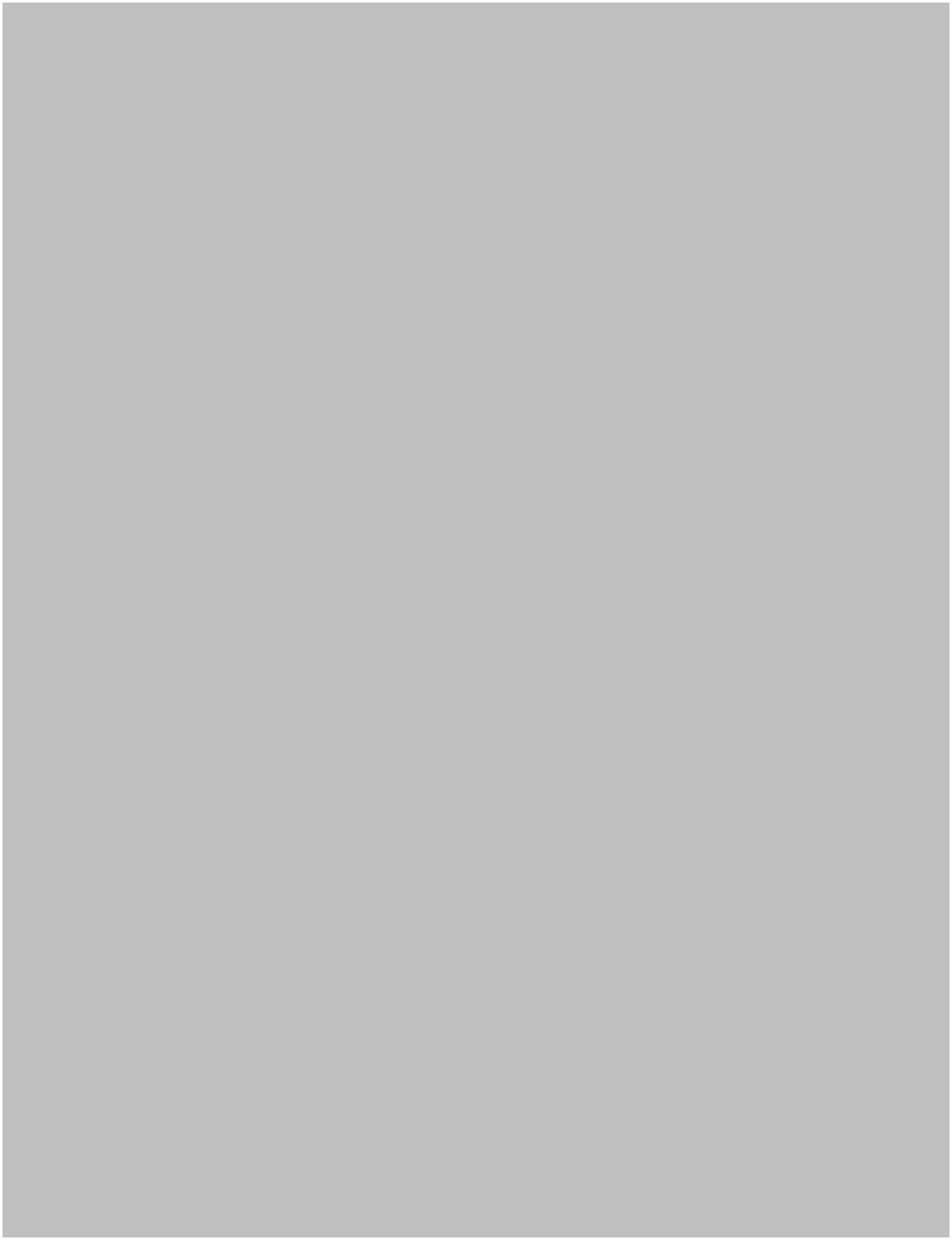

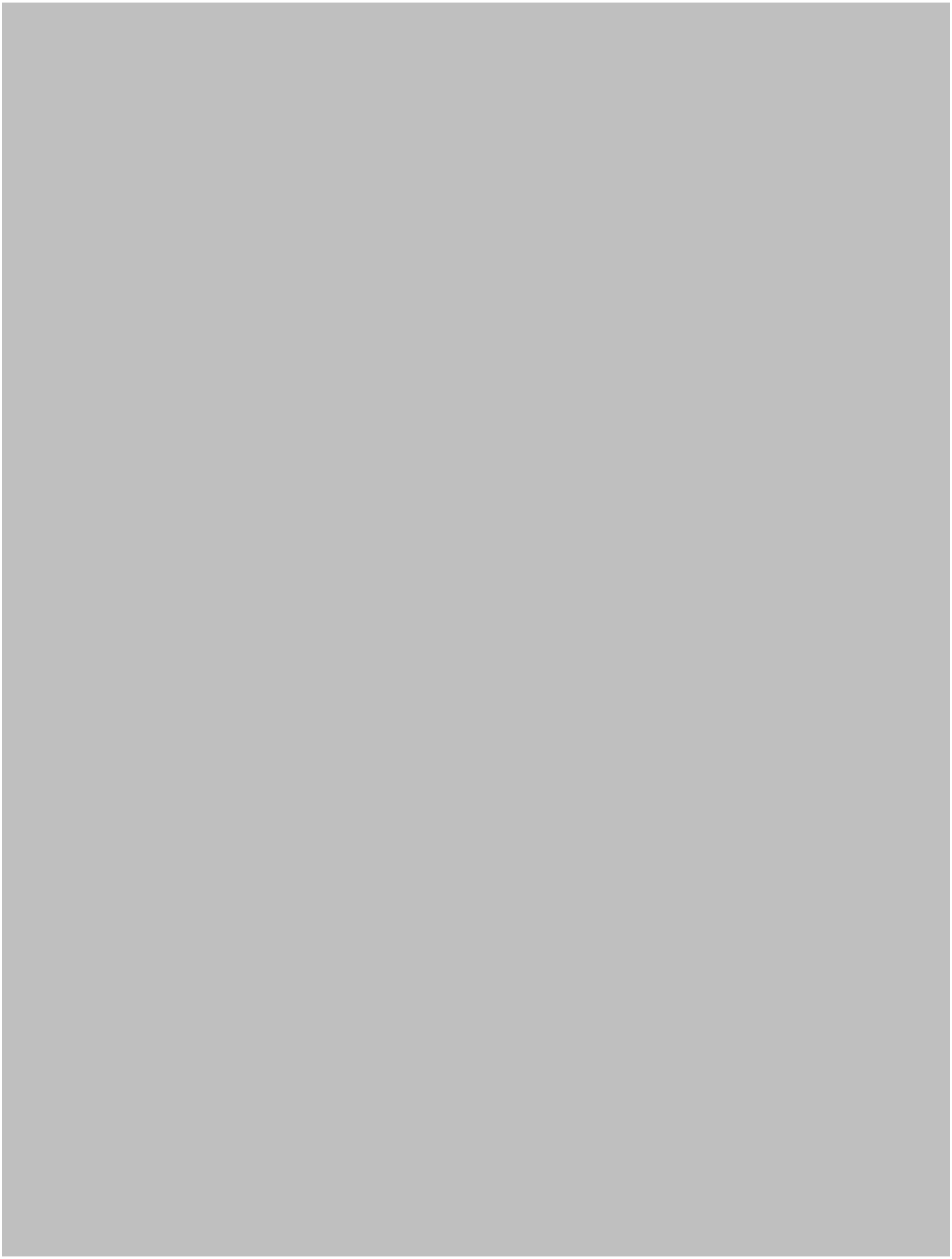

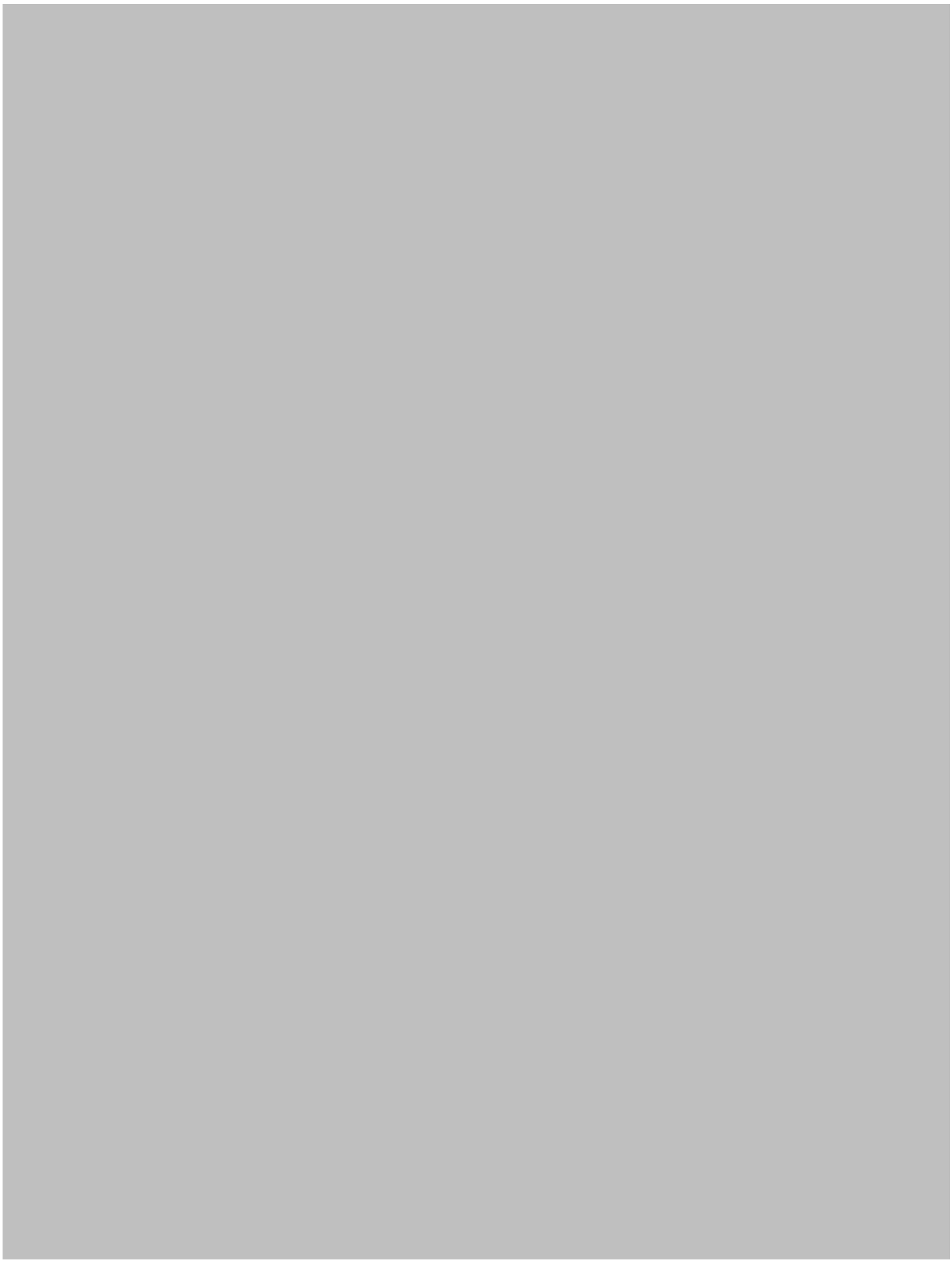

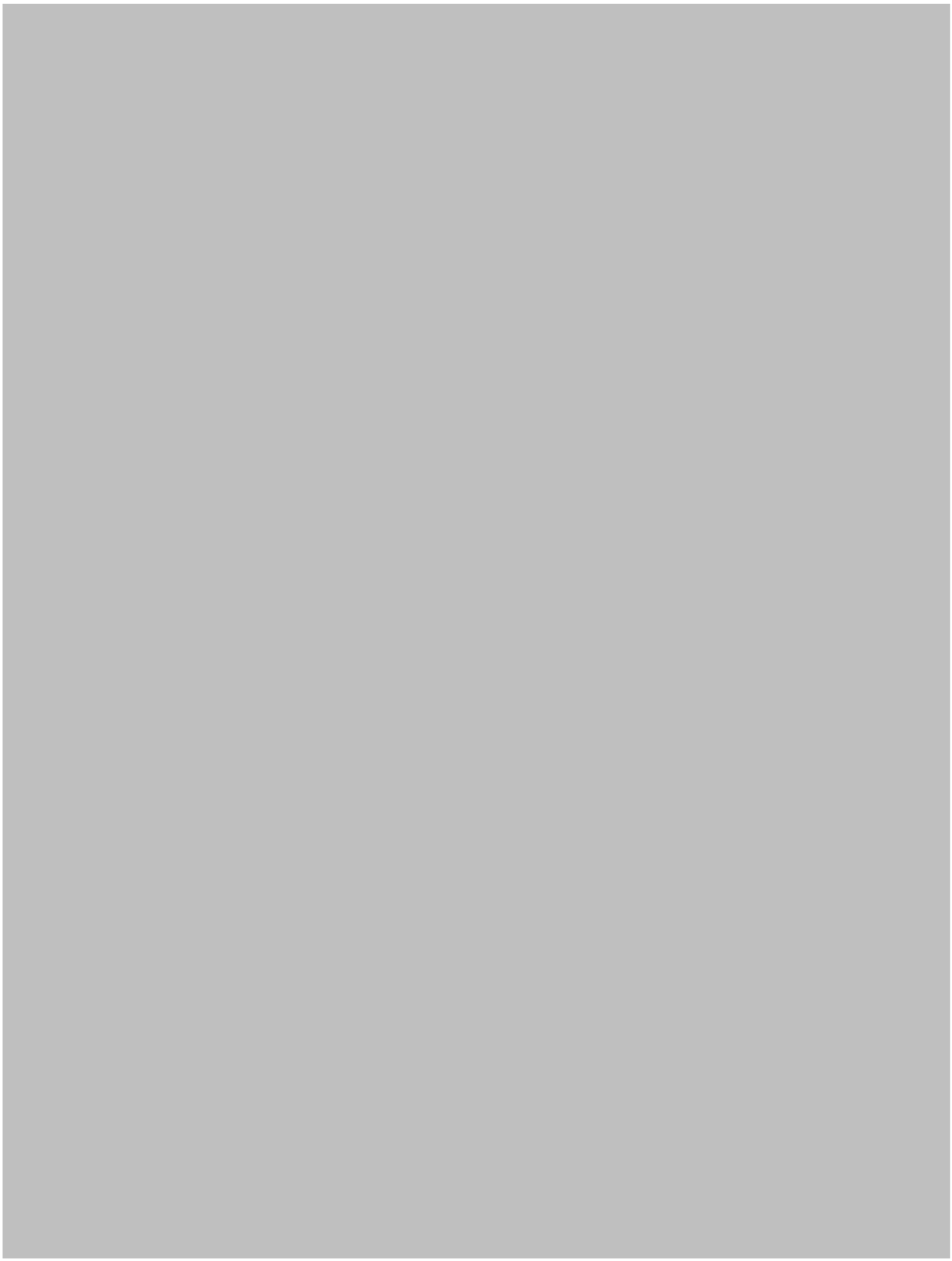

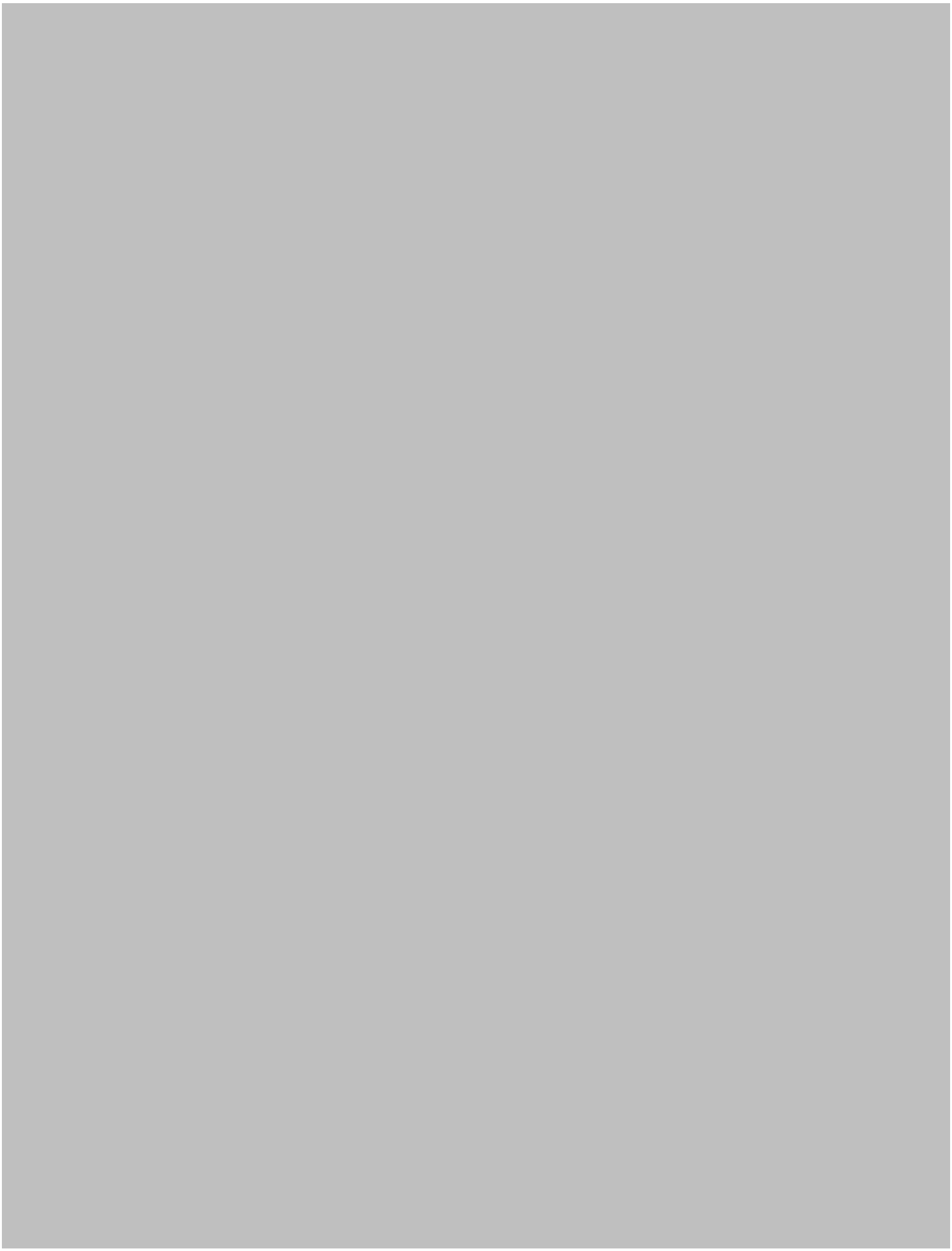

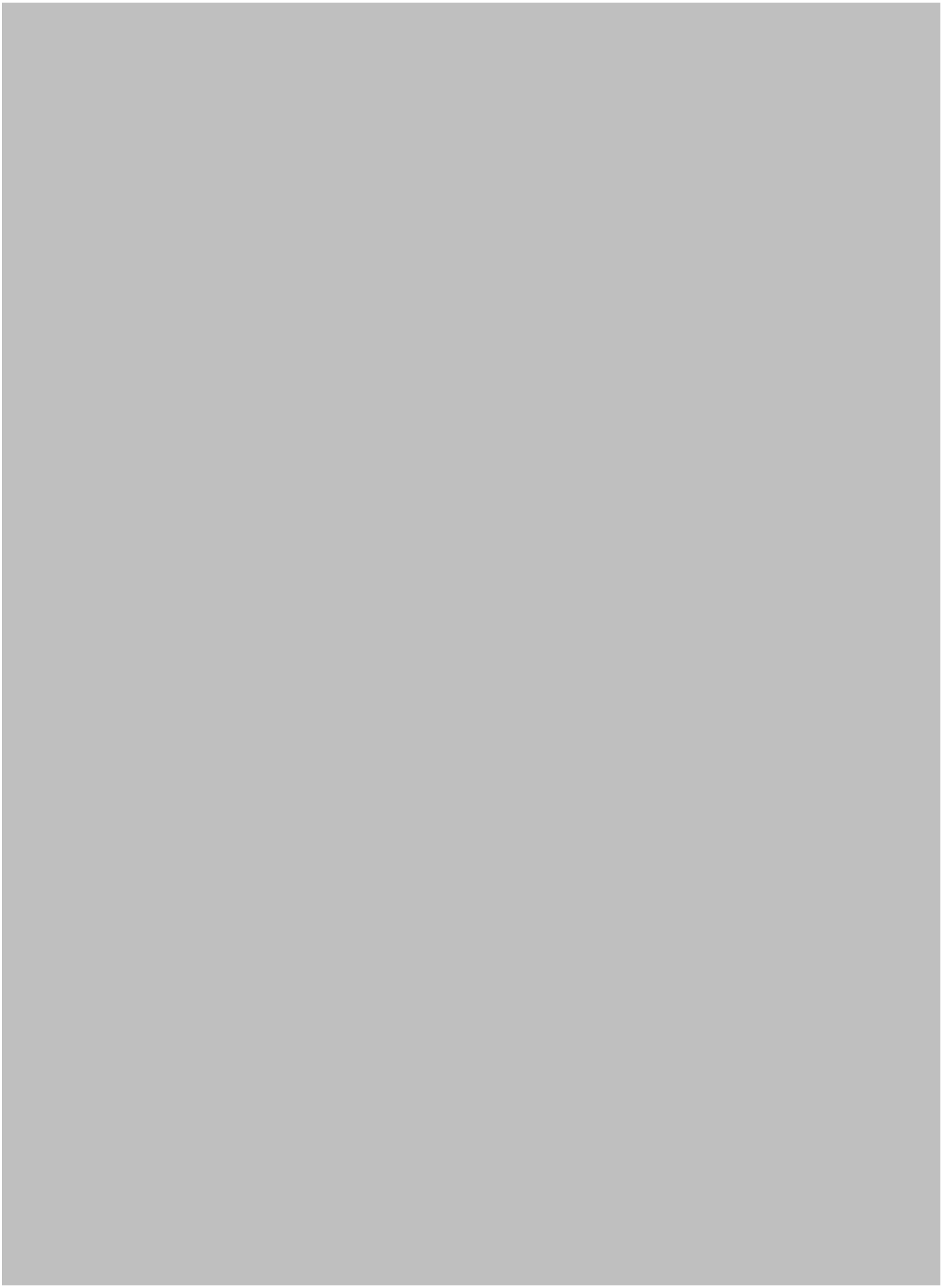

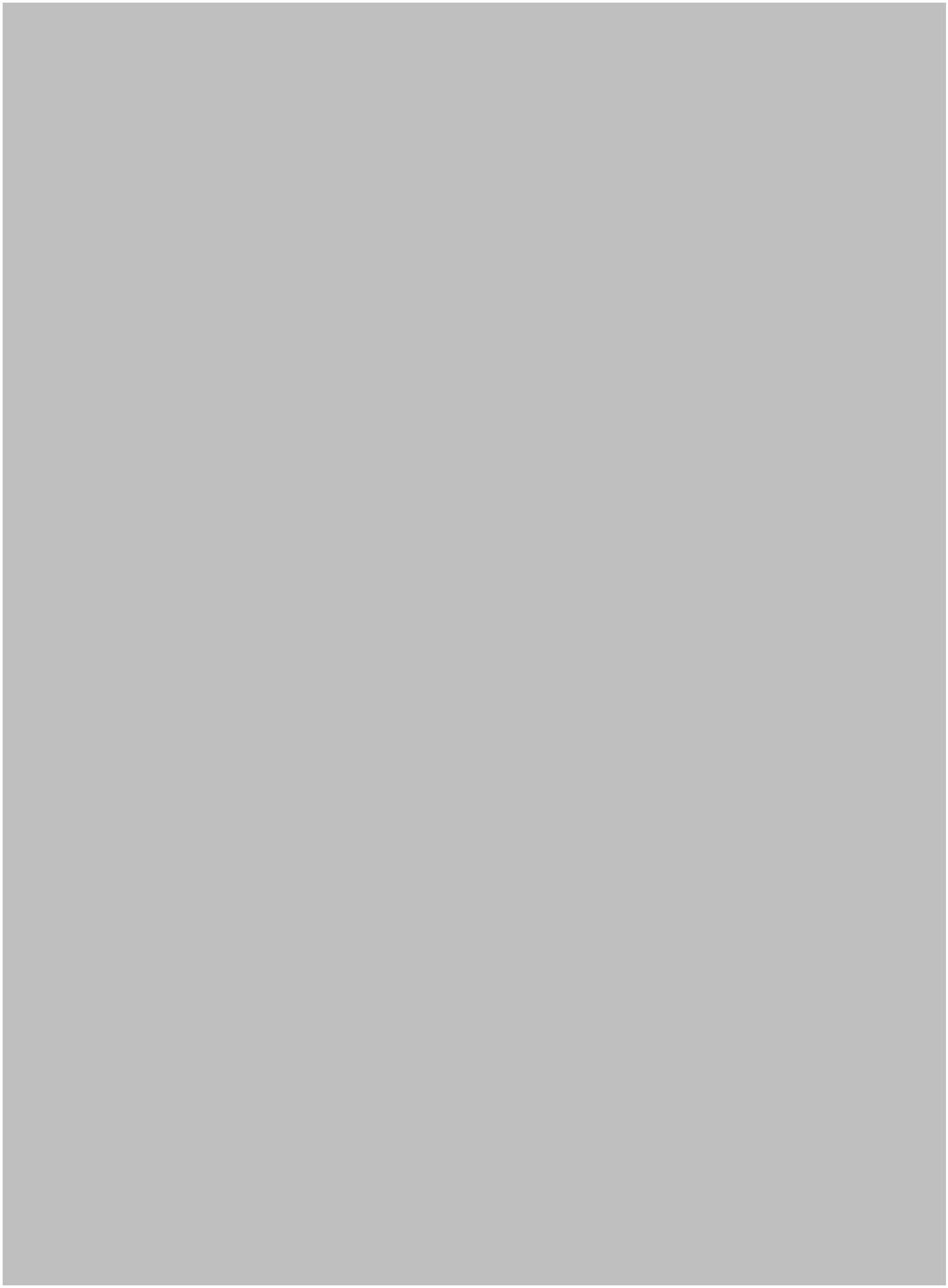

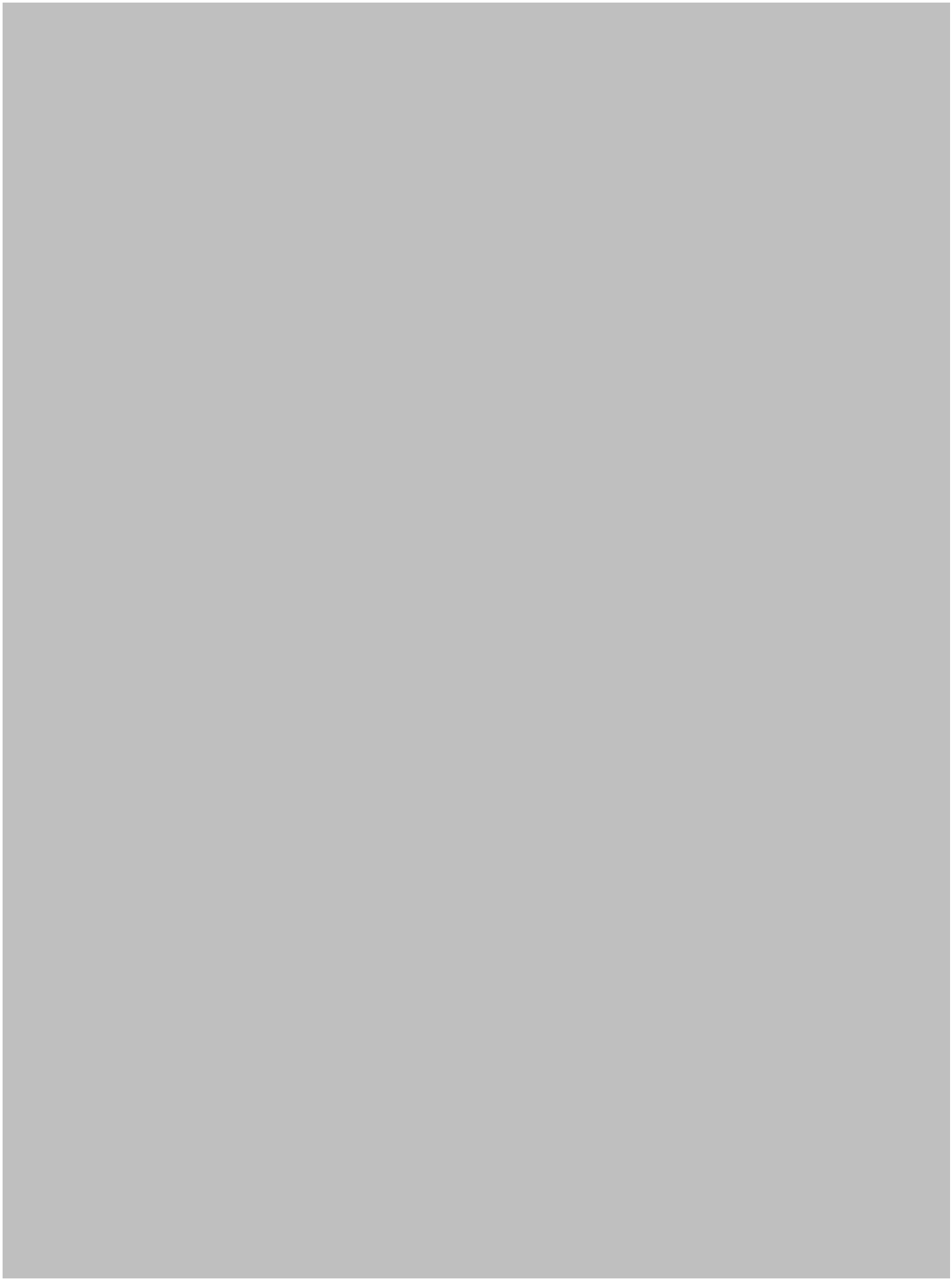

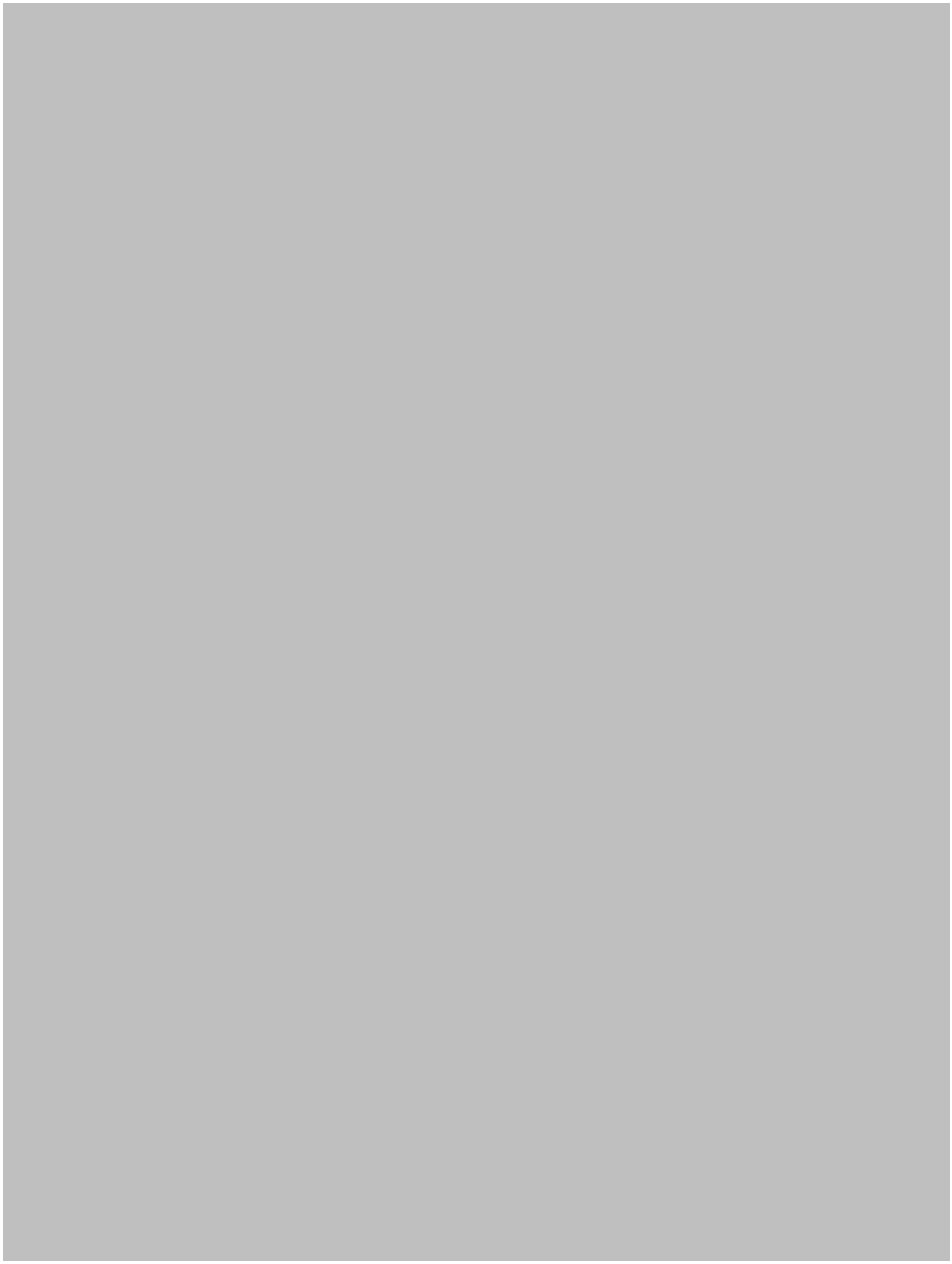

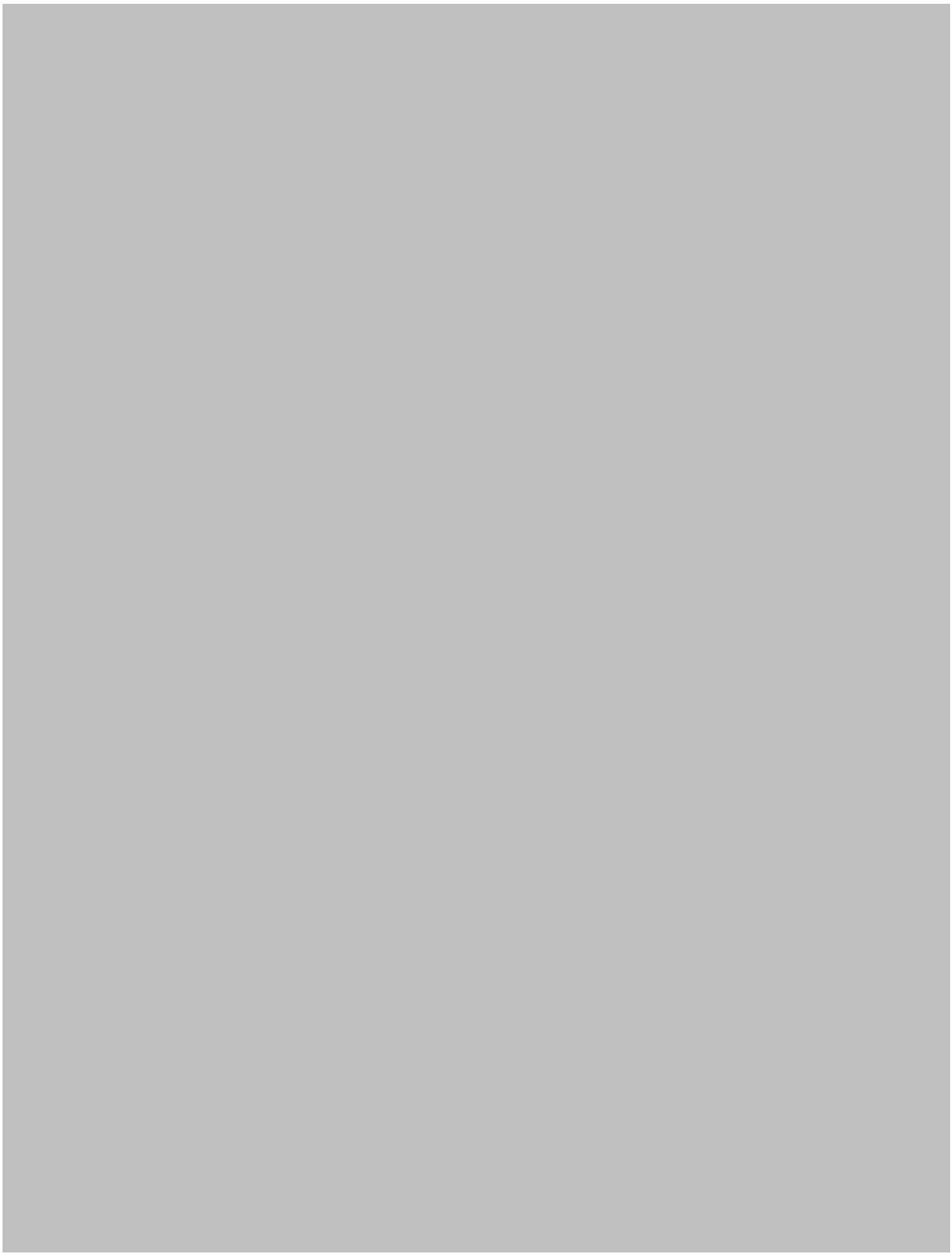

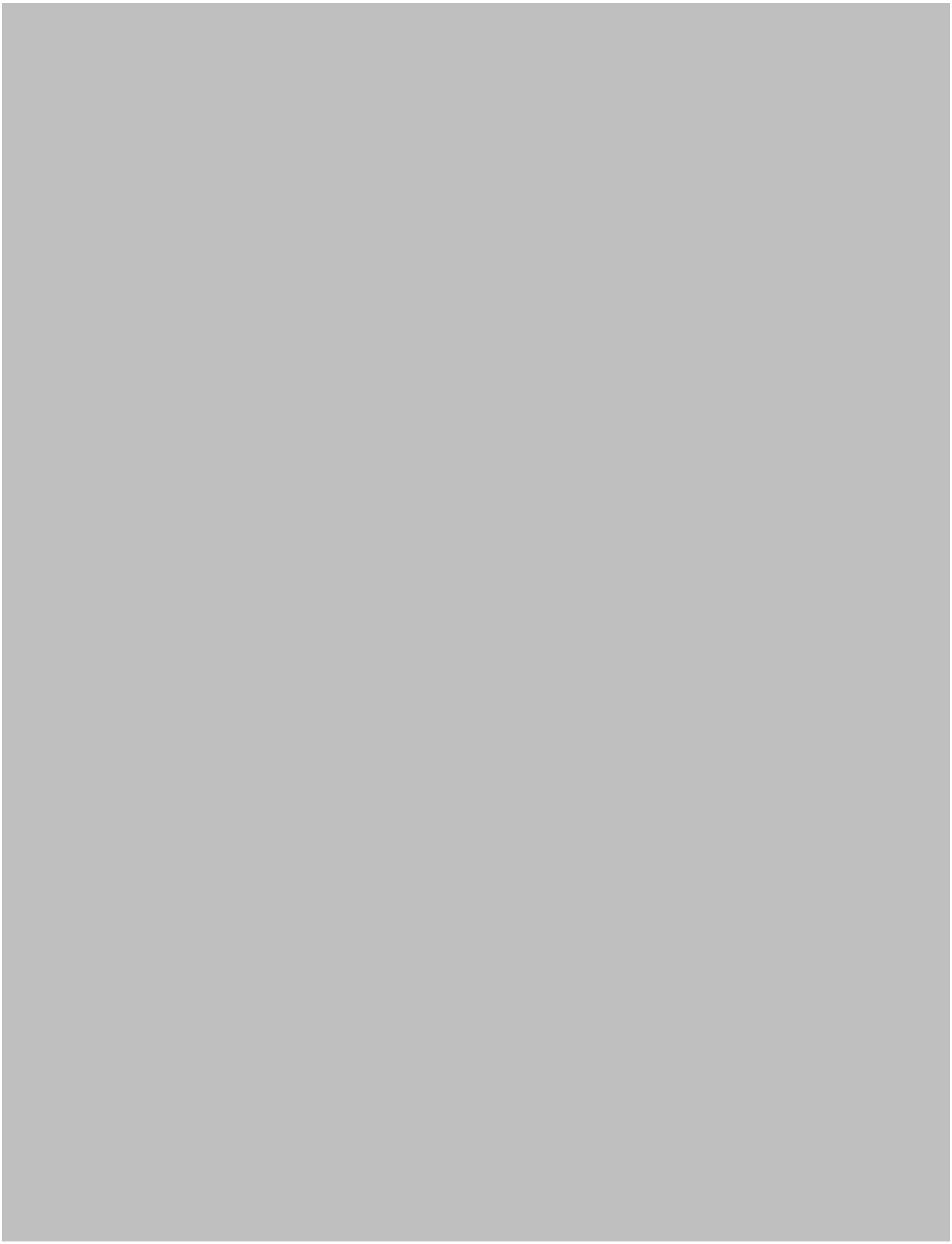

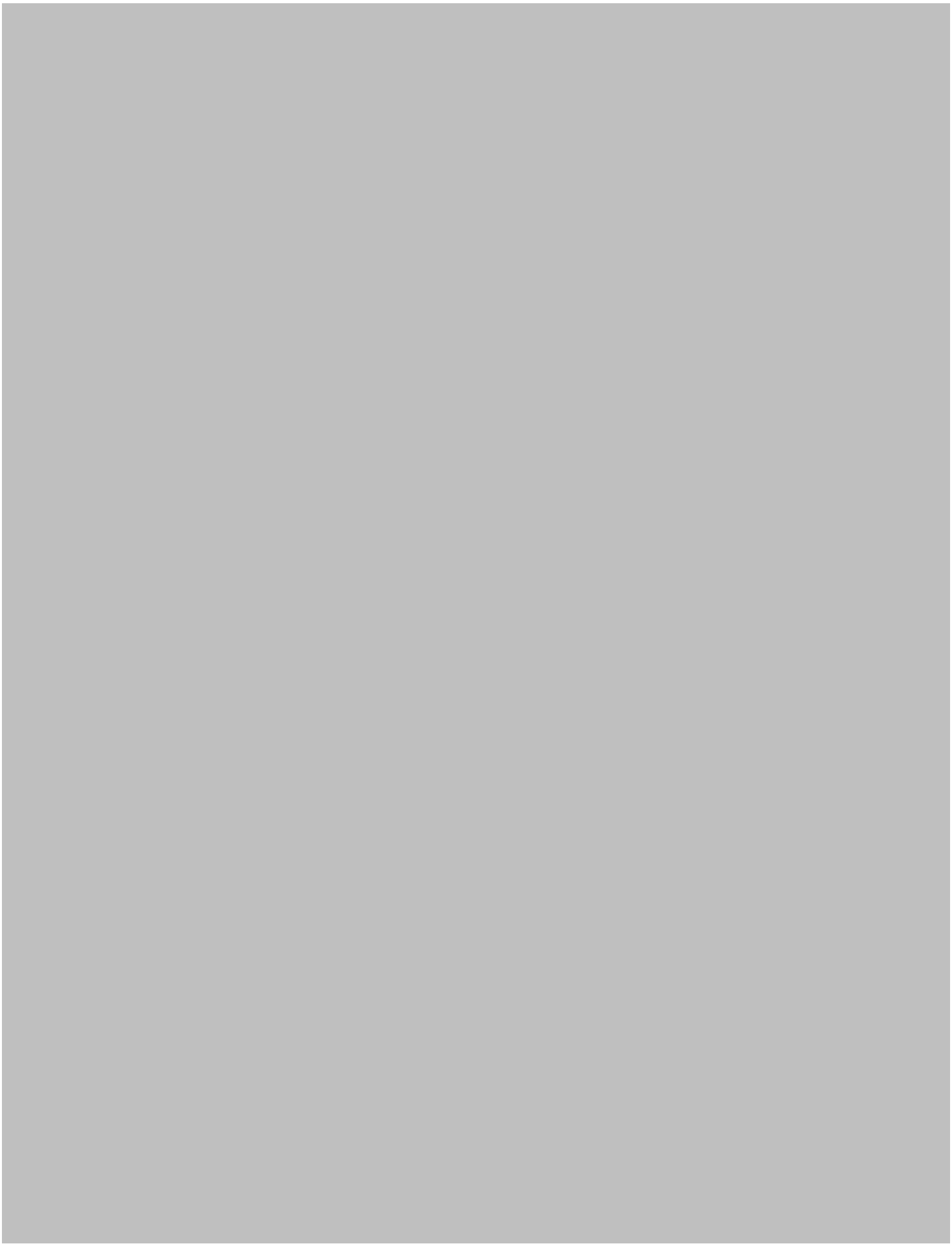

Appendix B

Bentonite

Powder

Berkbent 163 is a free flowing powder of premium grade high quality sodium carbonate activated Bentonite, specially formulated to provide rapid development of viscosity and gel strength for drilling and civil engineering slurries.

When dispersed in water, Berkbent 163 swells to many times its volume, rapidly forming a thixotropic gel.

PROPERTIES

Colour:	Light yellowish grey
Odour:	None
pH:	9 - 10
Specific Gravity:	800 to 950kg/m3
Moisture content %	10-14
% by weight passing BS410	
150 micron sieve	min 95%
Swelling*	
30 mins	27
1 hour	29
2 hours	30
24 hours	32
48 hours	34

- Test procedure - 10g Bentonite inserted into a 100 ml capacity 30 mm ID glass cylinder.
- Total swelling volume (mls) recorded with time. 100 ml water added to each cylinder

Packed in 25Kg paper bags, 40 bags per pallet.

Applications

- Sealing landfill gas wells
- Borehole sealing
- Grouting
- Isolating instrumentation and sampling

Features

- Easy to use
- Easy to mix
- High gel strength
- Stable suspension
- Rapid build up of viscosity
- Suitable for immediate use after mixing
- Can be used with traditional mixing equipment

Specifications may change without prior notice

Marton Geotechnical Services Ltd www.mgs.co.uk e info@mgs.co.uk t +44(0)1359 271167 f +44(0)1359 271168
Geotechnical Centre, Rougham Industrial Estate, Rougham, Bury St Edmunds, Suffolk IP30 9ND, England

Bentonite

Granules

~ 2-12mm

~ 1-6mm

High quality activated Bentonite in granule form with high swelling characteristics. A granular product with good handling properties and low dust content.

Available in two grades

~ 1-6mm Fast swelling

~ 2-12mm Slow swelling

Simple to use it can be poured straight into boreholes without the need for mixing equipment.

Where groundwater is not present then water must be added to provide the necessary swelling and sealing.

Packed in 25Kg paper bags, 40 bags per pallet.

Applications

~ Sealing landfill gas wells

~ Borehole sealing

~ Grouting

~ Geothermal wells

~ Isolating instrumentation and sampling

Features

~ Granular Form

~ Easy to use and hadle

~ Dust free

~ High swelling capacity

~ Low permeability

~ High plasticity

~ Different swelling rates available

Specifications may change without prior notice

Marton Geotechnical Services Ltd www.mgs.co.uk e info@mgs.co.uk t +44(0)1359 271167 f +44(0)1359 271168
Geotechnical Centre, Rougham Industrial Estate, Rougham, Bury St Edmunds, Suffolk IP30 9ND, England

Rugby®

CEM 2™ SUSTAINABLE CEMENT

Material Datasheet

CEMENT

Portland-fly ash cement BS EN 197-1 - CEM II / B-V 32,5 N

CEMEX is a world leader in packed cement, backed with excellent technical expertise in blended cements and fly ash for more than 20 years.

The Rugby® brand signals a refreshed, coherent and extended range for the future. It not only reinforces our CEM II products and our commitment to sustainable development, but also stands for improved reliability and availability.

More specific information on CEM II cements can be found on the reverse of this datasheet.

Rugby® Cement may be used in various general applications, for concrete, mortar and render.

Features/benefits/applications

- A value, general purpose cement for use in concrete, mortar and render
- Rugby® Cement can be used with admixtures* to produce concretes suitable for a wide range of applications
- Consistent in quality and performance
- Compatible with lime and plasticising admixtures** used to produce workable mortars for use in brick/block laying and rendering
- Chromium (VI) compliant

*If air entrainment is required in mortar or concrete Rugby+ Premium will generally fulfil this function without any admixture.

**If mortars are required to be mixed on site without use of lime or admixtures Rugby General Purpose Mortar is available.

Delivery and storage

Delivered by road in a curtain-sided vehicle, the standard load size is 28 - 30 tonnes. All CEMEX drivers are fully trained and experienced in the safe delivery and unloading of our vehicles, but please do all you can to ensure your site is accessible with no obstructions.

Rugby® Cement is available in paper sacks delivered as shrink-hooded, 1.4 tonne modules on non-chargeable pallets. To avoid premature deterioration of the reducing agent incorporated in the cement for control of soluble Chromium (VI), storage should be in accordance with the recommendations given on bags and despatch documents.

Health and safety

Contact with wet cement, concrete or mortar may cause irritation, dermatitis or severe alkali burns. Contact between cement powder and body fluids (e.g. sweat and eye fluids) may also cause irritation, dermatitis or burns. There is serious risk of damage to the eyes. Wear suitable waterproof protective clothing, gloves and eye/face protection. In case of contact with eyes, rinse immediately with plenty of clean water and seek medical advice. After contact with skin, wash immediately with plenty of clean water. Keep out of reach of children. Contains Chromium (VI), may cause allergic reaction, the risk of which is increased if the cement is used beyond the declared storage period shown on bags and despatch documents.

CEMEX

CEMEX UK Cement Ltd
CEMEX House, Evreux Way, Rugby, Warwickshire CV21 2DT
Tel: 0808 145 1900 Fax: 01788 514 742

Product applications

Concrete

Sharp (concreting) sand should be used, together with 20mm maximum size coarse aggregate and the minimum amount of water necessary for placement and compaction. Excess mixing water reduces both strength and durability of concrete. Use of separate sand and coarse aggregate is preferable to all-in aggregate (ballast).

The following table gives nominal mix proportions by volume for general applications.

General purpose mix application:

For most uses except foundation work and outdoor paving.

	Proportions by volume	Amount per M³ (approx)
Rugby+ Cement	**1**	**310 kg**
Sand	**2**	**655 kg**
20mm aggregate	**3**	**1130 kg**
(all - in aggregate)	(4)	(1785 kg)

Once in place, concrete requires moisture to develop its full strength and premature drying out must be avoided. In normal conditions and at temperatures in excess of 10°C, concrete should be cured under damp conditions for 1 to 3 days (cover with curing membrane, plastic sheeting or wet hessian); at temperatures below 10°C, this curing time should be doubled. Curing is particularly important with CEM II cements as early strengths may be slightly lower than for CEM I products. Protection of fresh concrete against freezing is essential and placement under such conditions should be avoided if possible.

Mortar

Rugby® Cement is fully compatible with hydrated lime and the plasticising admixtures* used to produce high workability mortars for use in brick/block laying and rendering. If, however, production of mortar on site without the use of lime or admixtures is required, then Rugby General Purpose Mortar is recommended.

*A plasticiser suitable for fly-ash will be required.

	Rugby+ Cement : Sand (with plasticiser)	Rugby+ Cement : Lime : Sand	Equivalent BS EN 998-2 Mortar class
General usage (low-rise housing)	**1 : 5**	**1 : 1 : 5**	**M 2,5**
Strong (free standing walls)	**1 : 3**	**1 : ½ : 4**	**M 5**

Rendering

In rendering applications, it is important when applying two-coat renders (normal practice) that the second coat is either thinner or weaker than the scratch coat to avoid problems with shrinkage and de-lamination. A suitable sand for rendering should be chosen. Mix proportions for rendering over strong and moderately strong backgrounds are given below.

	Rugby+ Cement : Sand (with plasticiser)	Rugby+ Cement : Lime : Sand
First coat **(strong backgrounds)**	**1 : 3**	**1 : ½ : 4**
First coat **(moderate backgrounds)** or Second coat **(moderate and strong backgrounds)**	**1 : 5**	**1 : 1 : 5**

Once placed, mortar requires measures to prevent premature loss of moisture and the advice given on curing of concrete is again applicable.

Product certification

Rugby® products are subject to rigorous third party certification procedures detailed in BS EN 197-2 (Cement – Part 2: Conformity evaluation), which lead to issue of EC certificates of conformity by an EU Notified Body. Products that carry EC Certification bear the CE marking to indicate conformity to all requirements of their harmonised technical specification and a presumption of conformity to the essential requirements of the Construction Products Directive.

CEM II information

CEMEX is committed to continuous improvement in environmental and sustainability performance, particularly through utilising recycled content, minimising landfill waste and improving our energy efficiency.

CEM II cements are factory produced Portland composite cements. Packed CEM II cements from CEMEX are of the Portland-fly ash type.

This product contains a minimum of 20% fly ash which is a by-product of Coal Fired Power Stations, making not only a more sustainable cement but also enhancing it's performance characteristics.

CEM 2™ SUSTAINABLE CEMENT

min. 20%

For further information please contact Customer Services on:

Tel: 0808 145 1900
Fax: 01788 514 742
E-mail: customerservices@cemex.co.uk

Hanson
HEIDELBERGCEMENT Group

REGEN

Brigg Road, Scunthorpe, North Lincolnshire DN16 1AW
Telephone : 01724 282211 Fax : 01724 294220

CUSTOMER SAMPLE
GGBS ANALYSIS CERTIFICATE

The sample was tested following the methods given in BS EN 196-1:2005 & BS EN 196-2:2005. Additions and modifications have been made in accordance with the Hanson Cement - Quality Department Laboratory Manual and Work Instructions.

Reference Details

Sample Source	Port Talbot Std	Date Sampled	04/10/13

Sample Reference	2020/64

Physical Analysis

Fineness : m²/kg	438	S.G. Typical : kg/m³	2890

Mortar Prism Compressive Strength			
50% : 50% GGBS : CEM I 52.5N		Activity Index	
7 Day : N/mm²	28 Day : N/mm²	7 Day : %	28 Day : %
29.1	50.0	62	84

XRF Analysis : %

SiO_2	Al_2O_3	Fe_2O_3	CaO
35.49	12.87	0.59	40.19

MgO	MnO	SO_3	TiO_2
7.74	0.45	1.93	0.65

Na_2O	K_2O
0.26	0.59

Chemical Analysis : %

Na_2O Equiv.	L.O.I.	V Ratio : (Ca+Mg)/Si	ih Value : (Ca+Mg+Al)/Si
0.65	0.79	1.35	1.71

Typical Analysis : %

IR	Cl^-	$S_{(Total)}$	S^{2-}
0.42	0.023	0.96	0.94

Glass Content	Moisture
95	0.037

The GGBS contained no additional materials other than those permitted. The above results and other tests demonstrate the conformity of the material sold during the month to the requirements of BSEN15167-1

CE

1333 – CPD – 00134

S C Chudley - Quality Manager

Date: 09/01/14

Appendix C

Options available for STDDPC

Pressure ranges

1MPa ✓
2MPa ✓
3MPa ✓
4MPa ✓

NB The most commonly-used pressure is 3MPa

Volume

200cc ✓

Standard Pressure/Volume Controller (STDDPC)

What is it?

The GDS Standard Pressure/Volume Controller (STDDPC) is a general-purpose water pressure source and volume change gauge. It is designed for use in commercial and teaching soil mechanics laboratories. A stepping motor and screw-drive actuate a piston which directly pressurizes water. The pressure is regulated under closed-loop control. The change in volume is measured to 1cu mm (0.001cc) by counting the steps to the stepping motor.

What are its uses?

The STDDPC, typically operating at 3MPa/200cc, provides a cost-effective direct replacement for conventional soil mechanics laboratory pressure sources and volume change gauges. Above all, the device has its own computer interface and so can be controlled directly from a computer. It is ideal as a back pressure source where it can also measure the change in volume of the test specimen. Also, it automatically protects itself from pressure and volume over-ranges.

In stand-alone mode, the instrument is a constant pressure source which can replace traditional laboratory pressure sources such as mercury column, compressed air, pumped oil and dead weight devices. It is also a volume change gauge resolving to 1 cu mm.

In addition, the instrument can be programmed through its own control panel to RAMP and CYCLE pressure or volume change linearly with respect to time. This means the device is also ideal for permeability testing by constant rate of flow or constant head.

A data logger can be connected to an analogue interface option which provides output readings of pressure and volume change.

Compressed air is not used with the STDDPC.

Technical specification

- **Pressure ranges**: 1, 2, 3, 4MPa
- **Volumetric capacity (nominal)**: 200cc for all pressure ranges
- **Resolution of measurement**: pressure = 1kPa, volume = 1cu mm
- **Accuracy of measurement**: pressure = <0.15% full range, Volume =< 0.25% measured value with +/- 30mm^3 backlash
- **Closed-loop microprocessor control of pressure:** regulated to 1kPa
- **Closed-loop microprocessor control of volume:** regulated to 1cu mm
- **Size**: 600mm x 230mm x 220mm
- **Weight**: 12kg
- **Power**: 92-265v, A.C. 48-440Hz, 65w maximum, single phase three wire earthed supply, 2A fuse x 2
- **Ambient temperature range**: 10°C to 30°C
- **Relative humidity**: 20% to 80% non condensing
- **Control panel**: 16 keypad membrane touch panel with audio feedback. Functions include zero pressure, target pressure, zero volume, target volume, fill, empty, test, ramp, stop, continue, reset, enter, +, -, >, <, yes, no
- **User interface:** 32 character, 2-line liquid crystal display
- **Computer interface**: optional RS232 serial computer interface for computer control and logging of pressure and volume
- **Maximum operational speed:** Fill/empty speed = 500 cu mm/sec

GDS Standard Controller quick reference guide (helpsheet 106)

Firmware

World Leaders in Computer Controlled Testing Systems for Geotechnical Engineers and Geologists

RESET

0 invokes SYSFUN

1 invokes DIAGNOSTICS

2 RAMP command

4 Target Volume

5 Zero Volume

6 Fill

+ Empty

7 Target Pressure

8 Zero Pressure

9 Power On Reset

- Select Volume or RFM display

"RESET" + "ENTER"
Remove Computer Control

SYSFUN MENU (RESET, 0)

4 Set Max pressure limit

5 Set RS232 Baud Rate

6 Set RS232 Stop Bits

+ Set RS232 Parity

8 Remove Pressure zero offset

ENTER Default Comms Parameters (4800, ODD, 2)

. RFM Functions

RFM FUNCTIONS MENU (RESET, 0, .)

0 Activate RFM
1 De-activate RFM
2 Set RFM Range
3 Set RFM decimal places
4 Set maximum RFM limit
5 Set minimum RFM limit
6 Soft Zero Offset
7 Remove Soft Zero Offset
+ Put RFM in control
- Remove RFM from control

DIAGNOSTICS MENU (RESET, 1)

0 Memory test
1 Display diagnostics
2 Keyboard diagnostics
3 Timer diagnostics
4 Forward limit
5 Reverse limit
6 Buzzer diagnostics
  1: 500Hz tone
  2: 2 kHz tone
  3: 4 kHz tone
7 A/D diagnostics
+ RFM A/D diagnostics

RAMP MENU (RESET, 2)

Slope cmd **1** = msecs
  9 = secs
Slope time interval per kPa or cu.mm
Lower Val
Upper Val
Execute cmd **7** = V,R,+
  39 = V,R,-
  15 = V,C,+
  47 = V,C,-
  23 = P ,R,+
  55 = P ,R,-
  31 = P ,C,+
  63 = P ,C,-